

NN31157.145

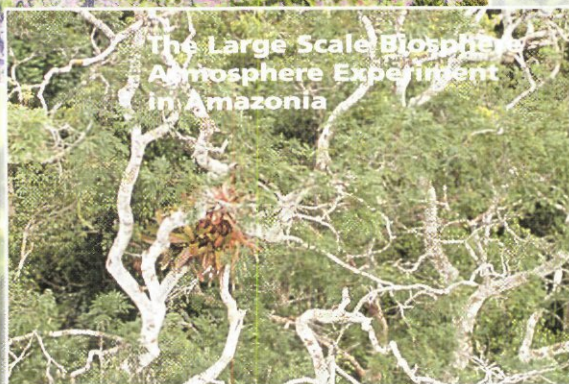
# Final Modelling for Design

## Final report

P. Kabat, A.J. Dolman, M. Ashby, J.C. Gash, I. Wright, A. Culf, J.C. Calvet, C. Delire, J. Noilhan, A. Jochum, M.A. Silva dias, G.A. Fisch, R.C. Santos Alvares, C.A. Nobre, S.D. Prince and M. Steininger



# LBA



The Large Scale Biosphere  
Atmosphere Experiment  
in Amazonia

32/607 (145) 2000

# Use of integrated modelling for experimental design

Final report

BIBLIOTHEEK "DE HAAFF"  
Droevendaalsesteeg 3a  
6708 PB Wageningen

- P. Kabat, A.J. Dolman, M. Ashby (DLO Winand Staring Centre, Wageningen, The Netherlands)
- J.C. Gash, I. Wright, A. Culf (NERC-Institute of Hydrology, Wallingford, UK)
- J.C. Calvet, C. Delire, J. Noilhan (CNRM Meteo France, Toulouse, France)
- A. Jochum (DLR, Oberpfaffenhofen, Germany)
- M.A. Silva dias (University of Sao Paulo, Sao Paulo, Brazil)
- G.A. Fisch (Centro Tecnico Aeroespacial, Sao Jose dos Campos, Brazil)
- R.C. Santos Alvala, C.A. Nobre (INPE/CPTEC, Cachoeira Paulista, Brazil)
- S.D. Prince, M. Steininger (University of Maryland, College Park, MD, USA)

Report 145

DLO-Staring Centre, Wageningen, 1999

Umg 66030

## ABSTRACT

Kabat, P., A.J. Dolman, M. Ashby, J.C. Gash, I. Wright, A. Culf, J.C. Calvet, C. Delire, J. Noilhan, A. Jochum, M.A. Silva dias, G.A. Fisch, R.C. Santos Alvala, C.A. Nobre, S.D. Prince and M. Steininger, 1999. *Use of integrated modelling for experimental design. Final Report*. Wageningen, DLO Winand Staring Centre. Report 145. 210 blz., 79 fig.; 18 tab.; .103 ref.

ISSN 0927-4537

### Project Participants:

Institute of Hydrology of the National Environmental Research Council (NERC-IH), Wallingford, United Kingdom

Central National de Recherche Meteorologique (CNRM), Toulouse, France

Deutsche Luft- und Raumfahrt (DLR), Oberpfaffenhofen, Germany

© 1999 DLO Winand Staring Centre for Integrated Land, Soil and Water Research (SC-DLO),  
P.O. Box 125, NL-6700 AC Wageningen (The Netherlands).  
Phone: +31 317 474200; fax: +31 317 424812; e-mail: postkamer@sc.dlo.nl

No part of this publication may be reproduced or published in any form or by any means, or stored in a data base or retrieval system, without the written permission of the DLO Winand Staring Centre.

The DLO Winand Staring Centre assumes no liability for any losses resulting from the use of this document.

## Contents

Summary of the main results	7
1 Introduction	19
1.1 Background of the research strategy for the current project	20
1.2 Objectives of the current project	22
2 Analysis of existing data	25
2.1 Climate and soil moisture data: extension of ABRACOS	25
2.1.1 The ABRACOS database	26
2.1.2 Estimates of annual evaporation from forest and pasture	26
2.2 Mapping of surface characteristics for mesoscale modelling (CNRM)	32
2.2.1 Data	32
2.2.2 Mapping processes	35
2.2.3 Discussion	43
2.3 Use of remote sensing data for monitoring rainforest extension and its changes: assessment of SAR data (DLR)	48
2.4 Biophysical stratification of the Amazon basin in support of LBA design (UMCP, DLR)	65
2.4.1 Introduction	65
2.4.2 Regression trees applied to land classification	68
2.4.3 Methods	69
2.4.4 Data sets	72
2.4.5 Results	73
2.4.6 Discussion	89
3 SVAT modelling (SC-DLO, CNRM, IH)	91
3.1 Introduction	91
3.2 Data description	92
3.3 Model descriptions	94
3.4 Model results	98
3.5 Discussion	114
4 Mesoscale modelling	115
4.1 Introduction	115
4.2 Mesoscale models and data	116
4.2.1 Model descriptions	116
4.2.2 Data	117
4.2.3 Aggregation of surface data for use in PERIDOT	118
4.3 Calibration of the land surface schemes	120
4.4 Mesoscale modelling	121
4.4.1 Data and model initialisation	121
4.4.2 MESO-NH 1D simulations	122
4.4.3 RAMS 3-D small-scale simulations	128
4.4.4 PERIDOT 3-D large-scale simulations	135

4.4.5	RAMS 3-D large-scale simulations - The effect of the Andes Mountains on the atmosphere over Rondônia	138
4.5	Discussion and conclusions	142
5	Implications for design of the LBA mesoscale field experiments	145
5.1	Introduction	145
5.2	1-D site based measurements	145
5.3	Boundary layer and mesoscale measurements	146
5.4	Experimental strategy	149
5.5	Surface flux measurements and small hydrological catchments in LBA	151
5.6	Land cover change mapping	151
5.7	Spatial distribution of LBA measurement sites	153
6	Planning and coordination activities	155
6.1	LBA planning activities	155
6.2	European co-ordination	156
6.3	Collaboration with Brazilian and other institutions	156
	References	159

### *Attachments*

1	ABRACOS electronic data base to which completion the current project contributed. Examples of data pages for micrometeorology and soil moisture. The data are in the public domain.	169
2	Pre-LBA data set initiative to which the current project contributed. The data are also included on a CD-ROM, which is being produced with contribution of the current project and under the auspices of the IGBP-BAHC and WCRP-GEWEX/ISLSCP.	185
3	The soil and natural vegetation categories obtained from the RADAMBRASIL (1978, 1979) Porto Velho and Guapore maps. For each soil and vegetation class, the measured median proportion of clay and sand (%) and estimated vegetation height (m) respectively, are indicated	191
4	Background note on European involvement in LBA	205

## Summary of the main results

(CEC-Environment & Climate Programme Project PL-931938 (CABARE); contract EV5V-CT94-0456)

### Introduction

The aim of the current project was to identify gaps in our current understanding of the interaction of tropical rainforest in Amazonia with the atmosphere. Identifying these gaps will then lead to a well designed and focused programme of experiments and field work for the Large Scale Biosphere Atmosphere Experiment in Amazonia (LBA). The leading two questions to be addressed by the land surface - atmosphere mesoscale experiment of LBA are the following: what are the mesoscale mechanisms by which differences in surface characteristics translate into large scale weather anomalies and what is the role of dry and moist convection in transferring energy and how will it change with different land use patterns?

The availability and use of existing data, such as that from ABRACOS and the Rondônia Boundary Layer Experiment was essential to the success of this project. In essence the project concentrated on three areas: ongoing collection of field data, mesoscale and 1-D modelling, and mapping of land cover and land cover change by remote sensing.

### Main results of the modelling programme and the implications for experimental design:

#### *a) SVAT (1-D) modelling and site based measurements*

Using the method of Culf and Gash to estimate incoming longwave radiation appears to work well in the SVAT models. However, for high net radiation the scatter in the results appears to be less than for lower values. For low values of net radiation the importance of simulating the surface temperature correctly becomes more important. Accurate measurements of surface temperature are therefore needed to reduce the number of degrees of freedom in the calibration of the SVAT models and as a further check on their performance.

All SVAT models applied in the current project are able to reproduce the latent heat fluxes for forest under both dry and wet conditions. This is in part due to the fact that there has been no observed water stress for forest in the available data, and this has not therefore been included as a stress function in the surface conductance models for the forest. During the wet season the water table at Reserva Jaru forest is within 2.0 m of the soil surface and this can considerably influence the soil moisture profile. For detailed soil moisture modelling a knowledge of the ground water level (GWL) is important and accurate measurements in LBA are therefore needed.

Although the soil heat flux beneath forest is a relatively small part of the energy balance, the canopy storage for a rainforest is significant and can be of similar magnitude to the sensible heat flux. In canopy measurements of temperature are therefore required to estimate this component.

The SVAT inter-comparison study carried out in the current project highlights the need, particularly for pasture, to make adequate predictions of soil moisture, and more specifically moisture stress in the surface conductance model. This goes alongside the need for accurate measurements of those parameters that describe the soil hydraulic properties. Note that a good estimate of soil moisture and rooting depth is vital for comparison of modelled with observed values. There may be a need to work out a more spatially based soil moisture sampling scheme. A specific measurement programme should be designed in LBA to estimate and parameterise soil hydraulic properties of the Amazonian soils, which show a different hydraulic behaviour compared to temperate soils. Especially needed are a proper estimation of the saturated hydraulic conductivity and measurements of moisture movement and the composition of the soil to generate the thermal properties of the top layer. Other required observations are: the deep (at diurnal damping depth) soil temperature; LAI; and the measurement of the pressure heads at a depth to determine the deep soil moisture fluxes. The rooting depth remains a crucial parameter for both the forest and the pasture.

***b) Mesoscale modelling and boundary layer and mesoscale measurements***

Given the importance of the boundary layer in transferring energy away from the surface into regions where it can be used to sustain convection, the inability of the models to predict the correct boundary layer growth and temperature and humidity structure over pasture is particularly worrisome. This failure of the models inhibits realistic simulations of the effect of regional deforestation on the precipitation, both in the dry and the wet season. Furthermore, it is noteworthy that both the simple slab models as well as the more developed mesoscale models do not perform well over the pasture. Simultaneous measurements of aerosol content and boundary layer structure during the dry season campaign is the most important experimental requirement.

The study area in Rondônia is affected by biomass burning at the end of the dry season, and a large part of the aerosols comprises soots, whose properties may differ significantly from standard continental aerosols. Therefore, future measurements should include a precise characterisation of the aerosols.

Biomass burning generally takes place over pasture areas and new forest land. The fact that the forest boundary layer heating is reasonably well described, suggests that the RJF was sufficiently far away from the burning areas, so as not be significantly affected during the period studied in this project. Nevertheless, the lateral and vertical distribution and spread of aerosols needs to be known to be able to make realistic mesoscale simulations.

In view of the under prediction of boundary layer warming, the turbulence structure over pasture areas also needs further study. An under prediction of the turbulence intensity may, if it affects entrainment at the boundary layer top, contribute to a loss

in heating at the inversion height. The mechanism of this would have to be sought in the interplay between, partly dissolved thermal circulations and the increased non linear contribution to the overall roughness of pasture areas by remaining patches of forests. Momentum transport could well be substantially increased at the edges of the remaining forests. This aspect needs to be further investigated by using a combination of boundary layer, tethered balloon, RASS and Sodar measurements at and around the forest/pasture interfaces. Using the 1D simulations, it has however been shown that an increase of the roughness length does not increase the height of the boundary layer. Low flying flux aircraft will be needed to assess the lateral and vertical variation in momentum, and possibly the sensible heat flux.

The deforestation map used was obtained by a simple forest/non forest classification. In reality, a significant part of the forest stripes may correspond to regrown vegetation. A more accurate classification, perhaps based on radar would be useful to identify these regrowth areas during LBA.

Topography influences the flows at both the large and the meso scale, as shown by the RAMS and PERIDOT simulations. At the meso  $\gamma$  scale a clear channelling effect was simulated. This needs to be taken into account generally when selecting sites and more specifically when setting up balloon stations and automatic weather stations for budget studies and initially, if the locations are chosen, simulations may be performed to assesses the possibility of deriving physically meaningful budgets.

The validation plans for the Tropical Rainfall Measuring Mission (TRMM) play an important role here as the objectives of the LBA mesoscale field campaigns and TRMM validation are very complementary. The TRMM field campaigns need to measure vertical air motion to a high resolution and will require surface and airborne radar, 4 to 5 radio sounding sites with more than 4 soundings per day for the duration of the campaign, and a network of surface raingauges. The radar has a quantitative range of about 150 km; the spatial scale of the required experimental domain should be the 150 km radius circle centred on the radar. Thus, at the larger scale a set-up of 4-5 radiosonde stations (three is the minimum, but some redundancy is required) is needed, complemented by tethered balloons for measuring the surface and lower boundary layer. The importance of these for adequate initialisation and validation of mesoscale models cannot be stressed enough. For the wet season AMC, the soundings should be near the perimeter of the 150 km circle centred on the radar. Preliminary sites of the radar are given in Fig. 1.

TRMM will also involve the NASA ER-2 high altitude aircraft, equipped with Doppler radar, multi-frequency passive microwave sensors, electric field sensors, visible/infrared sensors (and more) for 12-15 flights. The TRMM mission requires overflying major convective clouds and organised mesoscale precipitation systems. The aircraft's most likely base would be Brasilia. Efficient utilisation of the aircraft requires accurate six-hour forecasts from CPTEC of the existence of precipitation systems over the AMC domain.



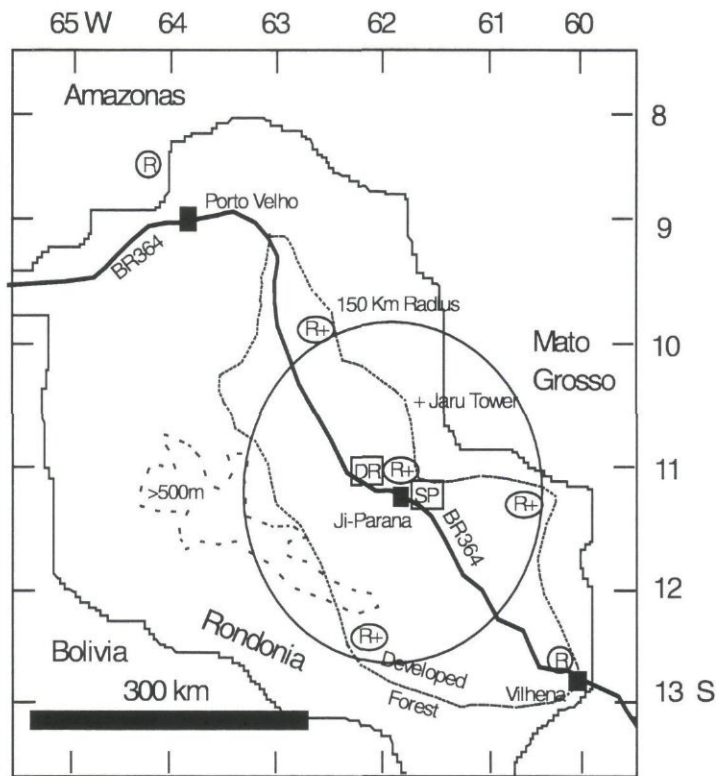


Fig. 1 Possible distribution of certain observing capabilities for LBA/TRMM Atmospheric Mesoscale Campaign (wet season). The candidate site for the S-POL radar (SP) is at Ji-Parana with the 2nd Doppler radar (DR) 40 km to the north west. Augmented rawinsonde launches (R) would take place at the operational sites at Porto Velho and Vilhena. Special rawinsonde sites, supplemented with tethersondes (R+) would be placed near the periphery of the quantitative radar coverage. A 4th peripheral site is highly desirable if practical. The "developed area" is, in fact, partially deforested, while the forested area is largely just that. Not shown are sites for 8 pilot balloons, 30 rain gauges, lightning sensors, 10 automatic weather stations, LIDAR, RASS, SODARS, flux balloon, two pasture towers, and a second forest tower. For reasons of accessibility most facilities will be located in the "developed area".

To estimate rainfall and windspeed US scientists propose bringing NCAR's S-POL radar, a state-of-the-art 10 cm radar with polarisation diversity. A second Doppler radar would be sited 30-50 km from the S-POL. This dual Doppler capability would be used to obtain 3-dimensional wind fields at the convective and meso- scale. The two radars would come in a total of 6-8 standard sea containers. Each requires a site with a clear field of view above half degree elevation for 360 degrees around the site. These radars would be of great use to check the modelled wind and rainfall fields.

At the larger scale the influence of the Andes becomes important as shown by the large scale RAMS runs. Not only is large scale subsidence in the dry season a result from circulations induced by the Andes, the mountain range also generates gravity waves, which may have implications for transport of atmospheric constituents. The subsidence induced by the Andes circulations may be important in suppressing boundary layer growth and convection in the dry season. This calls for the need to improve the 4DDA system of CPTEC with additional sounding locations over the whole LBA domain.

The ability of mesoscale models to simulate wet season conditions in the Rondônia area has not yet been adequately tested, largely because of the lack of observations of the boundary layer. Furthermore, the poor representation of the humidity profiles (e.g. when measured profiles are not used to initialise simulations) is alarming, and could be potentially disastrous for simulations of the wet season. Initial model studies are required to investigate the effect of the surface on boundary layer growth and convection, in particular the effect of the effective aerodynamic roughness or enhanced turbulence of the surface coupled with the rapid recycling of intercepted water.

*c) Experimental strategy*

The experimental strategy of the AMC reflects the deficiencies found in the current mesoscale models. These appear to be in the neglect of aerosols in the radiation and thermal budget equations, the possibility of enhanced turbulence over the pasture areas, and the interaction of the land surface with convective processes. The AMC should aim to provide the data needed to initialise, calibrate and validate the models. The following set-up was proposed and accepted for the *wet season* (Fig. 2).

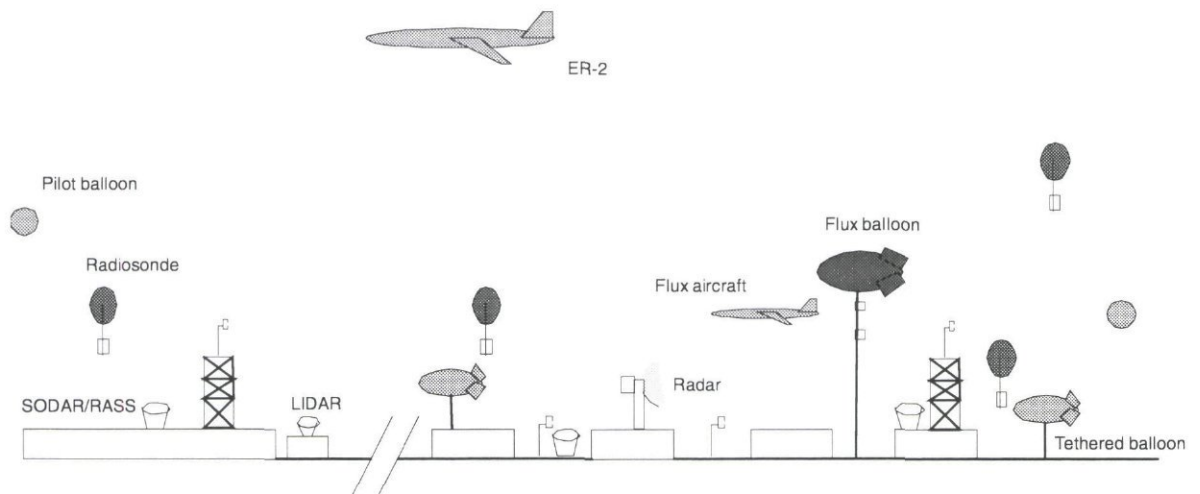


Fig. 2 Schematic of the proposed wet season AMC

To understand the boundary layer dynamics and turbulence of the pasture area, an array of RASS/Sodar systems is needed. Low flying flux aircraft are needed to sample area average flux, and a fixed tethered balloon system is needed to measure fluxes at two heights to sample the time variation of fluxes. Fully equipped tower sites are needed at undisturbed forest, at pasture and above the strips in pasture and forest. A Doppler lidar system should be available at the boundary of forest and pasture. Sun photometers are needed to sample biogenic aerosols. A quantitative Doppler radar such as the S-POL is needed for TRMM rainfall validation, with a second Doppler radar 30 - 50 km distant to provide 3-D wind fields. The vertical

velocities from these wind fields will be used to validate TRMM's algorithms for separation of convective from stratiform rainfall. This needs complementing with a network of tipping bucket rainfall gauges. For TRMM purposes the ER-2 will be available, a microphysics plane is also needed. Lightning detectors (3) are needed to correlate rainfall with lightning. Table 1 gives the optimum instrument deployment; an assessment of the likelihood of obtaining the instruments for LBA is also given.

*Table 1 The optimum instrument deployment and an assessment of the likelihood of obtaining the instruments for LBA*

Instrument	No	Avail- ability	Comments
Dual Doppler radar	2	+	available wet season only
Tower site grass	2	+	
Tower site forest	2	+	
Radiosonde station	4/5	+	2 exist in Brazil
Tethersonde	4/5	+	systems need upgrading with larger balloons
Flux balloon	1	+	
RASS	3	+	or 1 RASS & 2 SODARS
LIDAR	1	+/-	primarily for wind (CNRM not available 1999)
Raingauges	30	+	
Sun photometers	3/4	+	
Surface AWS	10	+/-	number includes tower flux sites
Pilot balloons	8	+	
Drop-size disdrometer	1	+	wet season only
Low flying flux aircraft	2	-	preference for Long E-Z, INPE a possibility
Lightning sensors	3	+/-	wet season only (but once installed should remain for many years)
ER-2	1	+	wet season only
cloud microphysics (Learjet)	1	+/-	wet season only
DC-8 with LIDAR	1	+	wet season only
NOAA P-3/Electra	1	-	wet season only
NCAR Aster surface flux network	1	-	

A *dry season* campaign will need a similar set-up (except for the measurements required specifically for rainfall detection and TRMM). The AMC dry season campaign should address the issues related to the failure of the models to predict the observed boundary layer structure, in an effort to understand what is happening at the scale of the pasture/forest strips. This information can then lead to new parameterizations where the effects of mesoscale flows and circulation at the scale of 20-200 km can be studied. In the dry season campaign aerosol detection from aircraft will be critical.

The timing of the wet and dry season campaigns depends to a large extent on the other components of LBA. It is essential that the wet season campaign links up with the TRMM validation effort. The timing of funding constrains the choice - a wet season campaign in Jan-February 1999 and a dry season campaign in July-August 2000 is the current plan.

## **Surface fluxes and small scale hydrology in LBA**

The evaporation from the pasture, both measured and modelled, is systematically less than that from forest. Over the sites tested in the current project the average total difference is 323 mm per year. During the wet season this will mainly be the result of the higher albedo of the grass reflecting more solar energy and resulting in less net radiation available for evaporation. No reduction in dry season evaporation from the forest has been observed in the measurements *available so far*. More long term measurements at several LBA-sites, covering wider range of the climatic and soil conditions are needed to support or reject this conclusion.

The modelled reduction in pasture evaporation during the dry season is smaller than expected but the estimated amounts of water extracted from the soil during the dry season are consistent with the variations in soil moisture observed. Additional measurements at several pasture sites covering wider a variety of climatic and soil regimes need to be done in LBA to assess the susceptibility of grasslands to the drought stress.

The differences in evaporation between primary forest and pasture will have an effect on surface runoff and river flows which will be relatively larger in the lower rainfall areas, such around Ji-Paraná and Marabá. In these areas the use of long term rainfall records and the estimated average reduction in evaporation (323 mm in present study) results in predicted increases in runoff of 48 and 41 per cent respectively. These preliminary estimates do not allow for any decrease in rainfall which might accompany the deforestation. In Central Amazon (Manaus) the predicted increase in runoff was 29%. These increases are large and it should certainly be possible to observe such changes by using conventional catchment experiment techniques which are planned in hydrology part of LBA.

LBA calls for measurements over a sample of five land covers associated with deforestation and re-growth: primary forest, freshly burnt and established pastures, and two types of re-growth forests. In terms of surface flux measurements the current modelling results show that this basic stratification would be adequate.

## **Land cover change mapping**

The current project has shown a crucial importance of a *combined* strategy to map and monitor the land surface and its change in the Amazon basin. Ideally, this combined strategy would employ geographical information comprising both existing (paper) maps for the natural landscape structures, the multi-resolution satellite data for current alterations and ground truth collection for verification of the inversion algorithm.

Optical satellite data have been shown to be highly accurate and valuable for cartography of tropical areas. Nevertheless monitoring of these areas is somewhat impeded by the poor availability of optical data, due to weather conditions (cloudiness). Furthermore optical data have limited use in estimating biomass.

Biomass estimation in the near infrared is possible but works only in the earliest stages of regrowth, due to rapidly increasing leaf biomass and the resulting saturation in the wavelength. Also, optical data do not detect sub-canopy floodings, a land-cover class high of great interest in climate modelling, due to its functions as a CO<sub>2</sub> source.

Radar sensors (SAR) have a different information quality and content depending on the frequencies and polarisations employed. C-band SAR, as available from ERS-1/ERS-2 and SIR-C, is satisfactory of forest/non-forest discrimination. ERS-1/2 data can be combined to multi-seasonal or multi-temporal products to further enhance and deepen information content. C-band data show stages of pasture degradation and different biomass levels of pastures in HV, VV and HH polarisations. Furthermore ERS-1/2 data are well suited for monitoring areas because of their 35 days repetition rate in the tropics.

The combination of optical and SAR data also gives good results in mapping land use patterns. In the current project a combined product of TM and ERS-1 is presented and classified. However, an improvement in the automatic classification could not be achieved by this method. More classes could not be detected compared to an optical data set alone. Nevertheless, the visual interpretability was highly improved by imbedding the relief information from the SAR data in the combination product.

In L-band SAR discrimination of forest and non-forest classes is especially good. L-HH is sensitive to sub-canopy floodings which are clearly discriminated. The Japanese JERS sensor delivers good results in detecting and mapping these areas. The correlation of biomass in HV polarisations is high and increases when data of two frequencies are used. The saturation level is about 100 to 150 tons/hectare. Thus, early to middle stages of regeneration areas not older than ten years are detectable. Correlation in L-HH to biomass is not that high, due to double bounce scattering on tree trunks. Different pasture stages are detectable. The use of biomass ratios improves the separability of pasture classes.

Using SIR-C/X-SAR data, discrimination of the following classes has been shown to be feasible in the current project: primary rainforest; sub-canopy flooding (flooded rainforest along rivers); pastures; degraded pastures (< 40% ground cover); overgrown pastures (with trees, palms or dead trunks, up to 10% ground cover); initial regrowth (1 - 4 years of age); intermediate re-growth (5 - 10 years); bare soils (dirt roads, badlands); and fresh clear-cuts (newly burned areas without vegetation cover).

The high quality and high resolution land cover and land use data are crucial to the success of almost every single study within the LBA. Each of the classification methods, either satellite or map-based, has its limitations. It is therefore a strong recommendation of the current project to focus within LBA on a combined strategy to classify the land cover and its change, rather than on one based on single, isolated data sources.

## Spatial distribution of LBA-measurement sites

The satellite data, vegetation maps and other model-derived products and a regression tree technique presented in current project may be applied to the selection of regions that should be represented with LBA- field measurement sites. Moreover the status of regions with existing field sites can be determined, perhaps with a view to augmenting certain types of measurements.

The existing field study sites that have been identified as potential LBA sites have been compared with the biophysical stratification of the Amazon basin. It is clear that an additional site in the high productivity region of Guyana (red) would be useful, possibly midway between Santarem and Boa Vista since the currently proposed site on Brazilian-Venezuelan border appears to be in a vegetation transition area. The transition from evergreen to semi-deciduous forest class (pink, yellow, light green) in the south west of the basin in Rondônia - Santa Cruz was distinct from that in Pará and should also be sampled; NE Santa Cruz province in Bolivia would be a possible location. The west Brazilian Amazon site near Tabatinga is also in an area of vegetation transition and may be better placed near Iquitos, Peru.

LBA has a major interest in the sustainability of various types of forest conversion, such as total clearance, selective logging, and traditional shifting agriculture. These human-induced transformations have affected a relatively small proportion of the total basin area at the present time and seem only to have influenced the current RTA classifications in areas of concentrated land conversion, such as in central Rondônia. Thus stratification for measurement design purposes at smaller scales (meso-scale) should be undertaken next at a more local scale using higher resolution data sets, such as Landsat.

The need to stratify at multiple spatial scales is inevitable when dealing with such a large area as the entire Amazon basin. The stratifications presented in the current project used  $8 \times 8$  km data at the highest resolution, but several data sets were at  $1^\circ \times 1^\circ$ , hence regional differences have been emphasized, not the variation at finer spatial resolution. Equatorial lowland forest is well known to exhibit much stronger  $\alpha$ -diversity than  $\beta$ -diversity, unlike temperate and arid regions. Thus much of the fine-scale variation may be lost at the scales explored here. The stratifications presented here are relevant to the  $1^\circ$  scale and they indicate which entire  $1^\circ$  area would give the optimal sampling of the basin-wide variation. Further stratification within each selected  $1^\circ$ , perhaps using similar techniques, is necessary to determine the optimal location of individual, point, field measurement locations.

These finer scale stratifications should be explicitly linked with the coarser, basin scale to ensure continuity in scaling up. At the basin scale, the RTA identified annual and monthly minimum PAR and minimum rain fall, and the number of months with less than 150 mm of rain fall as critical variables that determine  $R_n$ . These same variables are identified as critical for LE, although the first division of LE was on annual rainfall. Minimum NDVI, annual PAR, and the number of months with less than 150 mm rain fall were the most important variables in the tree model of NPP. Annual NDVI and rainfall were also important in the dryer, low NPP areas, while the

monthly minimums of NDVI, PAR and temperature were important in the more humid, high NP areas. The field measurement design should therefore emphasize measurement of these variables at the  $1^{\circ} \times 1^{\circ}$  scale.

The stratifications of the Amazon presented in current project were almost entirely based on climate data and, consequently, there were many seemingly obvious surface and vegetation features which have not been captured. Some vegetation classes which we would have liked to be able to distinguish include liana forests, particularly in Pará and Bolivia, bamboo forests, especially in southeastern Peru and Acre, palm swamps, and white sand vegetation such as that of the upper Rio Negro. There are no maps available which delineate these vegetation formations. Furthermore, all of these formations probably exist as mosaics with dense evergreen forest, and thus may not significantly influence bioclimate at the scale of the data used in this study. Stratification of only the Rondônia window did not successfully represent such classes as liana forest, seasonally inundated forest and palm swamp which are known to cover large portions of that area.

This is more an issue of data scale and availability rather than a failure of the RTA technique. RTA could be undertaken using finer resolution data, such as 1 km AVHRR data.

## **LBA - planning and coordination activities**

The design of LBA has evolved over a series of workshops and meetings held over the past three years. The results of the current project, together with the experience of the current project participants in organizing international experiments makes this project uniquely placed to play a major role in establishing LBA. Current project participants have been actively involved in the design, planning and preparation activities, not just by organizing and attending meetings, but also in the writing and preparation of the documentation.

### ***European co-ordination***

One objective of the project was to prepare a co-ordinated proposal for the European participation in LBA. Work towards this objective was initially concentrated on a co-ordinated bid in the European Union Framework IV Environment and Climate programme and following a meeting at the Staring Centre, Wageningen in March 1995 a proposal with 21 participants was prepared and submitted. This bid was not successful. Subsequently, two new projects have been prepared (LBA-EUSTACH and LBA-ERACO/ENRICH) and were submitted to the EU-DG XII Environment and Climate Programme in January 1997. The LBA-EUSTACH and ERACO projects build to a large extent on the results of the current project. Both projects have been proposed by the European Commission for funding.

Independent of these activities, the co-ordinator and the collaborators in the current project have been leading an effort to prepare European contribution to the main phase of LBA (over 1998 - 2002), which is to be supported by several EU - Directorates. In the course of the current project, a European LBA - co-ordination

office has been established at the SC-DLO in Wageningen, the Netherlands. A European LBA co-ordination workshop, supported by DG XI and DG XII was organized in June 1997 in Wageningen and attended by more than 150 participants from Europe, South America and USA.

#### ***Collaboration with Brazilian and other institutions***

Though the current project did not include any formal non-European partners or exchange of funds outside Europe, collaboration with Brazilian institutions was a major aspect of the present project. The help of Brazilian scientists contributed to making the different studies carried out in this project successful. All aspects of the present scientific work have been carried out in collaboration with Brazilian institutions: field measurements, data collection, and modeling.

The ABRACOS measurement network was operated as a continuing collaboration between IH and CPTEC/INPE, INPA, INCRA and the Federal Universities of Pará and Rondônia. The new site near Brasília is operated in collaboration with the National University of Brasília. The Brazilian RBLE III experiment provided the opportunity to combine the efforts of both European and Brazilian teams (from several institutions, including INPE, CTA, the University of São Paulo (USP), the Federal Universities of Alagoas and Pará and FUNCEME) during the field campaign.

The physiographic data collection (topography, soils, vegetation) was also a common effort: INPE/CPTEC provided Landsat data and INPE/DSM provided METEOSAT data and helped in classifying the satellite data and interpreting the RADAMBRASIL maps. This latter work was an opportunity for both European and Brazilian teams involved to gain experience in the use of geographical information systems.

USP and CPTEC/INPE joined EU teams in the modeling effort. Its help was fundamental since they have a long term experience in mesoscale modeling over Rondônia.

Based on a long term co-operation in previous projects (e.g. HAPEX-Sahel), University of Maryland, College Park, MD, USA collaborated with DLR and SC-DLO in producing Biophysical stratification of the Amazon basin (Section 2.4).

Establishing the above collaboration networks is a crucial step towards successful implementation of the future European LBA-projects.



## 1 Introduction

The consequences of the expansive growth of global population in humid tropical areas (between latitudes 23° North and 23° South) are already being experienced in the form of deterioration of the urban environment and devastation of the forest environment. Recent data show that a vast area of the Brazilian Amazon has been changed from forest into the pasture and agricultural land. Data from other rainforests in southeast Asia show a similar trend. A directly associated, and more complex, problem is the impact of deforestation on the local and global climate. The Amazon basin, because of its size, equatorial position and vast amount of biomass is a major heat and moisture source as well as carbon sink for the general circulation of the global atmosphere. It is a region where the processes enhancing global climate change are already happening parallel with the environmental impacts.

Studies with General Circulation Models (GCMs) have suggested that large scale changes in land surface cover may affect the regional climate (Rowntree, 1991). More specifically Nobre et al. (1991) and Lean and Rowntree (1993) have shown that large scale deforestation may lead to reduced rainfall and evaporation over the Amazon basin, and that a hotter, dryer climate is the likely outcome of a prolonged deforestation at its current rate. These suggested impacts, combined with a likely loss in biodiversity and effects on the global and regional carbon balance, make an interdisciplinary study into the combined hydrology, meteorology and ecology of the area a necessity.

Recent reviews of GCM deforestation studies for the Amazon basin suggest that evaporation and rainfall may fall by about 20% and 30% respectively with deforestation and that the air temperature can rise by as much 2 °C (Shuttleworth et al., 1991). Sensitivity studies with these models have shown that the inclusion of realistic descriptions of the land surface (forest/cleared forest) atmosphere interactions is critical to these results and that improved, calibrated descriptions provide a more realistic simulation of present day climate (Lean and Rowntree, 1993). The Lean and Rowntree (1993) study, for instance, shows a reduction in rainfall by 14% and evaporation by 24% when they incorporated improved descriptions of rainfall interception (Dolman and Gregory, 1992) in their GCM. Earlier studies with the same GCM (Lean and Warrilow, 1989), but with an "older" version of the land surface scheme had suggested reductions of 20% and 27% respectively. These reductions are accompanied by changes in circulation patterns, not only in the area which was deforested, but also outside this area. This results in a highly non-uniform pattern of generally rainfall reduction and occasional rainfall increases. A similar result was obtained by Henderson-Sellers et al. (1993) who, contrary to other studies, did not find an increase in surface air temperature.

Clearly these effects and the differences in model predictions need to be understood, both regionally and globally, if realistic predictions of the effects of deforestation on the water balance of the Amazon can be predicted. This implies that not only the role of regional recycling of moisture in the Amazon basin needs to be studied in more

detail, but that these studies need to be closely interlinked with studies of large scale moisture advection in the basin.

The broad objectives of mounting a large scale field experiment centred around the Amazon basin, the Large Scale Atmosphere Biosphere Experiment in Amazonia (LBA), are:

- To improve our understanding of the functioning of Amazonia as a regional entity.
- To improve our understanding of how changes in land use and climate may affect the biological, chemical and physical functions of Amazonia, including the sustainability of development in the region and the influence of Amazonia on global climate.

The overall research strategy of LBA (Nobre et al., 1996) consists of a large scale component which would concentrate on the transports of energy, heat, moisture and trace gas constituents over the entire Amazon basin, with an embedded mesoscale and local scale set of process studies. The LBA physical climate component should provide detailed information to support the formulation and validation of hydroclimatological, ecological and biogeochemical models, on the micro-, meso- and larger scales.

The main questions of the physical climate component of LBA are :

- What are the surface and meteorological controls on the fluxes of energy and water, and how do they vary both in space, over Amazonia, and in time, between seasons and from year to year, to affect the regional budgets of energy and water?
- What are the mesoscale mechanisms by which differences in surface characteristics translate into large-scale weather anomalies?

*The set-up, and experimental strategy needed to address these questions is the prime aim of the present CEC research project.*

## **1.1 Background of the research strategy for the current project**

### *The use of integrated mesoscale modelling to design large scale field experiments*

Mesoscale modelling of atmospheric and hydrological processes has proved to be a powerful and convenient tool for analysing and integrating experimental data obtained in large scale field experiments (e.g. Bougeault et al, 1991a,b & Noilhan et al., 1991). At present a point is reached where mesoscale models with advanced land surface atmosphere parameterizations should be used in the design of these experiments. In this way unique information about the influence of the variability of land surface characteristics on the spatial distribution of surface fluxes and on the development of the boundary layer at a variety of spatial scales can be obtained prior to the experiment.

This has direct consequences for the experimental design. A proper design of a land surface atmosphere experiment is critical to the success of these experiments in providing advanced aggregation algorithms for use in General Circulation Models. Experience with both EFEDA (Bolle et al, 1993) and HAPEX-Sahel (Goutorbe et al.,

1993) as well as the predecessor HAPEX-MOBILHY (Andre et al., 1988) has shown that the design of the network of surface flux stations, synoptic stations, soil moisture and boundary layer sounding stations as well as the aircraft flight patterns is essential in achieving a realistic and complete description of land surface heterogeneity on the scale of a typical GCM grid box. However, in none of the previous experiments modelling played an important role during the experimental design phase.

#### ***Role of Soil - Vegetation- Atmosphere- Transfer schemes (SVATs) calibration in improved GCM experiments***

SVAT models, describing the exchange of heat, momentum and CO<sub>2</sub> between the land surface and the lower atmosphere present the lowest vertical component of the mesoscale models and of the GCMs. The quality of future GCM experiments of Amazonia deforestation depends strongly upon good calibration of SVATs (Nobre et al., 1991). To test the physical validity of SVATs, intensive process studies are necessary.

Currently a large variety of SVAT schemes is used in GCMs and in the mesoscale models leading to considerable discrepancies between the simulation results. A number of intercomparison studies, such as PILPS (Project for Intercomparison of Land surface Parameterization Schemes), has been recently set up. These studies are driven by the knowledge about the sensitivity of the mesoscale models and of the GCMs to the parameterization of the SVATs. However, sensitivity of the SVATs to their parameters has up to now only occasionally been addressed in a systematic way (e.g. Dickinson et al. 1991).

The ABRACOS study (Wright et al., 1992) has set up a network of climate stations over the basin to provide essential data for calibration and validation of land surface schemes used in GCM's deforestation experiments. Several physically based submodels of land surface processes were parameterized and calibrated with these data (Wright et al., 1992, Bastable et al., 1993). Some data were already used to improve land surface parameterization in GCM's (Lean and Rowntree, 1993). In principle a very large number of parameters may be required to achieve adequate realism in the treatment of land-surface processes and there is not necessarily a unique set of parameters leading to correct results. The availability of the long term data of the ABRACOS network in combination with some recent SVAT developments offered in the context of the current CEC project a new prospect in addressing remaining deficiencies of SVAT-schemes and in guiding the future field efforts within LBA.

#### ***Role of the airborne and satellite remote sensing***

The remote sensing science was from the beginning one of the driving moments behind the large scale land-surface-atmosphere interaction experiments (Sellers et al., 1988, Andre et al., 1988, Bolle et al., 1993, Goutorbe et al. 1993) offering a unique possibility to collect the data for algorithm validations for scaling studies. The remotely sensed data played already a major role in the planning and design of the large scale experiments like EFEDA and HAPEX-Sahel. Information about the vegetation dynamics, in both space and time, obtainable through the NDVI-analysis (AVHRR) and the land cover maps obtained from the SPOT-data proved to be

inevitable for the final distribution of the individual measurements within the area of interest.

Methods to estimate surface evaporation and energy fluxes over large areas have been under development in parallel (e.g. Bastiaanssen et al. 1993, Jochum et al., 1993). Very important are the developments in using the remotely sensed data as driving variables for SVAT models (Sellers et al, 1992). All those aspects are expected to play an important role during the design and execution phases of LBA. Remote sensing will be used to provide information on surface radiation fluxes, precipitation, surface state (FPAR, leaf area index, photosynthetic capacity, minimum canopy conductance, biomass) and to identify the major physiographical land use and land cover types or strata within the Amazon basin.

All of the algorithms necessary to perform the inversion procedures to obtain these information require a rigorous feasibility test for the specific conditions of the Amazon basin using integrated sets of satellite, airborne and surface data. In the context of the current CEC project, the analysis focused on (i) use of the remote sensing radar data for mapping the tropical rainforest characteristics and their changes following deforestation, (ii) extensive land cover classification based on the satellite imagery, vegetation maps and ground survey in order to derive surface parameter fields for mesoscale meteorological models, (iii) assembling large sets of remotely sensed and mapped data to stratify the Amazon basin in terms of distribution of representative biophysical units.

## 1.2 Objectives of the current project

The main objectives of the current project were:

- I To use a nested mesoscale modelling approach together with calibration and sensitivity analysis of the SVAT models for *existing data*, and in combination with first estimates of areal distribution of land surface characteristics from airborne and satellite data, to improve our understanding of the main processes controlling the exchange of energy, water and momentum of the Amazon basin.
- II Based on this analysis, to develop a guidance to the design of the LBA mesoscale field experiment to be executed in 1999-2000. This includes ground flux and soil moisture measurements, vegetation measurements, boundary layer sounding and the aircraft measurements.
- III To continue the operation of the existing network of ABRACOS climate and soil stations and to investigate extending and enhancement possibilities of this network to meet the needs of LBA.
- IV To prepare a co-ordinated European contribution to the main field phase of LBA, stemming from the existing European network of the institutions involved in the land-surface processes studies.

This report describes the results obtained in the project. First the existing data is analysed and inventories of available data are presented. The main core of the project consisted of modelling including one-dimensional SVAT modelling and complex 3-D meso scale modelling. The results obtained using these models are presented in

Chapters 3 and 4. Consequences of the modelling for the experimental design are given in Chapter 5. The final chapter deals with the planning and co-ordination activities undertaken to implement LBA from a European perspective. One of the aims of the project also was to set up collaborative arrangements between European and Brazilian groups and institutions with a view to start joint work leading to the implementation of LBA; these collaborations are also briefly described in Chapter 6.

## 2 Analysis of existing data

### 2.1 Climate and soil moisture data: extension of ABRACOS

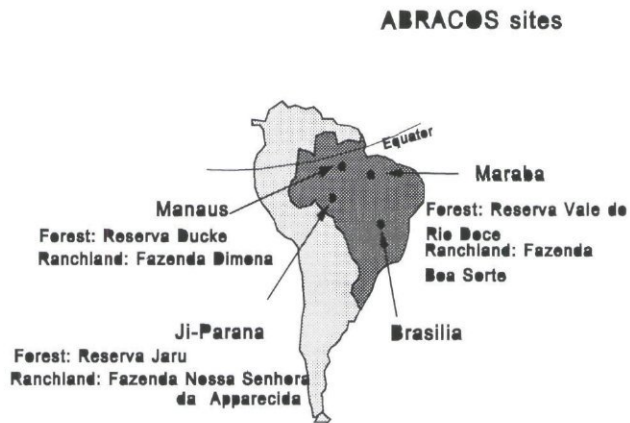


Fig. 2.1 ABRACOS observational network

ABRACOS (Anglo-Brazilian Amazonian Climate Observational Study) was a binational collaboration between Brazil and the United Kingdom with the objective of improving climate model predictions of the climatic effects of Amazonian deforestation (Gash et al., 1996). As part of ABRACOS a network of climate and soil moisture stations were established in Amazonia, with three pairs of forest and pasture climate and soil moisture monitoring stations positioned across Amazonia (see Fig. 2.1). An additional station was located in the city of Manaus in central Amazonia. Data collection continued under the present project from the three pairs of stations, but the instrumentation from the city station was redeployed to a new forest site near to Manaus. This site will be an LBA continuous flux measuring site, and flux measurements have already commenced in a collaborative study between IH, INPA, INPE, and the University of Edinburgh. This study has demonstrated the feasibility of continuous eddy correlation measurements in the rain forest environment. Analysis of the experience of this project leads to the following recommendations:

- a) the eddy correlation system can be run from solar power. Solar power should be used as it is more reliable than generators and does not produce CO<sub>2</sub> pollution which can affect the measurements.
- b) at least one complete set of spare parts is essential; the infra-red gas analyser is the least reliable component and should ideally have two spares.
- c) the instrumentation must be protected from lightning
- d) transmission of the data by direct or satellite radio link, to allow early identification and repair of faults, is advisable.

LBA covers the whole of the Amazon Basin including the headwaters to the south which are in the savannah, or cerrado, region north of Brasilia. An additional climate and soil station was therefore installed near Brasilia, where it is being run by the National University of Brasilia.

### 2.1.1 The ABRACOS database

During ABRACOS detailed measurements of the surface radiation and energy balances were made during seven micrometeorological campaigns in Amazonian pasture and forest (see Table 2.1). These data were central to the strategy of the present project of using calibrated SVAT and meso-scale models to investigate the design of LBA. Some model parameters such as albedo or aerodynamic roughness length can be applied directly to all models; these have been collated by Wright et al. (1996). Other parameters such as surface conductance are model-specific and must be derived by fitting each individual model to the data. Within the current project, the data were assembled into a database which was distributed to all the project participants and is now also available in the public domain. Copies of the database are available by electronic transfer from the Institute of Hydrology (<http://www.nwl.ac.uk/ih>) or CPTEC (<http://yabae.cptec.inpe.br/lba>); for more details see Attachment 1. The data are also included on a CD-ROM of data relevant to LBA, which is being produced with contribution of the current project and under the auspices of the IGBP-BAHC and WCRP- GEWEX/ISLSCP (for details see Attachment 2).

### 2.1.2 Estimates of annual evaporation from forest and pasture

Automatic weather station data are available from the three pairs of ABRACOS sites in Ji-Paraná, Rondonia; Manaus, in Central Amazonia and Marabá in Pará, in eastern Amazonia. By using these datasets in combination with an appropriate SVAT, evaporation can be estimated over sufficiently long periods to be useful for planning the components of LBA which operate on the hydrological timescale of months up to a year.

Table 2.1 Overview ABRACOS data set

Mission number	Site name	Year	Duration (days)	Start date	End date
Pasture sites					
1	Dimona	1990	45	18 Sept	2 Nov
2	Dimona	1991	74	29 Jun	11 Sept
3	Nossa Senhora	1992	62	6 Aug	7 Oct
4/5	Nossa Senhora	1993	119	31 Mar	28 July
6	Boa Sorte	1993	21	5 Oct	26 Oct
7	Nossa Senhora	1994	13	11 Aug	24 Aug
Forest sites					
3	Jaru	1992	58	8 Aug	5 Oct
4/5	Jaru	1992	113	4 Apr	26 July
6	Vale	1993	9	18 Oct	27 Oct
7	Jaru	1994	12	13 Aug	25 Aug

#### *Forest evaporation*

The evaporation from the three forest sites was estimated using a simple single-source SVAT comprising a Penman-Monteith big leaf model for transpiration and a Rutter model for estimating interception loss. The model is similar to that used by Shuttleworth (1988) except that the simple time of day surface conductance model used by Shuttleworth has been replaced by a Jarvis-Stewart type. For Reserva Ducke

(Manaus) the surface conductance model parameters derived by Dolman et al. (1990) and the interception parameters derived by Lloyd et al. (1988) have been used. At the Reserva Jaru site (Ji-Paraná) the values of the surface conductance model parameters were taken from Wright et al (1996a). As only very limited measurements of transpiration were made at the Reserva Vale site no surface conductance model parameters were derived and the values derived for Reserva Jaru have been used. The interception parameters derived by Ubarana (1996) have been used at the Jaru and Vale forest sites.

The dependence of forest transpiration on soil moisture was not sufficient to allow either Dolman et al. (1990) or Wright et al. (1996a) to optimise the relevant surface conductance parameters and the estimates of evaporation for the forest sites therefore do not contain a soil moisture dependence.

The evaporation has been estimated as the mean for each month by averaging the available estimates for each month over the two to three year record of data. For Reserva Ducke the data extends over three years and for the other sites two years. Small gaps in the data have been covered by interpolation.

The results of the model estimates for the individual sites are shown in Figure 2.2 and compared in Figure 2.3. There is little seasonal variation in forest evaporation, with the increased interception loss in the rainy season compensating for the reduced transpiration resulting from more clouds and greater periods of wet canopy. The average evaporation is generally between 3 and 4 mm per day, with the Reserva Ducke site being predicted to be systematically less. The annual totals and equivalent daily average are given in Table 2.2

*Table 2.2 The annual totals and equivalent daily average evaporation at three primary forest sites in the Amazon*

Forest site	Estimated total annual evaporation (mm)	Equivalent daily evaporation (mm per day)	Measured annual rainfall (mm)
Reserva Jaru	1384	3.8	2169
Reserva Ducke	1155	3.2	1931
Reserva Vale	1372	3.8	1364

### ***Pasture evaporation***

The evaporation from the three pasture sites was estimated using the MOSES-2S model described in Chapter 3. The parameters were taken from the table given by Wright et al. (1996b), with the exception of the soil saturated conductivity for the Fazenda Dimona site. The value of this parameter given by Wright et al. forces the soil to drain unrealistically quickly, creating problems of model stability. The standard value for a fine soil has therefore been used in this case. A rooting depth of 1 m has been assumed in all cases.



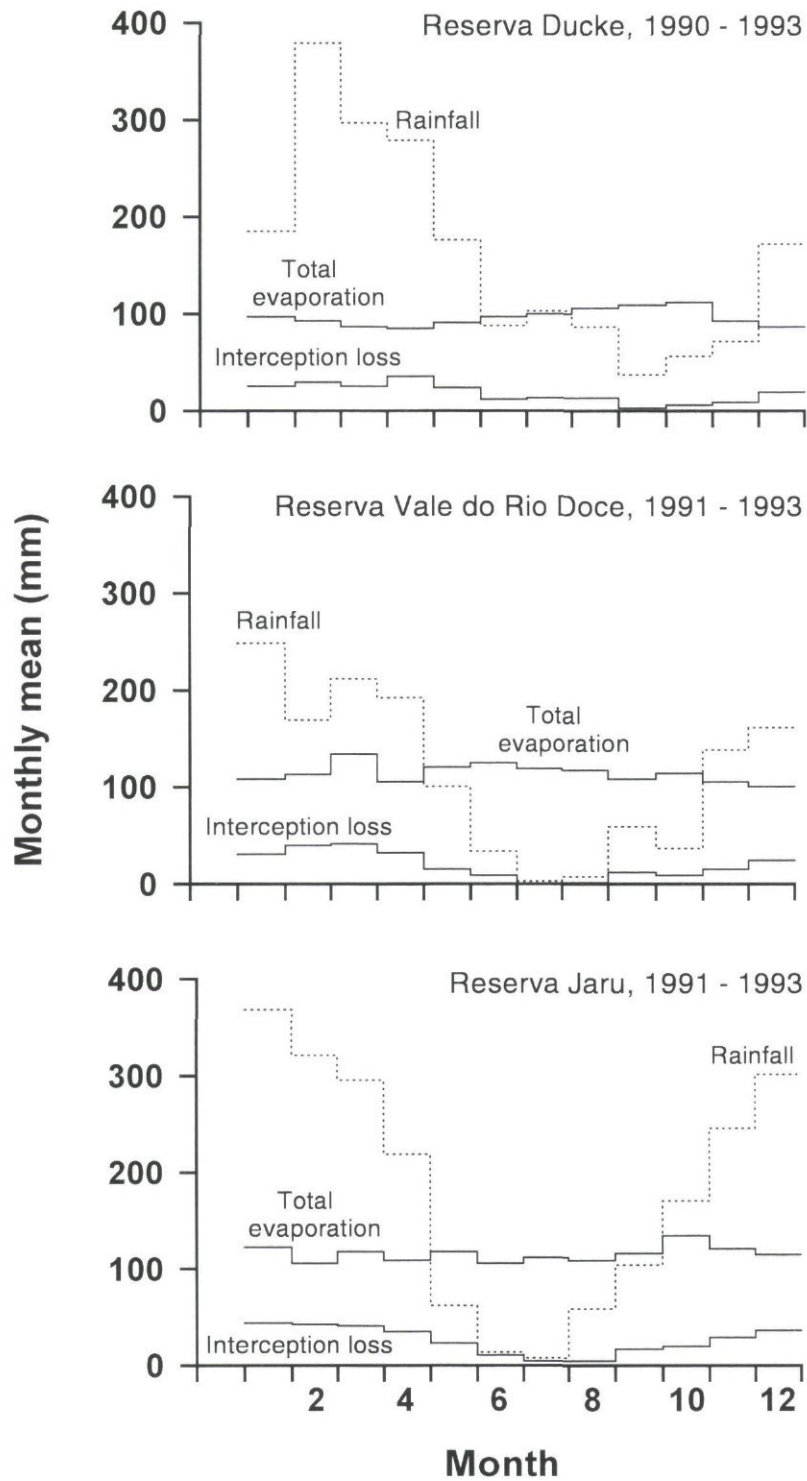


Fig. 2.2 Estimates of total evaporation and interception loss for three forest sites using a Penman-Monteith "big leaf" and Rutter model

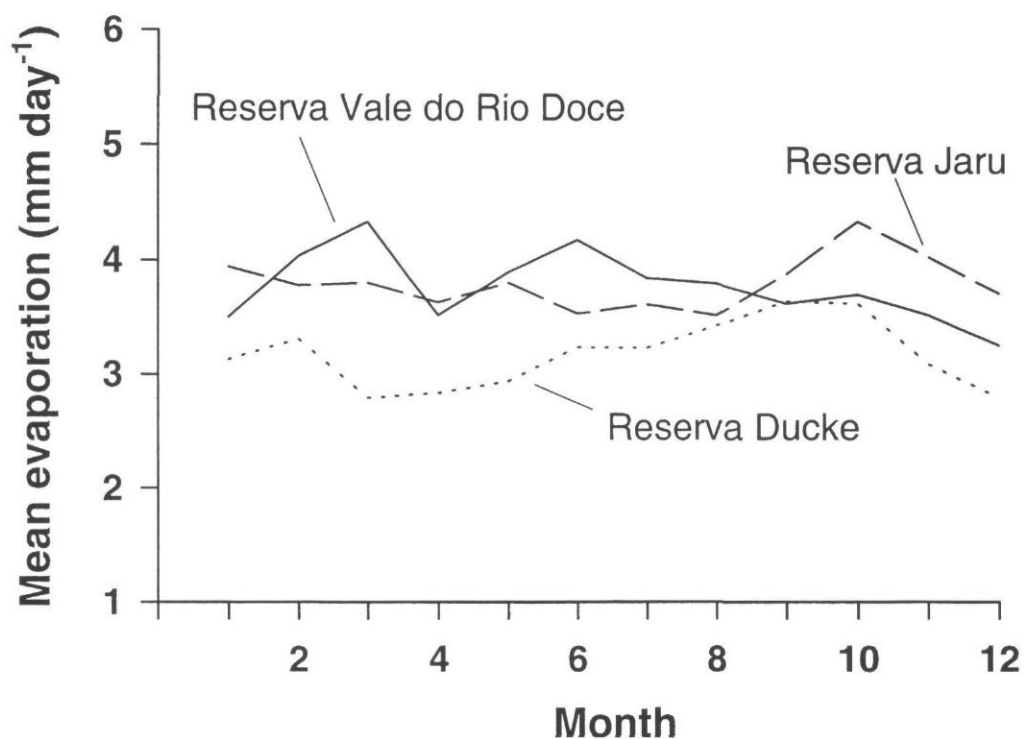


Fig. 2.3 Comparison of estimated evaporation for three forest sites

The mean monthly evaporations have been calculated in the same way as for the forest sites. The results are presented in Figures 2.4 and 2.5. At Fazenda Dimona (Manaus) the rainfall is greater than the evaporation in all months and the estimated evaporation shows no strong seasonal variation. At the other sites, there is a reduction in predicted evaporation for the dry season months: at Boa Sorte (Marabá) for May to October inclusive the evaporation exceeds the rainfall, implying a net amount of 264 mm being extracted from soil moisture storage. Similarly at Nossa Senhora (Ji-Paraná) evaporation exceeds rainfall in June and July implying that a net amount of 124 mm is extracted from soil moisture storage.

The annual total estimated evaporation, the equivalent daily rate and the measured annual rainfall are given in Table 2.3.

Table 2.3 The estimate annual and daily evaporation and the measured rainfall from the three ABRACOS pasture sites

Pasture site	Estimated total annual evaporation (mm)	Equivalent daily evaporation (mm per day)	Measured annual rainfall (mm)
Nossa Senhora	1024	2.81	1961
Dimona	915	2.51	2065
Boa sorte	1004	2.75	1585

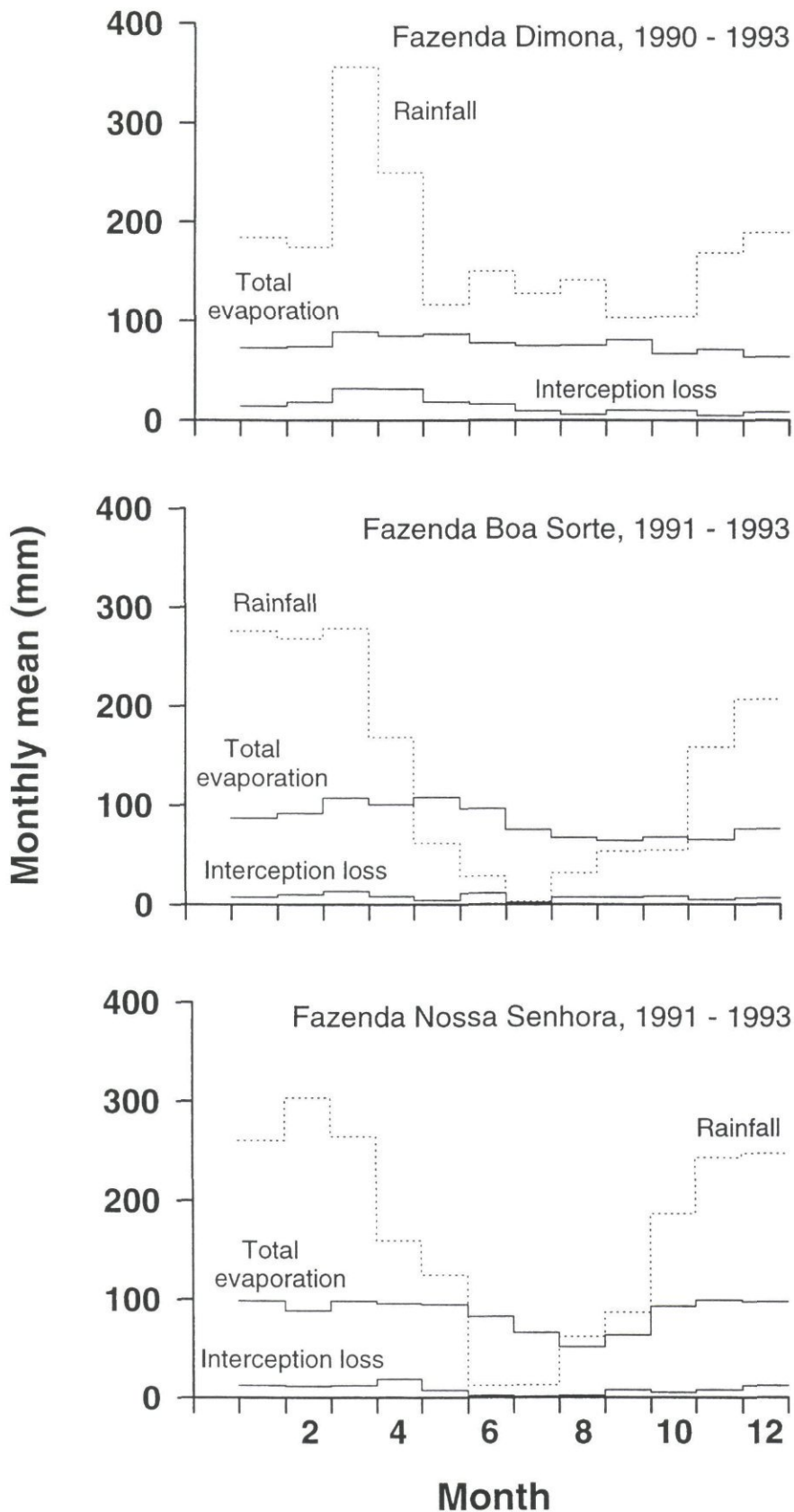


Fig. 2.4 Estimates of total evaporation and interception loss for three pasture sites using a Penman-Monteith 'big leaf' and Rutter model

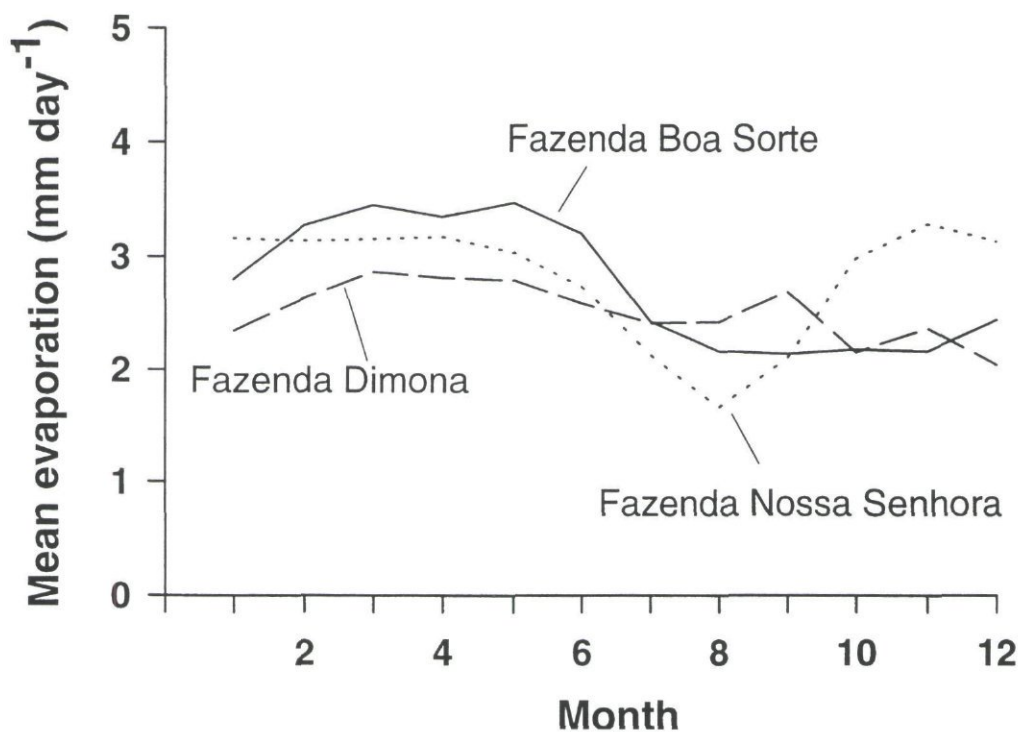


Fig. 2.5 Comparison of estimated evaporation for three pasture sites

### Discussion

The evaporation from the pasture is systematically less than that from forest. Over all sites the average total difference is 323 mm per year. During the wet season this will mainly be the result of the higher albedo of the grass reflecting more solar energy and resulting in less net radiation available for evaporation. No reduction in dry season evaporation from the forest has been observed in the measurements and none should be expected to be predicted from this analysis. The reduction in pasture evaporation during the dry season is smaller than expected but the estimated amounts of water extracted from the soil during the dry season are consistent with the variations in soil moisture observed by Hodnett et al. (1996).

These differences in evaporation will have an effect on surface runoff and river flows which will be relatively larger in the lower rainfall areas around Ji-Paraná and Marabá. In these areas the use of long term rainfall records and the estimated average reduction in evaporation (323 mm) results in predicted increases in runoff of 48 and 41 per cent respectively. These estimates do not allow for any decrease in rainfall which might accompany the deforestation. In Manaus the predicted increase in runoff is 29%. These increases are large and it should certainly be possible to observe such changes by using conventional catchment experiment techniques as are planned in LBA.

## **2.2 Mapping of surface characteristics for mesoscale modelling (CNRM)**

### **2.2.1 Data**

The employed geographical information consisted of both existing paper maps (for the natural landscape structures) and satellite data (for current alterations).

#### ***Printed maps and documentation***

Natural vegetation and soil maps over Rondônia at the 1:1,000,000 scale have been obtained from the RADAMBRASIL project (1978, 1979). Together with the printed color maps, very detailed notes are available (RADAMBRASIL 1978, 1979) (Fig. 2.6). The corresponding topography maps, at the same scale, are from IBGE (1979). These maps consist of the Porto Velho and Guapore sheets, (6-66°W, 8 - 12°S and 12-16°S, respectively). These two regions are presented in Fig. 2.7. The southern natural limit of this area is formed by the Guapore river, which separates Brazil (Rondônia state) from the Bolivian Republic.

The soil and vegetation maps of RADAMBRASIL (1978, 1979) combine information from radar images, airborne photographs and many field studies as basic mapping tools. In particular, measurements of soil properties, such as texture (clay, sand, silt proportions) are given in the technical notes for various profiles over the entire area. For vegetation, quantitative observations of the canopy height can be found in the Guapore map note. Information about the vegetation species making up the vegetation classes are also indicated.

#### ***Satellite Data***

In this study, both low resolution (METEOSAT) and high resolution (LANDSAT) satellite data are employed for spatial classification. The numerical counts are employed directly, without atmospheric corrections in particular.

#### ***METEOSAT data***

METEOSAT -75°W data in full spatial (-5 km) and temporal (30') resolution during RBLE-3 Experiment (August 11-25, 1994) were provided by Manzi (1994). They include the visible and infrared channels. The scenes have been geometrically corrected and put into a latitude-longitude coordinate system.

#### ***LANDSAT-TM data***

High resolution satellite data are needed to obtain accurate deforestation maps. Seventeen Landsat-TM full resolution (30 m) images (channels 1, 2, 3, 4, 5 and 7) of 1993 and 1994 acquired at INPE were provided by Nobre (1995). They cover the entire 5x5° studied area. The scenes have been geometrically corrected and put into a latitude- longitude coordinate system.

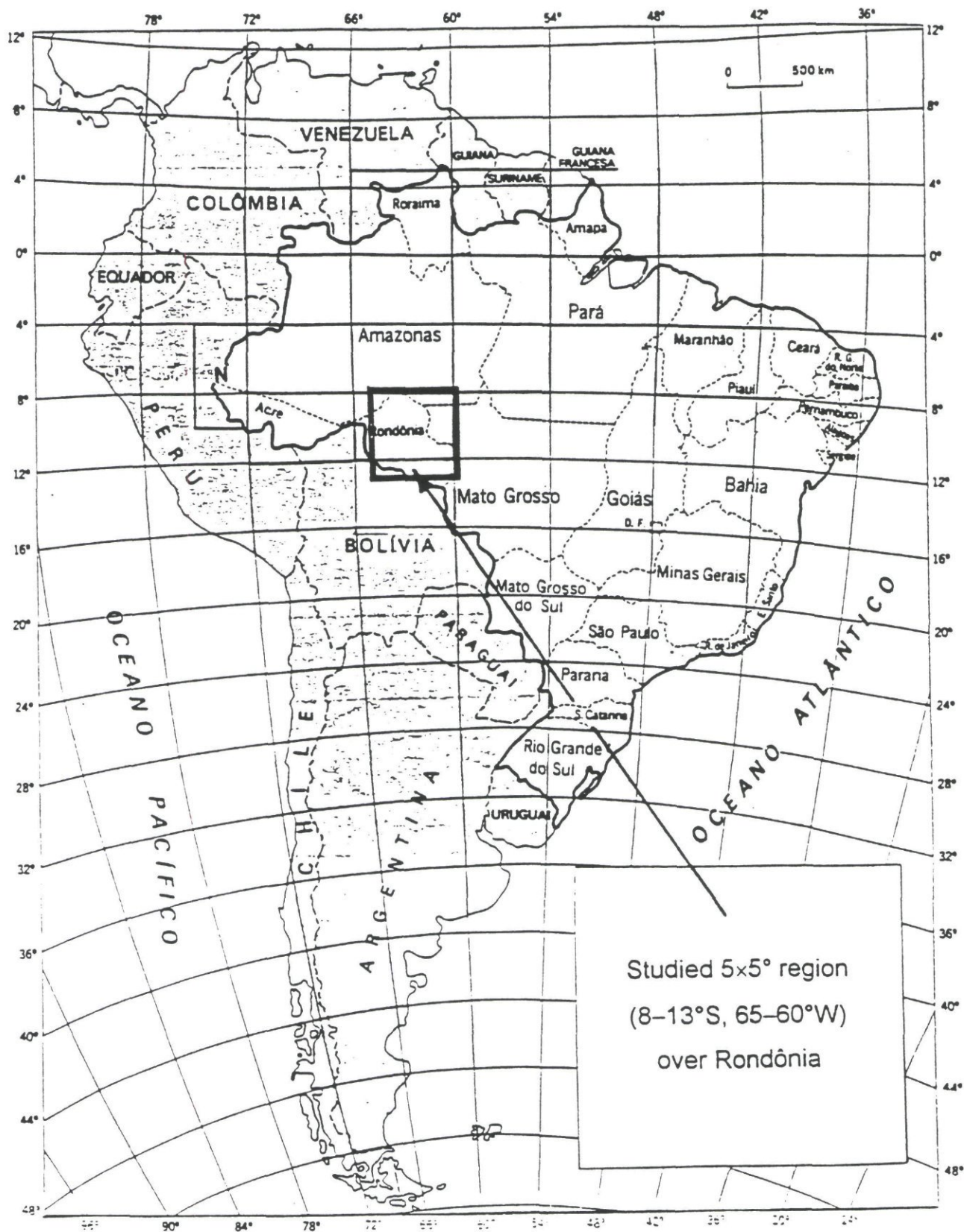


Fig. 2.6 The studied 5x 5° region in Brazil (adapted from RADAMBRASIL 1979)



### 2.2.2 Mapping processes

The natural vegetation, soil and relief maps on the millionth scale have been digitized over the 5x5° region (65 60°W, 8-1 3°S). Both digital elevation model and surface type classification were obtained by digitizing the contour lines of altitude class above sea level and of the RADAMBRASIL classes, respectively. The rasterizing process was performed by using the GRASS software (1995).

#### *Natural vegetation*

For natural vegetation mapping, airborne radar images and in situ field class observations were gathered by the RADAMBRASIL project. Many landscape units are described in both Porto Velho and Guapore maps. Because of North-South ecological gradients, the vegetation classes vary from one map to another.

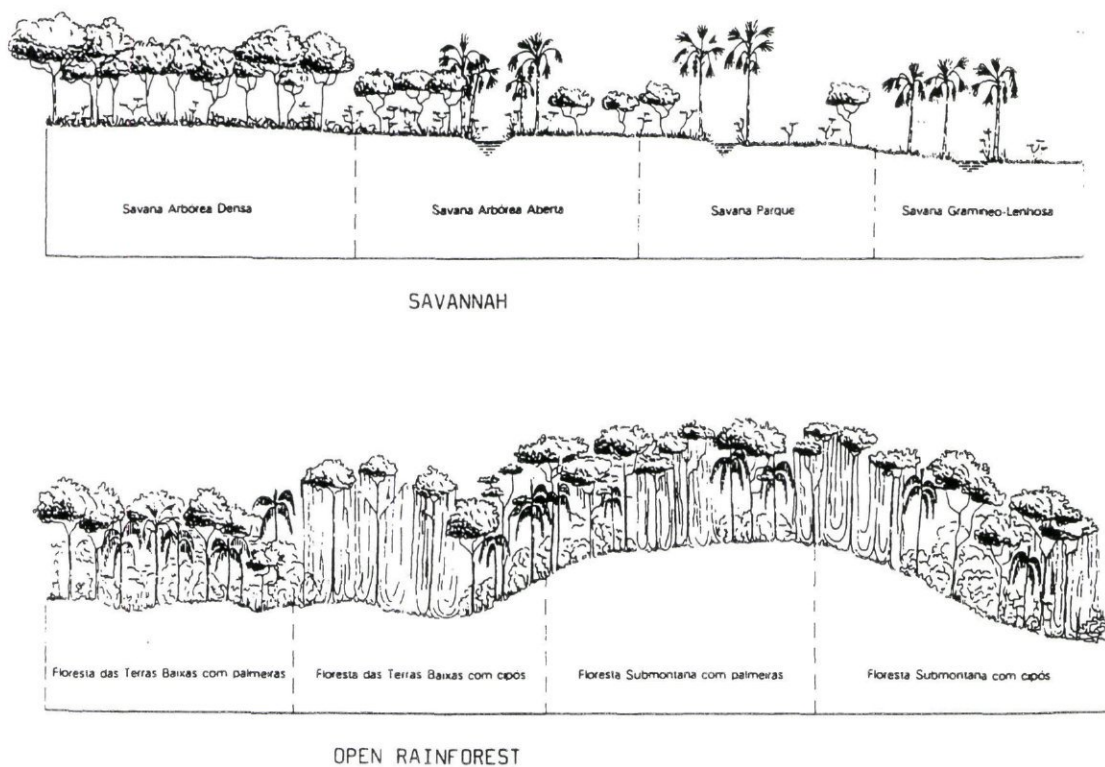


Fig. 2.8 Section diagrams of two natural vegetation main types: savannah and open rainforest (reproduced from RADAMBRASIL 1979)



# Vegetation

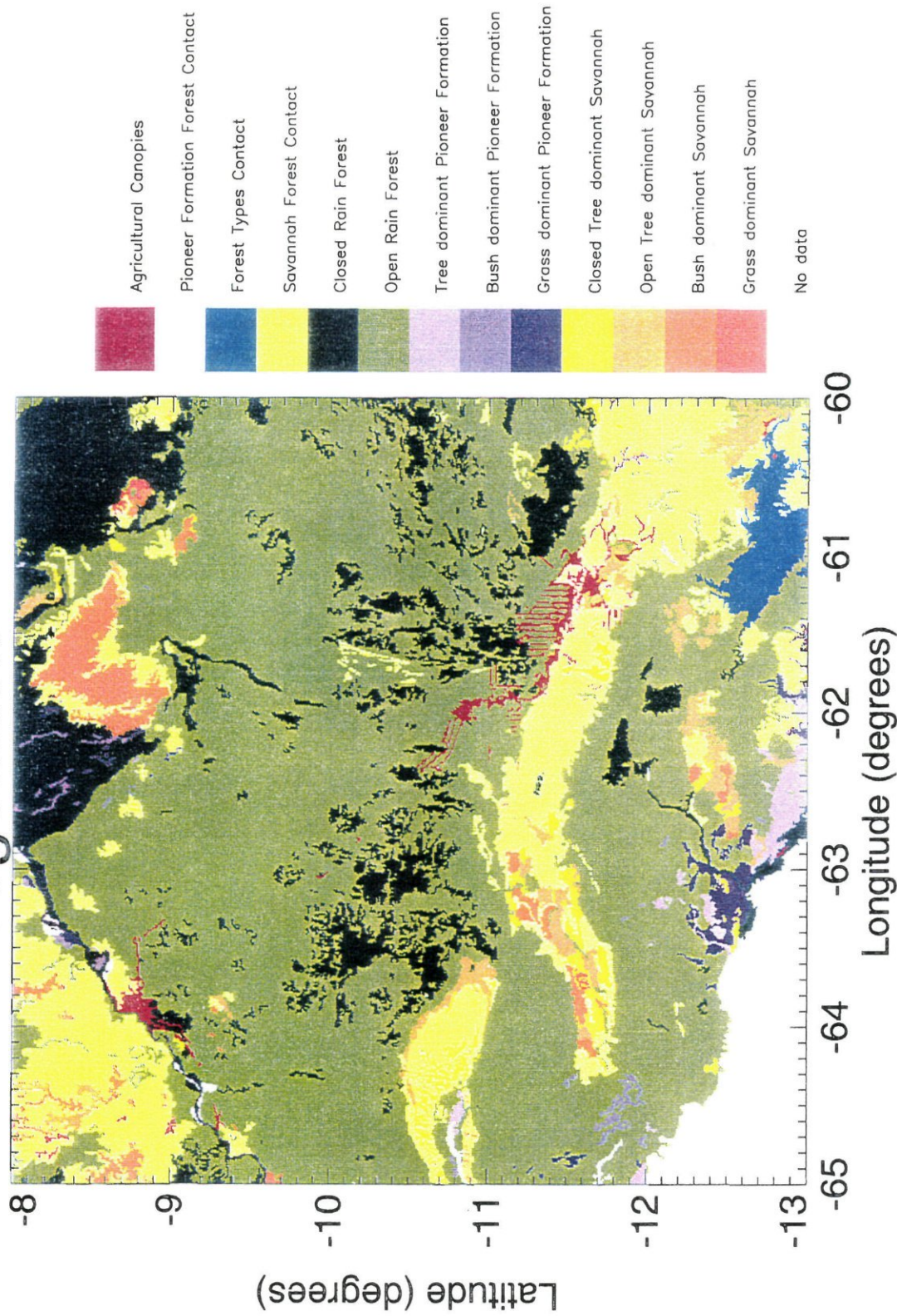


Fig. 2.9 Natural vegetation classes for the 5x5° region covering Rondônia (8-13°S, 65-60°W). This 600x600 digital map is derived from the 1 : 1,000,000 RADAMBRASIL maps of Porto Velho and Guaporé (1978, 1979)

The Porto Velho area is separated into four different ecological regions: 1- savannah, 2 pioneer formations, 3- closed and 4- open rainforest, along with the areas of ecological tension and anthropic action. The Guaroapé map comprises another main ecological class: 5- tropical semi-deciduous seasonal forest. These main vegetation units are further divided and described as ecological sub-regions. For example, Fig. 2.8 shows section diagrams of the main classes of savannah and open rainforest.

The sub-regions separate different canopy organizations (for example the proportion of grass, bushes and trees in the savannah main class), often associated with the relief structure. Also, in the Guaroapé map, the ecological sub-classes of a given ecological region often differ from the sub-classes of the Porto Velho map. The natural vegetation rasterized image is shown in Fig. 2.9. Over the area covered by the two maps, a total of 91 sub-classes are described (see the Attachment 3). For a better legibility, Fig. 2.9 presents only the 13 most representative vegetation classes in the studied  $5 \times 5^\circ$  region. Although a dominant vegetation unit in the region is open rain forest with palms, it appears that many different vegetation types are present. As illustrated by Fig. 2.9, the vegetation types are sometimes separated by more complex transition contact areas. Such regions are rather spread out. For example, the savannah-forest ecological tension areas constitute one major natural landscapes of the Ji-Paraná region ( $61^\circ 50'W$ ,  $10^\circ 50'S$ ).

#### **Soil data**

In the RADAMBRASIL maps, the soil classification is derived from the USDA taxonomy (1970). The following main categories of soil types have been identified: lithosols (or *lithic oxic troporthent* in the USDA taxonomy), alluvial alluvial soils, (*allic tropofluvent*), quartz sands (*allic quartzipsamment* and *spodic psammaquent*), latosols (*allic haplorthox* and *allic acrothox*), podzols (*oxic (ultric) tropudalf*, (*allic*) *orthoxic (distropeptic) tropudult*, *allic plinthic paleudult*), laterites (*allic superic plinthaquox*, *allic oxic plinthaquult*), cambisols (*aquic eutropept* and *udoxic dystropept*), gleyic soils (*allic tropaquept*), "terras roxas" (*oxic (ultric) tropudalf*, *rhodic paleudult*), and rocky outcrops. The soil classes are characterized by in situ 248 profiles obtained for most of the soil types. Such profiles are available for 78 soil classes. They are defined according to physical criteria such as the soil-forming processes (geology, topography, vegetation and climate), texture, color, and chemical properties. The spatial distribution of the classes in the RADAMBRASIL maps has been derived from the natural vegetation location, and from the topography, geology, and geomorphology maps. The alluvial red-yellow podzols and latosols are dominant. Fig. 2.10 presents the soil rasterized image. Again, a reduced number of classes is presented (11 classes). In reality, the map includes 132 sub-classes presented in the Attachment.

#### **Relief**

A digital elevation model obtained from the source 1 :1,000,000 maps of IBGE (1979) is presented in Fig. 2.11 as a rasterized image. As for vegetation and soil classes contours, the altitude contour lines have been digitized as vectors and converted into a raster grid. The interpolation process was done both manually by adding points (especially in flat areas) and automatically through an Akima's surface-fitting method (PV-WAVE, 1993).

There are marked differences in the relief structure within the studied area. The altitude varies from about 50 to 1100 m. The highest residual plateaux are part of the Pacaas Novos highlands (10°20' - 11°10'S, 65°15'-63°30'W). The lowest valley of the area is of the Madeira river, in Calama (8°05'S, 62°50'W).

### ***Deforestation Assessment***

The forest-non forest patterns are expected to be responsible for mesoscale circulations and changes in the atmospheric boundary layer structure. The main physical factor for such differences may be the presence of thermal contrasts. Therefore, the mapping of these patterns can be obtained from satellite data either from the viewpoint of the deforestation or thermal properties of the surface. The analysis of high resolution satellite vegetation indices enables one to map the deforested areas. On the other hand, low resolution infrared data from meteorological geostationary satellites can give access to the regional thermal structure of the area.

#### ***a) Meteosat-derived thermal map***

An estimation of the spatial extent of the warmest surfaces of the area was obtained by performing an automatic classification of the Meteosat infrared channel data. Four cloudless scenes (August 17, 19, 22, and 24 of 1994) at 0900 Local Standard Time (LST) were selected. A four-class map of the infrared numerical counts was made by using a k-means method (PV-WAVE, 1993). Fig. 2.12 presents the 'hot' class. Three main warmer areas appear very clearly: 1- the Porto Velho city (8°45'S, 63°50'W), 2- a deforested area close to Ji-Parana and 3- a large savannah area at about 150 km at the north of Reserva Jaru (8-9°S, 62°10'-61°W). It is interesting to note that the savannahs of the laterite plateaux are similar to deforested areas in terms of surface temperature.

#### ***b) Landsat-TM deforestation map***

A map of the deforestation on a zone of about 120x120 km is shown in Fig. 2.13. The selected scene (July 28, 1993) covers the RBLE-3 sites and contains pasture fields, forest, water surfaces and man-made features (roads and urban areas). The Landsat pixels were classified into three categories by using the same k-means method as employed for Meteosat: 1- forested areas (including regrowth), 2- non- forest areas (including pastures, urban areas, and natural savannahs), and 3 - water areas and missing data. The considered two variables in the automatic classification algorithm are normalized values of the greenness vegetation index (GVI) of Crist and Cicone (1984) and the channel 7 numerical count. The GVI is written as:

$$\text{GVI} = -0.2848 \times \text{TM1} - 0.2435 \times \text{TM2} - 0.5436 \times \text{TM3} \\ + 0.7243 \times \text{TM4} + 0.0840 \times \text{TM5} - 0.1800 \times \text{TM7}$$

where  $\text{TM}_i$  ( $i=1,7$ ) are the numerical counts of the Landsat-TM channels. The three classes presented in Fig. 2.13 show the deforestation patterns consisting of regularly spaced lines (about one every 3 km). Such patterns may have impact on the dynamics of the boundary layer at mesoscale.

# Soil

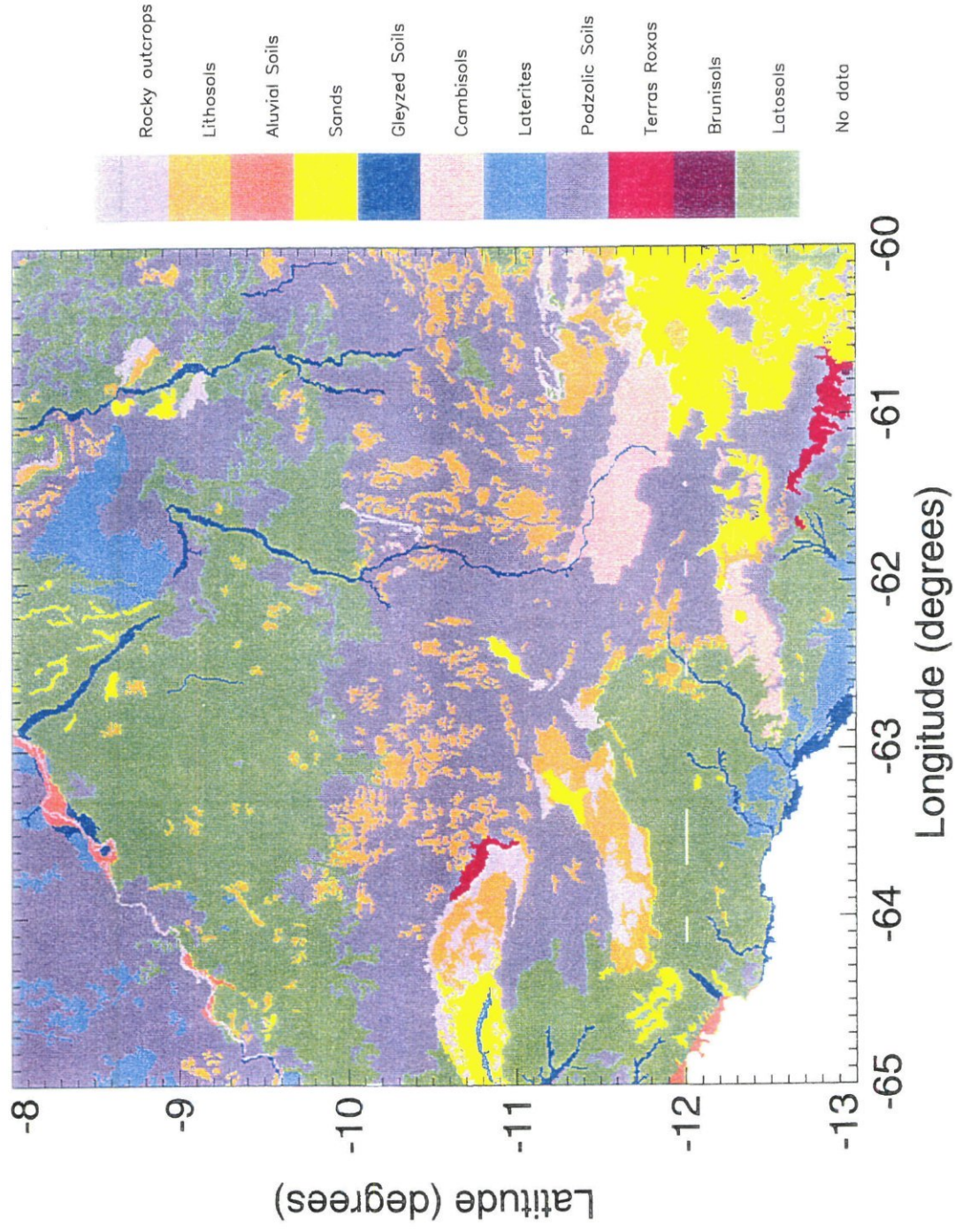
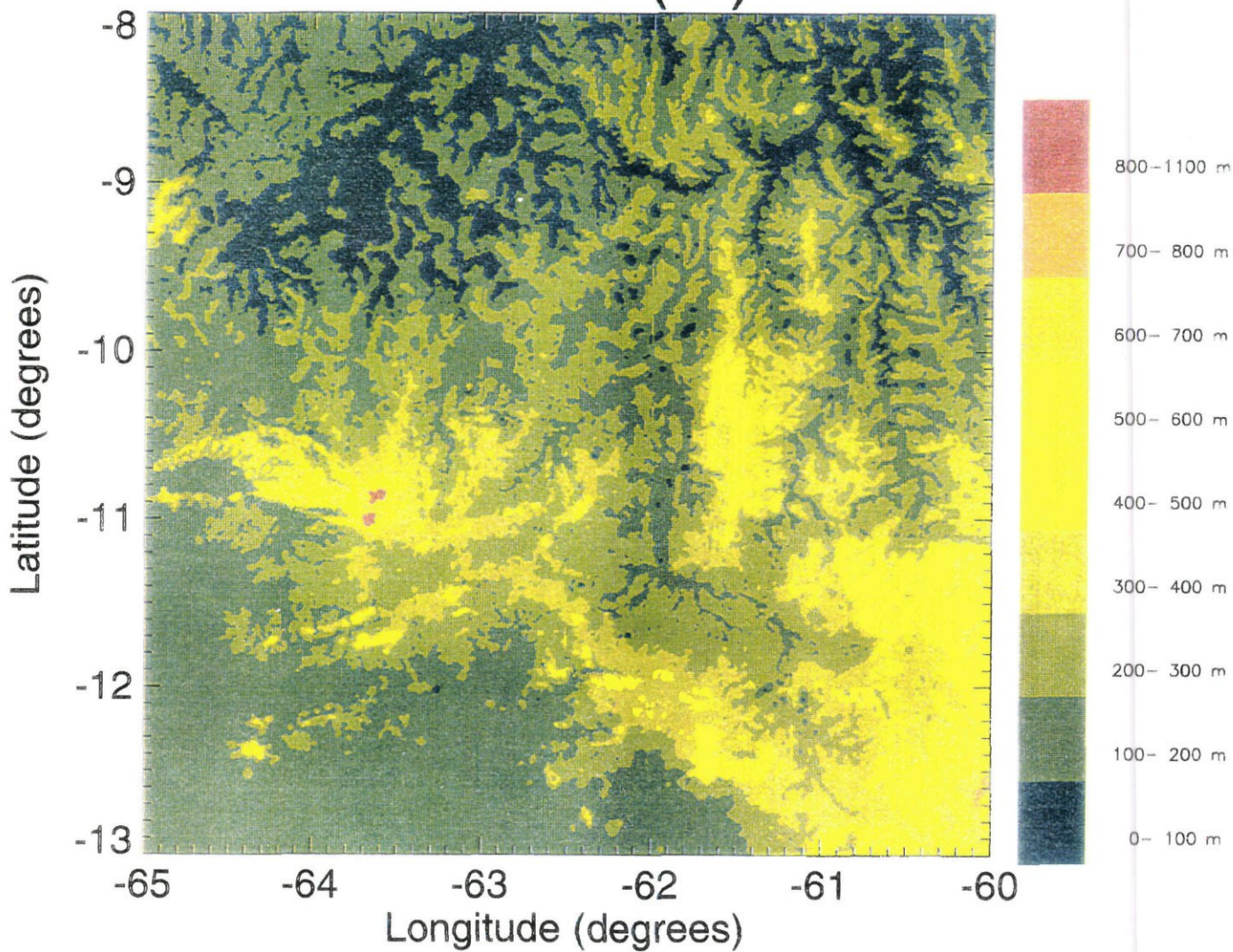


Fig. 2.10 As in Figure 2.9, except for soil

# Altitude (m)



*Fig. 2.11 Digital elevation model (600x600) covering the 8-13°S, 65-60°W region. This map is derived from the 1 : 1,000,000 IBGE maps of Porto Velho and Guaporé (1979)*

## Meteosat -75W Hot Class

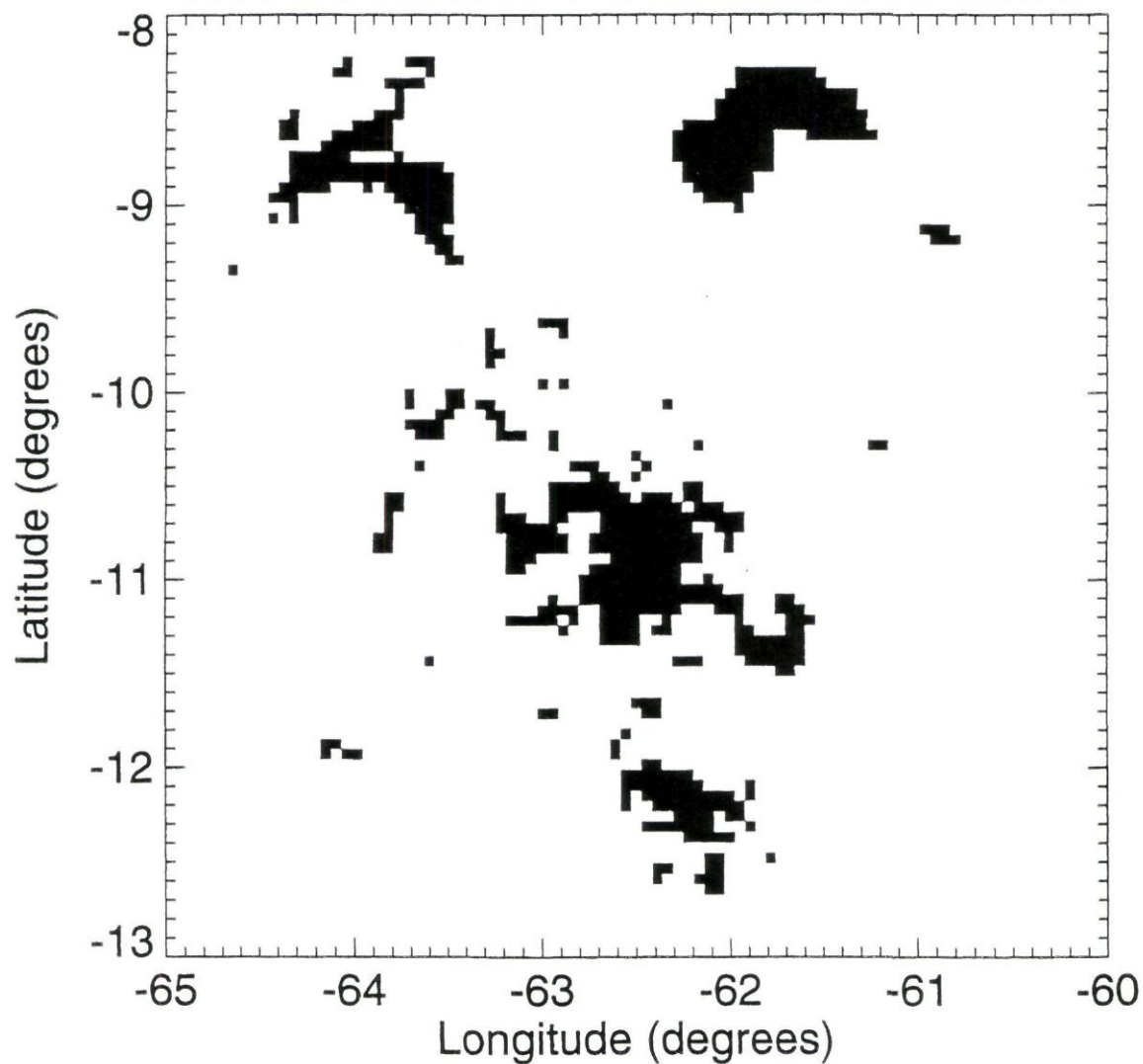


*Fig. 2.12 Meteosat infrared hot class (dark areas) at 0900 LST, during August 1994*

# Deforestation zones Ji-Parana region

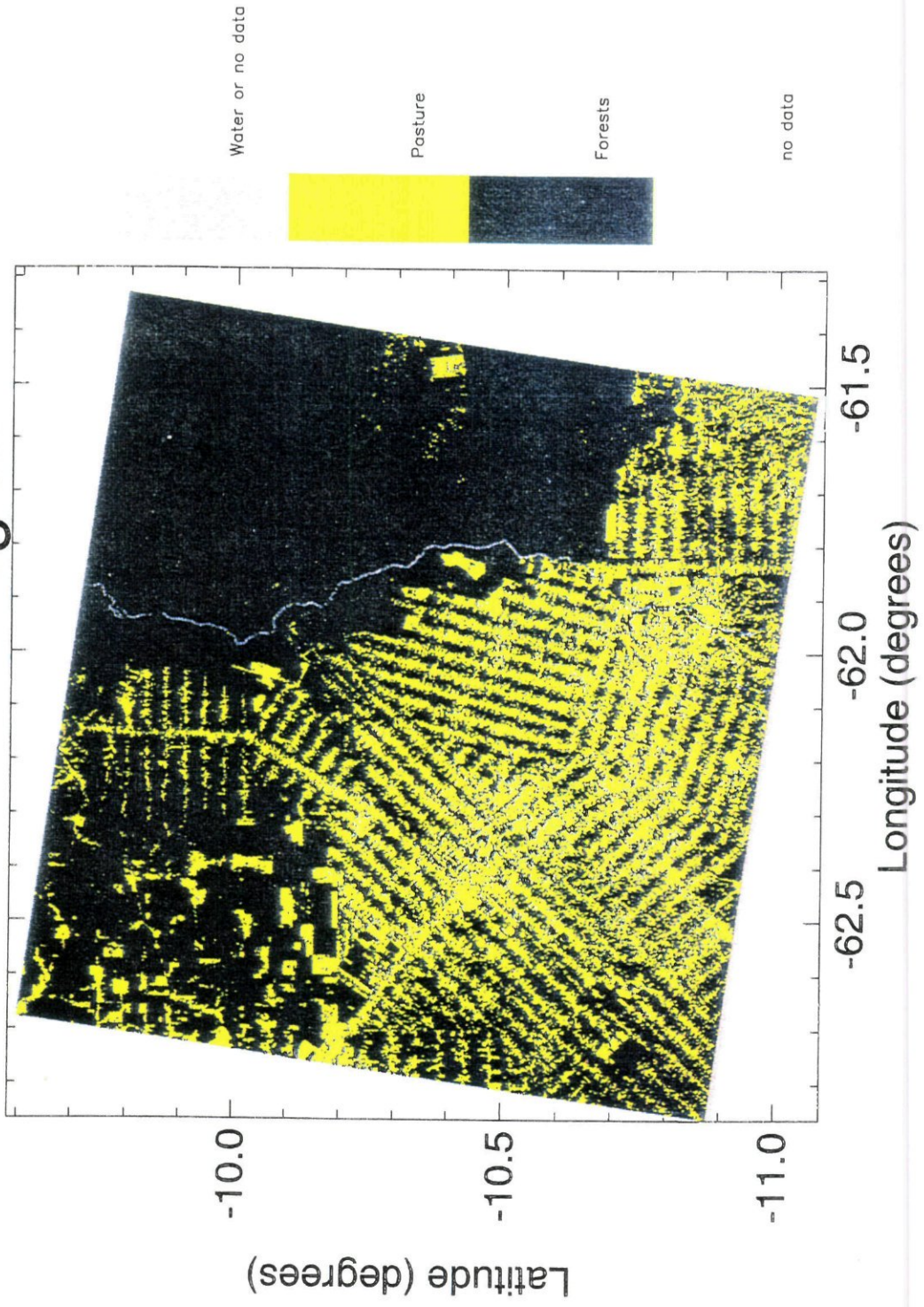


Fig. 2.13 Landsat-TM derived forest/non-forest classification of the RBLE-3 area of Ji Paraná (note that the scale is different from the other maps)

### 2.2.3 Discussion

In the relief presented in Fig. 2.11, the reported altitudes are only estimates of the reality. Indeed, the method used to obtain the digital elevation model induced a terracing effect: the distribution of the heights values is marked with a series sharp peaks corresponding to the digitized contour lines of the IBGE maps. Fig. 2.14 illustrates this effect. The terracing effect is common to all the terrain models obtained from contour line maps (USDC-NOM 1995). Although an interpolation is performed, the prescribed values of the digitized contour lines remain in the terrain model. This causes the altitude distribution to be discontinuous. In Fig. 2.14, the peaks correspond to multiples of 100-m, which is the interval between two contour lines on the source maps. The peak at 140 m corresponds to the prescribed value of the Bolivian portion of the Guapore map, for which no data were available at the same scale. It was checked that this part of Bolivia is a rather flat area containing many bogs.

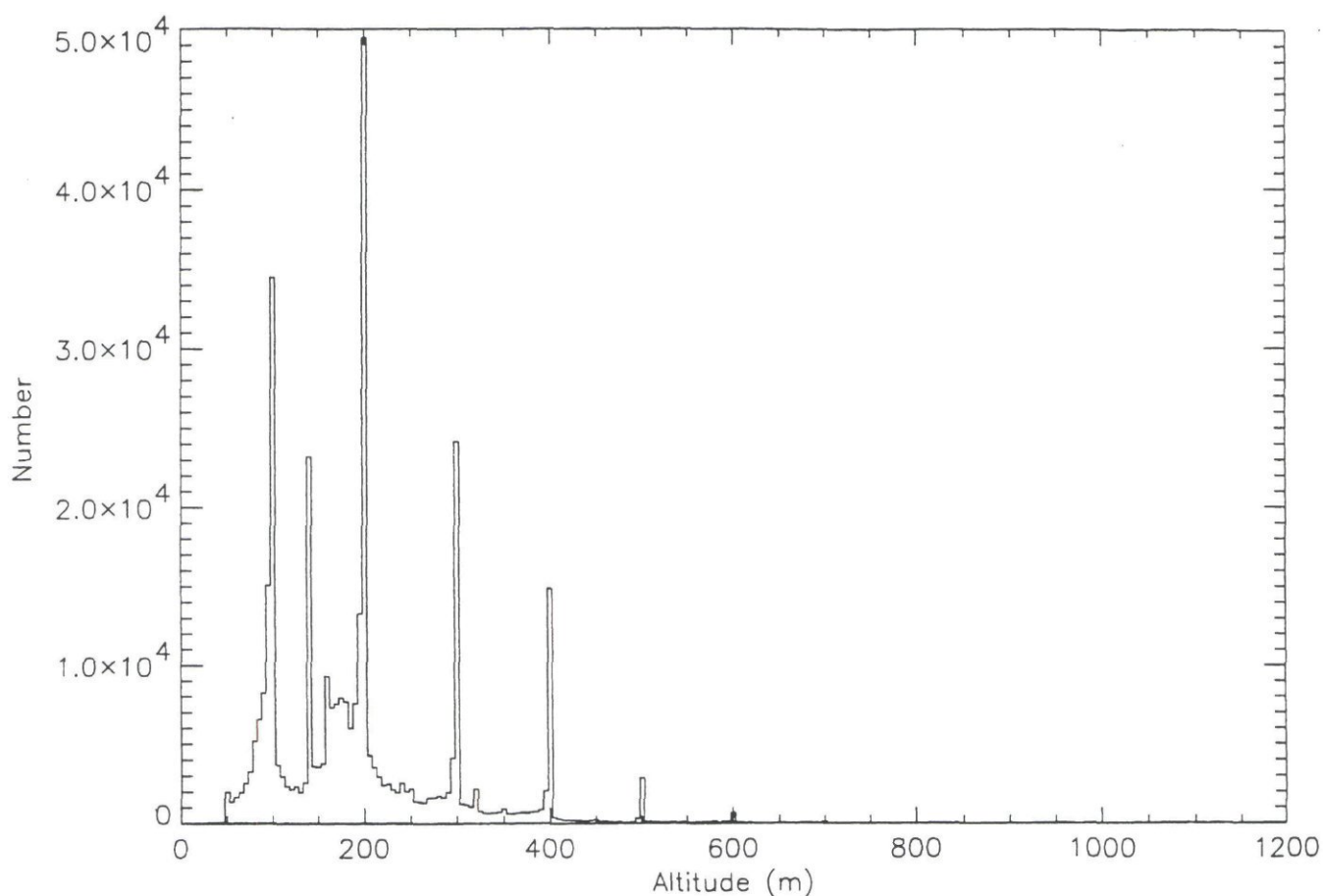


Fig. 2.14 Histogram of the altitudes reported in the digital elevation model Figure 2.11

The relief map presented before (Fig. 2.11) can be directly employed in a mesoscale model. On the other hand, the vegetation and soil types (Figs. 2.9 and 2.10) constitute a qualitative information. These maps have to be transformed into physical parameters of the surface scheme. In particular, the interaction of the vegetation with



the atmosphere depends on both structural and physiological parameters. The aerodynamic roughness of the canopy is related with the canopy height. The stomatal resistance depends also on the vegetation type. The hydraulic properties of the soils can be described by the soil texture and the soil depth involved in the vegetation transpiration. It is difficult to estimate the value of these parameters for each vegetation and soil classes. A method may consist of extrapolating the parameters obtained from the field measurements of ABRACOS, on specific sites. Table 2.4 presents the vegetation and soil structure parameters needed in surface schemes, as measured or estimated in the Rondônia ABRACOS sites of Nossa Senhora Pasture (NSP) and Jaru Reserve Forest (JRF). The same parameters for another type of (denser) forest near Manaus - the Ducke Reserve Forest (DRF) - are also indicated. It appears that the effective soil depth to be used in surface models depends more on the vegetation type (more or less deep roots) than on the soil type. For example, although the JRF and NSP sites correspond to rather similar soil types (Eutrophic red yellow podzol and allic red-yellow podzol, respectively), the fact that forest has been replaced by pasture at NSP has very significantly reduced the soil depth actually contributing to the vegetation transpiration. The leaf area index of the pasture site presents important seasonal variations. The lowest value is observed during the dry season (July-August). For all the sites, simple relationships between the canopy height and the aerodynamic parameters (zero plane displacement and roughness length) have been established during ABRACOS. These results can be used to draw aerodynamic parameters maps from a canopy height map derived from the RADAMBRASIL maps (for natural vegetation) and the Landsat classification (for recently deforested areas).

Table 2.4 Structure parameters of vegetation and soil for forest and pasture sites of the Amazon basin

Parameter	Nossa Senhora pasture	Reserva Jaru forest	Reserva Ducke forest	Source
Leaf area index ( $m^2 m^{-2}$ )	1.5 - 3.9	4.7	5.2	Roberts et al. 1996
Root depth (m)	2.0	> 4	> 4	Wright et al. 1996
Albedo	0.180	0.134	0.134	Culf et al. 1995
Canopy height $h$ (m)	0.5 - 0.6	30	35	Wright et al. 1996
Zero plane displacement $d$ (m)	$0.71 \times h$	$0.86 \times h$	$0.86 \times h$	Shuttleworth 1989, Wright et al. 1992
Momentum roughness length $z_0$ (m)	$0.12 \times h$	$0.09 \times h$	$0.06 \times h$	Shuttleworth, 1989, Wright et al. 1996
Soil bulk density ( $\times 10^3 kg m^{-3}$ )	1.3	1.5	1.1	Wright et al. 1996
Thermal diffusivity ( $\times 10^{-6} m^2 s^{-1}$ )	1.45	-	-	Santos Alvalá et al. 1996
Forest interception				
Canopy capacity (mm)	-	0.93	0.74	Ubarana 1996, Lloyd et al. 1988
Trunk storage (mm)	-	0.15	0.15	Lloyd et al. 1988
Free throughfall (%)	-	3.1	8.0	Ubarana 1996, Lloyd et al. 1988
% of rain to trunks	-	3.6	3.6	Lloyd et al. 1988

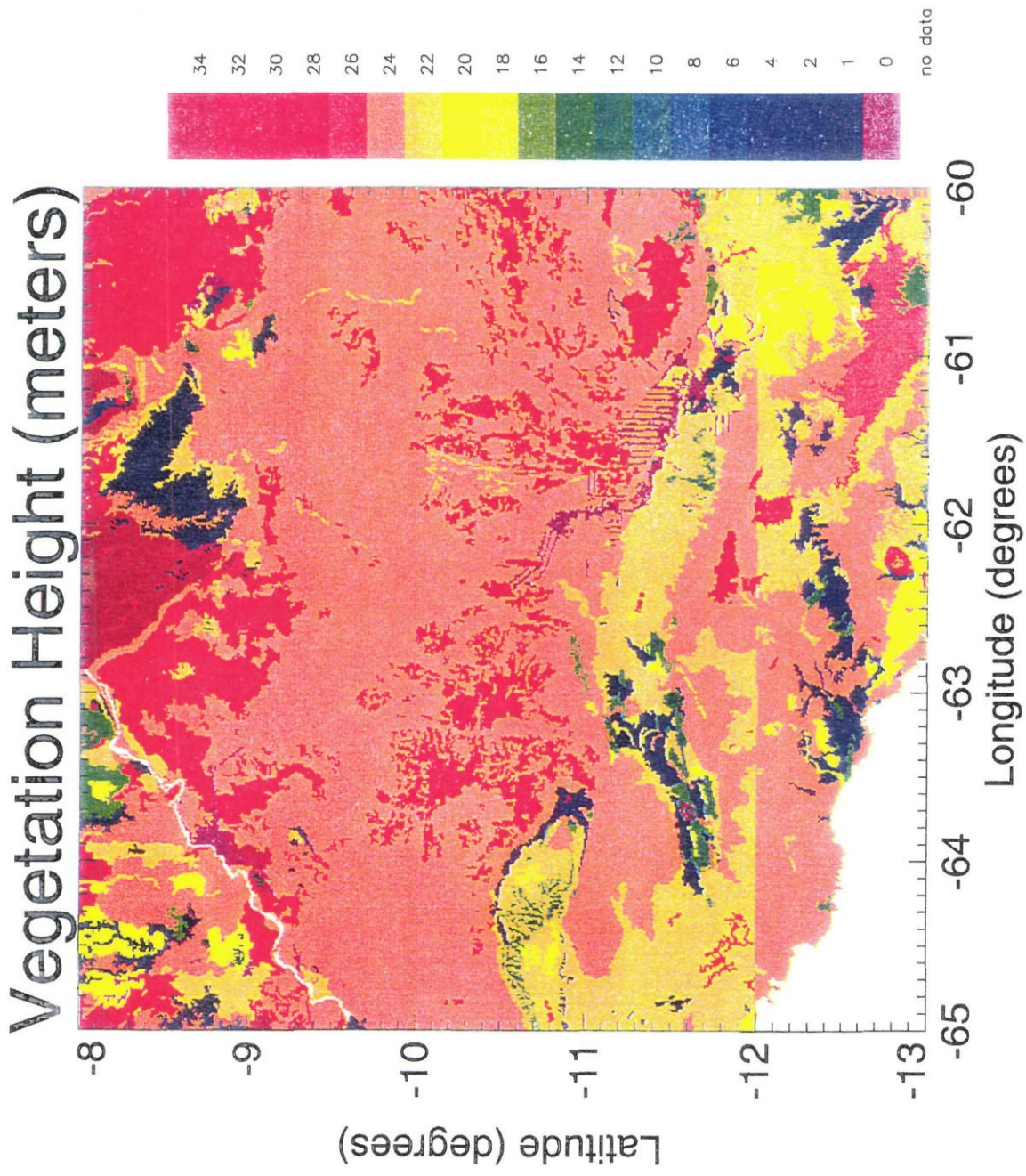


Fig. 2.15 Digital map of the natural-vegetation height obtained from the vegetation classes (Figure 2.9) and the RADAMBRASIL notes (1978, 1979)

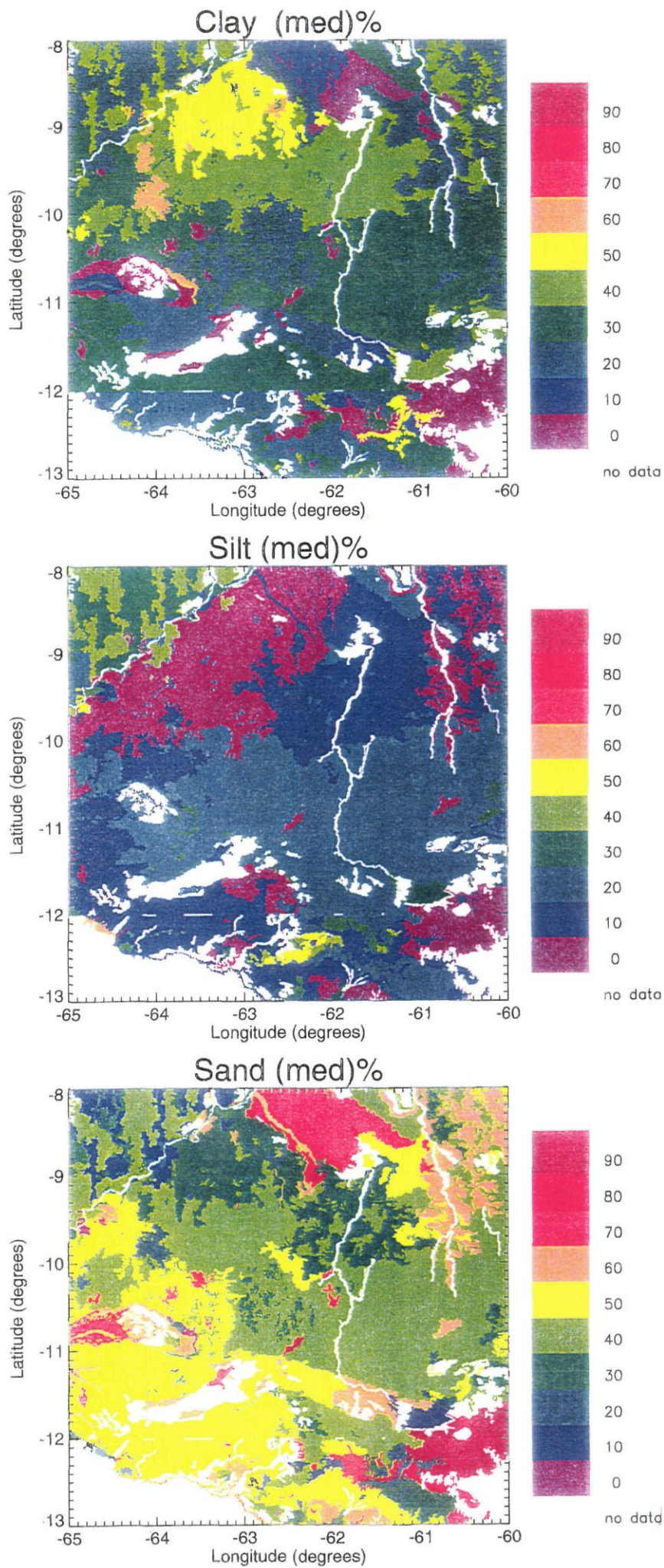


Fig. 2.16 Soil texture maps (percentage of clay, silt and sand) obtained from the soil map presented in Figure 2.10. The values employed for each soil classes are median of vertically averaged in situ profiles of RADAMBRASIL (1978, 1979)

The RADAMBRASIL maps of natural vegetation and soil types have to be interpreted in terms of natural vegetation height and soil texture. The information contained in the RADAMBRASIL notes has been analyzed in order to obtain a coherent correspondence between the landscape unit classes and these parameters. Figs. 2.15 and 2.16 present the derived maps of natural vegetation height and soil texture, respectively. In Fig. 2.16, the proportions of clay (particles diameter  $< 2 \times 10^{-6}$  m), silt (between  $2 \times 10^{-4}$  and  $5 \times 10^{-4}$  m), and sand (between  $5 \times 10^{-5}$  and  $2 \times 10^{-3}$  m) are mapped. A remarkable feature is the relatively low rate of silts in this area, whereas the proportion of either clay or sand is predominant. Deriving a soil texture map from a soil classification map is not an easy task. In this study, the 248 profiles of texture measurements were employed. It appears that the texture may vary a lot for a given soil type. To illustrate this variability, Fig. 2.17 shows the different profiles of the proportion of clay corresponding to a podzolic soil of the map. Surprisingly, the proportion of clay varies from less than 20% to more than 60% for the same soil type.

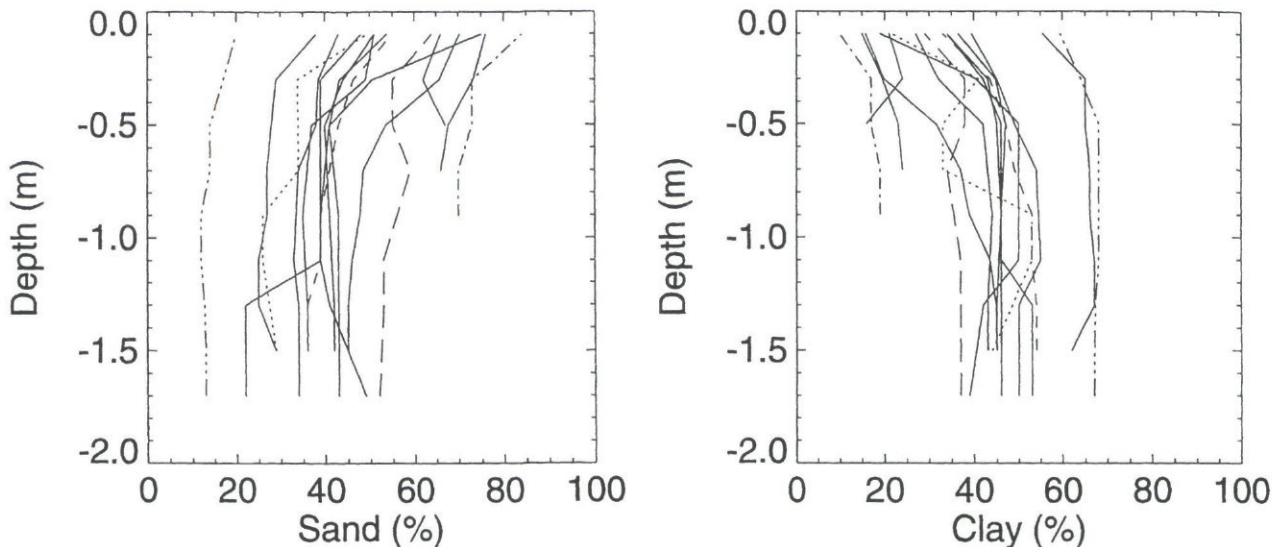


Fig. 2.17 Clay and sand proportion as measured over a 2-m depth for an allie red-yellow podzolic soil at 15 different places (RADAMBRASIL, 1978, 1979)

An explanation may be that the 1: 1,000,000 scale RADAMBRASIL map does not reproduce the actual variability of the soils. For example, the extreme values observed in Fig. 2.17 could correspond to inclusions 439 of other soil types which could not be mapped accurately. To tackle this problem and obtain the map presented in Fig. 2.13, a pragmatic solution was to calculate the median value of the vertically averaged texture, for each soil type. This process eliminated the extreme values. In both Figs. 2.15 and 2.16, discontinuities affect the transition between the RADAMBRASIL maps of Porto Velho and Guapore (at  $12^{\circ}$ S). This is due to a different classification of both vegetation and soil types from one the map to another. In the case of the vegetation height, quantitative information is only available in the

Guapore RADAMBRASIL notes. The extrapolation to the map of Porto Velho could be performed by prescribing a correspondence between the vegetation classes of the two maps, based on a thorough analysis of the RADAMBRASIL notes. Nevertheless, small differences at the boundary of the two IBGE maps remain (2 m for a forest canopy higher than 20 m).

The set of digital maps resulting from this work represents the currently available information about the surface structure of Rondônia, either natural or recently modified by human activities. This database can serve as a basis for mesoscale meteorological modeling.

### 2.3 Use of remote sensing data for monitoring rainforest extension and its changes: assessment of SAR data (DLR)

Multi-frequency and multi-polarimetric SAR data of the SIR-C/X-SAR missions of April and October 1994 were evaluated to show their potential for rainforest observation (see Fig. 2.18). Detection of sub-canopy flooding using HH-polarized L-band data is performed. In LHV and CHV polarizations a strong correlation of backscatter and biomass content was observed. Data of the ERS-1 satellite's Active Microwave Instrument (AMI) have been evaluated for their potential usefulness in monitoring deforestation and land use dynamics. The evaluation of SAR data has been performed in the state of Rondônia which is one of the deforestation hot spots in tropical rainforest of the Brazilian Amazon. Full-polarimetric and dual-polarimetric data of the SIR-C/X-SAR mission acquired in April and October 1994 and 5 ERS-1 scenes have been used to perform imaging work. Data collected during a field campaign in 1995 and 1996 served as reference data.

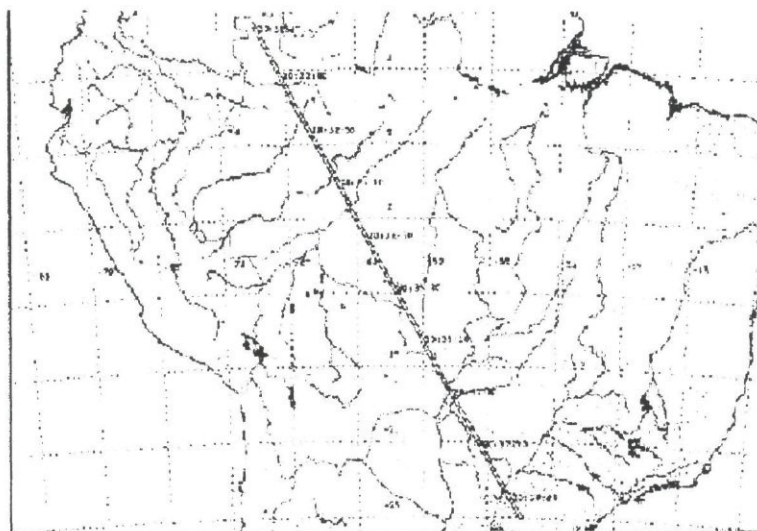


*Fig. 2.18 Coverage of South America of SIR-C/X-SAR Path 23.50 showing the strip of one SIR-C data set over South America. Beside the path 23.50 Rondônia is covered also by path 7.30. Data of both path were combined and evaluated*

The ERS-1 data have been acquired between June 1992 and October 1994. Image enhancement, filtering, and automatic classification tools have been used to improve discrimination of land use classes and to analyze the images. As an additional reference data set Landsat TM data of July 1994 have been used.

#### *Available data*

For the northern test site in the department of Jaru two SIR-C/X-SAR data sets have been used. For the southern test-site in the department of Ji-Parana only the dual-polarimetric data set has been evaluated because of its better ground resolution. Work has been done with MLC (MultiLook Complex) products of L- and C-band recorded on October 1st and 9th, 1994 and MLCs recorded on April 9th of 1994. Data sets of the full polarimetric and the dual polarimetric imaging mode were used. All dates were from descending passes. The dates for the former are: August 9th, 1992, October 10<sup>th</sup>, 1993, June 3rd, 1994. The dates for the latter are: January 15th, 1993, April 30th, 1993. The TM-scene was recorded on July 15th, 1994.

A total of 5 ERS-1 Images were used. Three images were GEC-products, the other two precision images (PRI). Three different dates were available for the test-site in Jaru, two dates for the testsite in Ji-Parana.

#### *Test site description*

Rondônia has been chosen as a testsite for its very distinctive and rather unique clearcut pattern (see e.g. Fig. 2.29). Large and small-scale clearings form the typical fishbone pattern of many of the Brazilian colonization areas which pose quite different problems to image enhancement techniques such as filtering and automatic classification algorithms.

In Rondônia the local and national authorities have developed the PAD colonization scheme (Projeto Assentamento Dirigido = Project of Directed Settlement). Settlers in Rondônia will receive a lot 2000 × 500 m (100 ha) - to cultivate (Walker, 1996). These areas are distributed in a certain pattern along development axis'. The axis' are laid out in a grid 4 km apart. Legally, each settler is allowed to clear 50% of his lot for cultivation. The intention was to keep a strip 2 km wide of forest between the pastures. Thus, soil loss through aeolian erosion was to be kept at a minimum and sufficient regenerating sources for the forest could be provided in case the lots were abandoned. Unfortunately the local settlers undermined this scheme by selling parts of their 100 ha lots to sub-owners who started clearing 50% of their sub-lots as well. So the actual forest cover in the PAD's dropped far below 50%, in some areas the forest strips vanished completely. Since the construction of the BR-364 (Brasil Rodovia) in 1984, the main paved highway connecting Rondônia with Acre and Mato Grosso do Sul, the stream of settlers coming to the state has increased considerably. In the early nineties the deforestation rate decreased due to diminished tax subsidies from federal government to increase again in 1995 to an even higher rate. Lately the regional planning authorities, namely INCRA (Instituto Nacional de Colonizacao e Reforma Agraria) have taken steps to a stronger surveillance of settlement in Rondônia. Consequently INCRA has a strong interest in remote sensing data to observe the settling processes.

### *Co-registration of data*

The three ERS data sets of the Jaru test site were delivered as GEC products (Geocoded Ellipsoid Corrected). These were used to correct the incomplete rectification of the Landsat TM scene which appeared slightly tilted to the north east. Also the SIRX data had to be corrected, which was done relative to the TM scene to retrieve a sufficiently large number of ground control points. X-SAR data were received as GEC products which showed the same geometry as the ERS-1 GEC products and could be used to verify the rectification of the SIR-C and Landsat TM data. The ERS-1 and SIR-C data of Ji-Parana, the southern test area, were rectified to the corrected TM full-scene. The land use pattern and Aver meanders provided sufficient ground control points to perform rectification.

### *Image enhancement*

The Landsat TM-scene showed zero percent cloud cover, no disturbing atmospheric haze or other influences disturbing image quality and interpretability. It could be used for interpretation and automatic classification without further enhancement. TM-data were used to generate a forest/ non-forest mask derived from look-up tables of channels 3,4 and 5. From this mask forest boundaries were extracted and used to check the forest/non-forest discrimination in the SAR-data. The SIR-C data were delivered by JPL as MLC (multi look complex) products. Using a software provided by JPL, different polarisations were extracted and combined for interpretation and classification. From full polarized data the polarizations HH, HV, VV, TP (horizontal/horizontal; horizontal/vertical; vertical/vertical; total power) were extracted, from dual polarized data the combinations HH, HV and TP were available.

The dual-polarized SIR-C data had to be brightness corrected due to a brightness loss from ground to slant range. Unfortunately this was only successful in the April scene (Fig. 2.25). However the brightness loss in the October scene seemed to pose no problems to the classification algorithm. The data sets were re-sampled to 25 m and mirrored to show the proper ground geometry (Fig. 2.27). Re-sampling was performed to reduce speckle. Several filters and filtering modes were applied to prepare the data for visual interpretation and for automatic classification. The LOCAL REGION, LEE, FROST and MAP filters were tested in up to two iterations and with various window sizes. Using the MAP filter in two iterations with a  $3 \times 3$  and  $5 \times 5$  moving window appeared best suited for the pixel-wise maximum likelihood approach and for visual interpretation.

To further enhance information various sets of multi-layer combinations were tested, combining different polarisation images of the SIR-C sensor and the three frequencies of X-, C- and L-band.

The ERS-1 images were analyzed following the experiences drawn from the image processing of the SIR-C data. For visual interpretation a Gamma-MAP filter was applied in two iterations. The first filtering was done using a  $3 \times 3$  moving window, the second iteration using a  $5 \times 5$  moving window. This method showed the best results in trail runs using the filters FROST, LEE and Gamma-MAP with different window sizes. The MAP filter showed the best compromise between eliminating speckle and preserving the information content of the SAR data. The ERS-1 data of

the department Jaru proved not suitable for an analysis based on a multi-temporal overlay, as they showed information of the years 1992, 1993, 1994 respectively. Clearing activities changed the actual landcover to a point that no statistically relevant data could be extracted of the cleared areas, being forest in one year and pastures in the following. Multi-temporal analysis was consequently limited to the southern test area in the department of Ji-Parana with data sets of one single year. Unfortunately, in this test area only two scenes could be acquired, one of January 1993 and one of April 1993. Thus, no multi-seasonal analysis in the actual sense could be performed as both scenes were imaged during rain season.

### *Applied classification tools*

For automatic classification of the SAR-images a set of training areas was used which was chosen according to data gained during a ground truth campaign in 1995. Fig. 2.19 shows the results of a visual interpretation using the ground truth data for a small sample of the SIR-C data set.

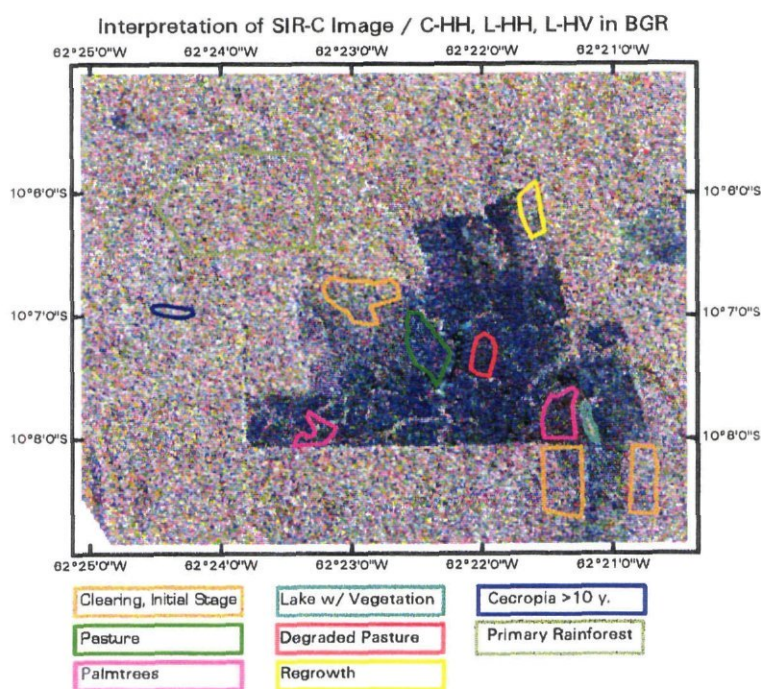


*Fig. 2.19 Visual Interpretation of Unfiltered SIR-C Image Texture classification*

For automatic classification two algorithms have been applied. On MAP-filtered images the maximum-likelihood method was chosen. In another approach unfiltered images were automatically classified using the EBIS (Evidence Based Interpretation of Satellite Images) texture classifier (Lohmann, 1991) EBIS was applied to one date images of 1992 and 1994 of both departments respectively.

The EBIS texture classifier uses the multi-nomial distribution besides the normal distribution to discriminate land use classes. Position and form of the local histogram are determined in a moving window of definable size in the range of  $5 \times 5$  to  $15 \times 15$  pixels. In addition EBIS provides the possibility to use texture



information derived from co-occurrence matrices or the local histogram in up to 6 different feature space files. Experience shows that either one or the other option should be used. Feature space files contain the information of the statistical measures to be applied as well as the window size of the data space and the increments of grey levels to be used. The co-occurrence matrix may be calculated by using the following directions: horizontal, vertical, left-diagonal and right-diagonal. To save computing time it is advisable to use only two directions of the four as the information gain is only minimal by additional directions.

Fig. 2.20 shows the ability of the EBIS classifier to recognize texture and set-up different classes accordingly. While the maximum-likelihood method defines class properties only by the grey value of a single pixel, EBIS goes one step further and supports co-occurrence matrices. Co-occurrence matrices do not only record the relative frequencies of grey values but additionally record the relative frequencies of the spatial distribution of grey values in direct neighborhood (Lohmann, 1994).

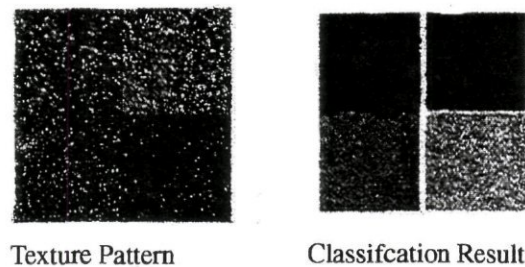


Fig. 2.20 Texture Evaluation by EBIS (Lohmann, 1991)

Fig. 2.21 shows an example of classes which are clearly distinguishable for the human eye but still have the same histogram. By using the co-occurrence matrix for the class decision EBIS is capable to separate the two classes in the sample shown above. In this approach various grey level and window sizes were tested. The classification results on multi-layer and one-layer images were compared.

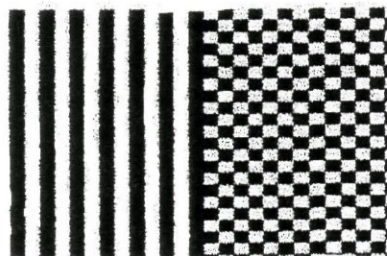


Fig. 2.21 Properties of texture - 2 different textures with identical histograms (Lohmann, 1991)

The difficulty for the human interpreter and user of EBIS is to pick the classes according to their textural features. Experience has shown that only a small number of AOI's is needed for this and that AOI's should enclose an image area large enough to generate a sufficiently distinctive class statistic based on the co-occurrence matrix.

**Classification approach**

The first step of the classification procedure was to evaluate and analyze the signatures of the desired classes. This was done by computing the statistical mean and standard deviation of the AOI derived from the ground truth campaign. This gives a first guess on separability by EBIS and a quite accurate estimation of performance of the maximum-likelihood classifier. Unfortunately, there is no statistical value which represents the properties of the EBIS texture parameters and so the estimation of separability of the classes by EBIS is more or less done on a trial and error basis. Different window sizes, co-occurrence directions and grey levels have to be tested on a subset of the image to judge separability of the desired classes and adapt the training sets accordingly.

To classify SIR - C/X-SAR data it was first necessary to evaluate the best combination of frequencies and polarisations to achieve the maximum output at reasonable computing time. Therefore the signature analysis was computed for different target classes and the various combinations of bands and polarisations. Furthermore, the different combinations were visually evaluated according to their information content.

The following figures show the signature analysis of full polarimetric SIR-C data for five classes.

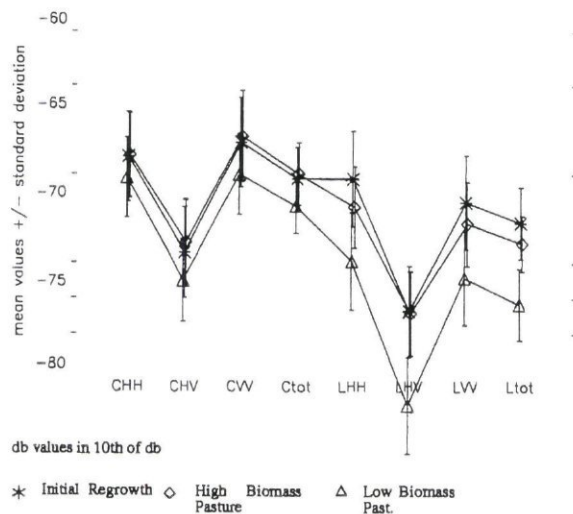


Fig. 2.22 Signatures Mean s and Stddev. from Full -Polarimetric SIR-C Data of April 1994

Fig. 2.22 shows the rather low separability of the classes High Biomass Pasture and Initial Regrowth in all polarisations in C-Band, because relative to this wavelength the classes High Biomass Pasture and Initial Regrowth have a similiar roughness.

Separability is somewhat better in L-HH, VV and L-band total power. Separability of Low Biomass Pasture against High Biomass Pasture is best in L-HV

Signature analysis assists in choosing the band combinations and polarisations which best represent the target classes. Experimenting with the SIR-C/X-SAR data showed that for biomass analysis the HV-polarisations are best suited, whereas for the detection of sub-canopy floodings L-HH gave best results (Fig. 2.23).

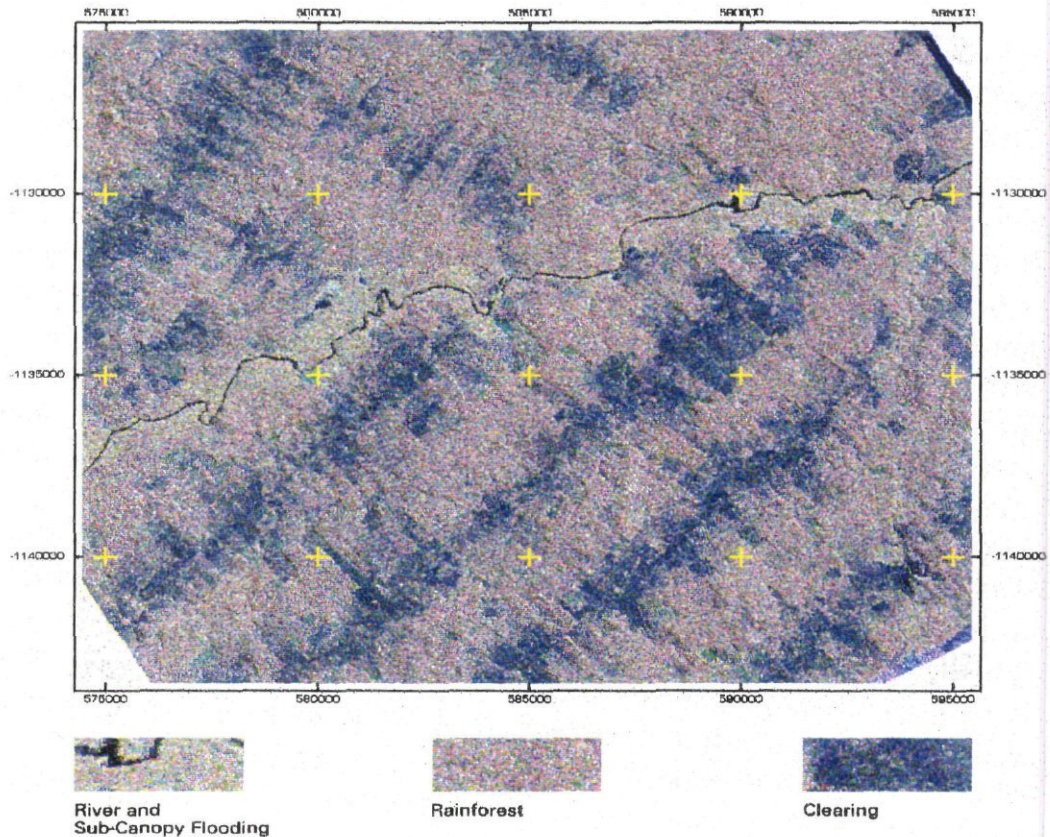


Fig. 2.23 Sub - Canopy Floodings in SIR-C Image L-HH, L-HV and C-HH in RGB

Fig. 2.24 shows the general difficulties in separating landuse classes containing higher biomass. Due to increased roughness the vegetation cover appears very much alike in radar images, especially at higher frequencies. Again L-band HV-polarisation discriminates the classes best. It seems amazing at first glance that in C-band the classes Forest and Initial Regrowth have an almost identical signal response. The fast increasing leaf biomass of young regrowth stands has a similar roughness as the crown layer of a mature rainforest, relative to the low penetration depth of Cband, thus these classes emit a similar backscatter. Again separability is best in L-HV. The separability of old regrowth and rainforest is generally low even in L-band, because of the high biomass levels and stand heights in these classes. Depending on the succeeding plant society (*Cecropia spec.*) regrowth stands of 6 years or older, having a stand height of 20 meters and more, could be observed.

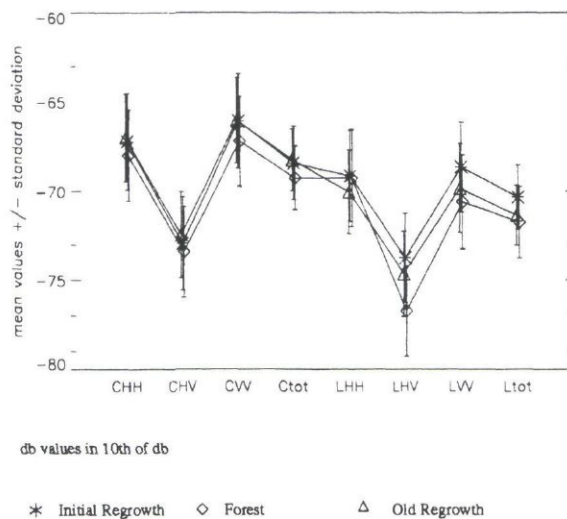


Fig. 2.24 Signature Means and Stddev from FulW Polarimetric SIR-C Data of April 1994

The figure above shows that discrimination of the class High-Biomass Pasture is rather poor in C-band and increases in L-band. L-band shows a good discrimination of rainforest and pastures High biomass and low biomass pastures are discriminable in L- and C-band.

For classification a combination of C-HV, LHH and L-HV proved best in October (Fig. 2.28), whereas for the April scene a combination of C-HH, L-HH and L-HV was chosen in order to enhance the detection of sub-canopy floodings (Fig. 2.26). The data were MAP-filtered twice with  $3 \times 3$  and  $5 \times 5$  moving windows and then classified with the maximum-likelihood classifier (Fig. 2.25). Also, several different EBIS approaches were applied to the SIR-C/X-SAR data but did not prove successful. The reason for this failure lies in the special pattern of the fazendas in this region. The EBIS classifier needs sufficiently large training sets to evaluate class statistics. Problems occur when small-scaled patterns, as the fish-bone patterned fazendas in Rondônia, lead to several landcover borders within the moving window's pixel environment. Thus, enough sufficiently sized training sets for more classes than forest/non-forest one could not be extracted. Discrimination of the classes with maximum-likelihood was faster, more accurate and more diversified in the Rondônia study site.

Table 2.5 gives an estimation of classification accuracy with maximum-likelihood for the SIR-C data of October 1994. Only the values for the bigger classes are shown.

Table 2.5 Classification accuracy for SIR-C data of October 1994

Class Name	Producer's accuracy (%)	User's accuracy (%)
Degraded pasture	71.74	97.06
Latest clearcuts	77.78	94.59
Pasture	82.93	100.00
Rainforest	100.00	100.00

Overall classification accuracy: 86.52%

Due to the nature of the statistical procedure to compute the confusion matrix, the values can be considered only as a first estimation. To compute a valuable statistical confusion matrix, more evaluation areas would have to be included, which are not at hand due to a lack of ground truth.

ERS-1 SAR data were used to enlarge spatial coverage of forest/non-forest mapping. Stronger limitations are caused by the lower wave-length of ERS-1 operating at C-band with VV-polarisation (Keil et al., 1996). Thus, working with a low penetration depth in the substrate, ERS-1 has a limited capability to discriminate classes like primary rainforest and older regenerating areas of an age older than 4 years.

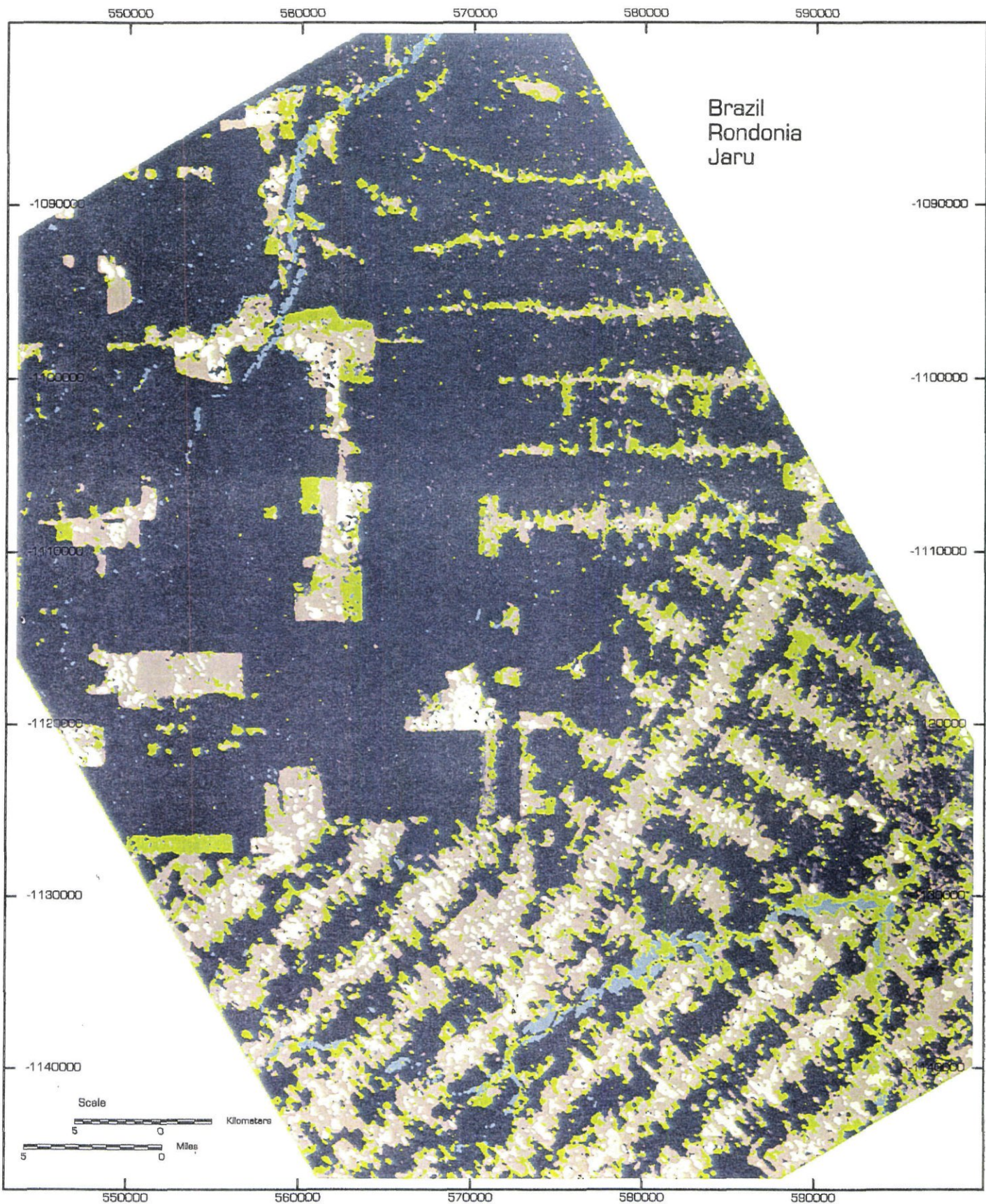
This has to be accounted for when trying to set-up a monitoring system or using automatic classifiers. The first step, however, in automatically classifying the ERS-1 data is to define target classes to be extracted. Due to the limitations of ERS-1 a mixed class of Forest and re-growth older than 4 years had to be defined. Multi-seasonal data sets can help to improve forest and re-growth separation but were not available. Other visually separable classes were Pasture in Good Condition and Degraded Pasture showing a vegetation cover lower than 40 percent. In the southern test-area another limitation of the ERS-1 sensor became evident. Due to the incidence angle of 23.5 degrees images of slopes of the same or similar angle towards the sensor contain little to no information at all. This effect severely degrades the interpretability of the ERS-1 image of the Ji-Parana test-site, as the south-eastern part consists of quite hilly terrain. This is Amplified by the nature of the slopes appearing in this area. Most of the hills consist of blocks of quartzite, resistant to erosion. This has the effect that many slopes have angles steeper than 45 degrees. Also the stronger shaded parts of hilly terrain lead to misclassifications, especially with the class degraded pastures. The following table gives a first assessment of classification accuracy for the forest/non-forest discrimination by EBIS, derived of 6 evaluation areas for each class. Within these areas a set of 100 points was chosen randomly to calculate the statistics.

*Table 2.6 Classification Accuracy for Forest / Non-Forest Discrimination of ERS-1 data*







Class name	Producer's accuracy (%)	User's accuracy (%)
Rainforest	67.57	100.00
Non-forest	100.00	52.00

Overall classification accuracy: 76.00%

The classification of Landsat TM data showed to be quite straight forward. A class overlap occurred only between the classes Settlements/Roads and Bare Soil. This had to be expected considering the nature of most roads of the area, being only caterpillared and not paved. By reducing the standard deviation for the smaller classes the separation of classes could be further improved and a total of 8 classes could be classified.



Legend

- |  |  |   |
|--|--|---|
|  Sub-Canopy Flooding |  Initial Regrowth |  Degraded Pastures     |
|  Forest              |  Pasture          |  Intermediate Regrowth |

Maximum Likelihood-Classification / Database: SIR-C Scene of April 1994  
 Rectified on ERS-1 GEC Product of August 1994  
 Multifrequency / Multipolarimetric SAR-Image CHH/LHH/LHV  
 MAP-filtered in 2 Iterations, 3\*3 and 5\*5 Moving Window



Fig. 2.25

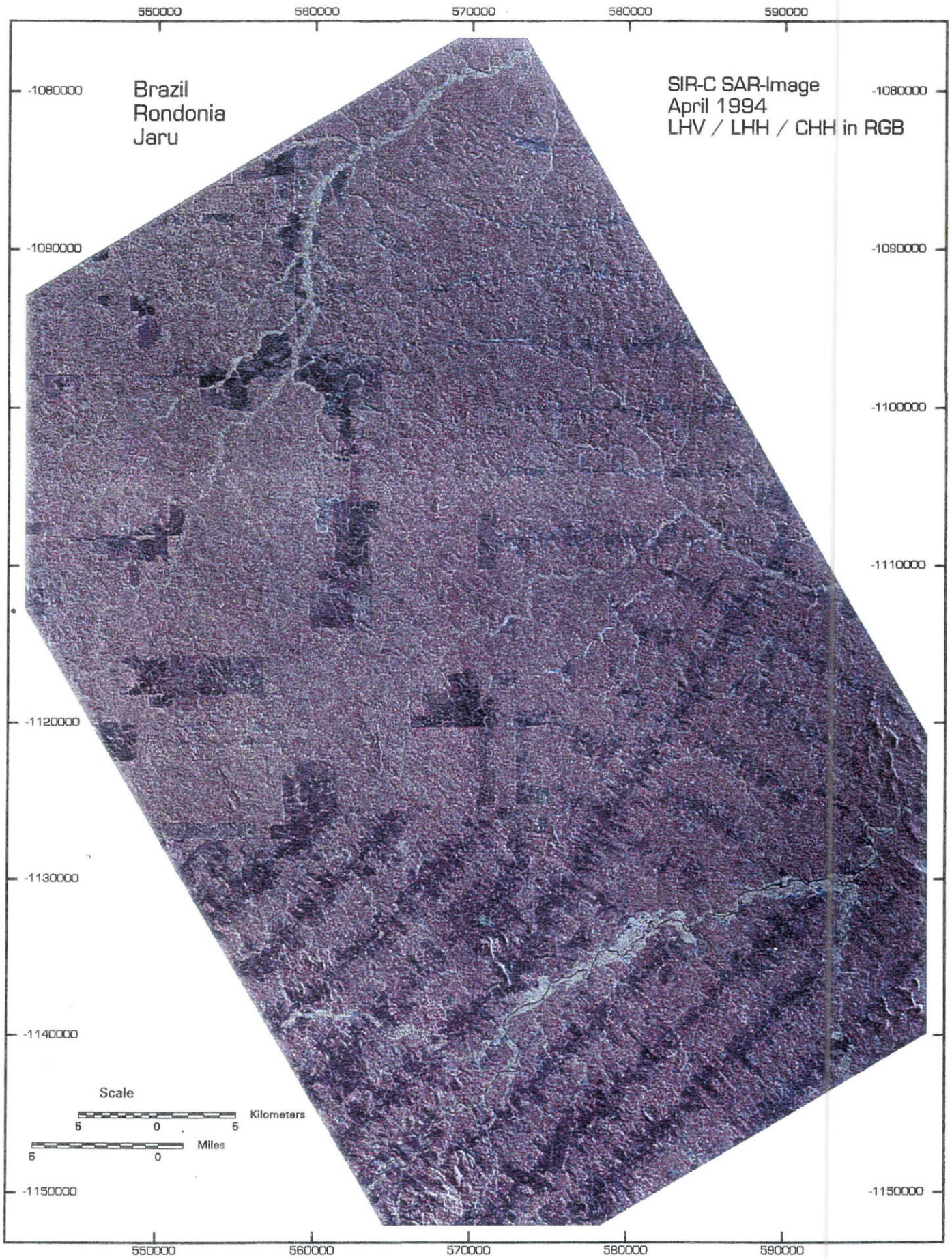


Fig. 2.26

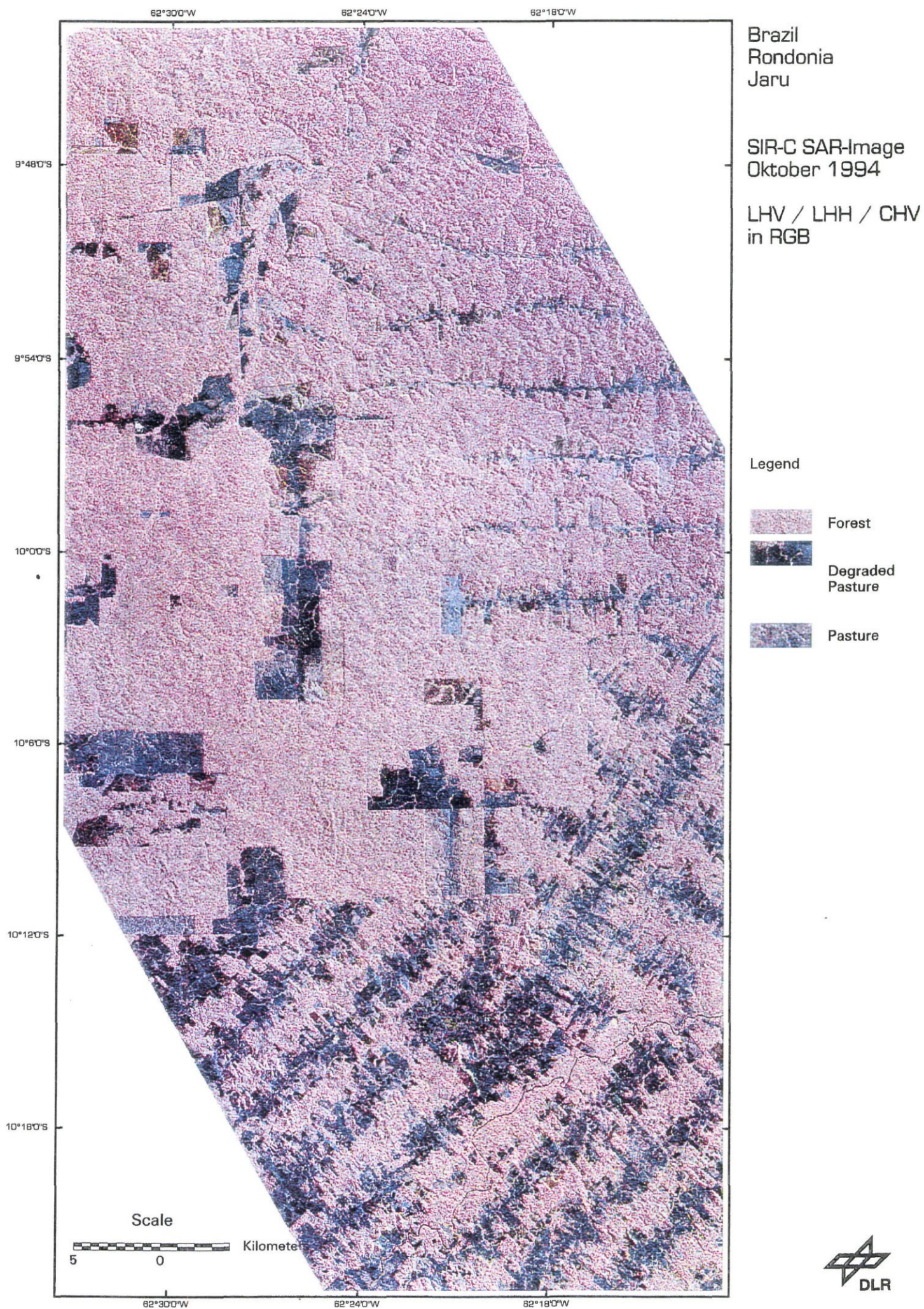
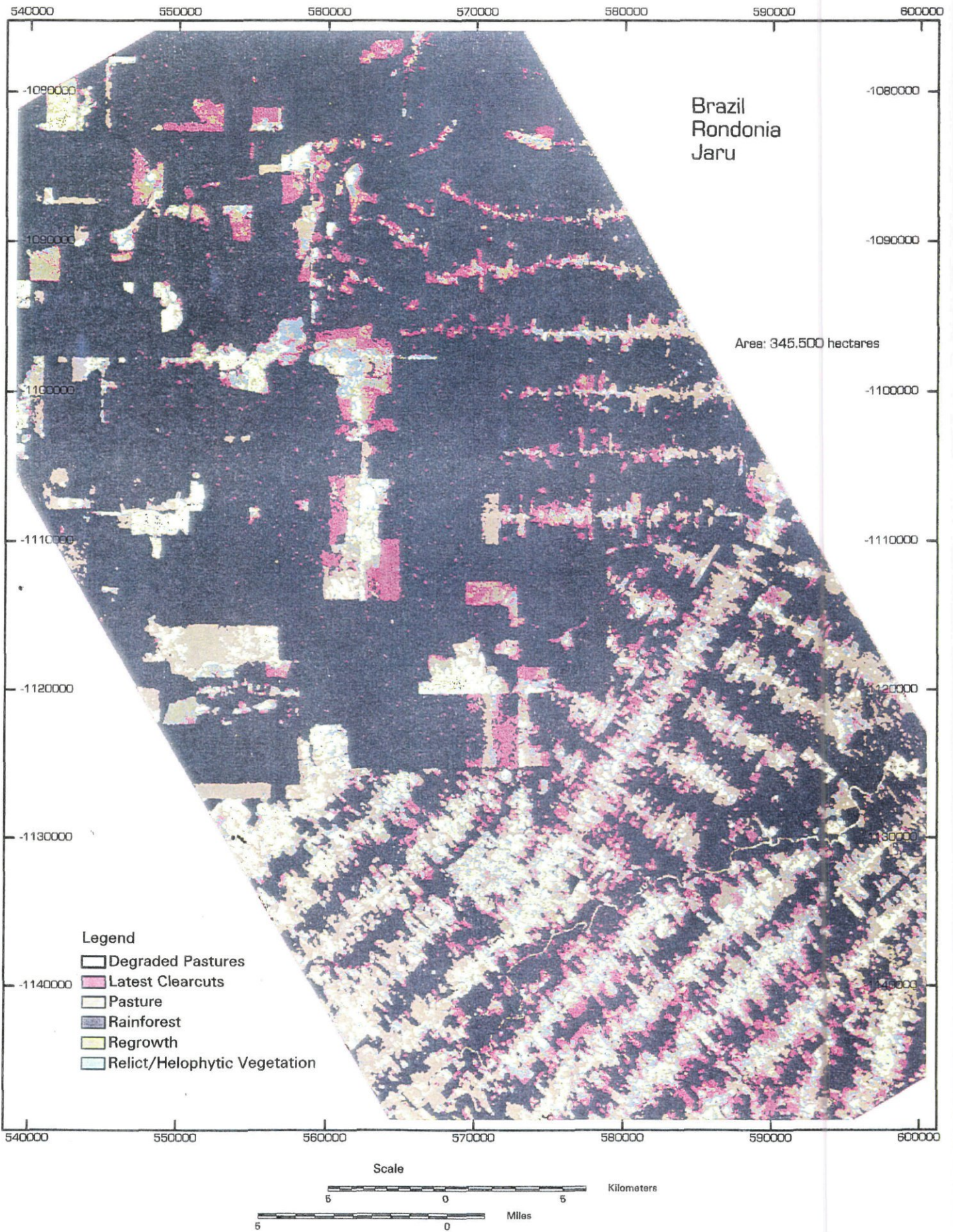


Fig. 2.27





Maximum Likelihood-Classification / Database: SIR-C Scene of October 1994  
 Rectified on ERS-1 GEC Product of August 1994  
 Multifrequency / Multipolarimetric SAR-Image CHV/LHH/LHV  
 MAP-filtered in 2 Iterations, 3\*3 and 5\*5 Moving Window



Fig. 2.28

### *Discussion of the results*

Optical satellite data have proved to be highly accurate and valuable for cartography of tropical areas. Nevertheless monitoring of these areas is somewhat impeded by the poor availability of optical data, due to weather conditions. Furthermore optical data have a low capability to estimate biomass. Biomass estimation in the near infrared is principally possible but works only in the earliest stages of regrowth, due to rapidly increasing leaf biomass and the resulting saturation in the wavelength. Also, optical data do not detect sub-canopy floodings, a land-cover class highly interesting for climate modelling, due to its functions as a CO<sub>2</sub> source.

SAR sensors have a different information depth and content depending on the frequencies and polarisations used. C-band SAR, as available from ERS-1/ERS-2 and SIR-C, offers quite satisfying abilities of forest/non-forest discrimination (Malingreau, 1994). ERS-1/2 data can be combined to multi-seasonal or multi-temporal products to further enhance and deepen information content. C-band data show stages of pasture degradation and different biomass levels of pastures in HV, VV and HH polarisations. Furthermore ERS-1/2 data are well suited for monitoring areas because of their 35 days repetition rate in the tropics. The combination of optical and SAR data also gives good results in mapping the land use pattern. In this work a combined product of TM and ERS-1 is presented and classified (see Fig. 2.29). An improvement in the automatic classification could not be achieved by this method. More classes could not be detected compared to an optical data set alone. Nevertheless, the visual interpretability was highly improved by imbedding of the relief information from the SAR data in the combination product.

In L-band SAR discrimination of forest and non-forest classes is especially well. L-HH is sensitive to sub-canopy floodings which are clearly discriminated (Fig. 2.26). The Japanese JERS sensor delivers good results in detecting and mapping these areas. The correlation of biomass in HV polarisations is high and increases when data of two frequencies are used. The saturation level is about 100 to 150 tons/hectare. Thus, early to middle stages of regeneration areas not older than ten years are detectable. Correlation in L-HH to biomass isn't that high, due to double bounce scattering on tree trunks. Different pasture stages are detectable. The use of biomass ratios improves separability of pasture classes.

Using SIR-C/X-SAR data discrimination of the following classes is possible:

- primary rainforest
- sub-canopy flooding (flooded rainforest along rivers)
- pastures
- degraded pastures (< 40% ground cover)
- overgrown pastures (with trees, palms or dead trunks, up to 10% ground cover)
- initial regrowth (1-4 years of age)
- intermediate regrowth (5-10 years)
- bare soils (dirt roads, badlands)
- fresh clearcuts (newly burned areas without vegetation cover)

Brazil  
Rondonia  
Jaru

TM-Bands: 3,4,5  
July 1994  
ERS-1-SAR Image  
August 1994

IHS-Transformation  
of TM 3,4,5  
Substitution of  
Intensity by ERS-1-Scene  
Retransformation to RGB

Legend

- Primary Rainforest
- Regrowth
- Pasture
- Fresh Clearcuts

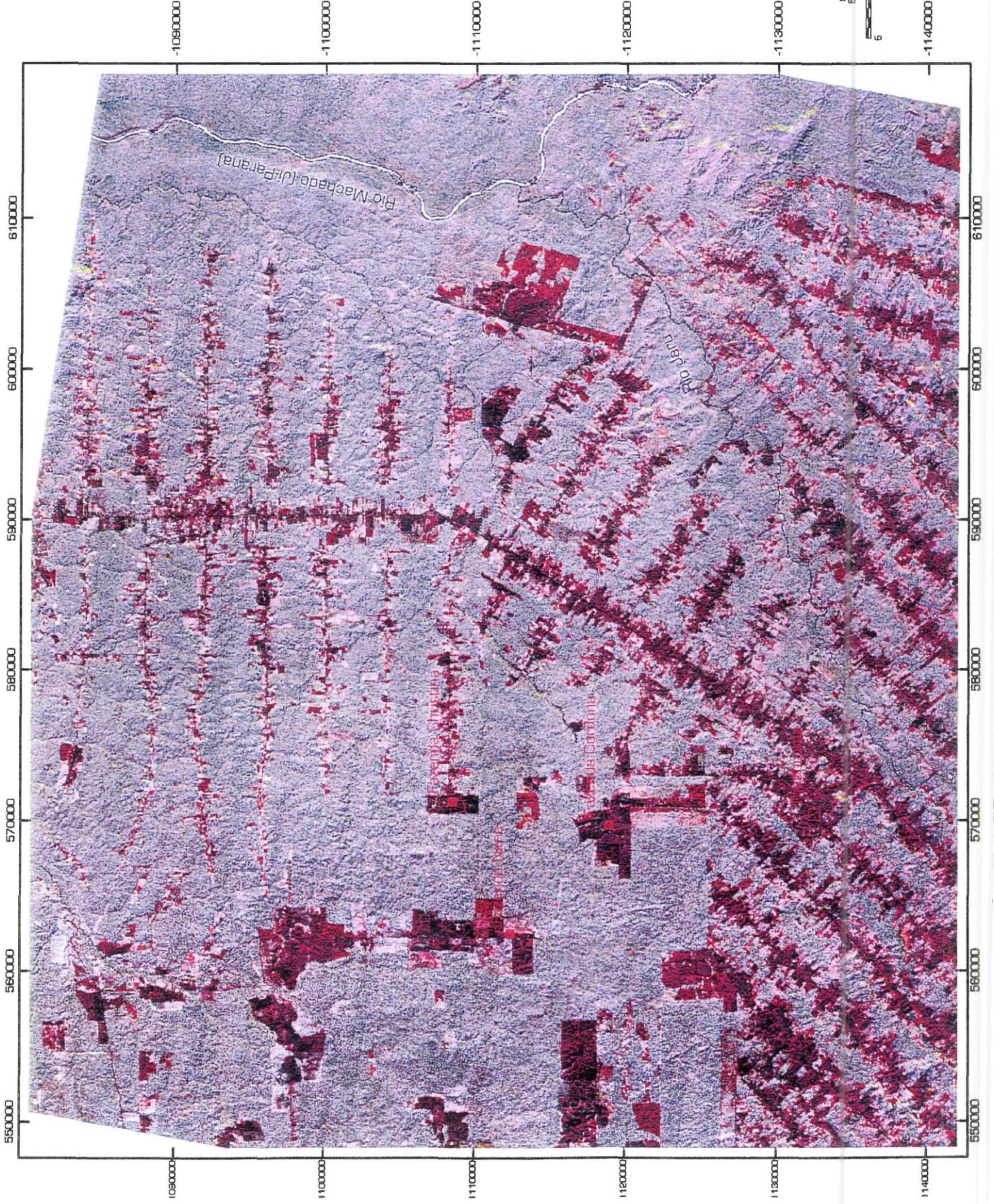


Fig. 2.29

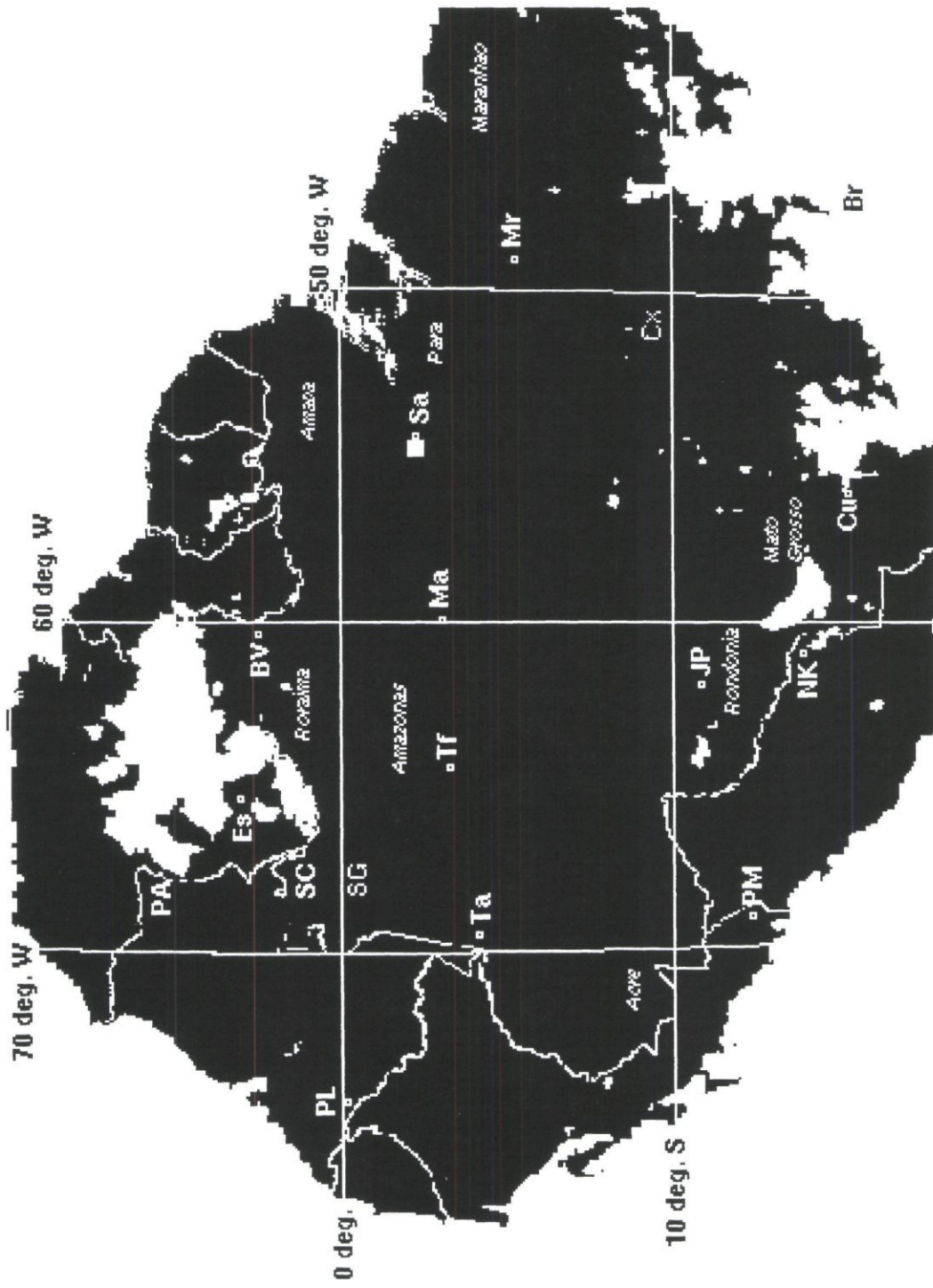


Fig. 2.30 Geographical locations mentioned in the text, including proposed study sites for L.B.I. State names are in italics. Site names are noted by initials: Br Brasilia, Cx Caixiana, Mr Maraba, JP Ji Parana, Cu Curitiba, Ma Manaus, Sa Santarem, Tf Tefe, Ta Tabatinga, BV Boa Vista, SG Sao Gabriel de Cachoeira, SC San Carlos del Rio Negro, Es La Esmeralda, PA Puerto Ayacucho, PL Puerto Leguisamo, PM Puerto Maldonado, NK Noel Kempff Mercado National Park.

The transfer of the experiences gained from the analysis of SIR-C L-band data to JERS data has yet to be done. However, SIR-C/X-SAR data with their high information content may be used to extrapolate information to the areas covered by sensors like JERS and ERS-1/ERS-2. Thus, SIR-C data being recorded in the rainy and dry season of 1994 data have to be regarded as profile data. These strips of high information density can be used to extrapolate information to data covering large-areas such as ERS-1/ERS-2 and JERS. Thus the small-scale landuse pattern of Rondônia and similar areas can be mapped accurately.

## **Glossary**

AMI Active Microwave Instrument: Imaging Microwave Sensor on board of ERS-1

AOI Area of Interest: Polygon used to extract an image section to train classifiers

EBIS Evidence Based Interpretations of Satellite Images: Classification algorithm

ERS-1 European Remote Sensing Satellite: SAR satellite

GEC Geocoded Ellipsoid Corrected: Image product projected on geoid

INCRA Instituto Nacional de Colonias e Reforma Agraria: Brazilian Institution

JERS Japanese Remote Sensing Satellite: SAR satellite

JPL Jet Propulsion Laboratory: American research centre

MLC Multi-Look Complex: Noise-reduced by averaging over multiple looks

PAD Projecto Assentamento Dirigido: Brazilian settlement directive

PRI Precision Image: Noise reduced-equal pixel sized image product

SAR Synthetic Aperture Radar: Sensor technique to achieve high ground resolution

SIR: Shuttle Imaging Radar-Mission C: Multifrequency / multipolarimetric SAR

TM Thematic Mapper: Optical Scanner on board of Landsat-5

X-SAR X-Synthetic Aperture Radar- X-band operating SAR

## **2.4 Biophysical stratification of the Amazon basin in support of LBA design (UMCP, DLR)**

### **2.4.1 Introduction**

Resources for field measurements are always limited, even in small field campaigns, and their optimal location is therefore a critical issue. The aim of this study was to explore techniques for sampling surface meteorological and vegetation conditions in a very large field measurement campaign. Not only did we require a sampling scheme that will optimize the information obtained from field measurements, but also a design for subsequent scaling up of the point field measurements to fields covering the entire study area. The immediate need for this work was in the context of the Large Scale Biosphere-Atmosphere Experiment in Amazonia (LBA) which will study the climatological, ecological, biogeochemical, and hydrological functioning of Amazonia, the impact of land use change on these functions and the interactions between Amazonia and the Earth system (LBA Science Planning Group 1996).

The study area in LBA has an area of approximately  $10^7$  km<sup>2</sup>, in which several intensive study sites, each sampling some local variation, will be arranged along two ecoclimatic transects. The approach adopted here applied techniques that have previously been explored for the design of a relatively small field measurement campaign (225 km<sup>2</sup> -the First ISLSCP Field Experiment - FIFE) (Michaelson et al., 1994).

Traditionally maps of land cover have been used for field stratification, since vegetation maps are considered to be highly diagnostic of surface conditions. Field sampling sites are usually allocated to the major vegetation types or along transects that follow the main gradients in vegetation variation. This is the approach that was adopted in the recent FIFE, BOREAS and HAPEX-Sahel field campaigns (Sellers et al., 1992; Goutorbe et al., 1994; Sellers et al., 1995a). Each of these field campaigns subsequently experienced problems in generalizing point measurements and processes to the larger domain and some of these problems may not have arisen if the field measurement resources had been more effectively deployed (Davis et al., 1990).

In the design of a measurement campaign it is important to recognize certain guiding principles. First, no one field sampling scheme is likely to be optimal for all purposes. Second, an explicit statistical design is essential if data are to be used to infer conditions anywhere beyond the field measurement points themselves. Third, the design of any set of measurements that will ultimately be applied to the basin as a whole must consider at the outset, not only the needs of each field measurement, but also its interpretation in the regional context.

The full list of variables needed for LBA will be long and complex. As a first step to experimental design we have selected net primary production (NPP), actual evapotranspiration (LE) and net surface radiation (Rn) at annual time steps to represent significant aspects of the carbon, energy and water balances. These three variables summarize the main themes of LBA at the most coarse spatial resolution to be addressed, that of the Amazon basin.

Although the temporal resolution used in this stratification is annual, this is not meant to imply that other time steps are less important, nor that only observations at an annual time step should be used in planning of the sampling schemes. Variables of interest may be more or less important in different places and at different times and there may be interactions. For example sites having the same annual integrated values could have very different seasonalities. Nevertheless the problem is best first addressed with the coarsest time resolution of interest and so annual total NPP, and mean LE and Rn are analyzed here.

Neither NPP, LE nor Rn, nor any other variables can be measured everywhere in the study region and so some selection of field measurement sites is necessary. How this should be done is the issue we addressed. Considerations of accessibility, logistics etc. are not explored. Subjective judgement and experience will always play a part in the final stratification but attempts at more objective decision making are valuable, even if they only act as guides and checks. The starting points here were fields of data for the region consisting of modeled fields of NPP, LE and Rn, spatial outputs of other models, satellite observations, interpolated fields from point observations. Some highly interpreted maps of surface properties such as vegetation and soils were used to analyze the results.

Various mechanistic models exist that can estimate fields of NPP, LE and Rn. If these models could be forced with the available fields of data, then sensitivity analyses could be undertaken and the sampling sites could then be selected on the basis of the spatial fields to which the models are most sensitive. The allocation of sampling sites might well be weighted by the proportion of the study area that experiences each level of the spatial variable, since it would not be worth allocating major resources to the accurate measurement of very extreme conditions that occurred in a very small part of the region. Equally those ranges of the controlling variables that have the strongest control over the dependent variable should be emphasized. The best models for spatial estimation of Rn and LE are climate reanalysis models which cannot be forced with the available spatial fields of data. In the case of NPP the available fields are adequate to drive a model such as GLO-PEM (Prince & Goward 1995), but a formal sensitivity analysis would be excessively complex.

The key requirement was to prioritize forcing variables in a hierarchical scheme that could identify the most important variables. If sensitivity analyses of well-validated, mechanistic models were available, the rank order of importance of variables could be determined and their geographical distributions used to locate optimal sampling sites. Without these sensitivity analyses, empirical, statistical models have been substituted here. Although subject to all the potential problems of non-mechanistic models, such as correlations that are specific to the calibration data set and do not apply to the study area as a whole, it must be recognized that the results of sensitivity analyses of mechanistic models themselves are notoriously model dependent (e.g. PILPS 2c, Y. Xue, personal communication).

Given that modeled, spatial fields of NPP, LE and Rn exist, it would be easy to stratify the study area using these dependent variables directly. This approach was rejected since, at best, the stratification would simply divide the range of values of the

variable in question and would not identify areas in which the same annual total was caused by very different seasonality, or different combinations of limiting factors. Moreover the classes would not take account of the areas in each range and, without adjustment, would overweight rare and extreme values. Our aim, rather, was to classify the region in terms of the correlation structure between the putative forcing variables and NPP, LE and Rn so that the mechanisms by which the values of NPP, LE and Rn arose would form the classification, and not simply to sample the range of values.

A crucial issue is the extent to which the correlation structure of the forcing variables, derived empirically, can represent the mechanisms by which they control the dependent variables. Here the choice of the independent, forcing variables used in the analysis was critical. Obviously non-mechanistic correlations will occur with a certain frequency, even among totally unrelated data sets. The independent variables should therefore be ones that are not only available as fields for the entire region but also are ones identified in mechanistic studies as being potential determinants. Beyond the use of well-chosen, independent variables, the desirable properties of the classification technique include a hierarchical structure in which the most significant class divisions are made first, an explicit dependent and independent variable structure and the ability to express non-linear and non-additive relationships in a simple form.

Michaelson et al. (1994) used regression tree analysis (RTA) for a very similar purpose in connection with the much smaller area of the FIFE measurement campaign. There were noted advantages of the method over more traditional linear and additive models, such as multiple regression, multi-way analysis of variance, indicator species analysis based on correspondence analysis, and linear discriminant analysis. As in many classification techniques, RTA divides the population of spatial samples into increasingly homogeneous subsets according to optimal decision rules that are derived from the relationship between the values of the independent and dependent variables for the samples. These splits create a hierarchical tree structure that can be pruned to obtain a robust tree and can be terminated at any desired level of significance or number of classes. Finally the tree can be used to classify the samples and the class membership can be displayed in a map.

It was anticipated that an objective, empirical model of key spatial LBA variables would find application not only in the development of an optimal sampling design for future field and airborne measurement campaigns in LBA, but also in the post-measurement campaign when point measurements will be used to estimate continuous fields of data for the Amazon basin as a whole. RTA will then be a candidate technique for developing empirical relationships between field measurements and variables that can be obtained for the whole basin using techniques such as remote sensing. The trees developed using the local field measurements and the corresponding remotely sensed variables can then be used to estimate the desired variables from those spatially-continuous, surrogate variables that are identified as the determinants.



RTA was applied to the entire Amazon basin with Rn, LE and NPP as dependent variables. In addition an RTA of NPP alone was performed for a smaller area extending from Rondônia, Brazil to northeastern Santa Cruz, Bolivia to assess the potential for this approach for finer-scale stratification. This smaller area was well known and several maps of the vegetation at high spatial resolution were available as well as detailed land cover maps of deforestation from Landsat TM (Skole & Tucker, 1993; Lawrence & Chomentowski, 1992). We report on the hierarchy of subdivisions of the population of pixels included in each analysis, identifying the most significant subdivisions of the values of the dependent variables. Also the geographical distribution of the final classes of pixels are examined, in particular from the point of view of measurements site selection.

#### **2.4.2 Regression trees applied to land classification**

The data set consisted of a set of two-dimensional arrays, each array having the dimensions of latitude and longitude. Arrays of dependent and independent variables were prepared in raster format at a spatial resolution of 8 x 8 km for the entire Amazon basin. The aim was to classify each grid cell according to the independent variables so that the best prediction of the dependent variables could be made. A classification technique was required that had the following characteristics.

1. Subdivides the study area into uniform domains of grid cells (strata) which could be used to indicate where field measurements are necessary.
2. Capture the full range of variability that is relevant to the estimation of the dependent variables (NPP, LE and Rn) throughout the study area.
3. Select the simplest stratification scheme with minimum within stratum variability and maximum between stratum variability.
4. Have an explicit dependent variable and independent, predictor variables to perform the classification.
5. Display results in a binary (single-link) tree-structure in which the most important classification criterion is specified first, with successively less important ones made in order.
6. Capable of expressing non-linear and non-additive empirical relationships in a simple form. Non-linear relationships exist where there are thresholds in the dependent variable as a result of smooth changes in predictor variables. Non-additive situations occur where the relationship between the dependent and predictor variables depends on the value of one or more of the other predictor variables; for example photosynthetically active radiation may be positively related to NPP in the cloud-covered central Amazon basin, but negatively related in the seasonal margins of the basin.
7. Can include categorical (class) and continuous (numerical) variables.

RTA is described by Breiman et al. (1984) and its application to the stratification of a biophysical measurement campaign is discussed in detail by Michaelson et al. (1994). Hansen et al. (1996) discuss the application of RTA to land cover classification using remotely sensed data and DeFries et al. (in press) and Cialella et al. (1997) give examples of other applications. On the basis of the results reported in these earlier studies, RTA was selected for the present application.

An RTA starts with the full set of grid cells and ends with a series of terminal nodes that contain homogeneous sub-sets of grid cells. The tree is composed of a series of divisions defined by specific values from the distributions of independent variables,  $x_1, \dots, x_n$ , that provide the best explanation of the distribution of a dependent variable,  $y$ . Beneath each division of an  $x_i$  are either further divisions of  $x_i$  or 'nodes' with estimated values of  $y$ . The hierarchical structure of regression trees allows reduction of very complex models to simple ones by 'pruning' the tree, i.e. by limiting the number of terminal nodes. Selecting a relatively simple tree with few estimates of  $y$  is thus a quantitative means of stratifying  $y$  based on its relationships with  $x_1, \dots, x_n$ .

### 2.4.3 Methods

In order to stratify the entire Amazon basin and neighboring humid tropical forest, we chose the best available data sets that are spatially continuous over lowland tropical South America and which can be expected to be related to the dependent variables. Table 2.7 lists the fields of climate and surface variables we obtained, their characteristics and sources. No doubt some of these variables are surrogates for the variables that actually determine  $R_n$ , LE and NPP. Some potentially important variables were excluded for lack of reliable, comprehensive data sets, such as soil organic matter, nutrient status, land cover and vegetation type.

The data sources used had a range of spatial and temporal resolutions. NDVI, PAR and inundation were derived from satellite data and had spatial resolutions from 8 km to  $1^\circ \times 1^\circ$ . Clearly the coarser resolution data sets are likely to have degraded amplitudes owing to the sampling. Temperature and rainfall were from long-term, climatological averages from ground stations interpolated and gridded to  $0.5^\circ$ .  $R_n$  and LE were from the ISLSCP CD-ROM and were at  $1^\circ \times 1^\circ$ , the coarsest resolution used. Most of the original data were monthly or 10-day averages. We re-calculated long-term monthly averages for all fields. From these we calculated long-term annual sums and indices of seasonality, e.g. monthly minimum, amplitude, and number of months below a threshold (Table 2.7). This last step was performed in order to exclude effects of temporal phase differences between the northern and southern hemispheres while preserving information about seasonality.

All data sets were geographically co-registered using nearest neighbor re-sampling where necessary. A sinusoidal projection was used with a  $60^\circ$  meridian (False Easting/Northing -6671692.500000 E, 0.000000 N). Since the study area was close to the equator, all grid cells were approximately of equal area ( $8 \times 8$  km). The values from coarser resolution data sets were replicated in neighboring pixels.

Table 2.7 Data sources and pre-processing for all fields in the regression tree analysis. Sources are 1) AVHRR Pathfinder University of Maryland Product (Agha et al., 1994), 2) Leemans and Cramer, 1991, 3) Eck and dye, 1991, 4) Choudhury, 1989, 5) ISLSCP CD-ROM (Sellers et al., 1992), and 6) Prince and Govard, 1995

Variable	Ref.	Spatial Scale	Yrs. of data	Pre-processing	Indices used in Tree
NDVI	1	8 km	'83-'86	4 yr. monthly avgs. calculated, PAL AVHRR 8km Pathfinder product, Solar zenith angle correction re-done at U. Md.	Monthly mean, min., amp.
Precipitation	2	0.5 deg.	Long-term	Reprojected from Lin. Lat. Lon., Long-term monthly avgs. calculated	Annual sum, monthly min., amp. No. months w/ > 50 mm, 100 mm, 150 mm
Minimum Temperature	2	0.5 deg.	Long-term	Reprojected from Lin. Lat. Lon., Long-term monthly minimum T° calculated	Monthly mean, min., amp.
PAR	3	1 deg.	'79-'89	Estimated from the Total Ozone Mapping Sensor (TOMS), Reprojected from Lin. Lat. Lon., Long-term monthly avgs. calculated	Monthly mean, min., amp.
Soil Inundation	4	0.5 deg.	'79-'85	Reprojected from Lin. Lat. Lon., Estimated from SMMR microwave polarization difference index (MPDI)	Monthly mean, min., max., amp.
Net Radiation	5	1 deg.	'87-'88	Reprojected from Lin. Lat. Lon., Monthly avgs. calculated	Annual sum
Latent Heat	5	1 deg.	'87-'88	Reprojected from Lin. Lat. Lon., Monthly avgs. calculated	Annual sum
NPP	6	8 km	'87	Monthly sums calculated from decadal (10 day) sums.	Annual sum

Table 2.8 Correlation coefficients among variables used in regression trees

	Rain sum	Rain min	Rain amp	Par sum	Par min	Par amp	NDVI mean	NDVI min	Tmin mean	SMMR mean	Rn sum	LE sum	NPP sum
Rain sum	1.000	0.718	0.241	-0.419	-0.466	0.020	0.256	0.421	-0.003	-0.162	0.100	0.327	0.430
Rain min		1.000	-0.453	-0.551	-0.647	-0.044	0.228	0.408	-0.002	-0.084	-0.060	0.176	0.409
Rain amp			1.000	0.383	0.379	0.231	-0.043	-0.081	-0.008	-0.038	0.360	0.288	-0.084
Par sum				1.000	0.872	0.354	-0.298	-0.396	-0.008	0.125	0.525	0.279	-0.458
Par min					1.000	-0.085	-0.267	-0.406	-0.003	0.093	0.370	0.132	-0.460
Par amp						1.000	-0.093	-0.063	-0.016	0.046	0.327	0.259	-0.047
NDVI mean							1.000	0.885	0.006	-0.397	-0.020	0.096	0.731
NDVI min								1.000	0.003	-0.355	0.042	0.220	0.777
Tmin mean									1.000	-0.044	-0.015	-0.015	0.008
SMMR mean										1.000	-0.029	-0.079	-0.315
Rn mean											1.000	0.948	0.024
LE mean												1.000	0.208
NPP sum													1.000

Table 2.9 Total variance and unexplained variance in tree models of net radiation (Rn), latent heat (LE) and net primary production (NPP). Values in parentheses are percent unexplained variance

	Total variance (%)	7 node tree variance	13 node tree variance
<b>Entire Area:</b>			
Rn	5.16 x 10 <sup>15</sup> (100)	2.13 x 10 <sup>15</sup> (41)	1.52 x 10 <sup>15</sup> (29)
ET	4637 (100)	2125 (63)	742 (37)
NPP	9.49 x 10 <sup>8</sup> (100)	3.56 x 10 <sup>8</sup> (38)	3.18 x 10 <sup>8</sup> (34)
<b>Rondonia Window:</b>			
NPP	7.34 x 10 <sup>7</sup> (100)	3.53 x 10 <sup>7</sup> (48)	3.02 x 10 <sup>7</sup> (41)

The study area in this exercise was defined as broader than the Amazon basin alone. A window was selected from 12° N, 81° W to 18° S, 41° W. Within this window we analyzed only areas below 500 m and with an annual mean NDVI above a lower limit (1.68 NDVI months) which effectively selected all South American tropical lowland forest and *cerrado* (seasonal woodland), most of which are in the Amazon and Orinoco basins. A regular grid was then used to sample 8 km pixels from within this area. This sample, totaling 23,000 observations, was used to develop the regression trees. A smaller area, in which only NPP was analyzed, spanned the Brazilian-Bolivian border between Rondônia and northeastern Santa Cruz (9°9'30" S, 64°20' W to 15°12'20" S, 59°30'10" W). All 8 km pixels within this area were analyzed.

RTA was undertaken using the S Plus statistical package (Becker et al., 1988). Following the approach suggested by (Venables et al., 1994), we grew trees using 60% of the sample data, pruned trees with an independent 20% of the data, and estimated model errors with the remaining 20%. For each dependent variable, we estimated trees with 7 and 13 nodes. These numbers of classes were chosen since the LBA expects to have resources for less than 20 study sites. Maps of these trees were created by applying the binary divisions to the entire image data.

#### **2.4.4 Data sets**

The data sets that were used in the RTA are listed in Table 2.7. Below we give additional information where necessary to assist in the interpretation of the results.

##### ***Inundation***

Following (Giddings & Choudhury 1989) we used the microwave polarization difference index (MPDI) calculated from the Scanning Multichannel Microwave Radiometer (SMMR) carried on the Nimbus-7 satellite. The signal responds to open water and is thus able to detect *igapó* and *várzea* forests as well as inundated savannas. There is evidence that its sensitivity is limited by closed tree canopies (J. Melack, personal communication) and so it is probable that the MPDI indicates only the more open flooded areas.

##### ***Normalized Difference Vegetation Index (NDVI)***

The NOAA NASA AVHRR Land Pathfinder 8 x 8 km monthly composite NDVI product was used (Agbu & James 1994). These data were re-corrected for solar zenith angle at the University of Maryland Laboratory for Global Remote Sensing Studies.

##### ***Photosynthetically Active Radiation (PAR)***

Monthly estimates of incident photosynthetically active radiation were obtained from the data set prepared by Eck & Dye (1991) and Dye et al. (1995) using the Total Ozone Mapping Spectrometer (TOMS).

##### ***Precipitation and Air Temperature***

Climatological air temperature and precipitation was obtained from the Leemans & Cramer (1991) data base at 0.5° x 0.5° resolution.

### *Net radiation and Latent Heat*

We obtained fields of the dependent variables Rn and LE from the International Satellite Land Surface Climatology Project (ISLSCP) Initiative 1 data sets (Meeson et al., 1995; Sellers et al., 1995b). ISLSCP calculated Rn and LE from climate assimilation-forecast models of the European Centre for Medium Term Weather Forecasts (ECMWF) and the National Meteorological Center (NMC).

### *Net Primary Production (NPP)*

NPP was obtained from the GLObal Production Efficiency Model (GLO-PEM) (Prince & Goward 1995), a mechanistic model forced by global satellite data that takes account of the PAR absorbed by the vegetation, and the limitation to potential production owing to vapor pressure deficits, high and low air temperature and soil moisture. NPP was obtained from gross primary production using a respiration algorithm based on biomass.

## **2.4.5 Results**

### *Amazon basin*

Net radiation and latent heat were the most strongly correlated variables in the data set used for this study (Fig. 2.31, Table 2.8). These variables were both products of climate assimilation-forecast models and were derived from the same data sources (Sellers et al., 1995b). Their correlation is no doubt a result of the fact that they are both strongly related to the total energy available at the land surface. Annual NPP was highly correlated with annual NDVI, as is expected since  $F_{APAR}$  is a primary driver in the NPP model used to generate NPP (Prince & Goward, 1995) and, as Fig. 2.31 suggests, annual NDVI together with incident PAR defines a maximum, or potential annual NPP. With the exception of the high correlation between annual NPP and NDVI, all other correlations between independent variables and Rn, LE and NPP were at a level less than  $r = 0.53$ . Among the other variables, the highest correlations were between annual averages and minimums of the same variable, e.g. rainfall, PAR and NDVI. Annual rainfall and PAR were inversely related, suggesting that clouds influence tropical PAR distribution (Dye, 1992) and NPP (Grace et al., 1995).

The RTA models for Rn and LE were somewhat similar, as was to be expected since these two variables were highly correlated (Table 2.8). 59% of the variation in Rn was explained by a 7-node tree, and 71% by a 13-node tree. Likewise, 54% of the variation in LE was explained by a 7-node tree, and 62% by a 13-node tree (Table 2.32). For both Rn and LE, annual and monthly minimum rainfall and PAR were selected to form most of the binary splits, with minimum temperature and number of months with less than 150 mm rainfall being next in importance (Figs. 2.32, 2.33).

In the RTA model of NPP, 62% of the variation in NPP was explained by a 7-node tree, and 66% by a 13-node tree (Table 2.9). Monthly minimum NDVI, annual NDVI and annual PAR formed most of the splits in the NPP tree, with minimum temperature and number of months with less than 150 mm rainfall at lower levels of significance (Fig. 2.34).

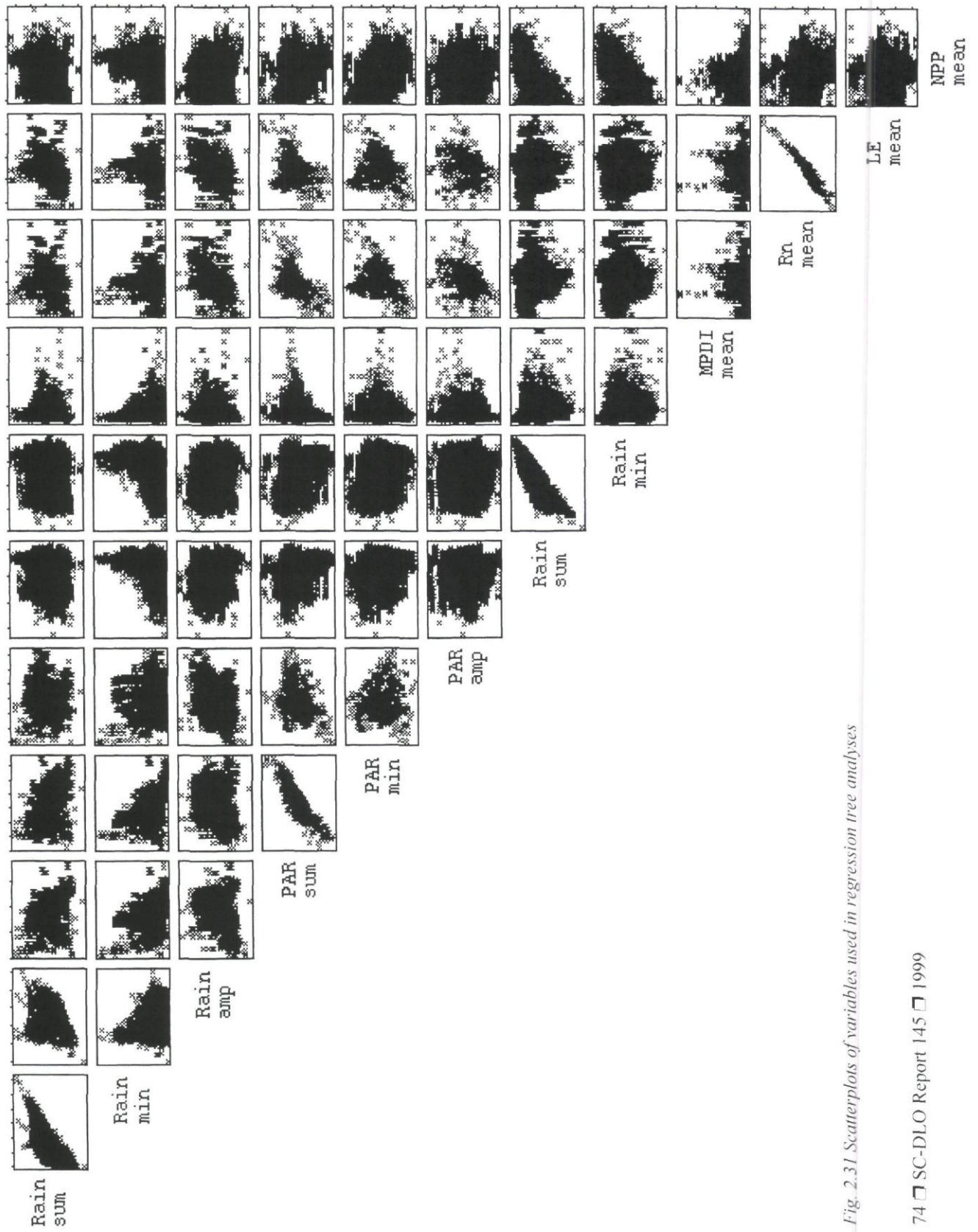


Fig. 2.31 Scatterplots of variables used in regression tree analyses

netrad2.test.best13.tree

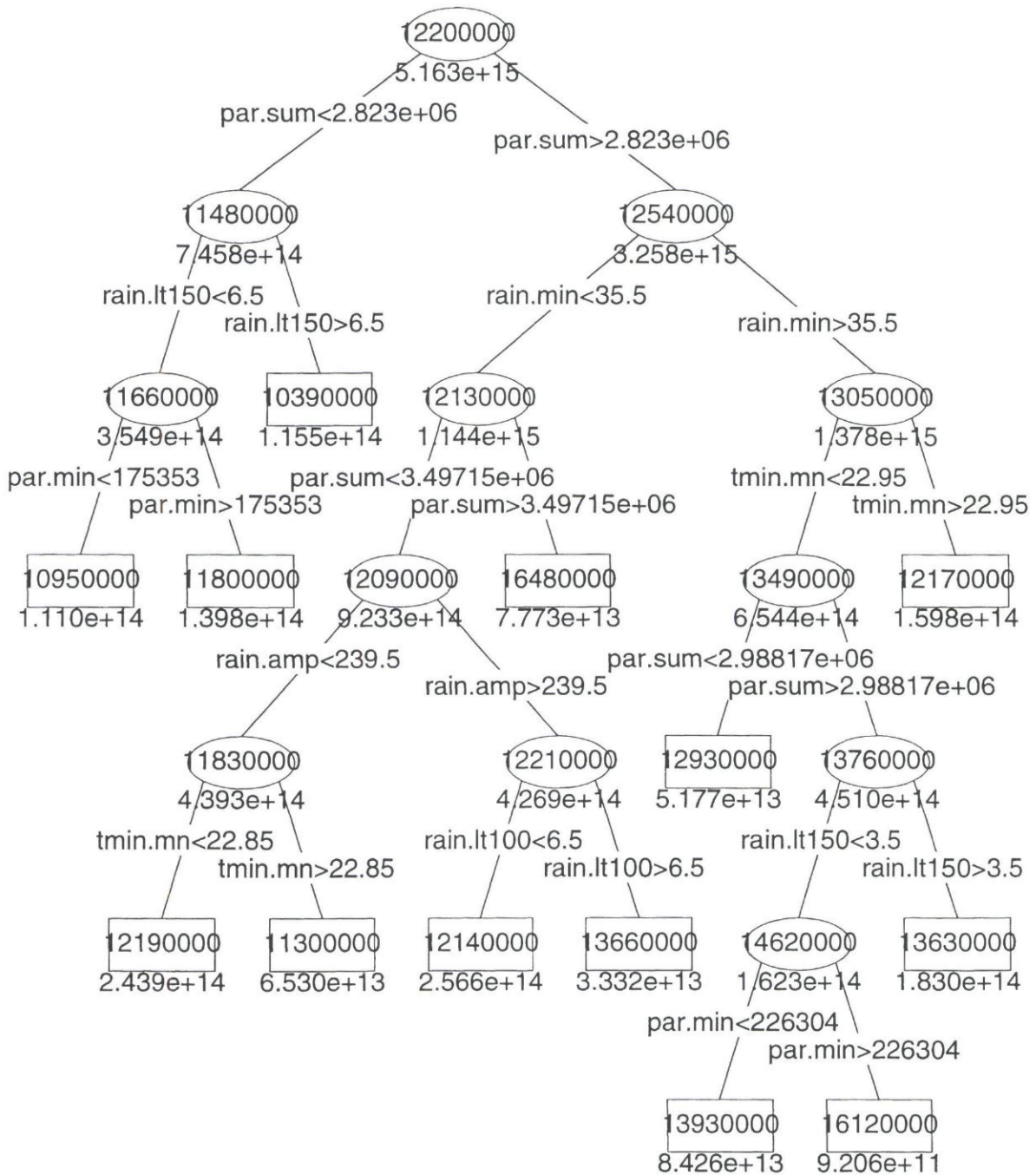


Fig. 2.32 Regression tree of annual net radiation (Rn). Values in boxes are means of predicted Rn values for terminal nodes; values in ellipses are means for branched nodes. Values underneath are within class variances. Units are  $W m^{-2}$ .



le3.test.best13.tree

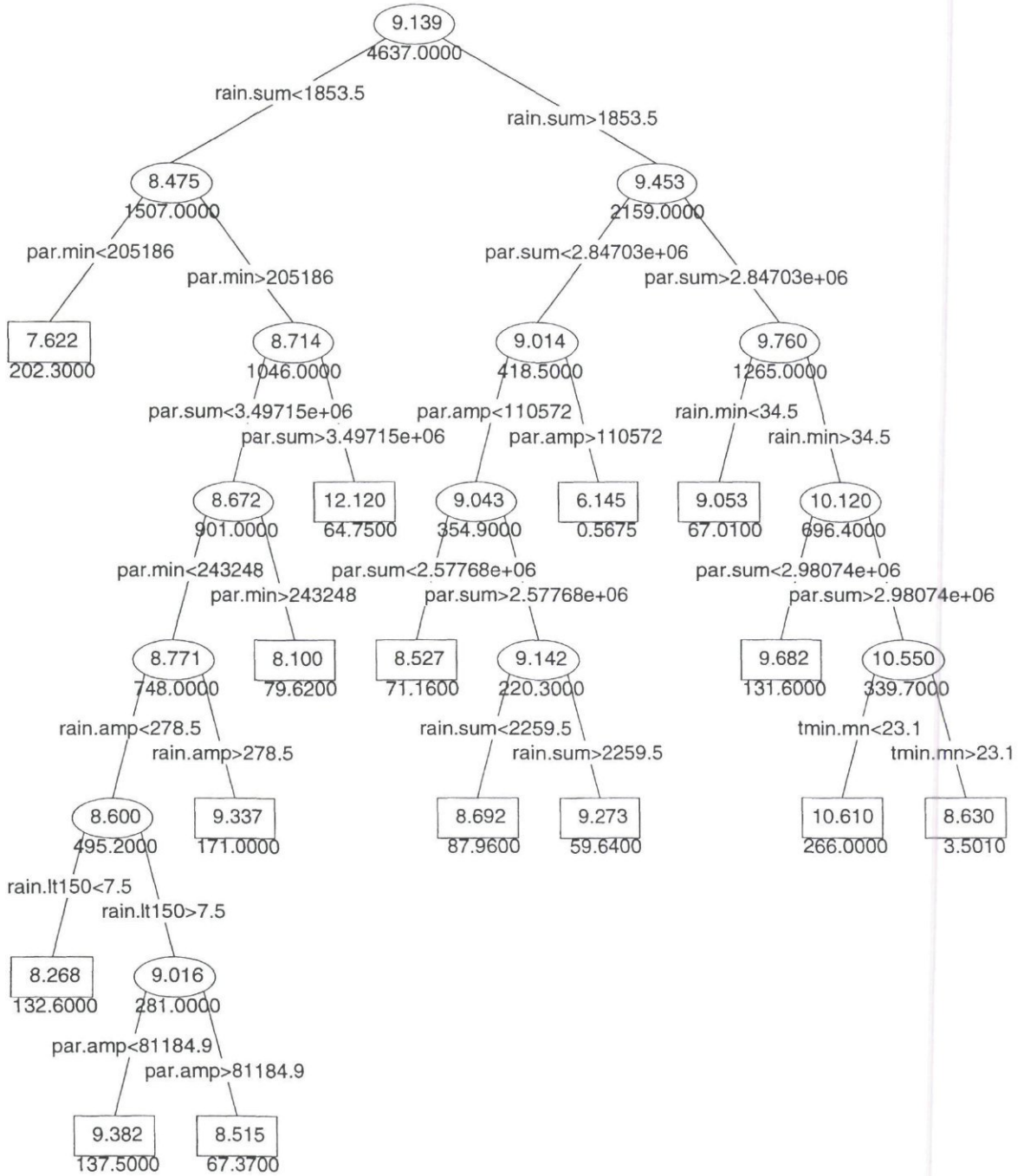


Fig. 2.33 Regression tree of annual latent heat (LE). Values in boxes are means of predicted LE values for terminal nodes; values in ellipses are means for branched nodes. Values underneath are within class variances. Units are  $\text{mm } 12d^{-1}$ .

npp.win1.test.best13.tree

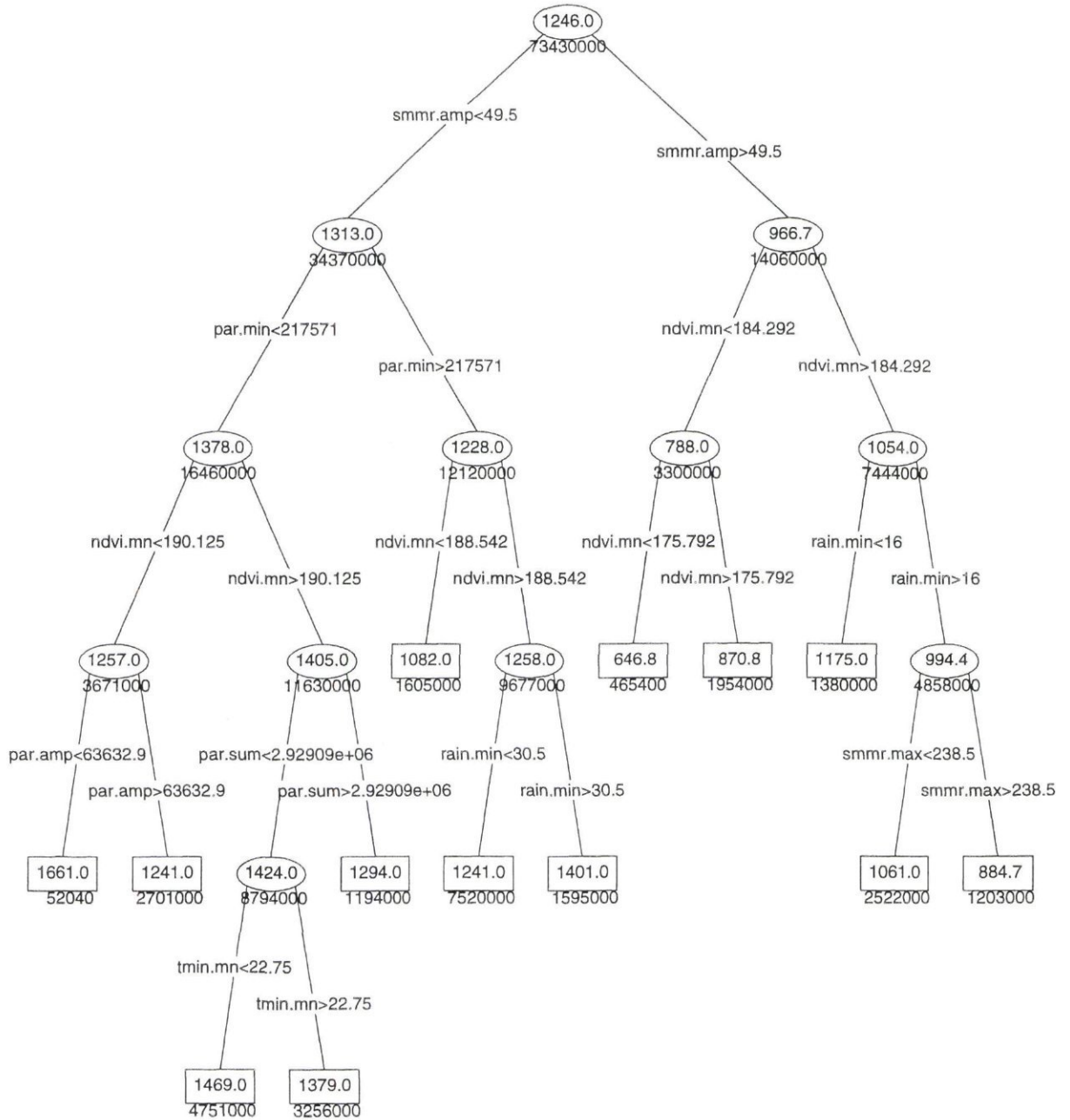


Fig. 2.34 Regression tree of annual net primary production (NPP). Values in boxes are means of predicted NPP values for terminal nodes; values in ellipses are means for branched nodes. Values underneath are within class variances. Units are  $gC\ m^{-2}\ yr^{-1}$ .

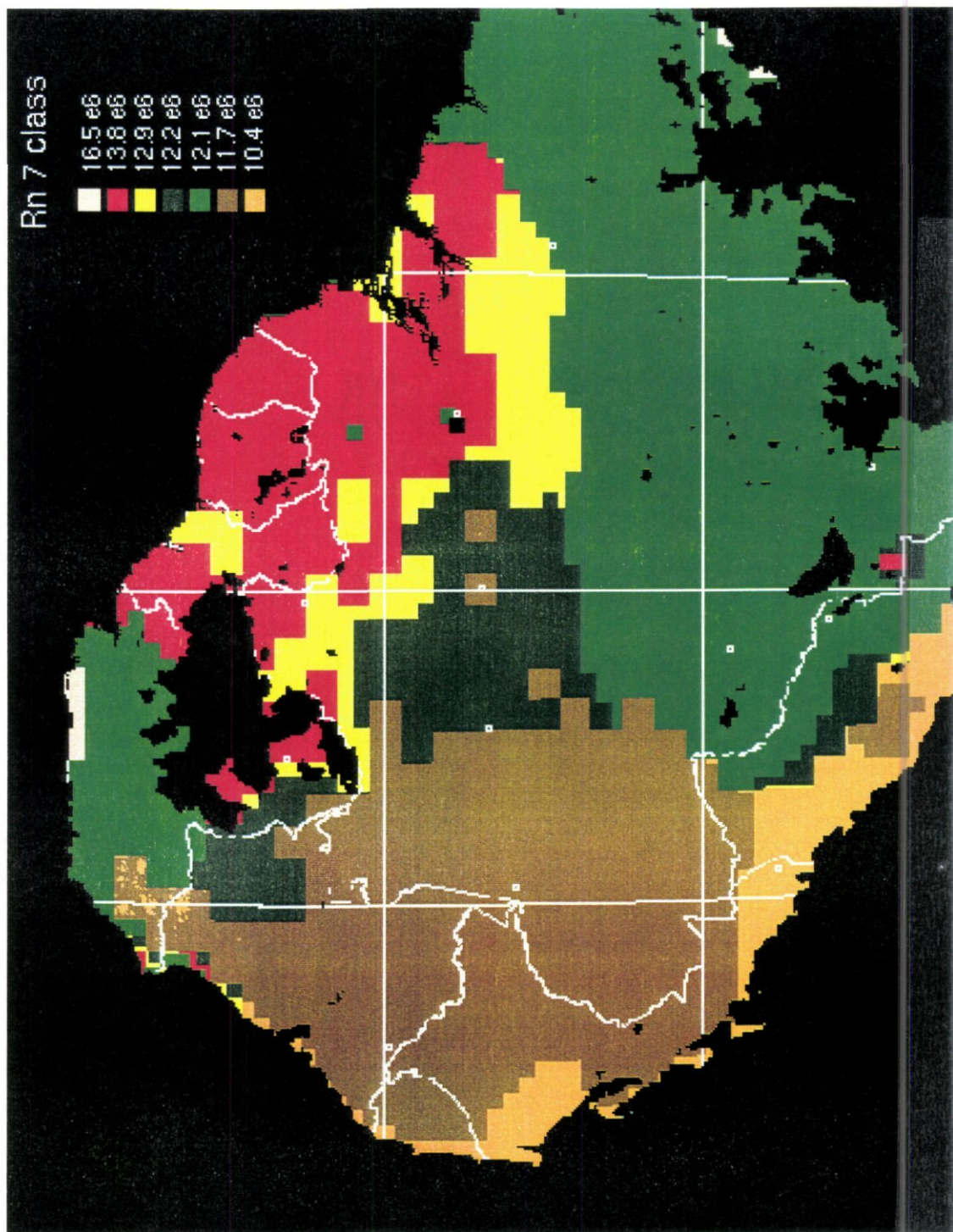
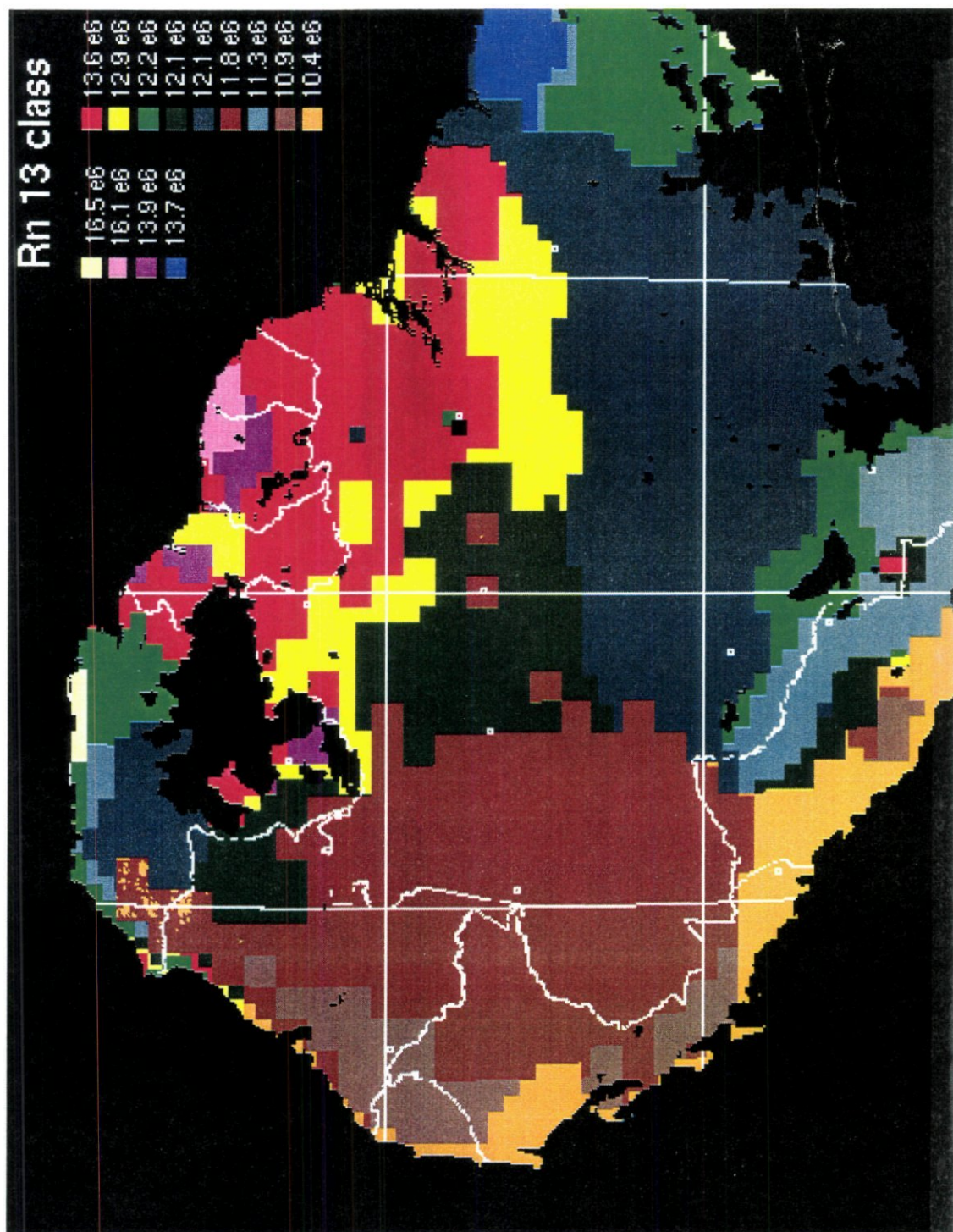


Fig. 2.35a Maps of classes derived from regression tree analyses: net radiation (Rn) 7-class



*Fig. 2.35b Maps of classes derived from regression tree analyses: Rn 13-class.*

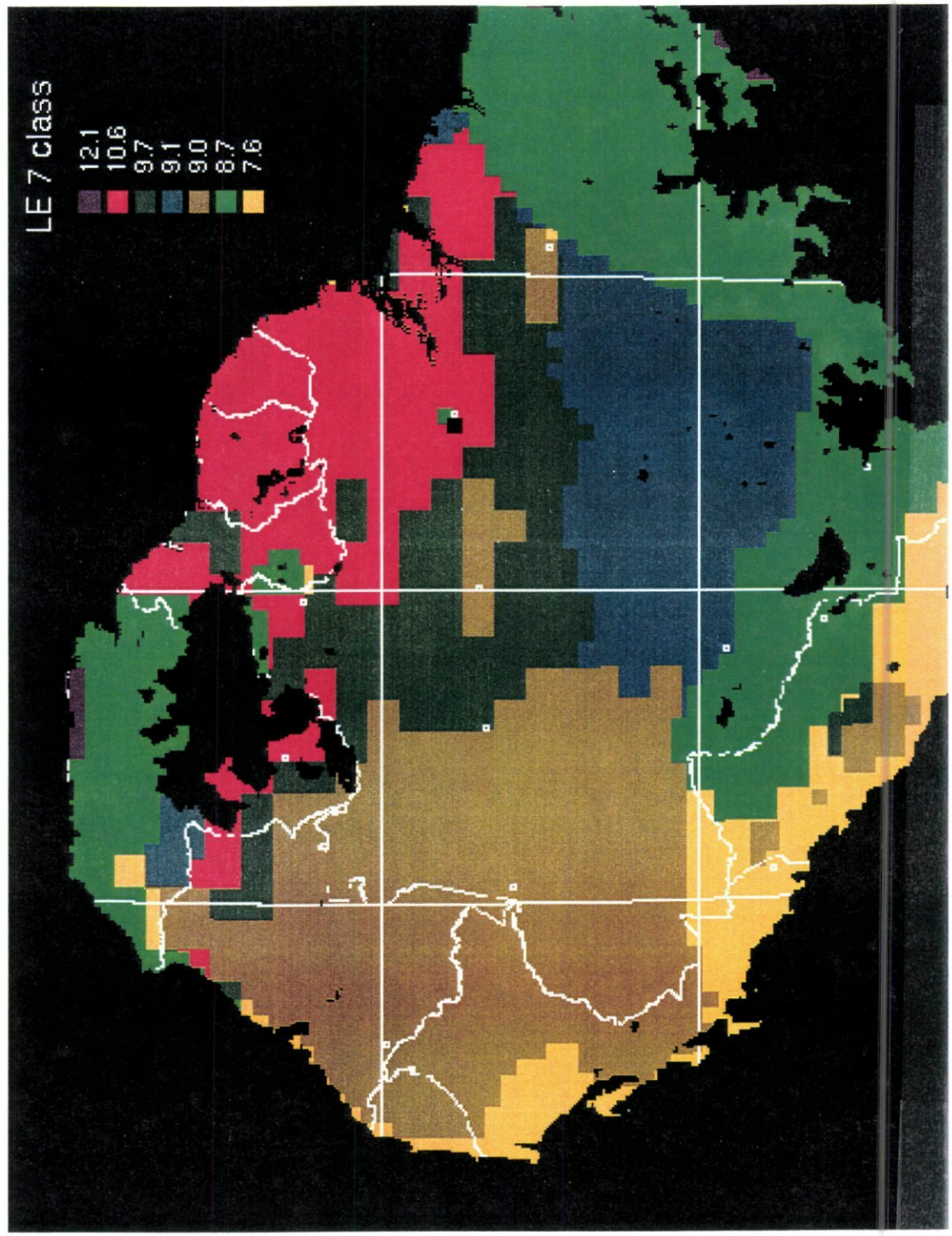


Fig. 2.35c Maps of classes derived from regression tree analyses: latent heat (LE) 7-class

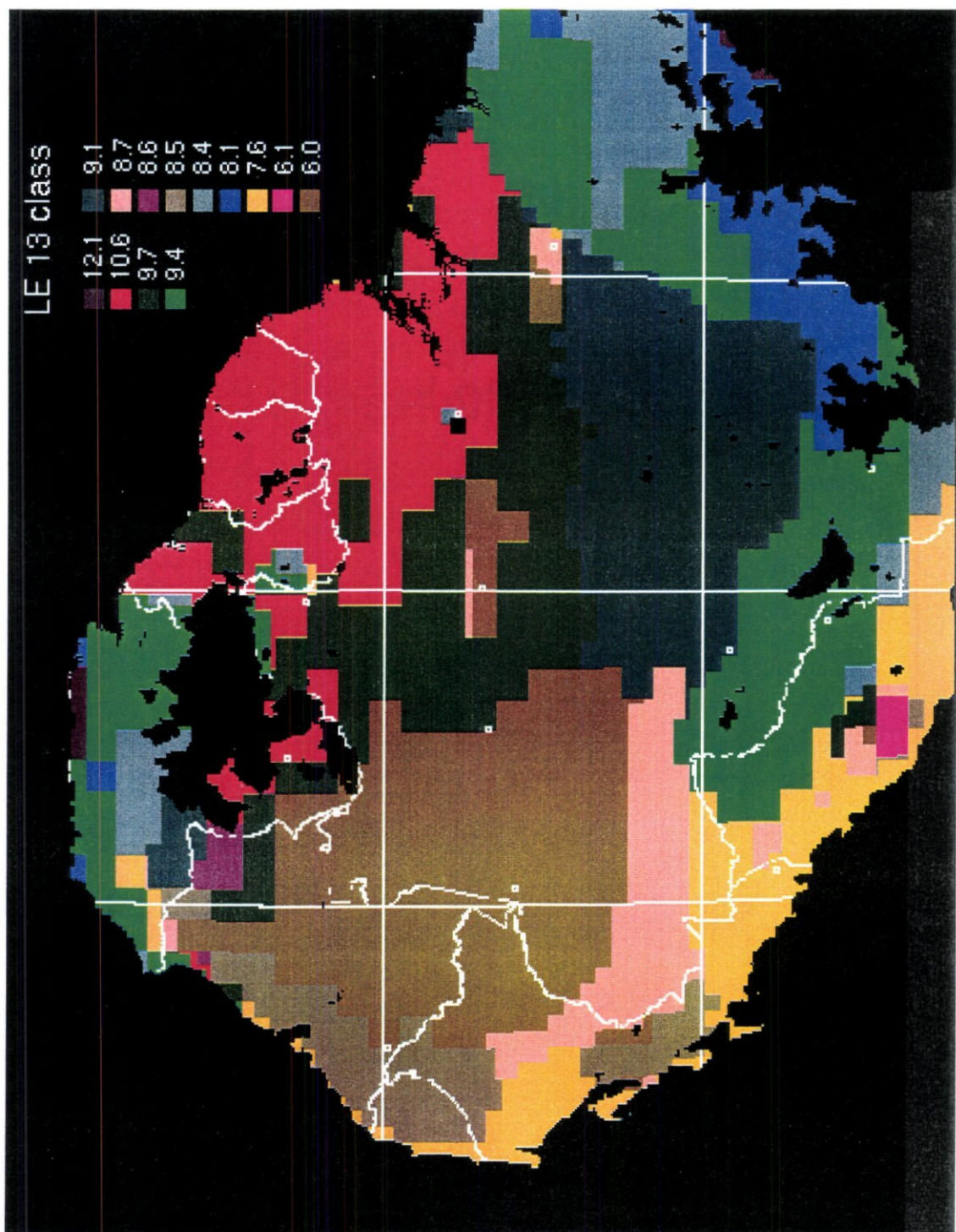


Fig. 2.35d Maps of classes derived from regression tree analyses: latent heat (LE) 7-class; LE 13-class,

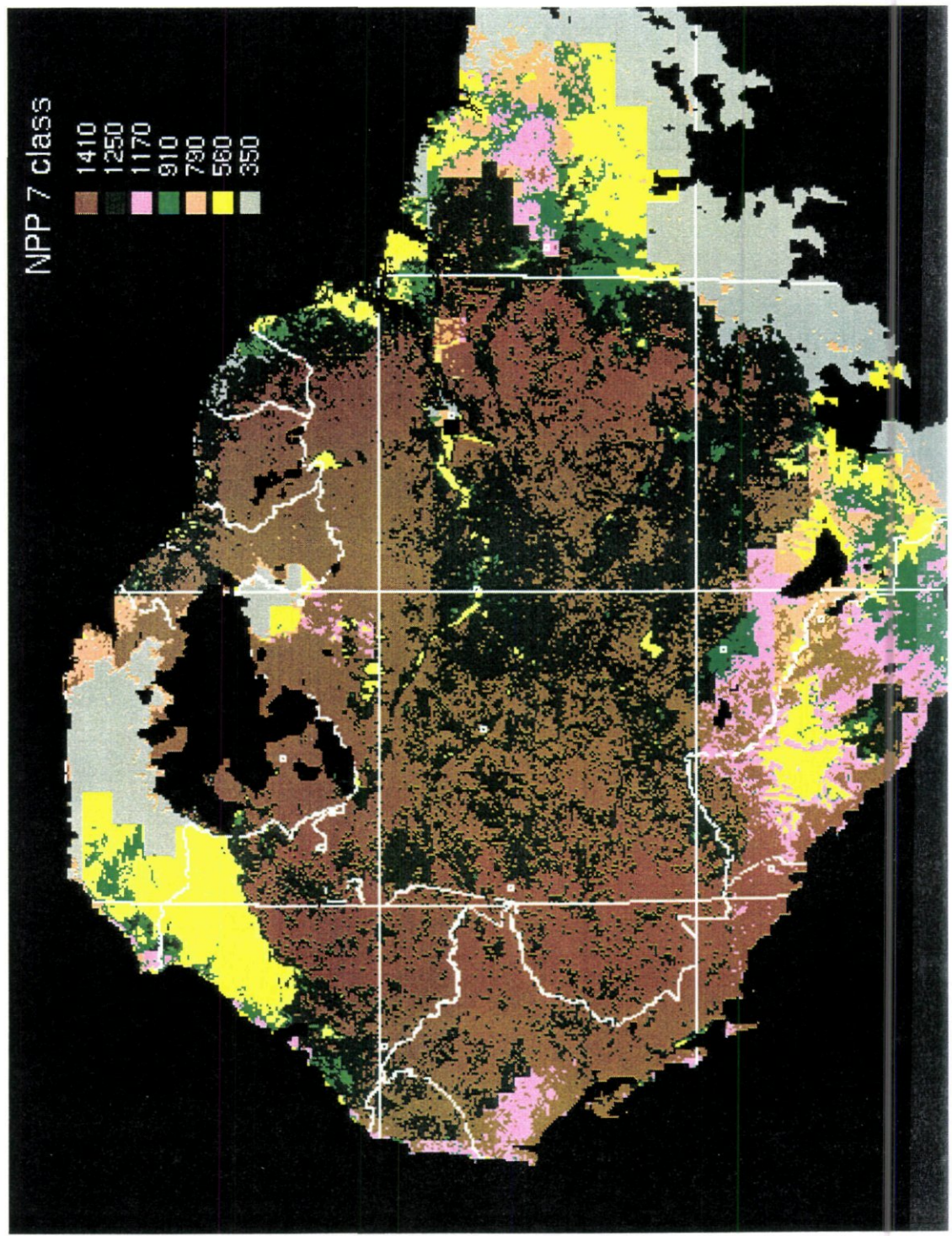


Fig. 2.35e Maps of classes derived from regression tree analyses: latent heat (LE) 7-class: net primary productivity (NPP) 7-class

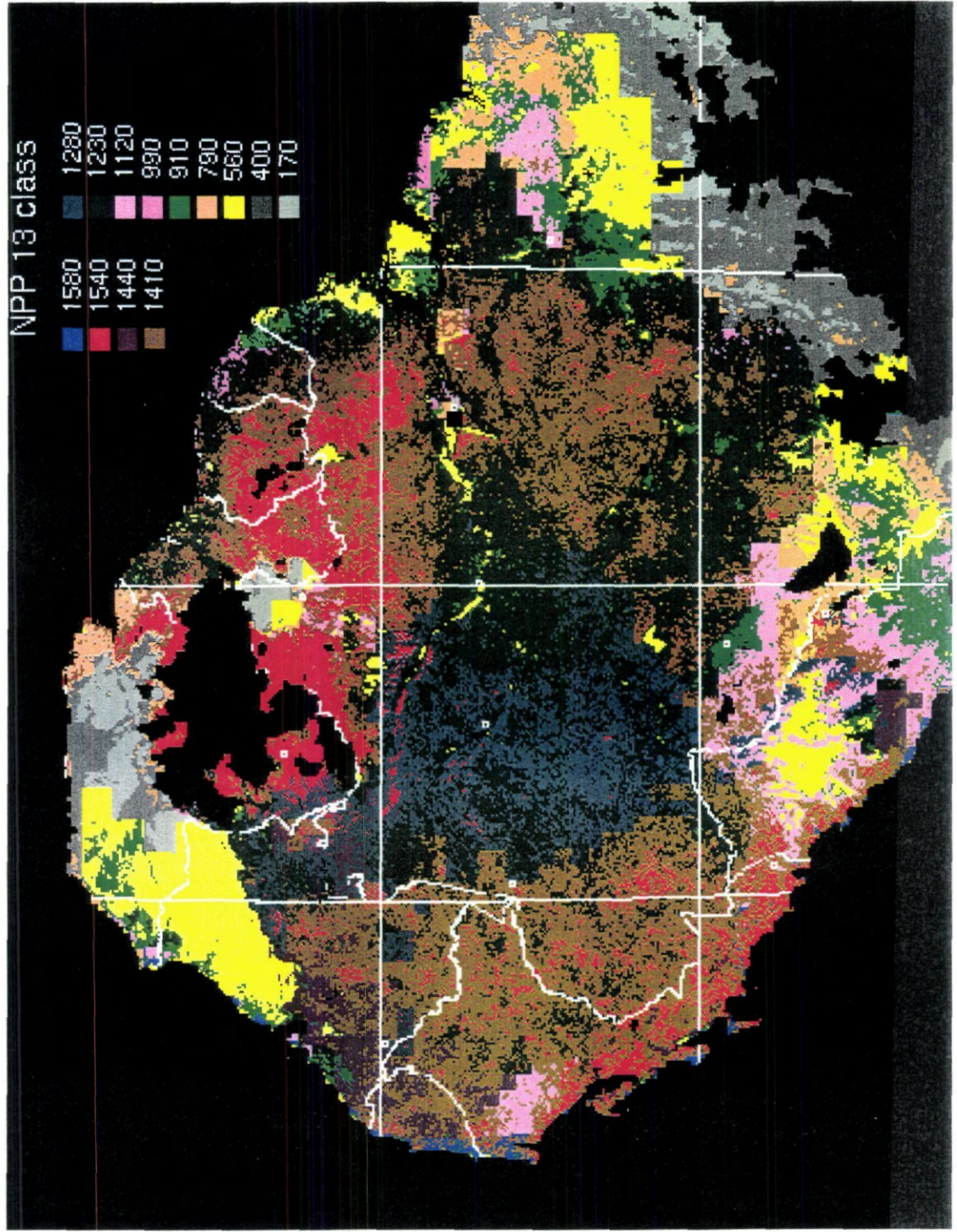


Fig. 2.35f Maps of classes derived from regression tree analyses: latent heat (LE) 7-class: net primary productivity (NPP) 7-class: NPP 13-class. Units for Rn are  $W m^{-2}$ , for LE are  $mm 12d^{-1}$ , for NPP are  $gC m^{-2} yr^{-1}$ .



The basin-wide geographical distributions of the pixels placed in each of the terminal nodes are shown in Fig. 2.35. All pixels having the same color belong to the same terminal node or class. The strength of the relationships between each node can be found by reference to the appropriate RTA tree (Figs. 2.32, 2.33 and 2.34). The 13-node results are nested within the 7-node tree, for example in the NPP maps the red (mean NPP = 1540 gC m<sup>-2</sup>yr<sup>-1</sup>), blue-gray (1280 gC m<sup>-2</sup>yr<sup>-1</sup>) and brown (1410 gC m<sup>-2</sup>yr<sup>-1</sup>) in the 13-node tree are all combined as brown (1410 gC m<sup>-2</sup>yr<sup>-1</sup>) in the 7-node tree.

The distribution of classes of Rn and LE were quite similar (Figs. 2.35 a, c). In both 7-class maps, the entire western Amazon basin was one large class of low PAR and Rn and moderate LE (dark brown; Rn=11.7x10<sup>6</sup>, LE=9.0), flanked by a class (light brown; Rn=10.4x10<sup>6</sup>, LE=7.6) along the southwestern Andean foothills (note, all land over 500m was eliminated from the analyses). Both Rn and LE 7-class maps had a class in the center of the basin around Manaus (dark green; Rn=12.2x10<sup>6</sup>, LE=9.7) and large classes for Guianan forest (red; Rn=13.8x10<sup>6</sup>, LE=10.6) and southeastern Amazonia (LE light green, =8.7 and blue-gray =9.1; Rn light green = 12.1x10<sup>6</sup>). The latter class also occurred in the Venezuelan Llanos. The central Amazonian and Guianan regions had the highest estimates of annual Rn and LE while the central and southeastern regions had moderate estimates of Rn and LE. Lowest values were consistently in the cloudy Andean foothills.

Comparison of the 13-class and 7-class maps for both Rn and LE suggest that the variation in these two variables can be captured in relatively few classes. Several of the additional classes in the 13-class map are small areas in northern Venezuela. Three classes of Rn in seasonal forest occur; in Maranhão (blue) and western Mato Grosso and Rondônia (light green, light blue); they are distinguished from the large southeastern Amazonian basin class in the 13-class map (blue-gray) based on the number of months with less than 150 mm rainfall and minimum temperature. The only other large class in the 13-class maps of Rn (light brown, 10.9x10<sup>6</sup>) and LE (light brown, 8.5) is one along the northwestern Andean foothills which is less seasonal than its southwestern counterpart.

Some regions separated by the stratifications of Rn and LE are also distinguished in the maps of the stratification of annual NPP. The largest class in the 7-class map of estimated NPP represents the highest predicted value of NPP (brown, 1410 gC m<sup>-2</sup>yr<sup>-1</sup>), and includes most of the western Amazon and Guianan forests. A central Amazonian class around Manaus again appears, identifying a region of lower NPP than the surrounding areas (dark green, 1250 gC m<sup>-2</sup>yr<sup>-1</sup>). This class extends into northern Rondônia and parts of eastern Pará.

The classes with the lowest predicted NPP are found the eastern and southern Amazon basin (light green, 910 gC m<sup>-2</sup>yr<sup>-1</sup>) and gray 350 gC m<sup>-2</sup>yr<sup>-1</sup>). These classes are distinguished by high values of annual PAR and number of months with less than 150 mm of rainfall. The Venezuelan Llanos, the Bolivian Beni, the Pantanal and *várzea* forests along the lower Amazon are all represented as a single class, also with low annual NPP (yellow, 560 gC m<sup>-2</sup>yr<sup>-1</sup>). Brazilian *cerrados* and Venezuelan deciduous woodlands also have low predicted NPP (gray, 350 gC m<sup>-2</sup>yr<sup>-1</sup>). Another class of seasonal forest, distinguished by relatively high NDVI and NPP appears to

include most of the fragmented seasonal forests of Pará, Rondônia, Mato Grosso and eastern Bolivia (light green, 910 gC m<sup>-2</sup>yr<sup>-1</sup>).

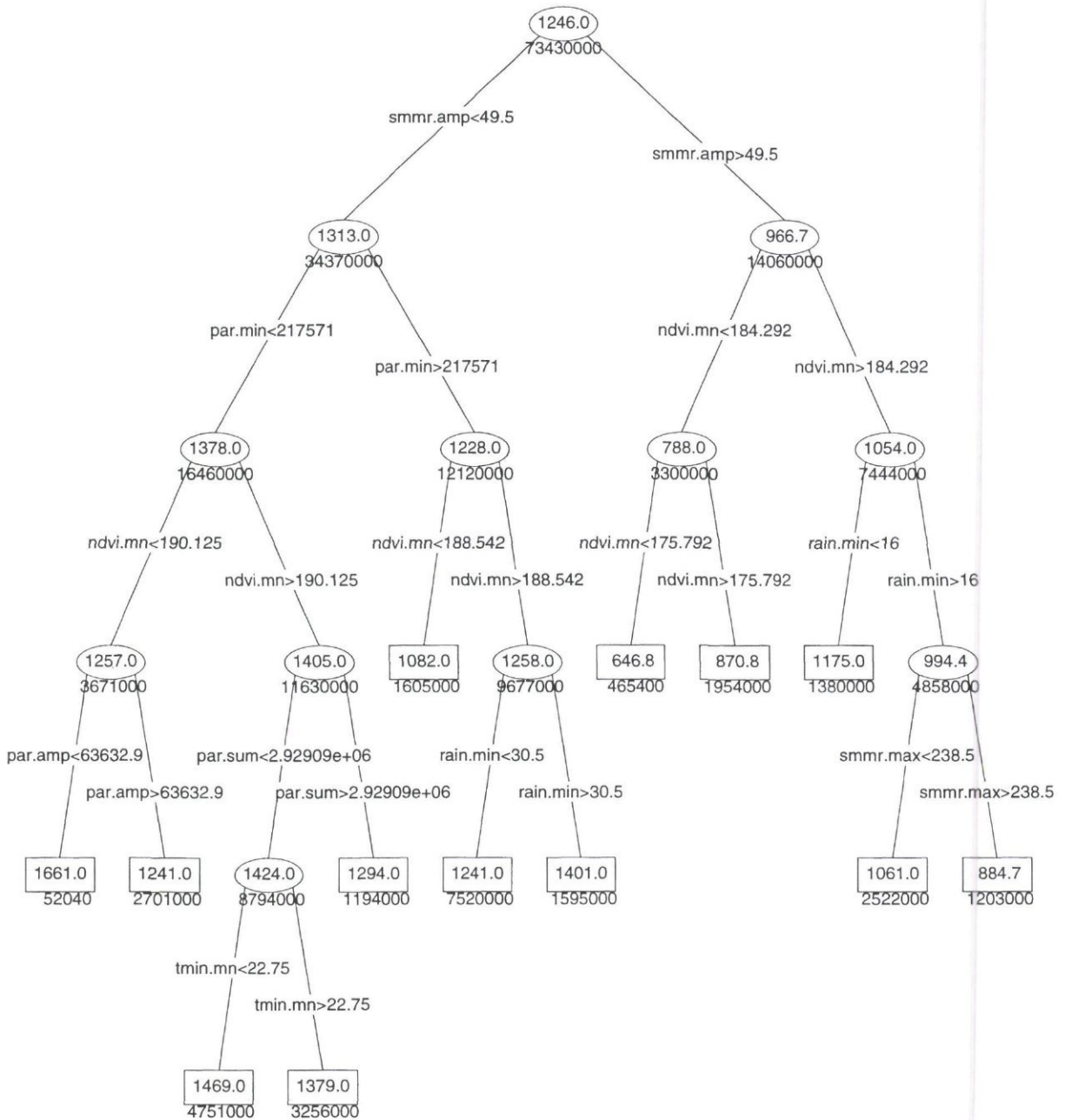
As in the case of the stratification of Rn and LE, comparison of the 7 and 13-class NPP maps suggests that there is little need to stratify beyond 7 regions in this study area. Several of the new classes in the 13-class map represent small areas around the periphery of the study area. In the 13-class map, narrow strips of pre-montane forest are delineated along the Andean foothills in Colombia and Ecuador (dark purple and bright blue). These classes are distinguished by their unusually low PAR and minimum temperature and high NPP. Seasonal forests in the southern and eastern Amazon are further divided in the 13-class map based on annual PAR (light brown, 790 gC m<sup>-2</sup>yr<sup>-1</sup>) and minimum temperature (light pink, 1120 gC m<sup>-2</sup>yr<sup>-1</sup>). Other classes of seasonal forests, *cerrados* and inundated savannas were unchanged from the 7-class map (light green, yellow, light brown).

The most significant difference between the 7 and 13-class maps of predicted NPP was the subdivision of the large class of high NPP in the Guiana and Surinam and to a lesser extent in the SW Andean foothills. The new class had a very high annual NPP (red, 1540 gC m<sup>-2</sup>yr<sup>-1</sup>). In Venezuela the boundary of this class closely follows the boundary between 'tall non-inundated evergreen forest' and sclerophyllous (*caatinga*) forest (Huber 1995). An intermediate class between the western and central Amazon basin regions was distinguished (blue-gray, 1230 gC m<sup>-2</sup>yr<sup>-1</sup>) having a lower mean monthly minimum temperature than western Amazon basin and a higher minimum NDVI than central Amazonia. The spatial pattern from central to western Amazonia was thus primarily defined by differences in monthly minimum NDVI, PAR and minimum temperature. These variables probably indicate differences in cloudiness and altitude.

#### **Rondônia - NE Santa Cruz**

The RTA for Rondônia, Brazil to northeastern Santa Cruz in Bolivia allowed the results to be validated at a finer scale than was possible for the larger domain. The primary split of NPP in the Rondônia window (Fig. 2.36) was on the annual amplitude of the SMMR MPDI, an index of inundation. Seasonally inundated savannas were further divided based on mean NDVI and monthly minimum rainfall (light and dark brown). PAR and NDVI accounted for the splits among non-inundated areas, where NPP appeared inversely related to PAR, perhaps because of the interaction of rainfall and cloudiness, or perhaps an indication of limited usefulness of data with only 1° latitude x 1° longitude resolution for stratification of a small region such as this. Heavily fragmented forest was distinguished with lower NPP and annual mean NDVI (green). In the 13-class stratification, further splits were made in the inundated savannas based on maximum MPDI and mean NDVI. Another split defined by mean NDVI delineated a heavily-fragmented forest class in the region of Rondônia and Mato Grosso where PAR is lower and which included the dry savannas of the Huanchaca Plateau in Noel Kempff Mercado Park, Bolivia. Forested areas were again divided based on climate variables, PAR, rainfall, and minimum temperature. The geographical pattern of these classes (Fig. 2.37) agreed closely with the well-known pattern of forest clearance in central and western Rondônia, with evergreen forests and seasonal forest to the south.

npp.win1.test.best13.tree



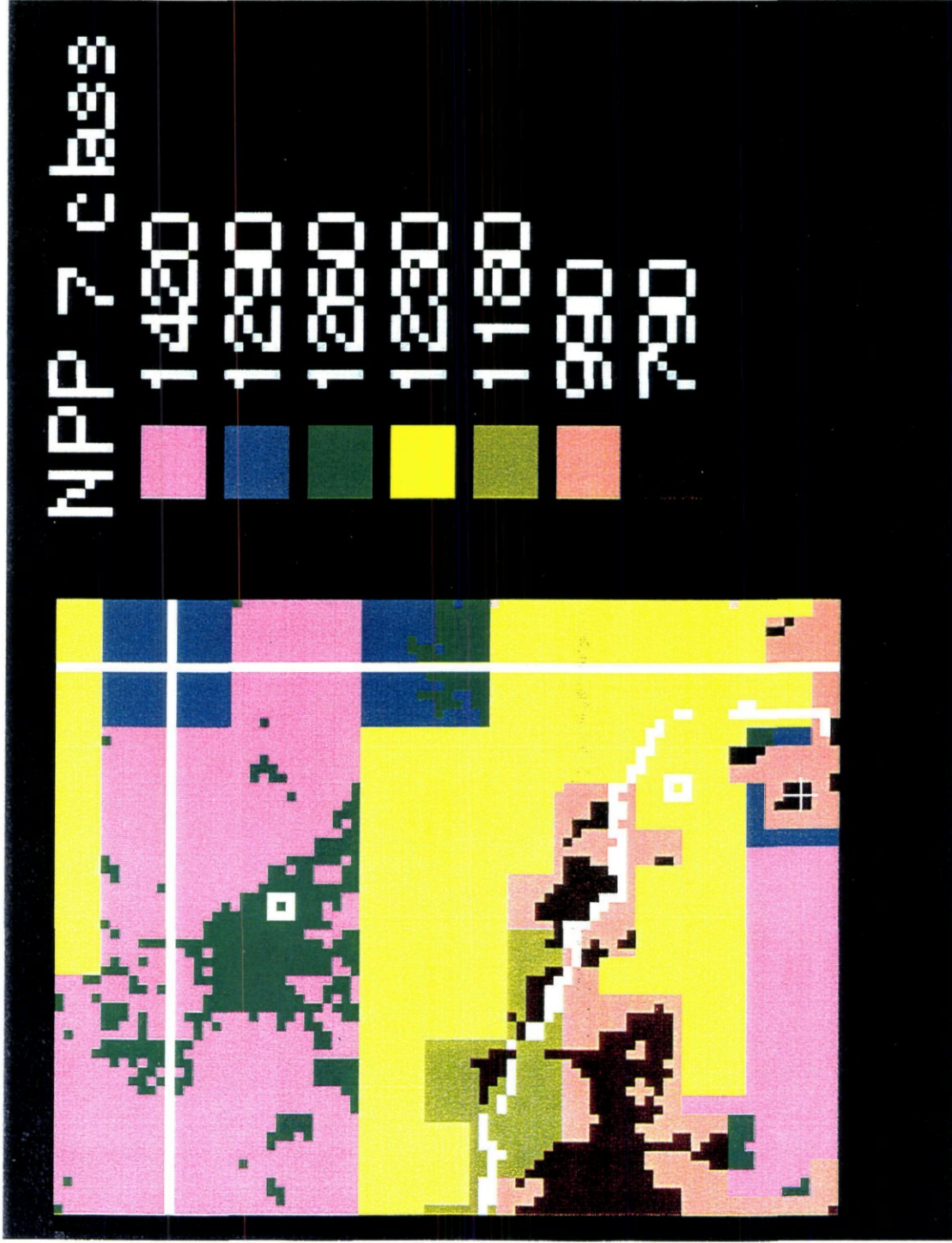


Fig. 2.37a Maps of classes derived from regression tree analyses of the Rondonia - Santa Cruz window: a) NPP 7-class, b) NPP 13-class. Units are  $gC\ m^{-2}\ yr^{-1}$ .

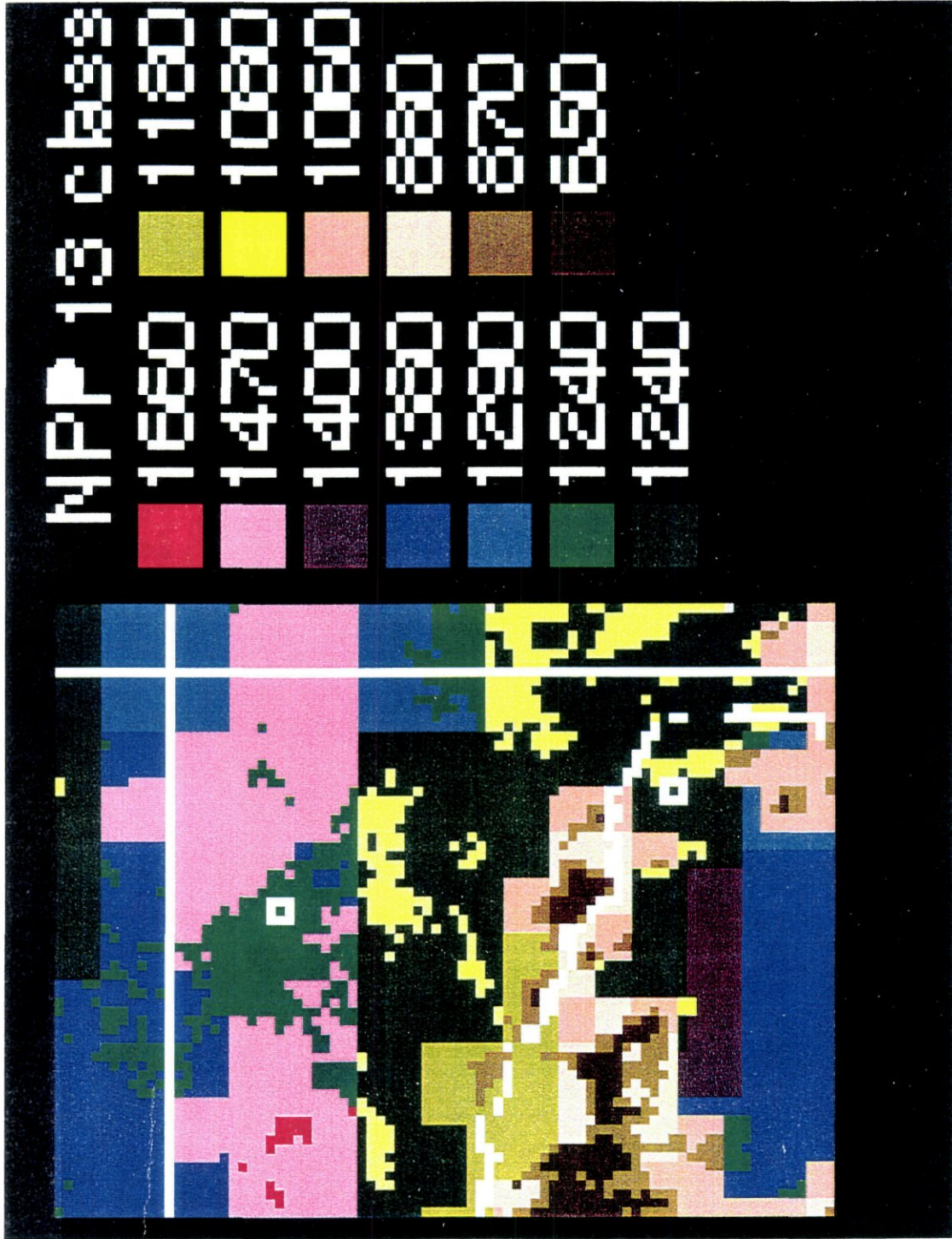


Fig. 2.37b Maps of classes derived from regression tree analyses of the Rondonia - Santa Cruz window: NPP 13-class. Units are  $gC\ m^{-2}\ yr^{-1}$ .

## 2.4.6 Discussion

The patterns of NPP, Rn and LE mapped using the RTA classifications (Figs. 2.35, 2.37) were compared with vegetation maps of the Amazon basin. Overall the RTA technique produced classes that shared some boundaries with the vegetation maps but, unlike the vegetation maps, each class division had a position in a hierarchical tree.

The wedge-shaped pattern of lower NPP (Fig. 2.35, dark green,  $1230 \text{ gC m}^{-2}\text{yr}^{-1}$  and blue-gray,  $1280 \text{ gC m}^{-2}\text{yr}^{-1}$ ) versus higher NPP (brown,  $1410 \text{ gC m}^{-2}\text{yr}^{-1}$  and red  $1540 \text{ gC m}^{-2}\text{yr}^{-1}$ ) followed closely the 150m contour and was similar to the pattern formed by the boundary between 'lowland' and 'sub-montane' evergreen forest in the IBGE map of Brazilian vegetation ([IBGE), 1993 #4121]). Two north-south boundaries delimiting western Amazonia were defined in the analyses; one from the stratifications of Rn and LE was at  $65^\circ \text{ W}$ , and another from the stratification of NPP at about  $69^\circ \text{ W}$ . The latter agrees roughly with boundaries distinguishing western Amazonia in the map of ecoregions produced at the World Wildlife Federation (Dinerstein et al., 1995), which incorporates both climatological and floristic data. It also follows a boundary distinguishing 'open ombrofile' forest to the west in Acre from 'dense ombrofile' forest to the east in the IBGE map of Brazilian vegetation. This vegetation class, however, was probably meant to distinguish mixed bamboo forests in Acre; the western Amazonia class produced from this study was mostly dense evergreen forest.

There were, nevertheless, marked differences between the RTA maps and the various vegetation maps. For example, classes of seasonal forest extended further west into Bolivia than was expected, perhaps because 1987, the year for which NPP was available, was particularly dry throughout most of the Amazon basin. The stratifications of the Amazon presented here were almost entirely based on climate data and, consequently, there were many seemingly obvious surface and vegetation features which have not been captured. Some vegetation classes which we would have liked to be able to distinguish include liana forests, particularly in Pará and Bolivia, bamboo forests, especially in southeastern Peru and Acre, palm swamps, and white sand vegetation such as that of the upper Rio Negro. There are no maps available which delineate these vegetation formations. Furthermore, all of these formations probably exist as mosaics with dense evergreen forest, and thus may not significantly influence bioclimate at the scale of the data used in this study. Stratification of only the Rondônia window did not successfully represent such classes as liana forest, seasonally inundated forest and palm swamp which are known to cover large portions of that area (Killeen et al., 1997). This is more an issue of data scale and availability rather than a failure of the RTA technique. RTA could be undertaken using finer resolution data, such as 1 km AVHRR data.

The maps and regression trees presented here may be applied to the selection of regions that should be represented with field measurement sites. Moreover the status of regions with existing field sites can be determined, perhaps with a view to augmenting certain types of measurements.

The existing field study sites that have been identified as potential LBA sites are marked on the RTA maps as white rectangles (Figs. 2.35 and 2.37). It is clear that an additional site in the high productivity region of Guyana (red) would be useful possibly midway between Santarem and Boa Vista since the currently proposed site on Brazilian-Venezuelan border appears to be in a vegetation transition area. The transition from evergreen to semi-deciduous forest class (pink, yellow, light green) in the south west of the basin in Rondônia - Santa Cruz was distinct from that in Pará and should also be sampled; NE Santa Cruz province in Bolivia would be an ideal location. The west Brazilian Amazon site near Tabatinga is also in a vegetation transition and would be better placed perhaps near Iquitos, Peru.

LBA has a major interest in the sustainability of various types of forest conversion, such as total clearance, selective logging, and traditional shifting agriculture. These human-induced transformations have affected a relatively small proportion of the total basin area at the present time (Skole & Tucker, 1993) and seem only to have influenced the current RTA classifications in areas of concentrated land conversion, such as in central Rondônia. Thus stratification for management must be undertaken at a more local scale using higher resolution data sets such as those prepared by the Universities of Maryland and New Hampshire as part of the NASA Landsat Tropical Deforestation project (Lawrence, 1992).

The need to stratify at multiple spatial scales is inevitable when dealing with such a large area as the entire Amazon basin. The stratifications presented here used 8 x 8 km data at the highest resolution, but several data sets were at 1° x 1°, hence regional differences have been emphasized, not variation at finer spatial resolution. Equatorial lowland forest is well known to exhibit much stronger  $\alpha$ -diversity than  $\beta$ -diversity, unlike temperate and arid regions (Brown, 1995), thus much of the fine-scale variation may be lost at the scales explored here. A corollary of this point is that the presence of an existing field site in any particular stratum does not necessarily indicate that it is being adequately sampled. The stratifications presented here are relevant to the 1° scale and they indicate which entire 1° area would give the optimal sampling of the basin-wide variation. Further stratification within each selected 1°, perhaps using similar techniques, is necessary to determine the optimal location of individual, point, field measurement locations.

These finer scale stratifications should be explicitly linked with the coarser, basin scale to ensure continuity in scaling up. At the basin scale, the RTA identified annual and monthly minimum PAR and minimum rain fall and the number of months below 150 mm of rain fall as critical variables that determine  $R_n$ . These same variables are identified as critical for LE, although the first division of LE was on annual rainfall. Minimum NDVI, annual PAR, and the number of months below 150 mm rain fall were the most important variables in the tree model of NPP. Annual NDVI and rainfall were also important in the dryer, low NPP areas, while the monthly minimums of NDVI, PAR and temperature were important in the more humid, high NPP areas. The field measurement design should therefore emphasize measurement of these variables at the 1° x 1° scale.

### **3 SVAT modelling (SC-DLO, CNRM, IH)**

#### **3.1 Introduction**

Soil Vegetation Atmosphere Transfer schemes form the lungs of global and meso scale models of the atmosphere. They are the main tool to estimate the transfer of water, energy and carbon from situations where the residence time of these properties is long, to the atmosphere, where the residence time is short.

It is now well recognised that for a correct prediction of global and regional climate change with respect to increasing carbon dioxide levels and land use change, the specification of the interaction of the land surface vegetation with the atmosphere is of crucial importance (e.g. Sellers et al., 1995). To be able to predict the seasonal to inter-annual variation in climate and weather, adequate parameterization is required of processes operating at both the short, diurnal time scale and the long, seasonal time scale where significant memory of the system presents a major complication.

GCM studies of deforestation of the Amazon basin show a strong sensitivity of the predicted change in climate to surface forcing (e.g. Lean and Rowntree, 1993). Generally the important factors are albedo, surface conductance and aerodynamic roughness, although the specification of interception loss (Dolman and Gregory, 1992) and soil properties (da Rocha et al., 1996) is also important. It is therefore of crucial importance in modelling studies that the land surface is correctly specified. This is required for both short and long term predictions.

The main objective of this SVAT modelling part of the project is to produce calibrated SVAT models for use in mesoscale meteorological models. Related to this are two further objectives: obtaining a better understanding of the underlying processes involved in interactions between the soil, vegetation and atmosphere; and highlighting the future needs in the design of the mesoscale measuring campaign of LBA.

For this study three SVAT models (ISBA, MOSES-2S and SWAPS) have been used. They differ in complexity, but all have been run decoupled from the overlying atmosphere. MOSES-2S and SWAPS are run primarily to investigate the capability of these models to predict energy partitioning of forest and pasture with a view to highlighting model deficiencies and areas of experimental uncertainty. These two models are the two more complex of the schemes. ISBA is also used in the mesoscale models and has a relatively simpler structure. The calibration of the RAMS surface model is described in the mesoscale modelling part of this report (Chapter 4) and in Dolman et al. (1997).



### 3.2 Data description

Data from the Anglo-Brazilian ABRACOS project have been used in this project for the SVAT modelling. ABRACOS involved both long and short term measurements undertaken in Brazil. The long term measurements included continuous measurements of soil moisture. The short term measurements (in the form of missions lasting several weeks or months) focused on studying meteorological and physiological processes. These missions provided data during the dry and the wet seasons at various sites. The long and short term measurements were made at both forest and pasture (i.e. deforested) sites. Gash et al. (1996) give a summary of the ABRACOS project.

The ABRACOS missions and the corresponding sites and seasons *used in this project* are summarised in Table 3.1. ABRACOS data have been used for forcing the SVAT models and comparison with the model results. Data from the sites at Reserva Jaru forest (RJF) and Nossa Senhora pasture (NSP) were chosen for various missions for a number of reasons given below. Besides providing forcing and comparison data, the ABRACOS data have also been used to derive parameters which are required as model inputs. Mission 3 is thus included in Table 3.1 because data from this mission were used to obtain parameters for the surface conductance models for forest and pasture.

Table 3.1 ABRACOS missions used in the CABARE project

Mission	Site	Period	Year	Season
3	Reserva Jaru forest	8 August - 5 October	1992	Dry
3	Nossa Senhora pasture	6 August - 7 October	1992	Dry
4/5	Reserva Jaru forest	4 April - 26 July	1993	Wet, Dry
4/5	Nossa Senhora pasture	31 March - 28 July	1993	Wet, Dry
7	Reserva Jaru forest	13 August - 25 August	1994	Dry
7	Nossa Senhora pasture	11 August - 24 August	1994	Dry

#### **Mission 4/5**

Missions 4 and 5 combined give a 3 - 4 month period running from the wet to the dry season. Mission 4/5 is a good test for rainfall interception models, and for soil moisture models over a relatively long period with highly varying soil moisture. In particular there is strong depletion in soil moisture in the top few metres at the forest site, with little influence on transpiration. During this period at this site the groundwater table is also important. For the pasture site soil moisture slowly decreases over this period.

#### **Mission 7**

This mission is concurrent with the third campaign of the Rondônia Boundary Layer Experiment (RBLE III) to which this project contributed (see Kabat et al., 1996). RBLE III corresponds to the dry season in Rondônia. During RBLE III atmospheric soundings were made over the forest and pasture sites simultaneously. The RBLE III data show that there can be a significant difference in PBL growth over forest and pasture surfaces, and this is obviously important with respect to mesoscale meteorological modelling.

### ***Forcing data***

The SVAT models have been run decoupled from the overlying atmosphere and thus require measured (or derived) reference height variables for forcing at the upper boundary. All SVATs in this project use the following as forcing variables: air temperature; relative humidity; incoming shortwave radiation; incoming longwave radiation; barometric pressure; wind speed; gross precipitation. Pressure was not measured, and has been estimated as a function of site elevation. Incoming longwave radiation was also not measured, and has been estimated following Culf and Gash (1992) with an empirical adjustment for Amazonia. The forcing data were taken from micro-meteorological/AWS measurements which are time-averaged over hourly periods.

### ***Comparison data***

Micro-meteorological and soil moisture data have been used for comparison with the model results. For each mission fluxes of latent heat, sensible heat, net radiation and soil heat were available from the micro-meteorological/AWS stations. In addition aerodynamic and surface conductances, atmospheric stability functions and friction velocity have been derived from the measurements. For the forest sites the flux density of energy stored in the forest canopy has also been calculated as a residual of the energy balance. All of these data are available time-averaged over hourly periods. At or near each AWS site soil moisture was measured at various depths. The soil moisture data are continuous for a period that covers all the ABRACOS missions. These data are available at approximately weekly intervals, and at shorter intervals during the missions themselves.

### ***Derived model input parameters***

Various input parameters are required by the SVATs. For a detailed description of all surface (soil, vegetation, surface conductance etc.) parameters derived for Amazonia based on ABRACOS (and other) data the reader is referred to Wright et al. (1996b).

The reader is also referred to Wright et al. (1996a) for details on the Jarvis-Stewart surface conductance model applied to ABRACOS sites, and the resulting calibrated parameters. The surface conductance calibrations for Reserva Jaru forest and Nossa Senhora pasture are based on data from Missions 3, 4 and 5. Parameters for these sites are available based on optimisations for each of these missions separately, and for an optimisation using data from all three of these missions.

The semi-empirical description of soil hydraulic properties of van Genuchten (1980) has been applied to obtain parameters for different sites at a number of depths. These are described by Wright et al. (1996b) and the reader is also referred to Tomasella and Hodnett (1996). It should be noted that there is some uncertainty in the values presented for the saturated hydraulic conductivity.

The use of input parameters varies between the models. The van Genuchten parameters given by Wright et. al. (1996b) have been used for both the SWAPS and MOSES-2S models. For ISBA these parameters have been converted to the corresponding Clapp and Hornberger values (Delire et al.,1997). Similarly SWAPS and MOSES use the functions and parameters given by Wright et. al. (1996a, b) in the

surface conductance models. Note that for Mission 7 pasture the surface conductance parameters used in SWAPS are those obtained from Missions 3, 4 and 5 whereas for Mission 4/5 SWAPS and MOSES employ the mission specific parameters for pasture. For ISBA the surface conductance model and parameters have been optimised using the measurements (Delire et al., 1997). The parameters derived from ABRACOS data used in this project are summarised in Tables 3.2 and 3.3.

Table 3.2 Parameters from ABRACOS missions used in this project

Site/vegetation	Nossa Senhora pasture		Reserva Jaru forest	
Mission	4/5	7	4/5	7
Reference height (m)	5.5	3.8	53.5	
Vegetation height (m)	0.6	0.58	30.0	
Canopy cover (%)	85	85	97	
Root zone depth (m)	2.0	2.0	> 4	
LAI	2.73	3.00	4.6	5.2
Total albedo	0.190	0.187	0.134	0.144
Roughness length (m)	0.1 × height		2.6	
Displacement height (m)	0.66 × height		0.86 × height	
Rainfall interception parameters				
Canopy capacity (mm)	0.5		1.03	
Trunk capacity (mm)	-		0.09	
Trunk input	-		0.1 × Rain	
Surface conductance parameters for use with reference height data <sup>(1)</sup>				
Mission	4/5	3 and 4/5	4/5	
$a_1$ (mm s <sup>-1</sup> ) = LAI × $g_{sMax}$	32.0	33.1	65.2	
$a_2$ (kg g <sup>-1</sup> )	0.0922	0.1127	0.1064	
$a_3$ (°C)	22.9	-	44.6	
$a_4$ (Wm <sup>-2</sup> )	654	671	743	
$a_5$ (m <sup>3</sup> m <sup>-3</sup> )	0.27	0.259	-	

Vegetation emissivity = 1.00

Soil emissivity = 0.95

<sup>(1)</sup> See Wright et al. (1996a) for a description of the stress functions used in the surface conductance model

### 3.3 Model descriptions

For this study three SVAT models (ISBA, MOSES-2S and SWAPS) have been used. They differ in complexity, but all have been run decoupled from the overlying atmosphere, and thus require variables, listed above, for forcing at the top boundary. These variables are the same for each model.

All three models make the assumption that there is energy and water balance closure. The models aim at partitioning the total latent heat flux into plant transpiration, bare soil evaporation and interception evaporation components. The transpiration is regulated by a surface conductance. In all three SVATs the surface conductance is based on the stomatal conductance model of Jarvis (1976) which was later modified by Stewart (1988) for a surface conductance. Although the exact form of the surface conductance model is not the same for each SVAT, each employs a maximum surface conductance which is then reduced by stress functions based on environmental

variables (air temperature, air humidity deficit, incoming solar radiation and soil moisture over the effective rooting depth). The bare soil evaporation is a function of the soil moisture content near the soil surface.

Table 3.3 Van Genuchten and soil physical parameters (see Wright et al. (1996b) for a full description of the symbols)

Depth	n	$\alpha$	l	$\theta_{\text{Sat}}$	$\theta_{\text{Res}}$	$K_{\text{sat}}$	Bulk density (Mg m <sup>-3</sup> )	Clay	Sand
(m)	(-)	(kPa <sup>-1</sup> )	(-)	(m <sup>3</sup> m <sup>-3</sup> )	(m <sup>3</sup> m <sup>-3</sup> )	(mm h <sup>-1</sup> )		(%)	(%)
Nossa Senhora pasture (NSP)									
0.0	-	-	-	-	-	6 <sup>(1)</sup>	1.50	7	85
0.2	1.92	0.202	0.5	0.259	0.046	20-60 <sup>(1)</sup>	1.50	12	78
0.4	1.77	0.359	0.5	0.309	0.109	-	1.30	16	72
0.6	1.16	0.730	0.5	0.389	0.131	-	1.30	33	58
0.8	1.35	0.293	0.5	0.418	0.257	-	1.30	33	58
1.0	1.56	0.251	0.5	0.465	0.298	-	1.24	33	53
1.2	1.59	0.206	0.5	0.425	0.275	-	1.24	36	53
1.5	1.25	1.103	0.5	0.383	0.191	-	1.24	36	53
Reserva Jaru forest (RJF)									
0.0	-	-	-	-	-	-	1.38	4	85
0.2	1.34	2.209	0.5	0.483	0.025	63	1.55	4	82
0.4	1.60	0.164	0.5	0.305	0.079	66	1.52	6	77
0.6	1.73	0.304	0.5	0.343	0.155	10	1.49	18	63
0.8	1.46	0.209	0.5	0.397	0.212	(10)	1.49	35	58
1.0	1.39	0.212	0.5	0.410	0.231	-	-	35	58
1.2	1.40	0.252	0.5	0.408	0.207	-	-	36	53
1.5	1.57	0.213	0.5	0.418	0.189	-	-	36	53

<sup>(1)</sup> Saturated hydraulic conductivity was not optimised - measured by ABRACOS.

### **ISBA (Interactions Surface Biosphere Atmosphere)**

The ISBA scheme is the simplest SVAT used for this study. This scheme has been tested and calibrated for various sites in stand alone simulations and has been coupled to mesoscale and global climate models. ISBA is currently used in operational meteorology at Météo-France. The main calculations in ISBA determine the evolution of 5 prognostic variables: a deep soil temperature  $T_2$ , a total water content over the rooting depth  $w_2$ , a single temperature for the soil surface and the vegetation  $T_s$ , a small superficial water reservoir  $w_g$  (included in  $w_2$ ), and a canopy interception reservoir  $S$ . The evolution of both  $w_g$  and  $T_s$  is described using the force-restore method (Bhumralkar, 1975). The respective contributions of bare soil and vegetation to the surface energy balance are determined by the vegetation fraction (veg). The value of  $w_g$  is driven by the non-intercepted precipitation and the bare soil evaporation (at a rate given by a coefficient  $C_1$ ), and is also restored to  $w_2$  according to a coefficient  $C_2$ . The value of  $w_2$  is directly driven by the non-intercepted precipitation, the bare soil evaporation and the transpiration. Above field capacity, gravitational drainage occurs at a rate determined by the coefficient  $C_3$ . The coefficients  $C_1$ ,  $C_2$ , and  $C_3$  depend on the water content and on the average clay and sand proportions. In ISBA, these coefficients are related to the soil texture through the Clapp and Hornberger (1978) soil water model. In the same way, the soil heat capacity depends on the soil texture and water content.

The critical water contents (saturation, field capacity and wilting point) also depend on the soil texture. As pointed out by Tomasella and Hodnett (1996), some Amazonian soils behave in a totally different way from temperate ones. In the framework of this programme, the texture dependence of these coefficients and critical water contents have been recalibrated according to the ABRACOS measurements.

The turbulent fluxes are calculated by means of classical aerodynamic formulae (Louis, 1979): the sensible heat flux is related to the vertical temperature gradient and the latent heat flux to the specific humidity deficit. The bare soil evaporation is limited by the surface soil water content and occurs at the potential rate when  $w_g$  is at field capacity. The transpiration is regulated by the stomatal resistance. The interception reservoir evaporates at the potential rate. A complete description of ISBA can be found in Noilhan and Mahfouf (1996).

#### ***MOSES-2s (Meteorological Office Surface Energy Scheme - 2 sources)***

This model is an adaptation of MOSES-I (Cox et al., 1997) which is due to become the surface scheme in the UK Met Office Unified Model in 1997. The adaptation concerns the separation of the energy and water balance between the vegetation and the soil. A fraction of the surface is assumed to be covered by vegetation, and the rest is exposed soil. Rainfall and incoming shortwave radiation can reach the soil underneath the vegetation however, and this part of the soil is referred to as the shaded soil. The vegetation and soil have different surface temperatures but the shaded and exposed soil have the same surface temperature. Water enters the SVAT as rainfall, and leaves as surface runoff, drainage and evaporation. The rainfall intercepted by the vegetation is calculated using the Rutter interception model. This water is evaporated from the canopy at the potential rate. The water incident at the soil surface is the sum of the throughfall on the shaded soil and the rainfall on the exposed soil. There is no ponding on the soil, so this incident rain either infiltrates into the top layer of the soil model or is assumed to be surface runoff. The incident short wave on the vegetated fraction is partitioned between the vegetation and the soil according to Beer's Law while the long wave radiation which is incident on the vegetation is fully intercepted. The albedos of the soil and vegetation are different as are their surface temperatures, so each surface type has a different net radiation in the energy balance calculation. The energy balance of the soil/vegetation mix is calculated in one iteration using the method proposed by Shuttleworth and Wallace (1985). This method is based on the Penman-Monteith equation and the surface temperature of both the soil and vegetation are diagnostics of the solution. Three aerodynamic resistances control the flux/gradient relationships of heat and moisture between the two surfaces and the reference height. The equations for these resistances are given in Dolman (1993) and in Huntingford et al. (1995). The evaporation from the soil is limited by the soil moisture in the top layer, while the evaporation from the transpiring vegetation is limited using a surface resistance which is calculated using the Jarvis functions. The soil model for both heat and moisture has four layers: 0.1, 0.25, 0.65 and 2 m. The soil heat model is driven by the diagnosed surface temperature of the soil. The soil water model is driven by the incident rainfall and the energy balance solution, which diagnoses the soil evaporation. There is water and heat flow between the four layers. The flow of water is calculated by solving the

Darcy-Richards equations, using the Brooks and Corey functions of the conductivity and suction.

### ***SWAPS (Soil Water Atmosphere Plant SVAT)***

SWAPS is a land surface model comprising an unsaturated soil moisture flow scheme and a one or two layer evaporation-interception scheme. Two types of two layer model may be used. First, in terms of radiation and precipitation, the upper layer is pictured as overlying the lower layer (Shuttleworth and Wallace, 1985) and the radiation and precipitation reaching the lower layer are determined by an extinction coefficient and free throughfall coefficient respectively. Second, the two layers are pictured as adjacent patches (Dolman, 1993) where it is assumed that each layer receives the same incoming fluxes of radiation and precipitation. For all runs in this study SWAPS was set up for the first two layer configuration (with an upper vegetation layer overlying a soil layer), and we concentrate on this configuration in the description of the model. For a full description of the model the reader is referred to Ashby et al. (1996).

For the evaporation a Penman-Monteith model is applied to each layer following the original "sparse canopy" model of Shuttleworth and Wallace (1985). This assumes that the upper layer is sparse enough to allow the existence of a mean or in-canopy flow. The latent heat fluxes of each layer are then linked by the in-canopy vapour pressure deficit.

The interception module is based on the model of Rutter (1971) where an interception layer is modelled as a reservoir or bucket. A fraction of the precipitation incident above the layer is intercepted and stored in the reservoir. Evaporation from water in the reservoir will occur, as will drip if the capacity of the reservoir is exceeded. Unlike the original Rutter model there is no drainage (simulated by a hole in the bucket) when the reservoir is not completely full.

For each layer the surface conductance is needed for the evaporation model. In the case of vegetation a modified version of the model proposed by Jarvis (1976) is used, where the conductance is controlled by prevailing environmental conditions. In the case of a soil layer an effective soil surface resistance to evaporation is determined based on the soil moisture and soil thermal status (Bastiaansen, 1995).

For a layer whose interception reservoir is completely full the surface resistance is set to zero and the latent heat flux from that layer comprises interception evaporation only. This is also assumed for a soil with ponding or a soil with a wet litter layer. The latent heat flux from a partially wet layer (where the interception reservoir is not full) comprises both transpiration and interception evaporation components. Transpiration is calculated assuming completely dry conditions using the surface conductance. Interception evaporation is then calculated assuming completely wet conditions (i.e. zero surface resistance). The actual transpiration is then assumed to be the dry transpiration reduced by the fraction of the canopy that is actually dry. This fraction is derived from the status of the interception reservoir. Similarly the actual interception evaporation is assumed to be the above interception evaporation reduced by the fraction of the canopy that is actually wet.

The soil moisture module of the model (see Kabat et al., 1992) is based on the Darcy-Richards equation where a sink term is used to represent processes that remove water from the soil, such as root water uptake, soil evaporation and lateral drainage. The relations between pressure head, soil moisture content and soil hydraulic conductivity for each soil layer are given either by specifying the parameters for the semi-empirical model of Van Genuchten (1980); or by specifying corresponding values of these variables in tabular form. Each soil layer may comprise several compartments. The soil moisture equations are solved for each compartment by using a fully implicit, one-dimensional finite difference scheme where boundary conditions and initial soil moisture status is required. The upper boundary condition will be head or flux controlled depending on the prevailing conditions and is determined within SWAPS. The lower and lateral boundary conditions are specified by the user.

Soil heat transport is modelled as a conduction process using Fourier's equation. The soil thermal calculations are performed using a fully implicit one-dimensional finite difference scheme with the same vertical discretisation as the soil moisture calculations. In general these calculations are performed at a longer time step than the soil moisture calculations. The upper boundary condition is calculated in SWAPS using the prevailing values for the energy fluxes and aerodynamic resistances. The lower boundary conditions are specified by the user. The soil heat capacity and the soil thermal conductivity are determined from the soil composition following the model of De Vries (1963).

### **3.4 Model results**

In this section the results are first described separately for each mission. For brevity not all results for all the models are shown. Those presented here have been chosen to highlight various points arising from the simulations.

#### *Mission 4/5 - Reserva Jaru forest*

Figs. 3.1, 3.2 and 3.3 show results produced by ISBA. Fig. 3.1 shows simulated versus observed net radiation for each hour during the mission for ISBA. Incoming longwave radiation has been used to force the model and, as this was not measured, it has been estimated following Culf and Gash (1992) with an empirical adjustment for Amazonia. The results agree well with the observations. Similar results are produced by SWAPS, indicating that the method of Culf and Gash (1992) appears to be a good estimate of incoming longwave radiation.

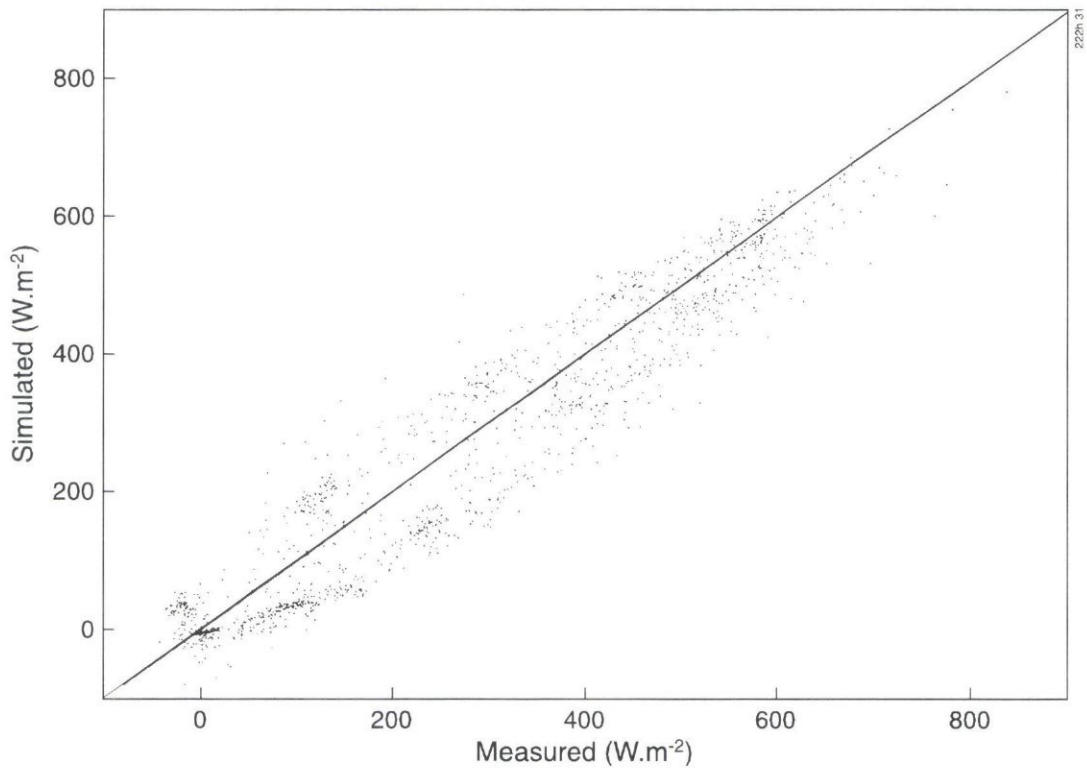


Fig. 3.1 ISBA: simulated versus measured net radiation for R/JF Mission 4/5 (with incoming longwave radiation estimated following Culf and Gash, 1992).

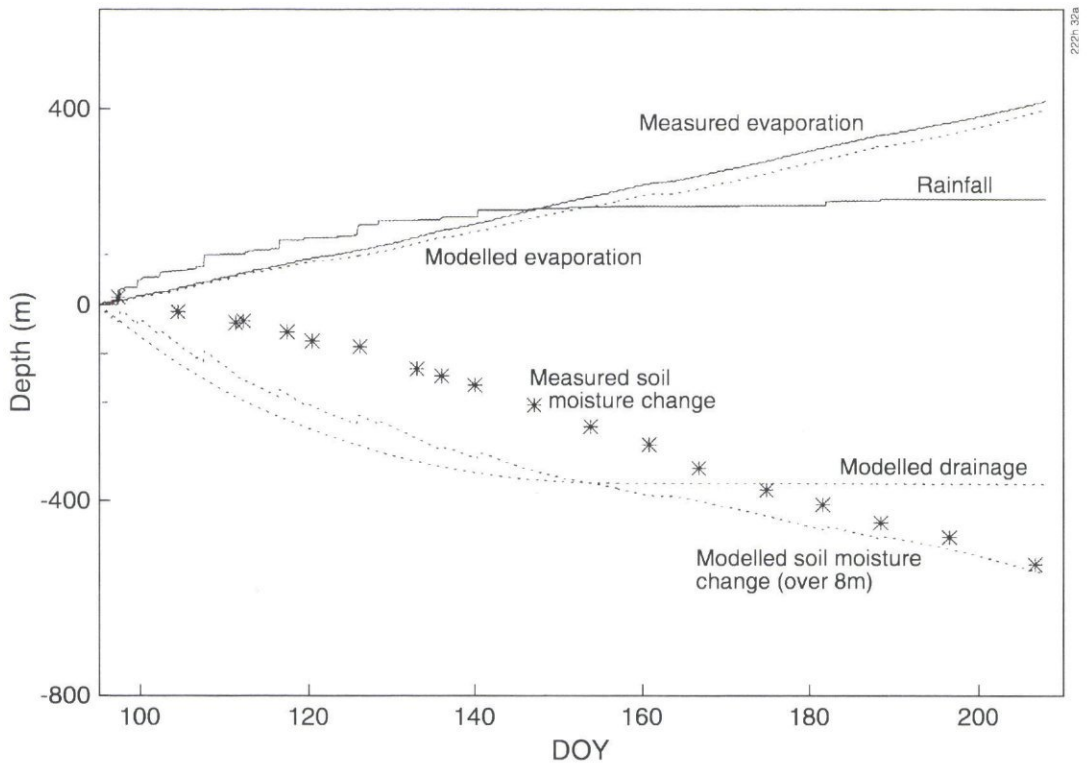


Fig. 3.2 ISBA: cumulative gross precipitation, total evaporation (measured and simulated), total soil moisture change (measured and simulated), drainage (simulated) for R/JF Mission 4/5.



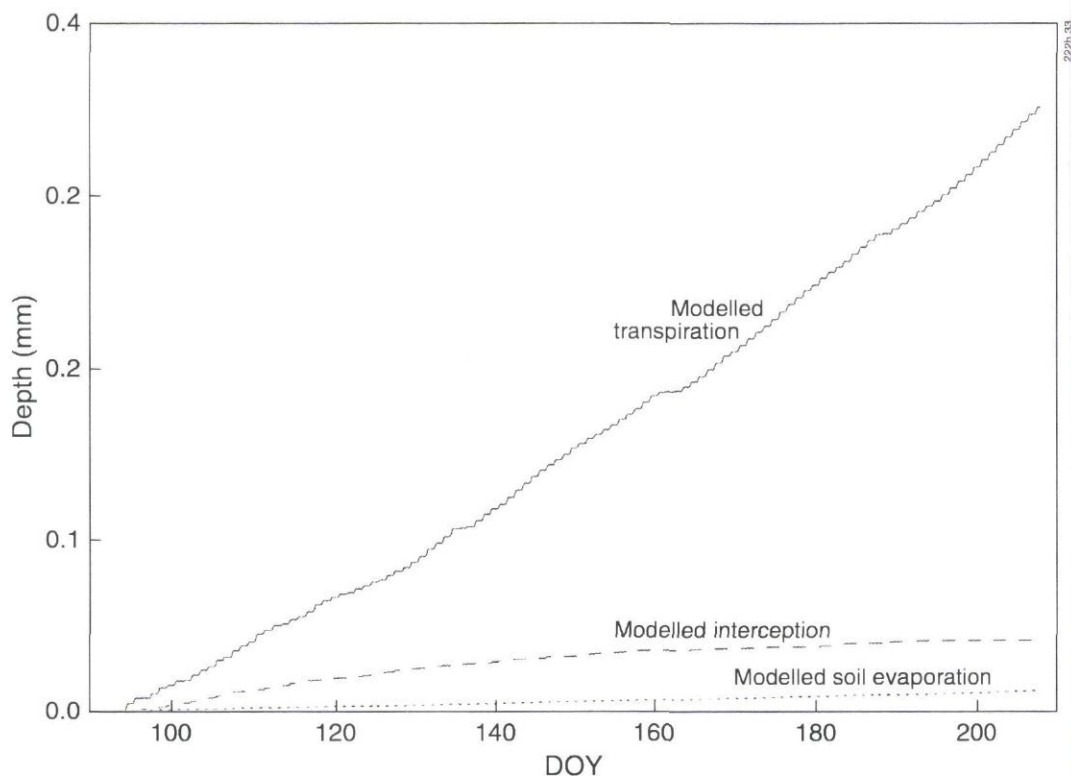


Fig. 3.3 ISBA: simulated cumulative transpiration, interception loss, bare soil evaporation for R/JF Mission 4.5.

Fig. 3.2 shows cumulative values of the following variables: rainfall, observed and modelled total evaporation, observed and modelled soil moisture *change*, and modelled drainage. Note that for this figure (and Figs. 3.12 and 3.13) drainage is negative out of the system. There is a slight underprediction of the total evaporation from the forest site. In comparing modelled and measured soil moisture change it should be noted that because of the temporal resolution of the measurements, spikes due to rainfall inputs are not seen in the measurements although they do occur in the simulation. Obviously interpolation of measured soil moisture data to model output times is not valid if the latest soil moisture measurement occurs after a rainfall input. In this simulation the model soil and root depth is 8m in order to keep the forest transpiration unstressed with respect to soil moisture. Therefore the modelled and measured soil moisture changes are not directly comparable since soil moisture measurements are only available to a depth of 3.6 m. As expected the cumulative modelled drainage shows little change towards the end of the period when the soil is dry.

Fig. 3.3 shows modelled cumulative transpiration, bare soil evaporation and interception loss. For the forest, modelled bare soil evaporation is small but significant. The modelled interception loss (interception evaporation/rainfall) amounts to some 18% in this simulation (see also Fig. 3.2). The plateaux in the transpiration curve obviously correspond to zero night-time transpiration.

Figs. 3.4 and 3.5 show results for SWAPS similar to Figs. 3.2 and 3.3 for ISBA. Fig. 3.4 shows the following cumulative variables: modelled and measured total, bare soil and interception evaporation, transpiration and precipitation. Again modelled bare soil evaporation is small but significant. The modelled interception loss is 20%. The total evaporation in this simulation agrees well with the measurements. Fig. 3.5 shows the total observed and modelled soil moisture to a depth of 3.6 m. The bottom boundary condition in this simulation is a given but varying groundwater level which has been estimated by comparing observed volumetric soil moisture content with the saturated values given in Table 5.3. During the wet season the groundwater has been observed to reach within 2 m of the surface at this site (Hodnett et. al., 1996) and is thus important. In this case the modelled and measured soil moisture are directly comparable. Again spikes in the simulation correspond to rainfall inputs which are not presented by the measurements. The model results appear to be quite good until the end of the mission where SWAPS starts to underestimate the soil drying. More detailed groundwater information (or e.g. a measurement derived flux) would be required for the bottom boundary condition, as a thorough test of the model performance.

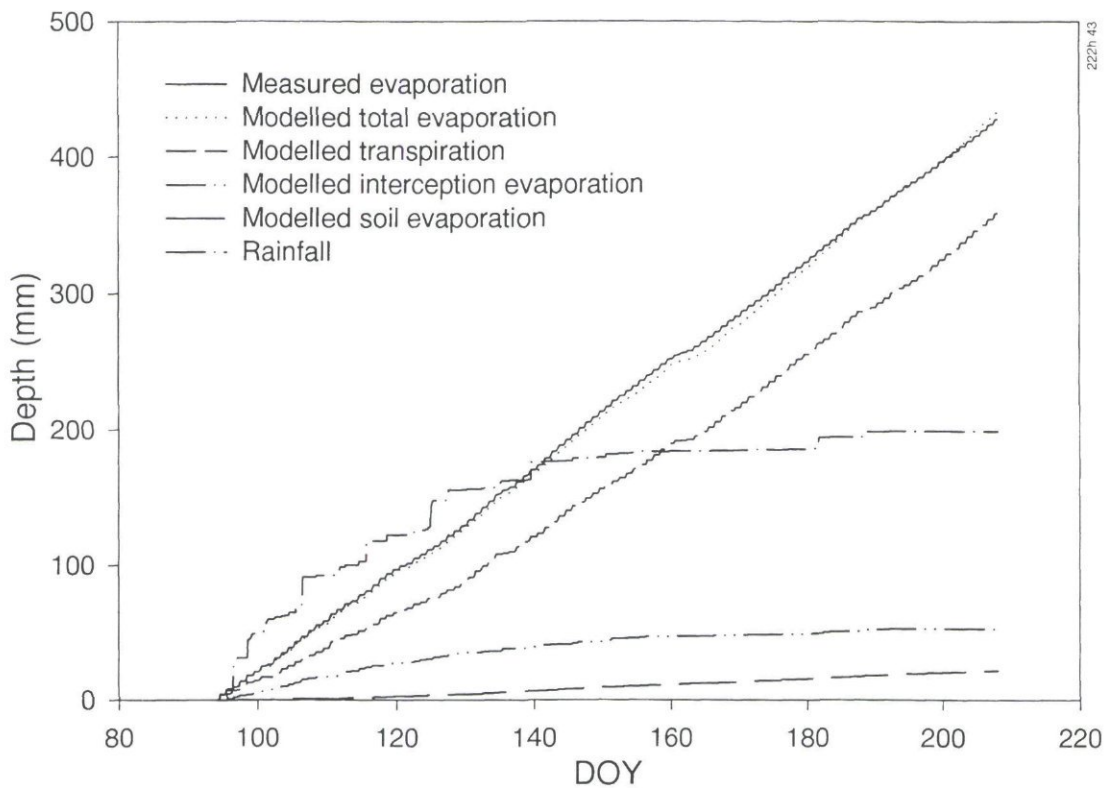


Fig. 3.4 SWAPS: simulated and measured cumulative total evaporation; simulated cumulative transpiration, interception evaporation, bare soil evaporation; cumulative measured rainfall for R/JF Mission 4/5.

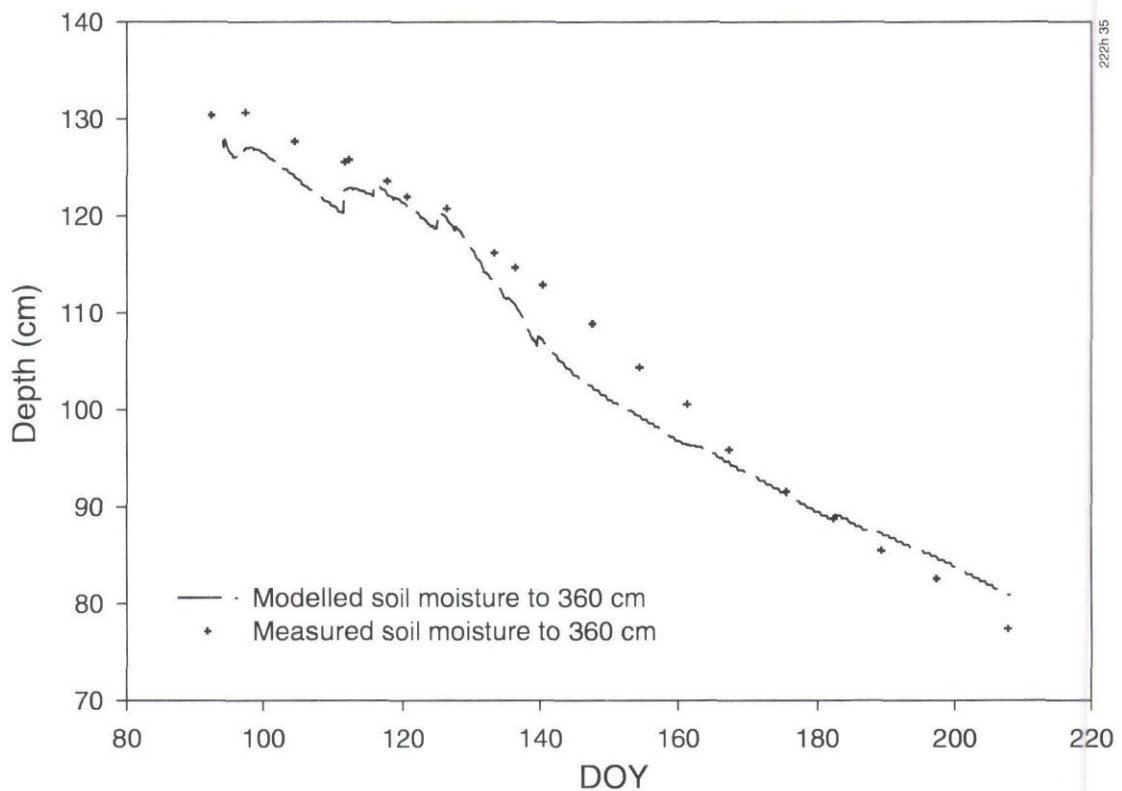


Fig. 3.5 SWAPS: simulated and measured total soil moisture to a depth of 3.6 m for R/JF Mission 4 5.

Time series of simulated and measurement derived surface temperatures are shown in Figs. 3.6 and 3.7 for SWAPS (upper vegetation layer) and ISBA respectively. Note that these correspond respectively to periods in wet (SWAPS) and dry (ISBA) parts of the mission. The effective surface temperature has been derived by inverting the flux-gradient relationship and using the measured sensible heat flux, air temperature, and derived aerodynamic resistance (i.e. assuming a single layer model). For both of these periods for both models there is good agreement between simulated and 'observed' daytime values although at night both ISBA and SWAPS tend to underestimate the surface temperature. Note that for a two layer model configuration comparison of the effective surface temperature to the modelled in-canopy temperature may be more appropriate since these temperatures correspond to the temperature variable below the aerodynamic resistance. However for this simulation there is a negligible difference between (upper) surface and in-canopy temperatures produced by SWAPS so the latter is not shown.

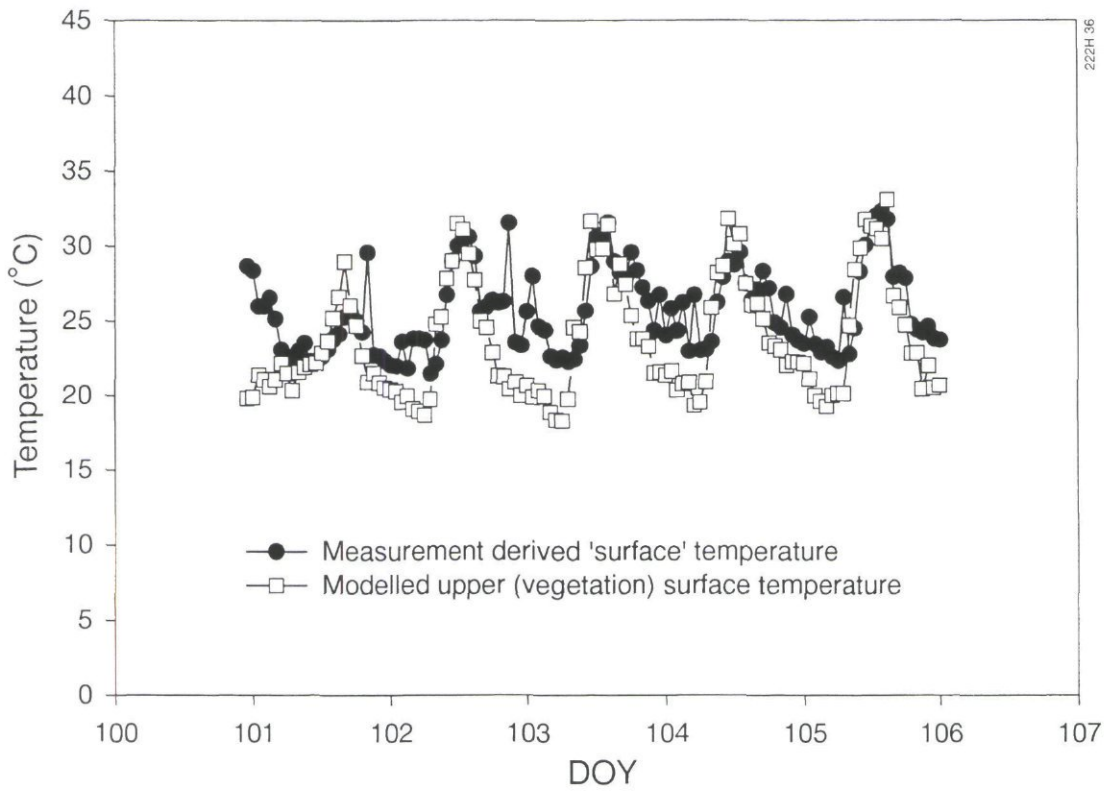


Fig. 3.6 SWAPS: simulated (upper vegetation layer) and measurement derived surface temperature for R/JF Mission 4/5 (wet part).

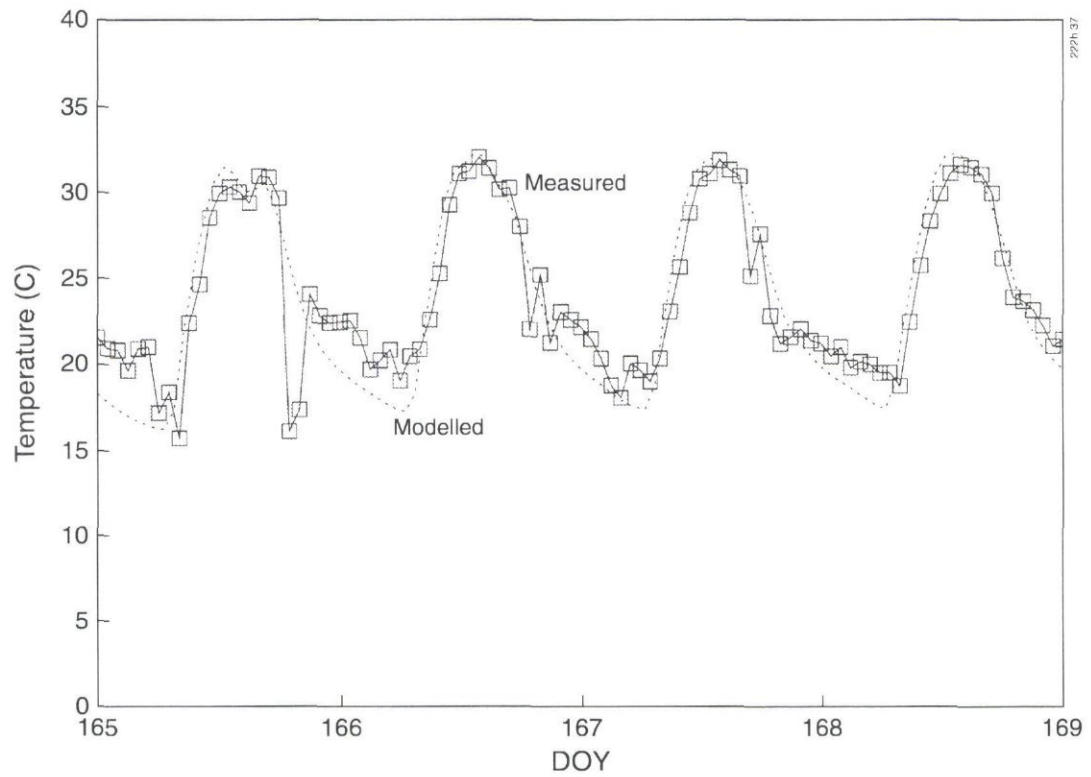


Fig. 3.7 ISBA: simulated and measurement derived surface temperature for R/JF Mission 4/5 (dry part).

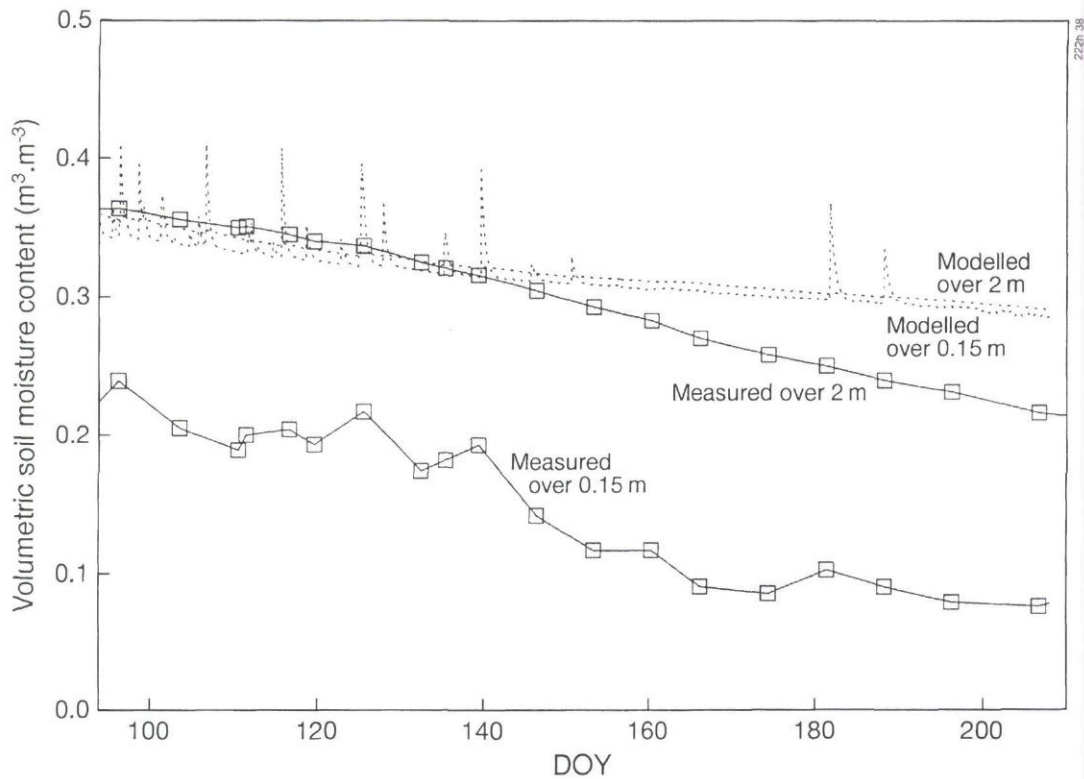


Fig. 3.8 ISBA: simulated soil moisture to depths ~15 cm and 2 m for RJF Mission 4 5.

Soil moisture produced by ISBA to two depths (~15 cm and 2 m) is shown in Fig. 3.8. Spikes in the simulated surface moisture content correspond to rainfall inputs. ISBA does not reproduce steep vertical gradients in soil moisture. The force-restore method used in the model implies that the surface moisture content is restored to the equilibrium (i.e. between gravitational and capillary forces). This is close to the total moisture (as shown in Fig. 3.6) and explains the overpredicted surface moisture. In turn this explains the relatively high bare soil evaporation (Fig. 3.3) from ISBA although this is still slightly less than that produced by SWAPS (see below) using an explicit soil surface resistance. A direct comparison of total (mean) volumetric soil moisture with the measurements is not valid, again due to differences in model and measurement depths.

For SWAPS Fig. 3.9 shows the volumetric soil moisture at 15 cm and 2 m. The measured values have been interpolated to the model output times and depths. At 15 cm SWAPS predicts saturation after some rainfall inputs as shown by the highest spikes. These spikes are obviously not shown by the interpolated measurements of moisture, neither is saturation. This simulation fails to reproduce the soil drying near the surface, although at small depths higher uncertainty in the soil moisture measurements are expected. Since the model discretisation has small compartments near the surface the effect of this on the total soil moisture (Fig. 3.5) is small. This also explains why for this simulation the soil evaporation from SWAPS is greater than that produced by ISBA. At 2 m the model appears to reproduce the soil moisture well apart from the kink at the beginning of the simulation which is probably an initialisation problem.

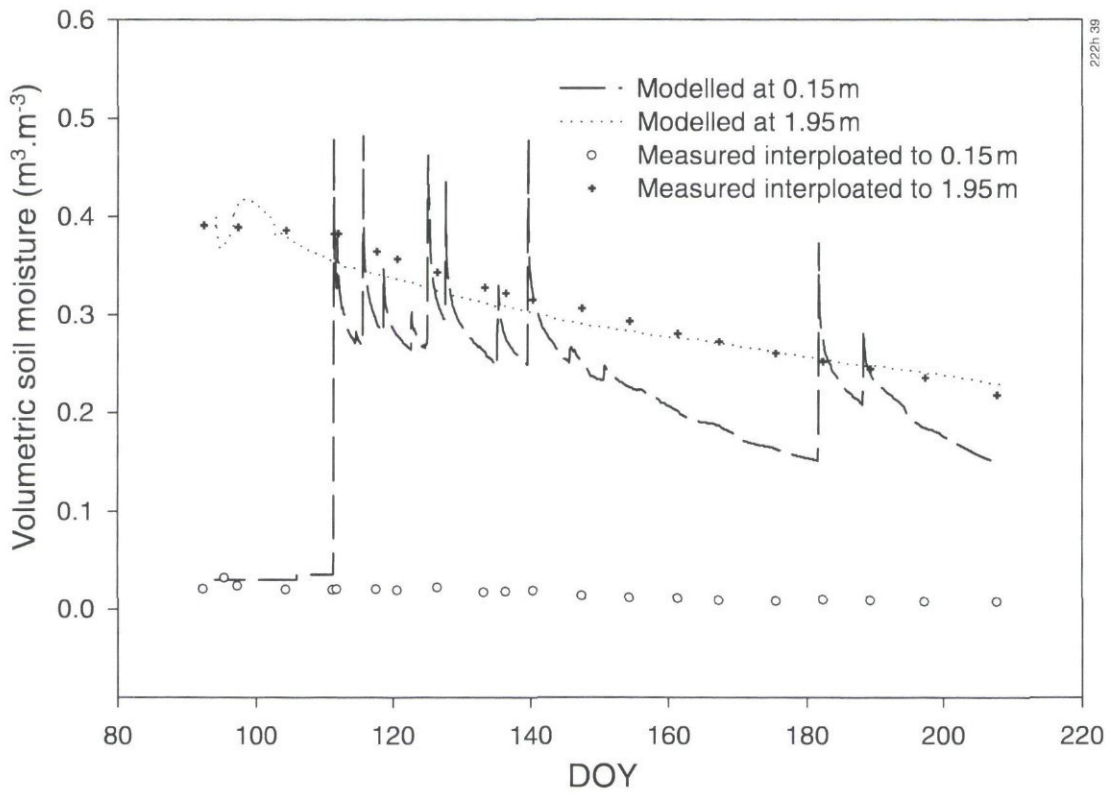


Fig. 3.9 SWAPS: simulated and measured (interpolated to model depths and times) volumetric soil moisture at 15 cm and 2 m for RJF Mission 4 5.

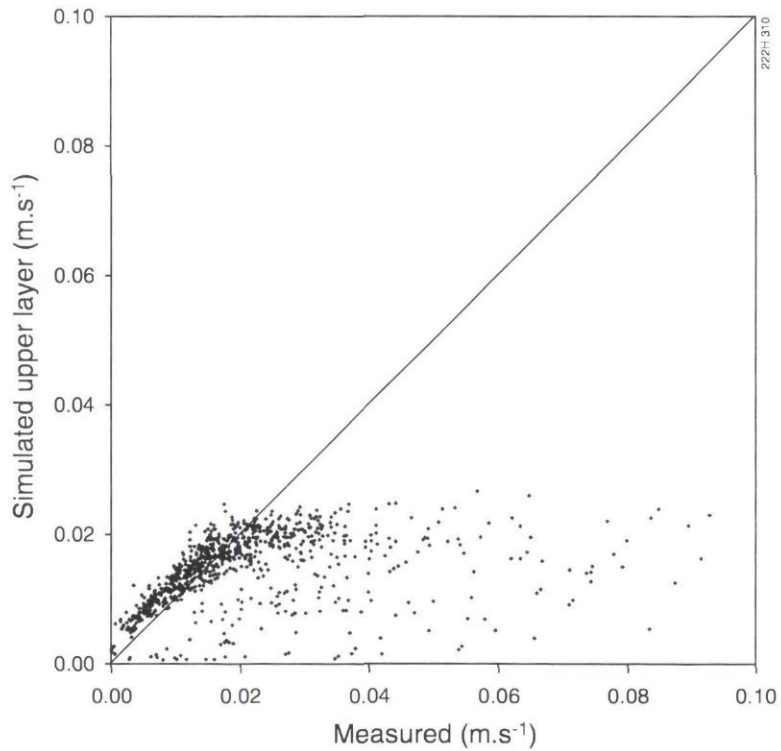


Fig. 3.10 SWAPS: simulated upper vegetation layer versus measurement derived surface conductance for RJF Mission 4 5.

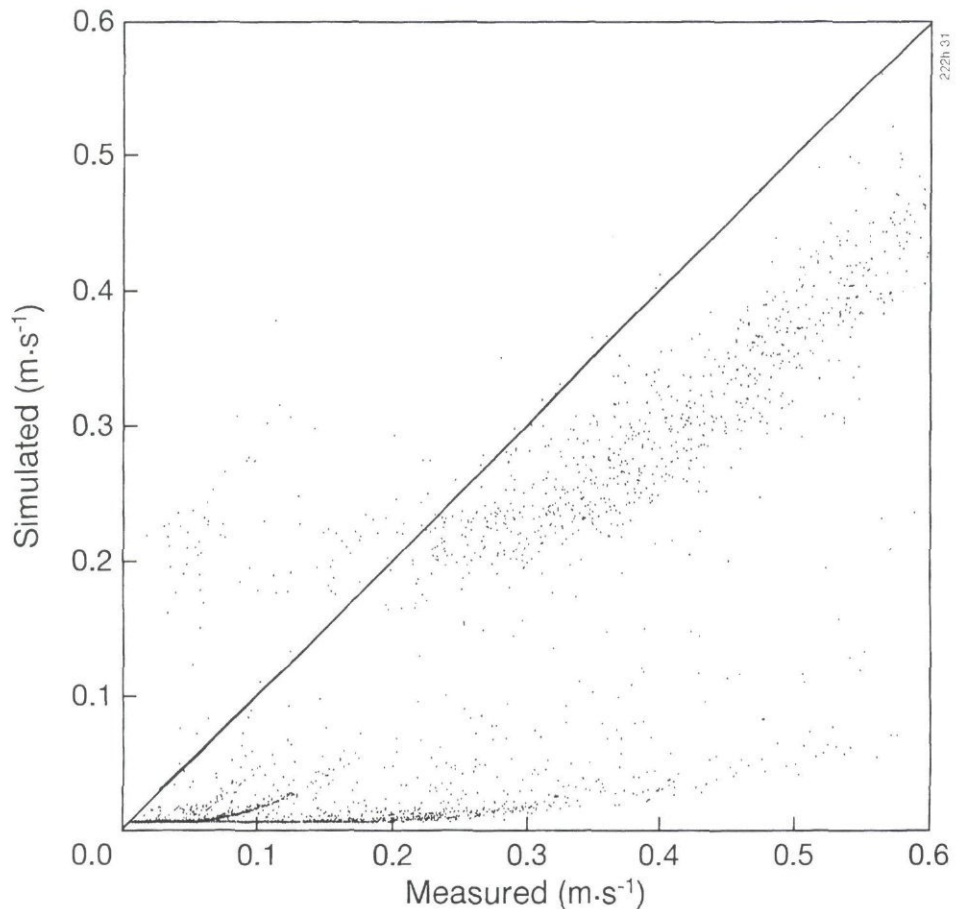


Fig. 3.11 ISBA: simulated versus measured friction velocity for RJF Mission 4/5.

Fig. 3.10 shows the modelled *upper* vegetation layer versus derived surface conductance for SWAPS. Note that at high values of derived surface conductance SWAPS appears to underpredict and this is also true of the other models. This may be due to the high derived values actually applying to times when the canopy is still wet whereas modelled values apply to a dry canopy.

Fig. 3.11 shows the modelled versus simulated friction velocity for ISBA. At night there are problems with the simulated friction velocity.

***Mission 4/5 - Nossa Senhora pasture***

For net radiation the same comments apply here as for the forest site, namely there is good agreement between observations and measurements for all models.

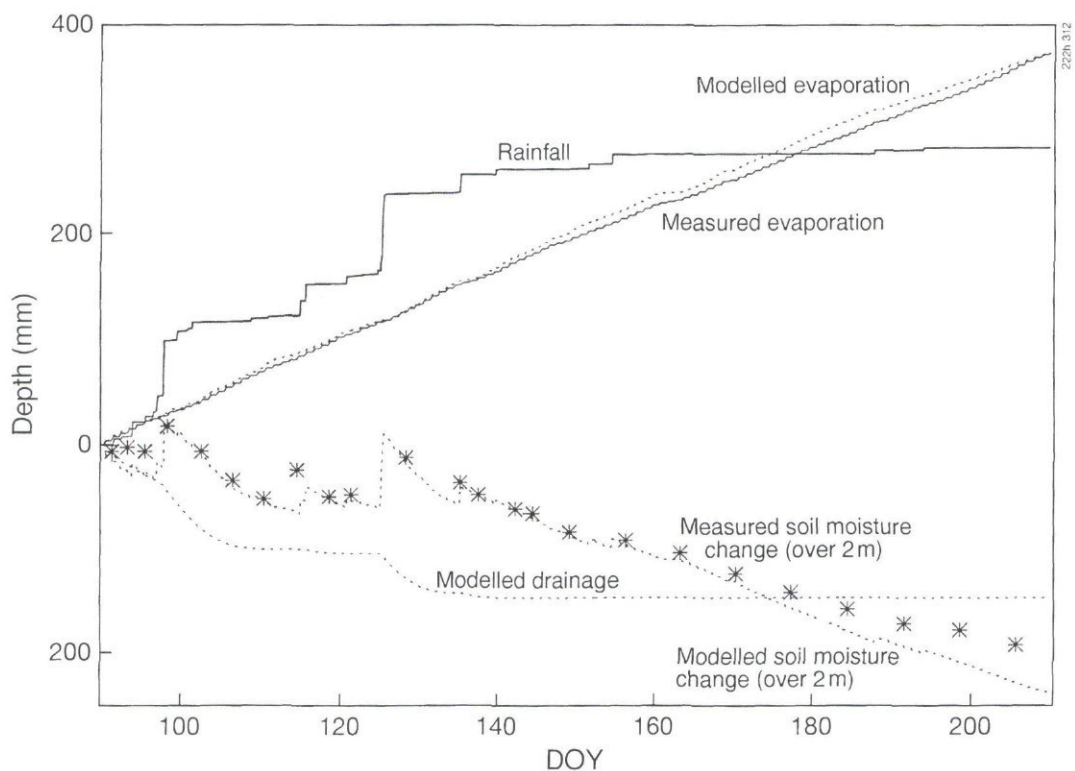


Fig. 3.12 ISBA: cumulative gross precipitation, total evaporation (measured and simulated), total soil moisture change (measured and simulated), drainage (simulated) for NSP Mission 4.5.

Fig. 3.12 shows the same cumulative water balance variables produced by ISBA for the pasture as those in Fig. 3.2 for the forest. In this simulation the total evaporation from the pasture site is slightly overpredicted by the model in some parts of the mission. Note that comparison with Fig. 3.2 shows there is less total (modelled and measured) evaporation from the pasture compared to the forest. A direct comparison of modelled and measured the soil moisture change is valid for this simulation for ISBA since the model soil and root depth is only 2 m. ISBA is able to reproduce the soil moisture change well, but with stronger than observed drying at the end of the mission.

Fig. 3.13 shows the cumulative water balance variables for pasture for MOSES. Note that for this figure drainage is *positive* out of the system. For this Mission and site MOSES (and SWAPS was run with a free drainage boundary condition at the bottom of the soil profile. Again as expected the model predicts a flattening out of the cumulative drainage as the soil dries. The model underpredicts the total evaporation (85% of the measured values). The soil moisture change over 2 m is well predicted except at the beginning of the mission. For SWAPS (not shown) the total cumulative evaporation is overpredicted by some 11%. This is due to the model failing to reproduce the soil drying after rainfall inputs during the first part of the mission, and the pasture thus failing to suffer water stress in the simulation.



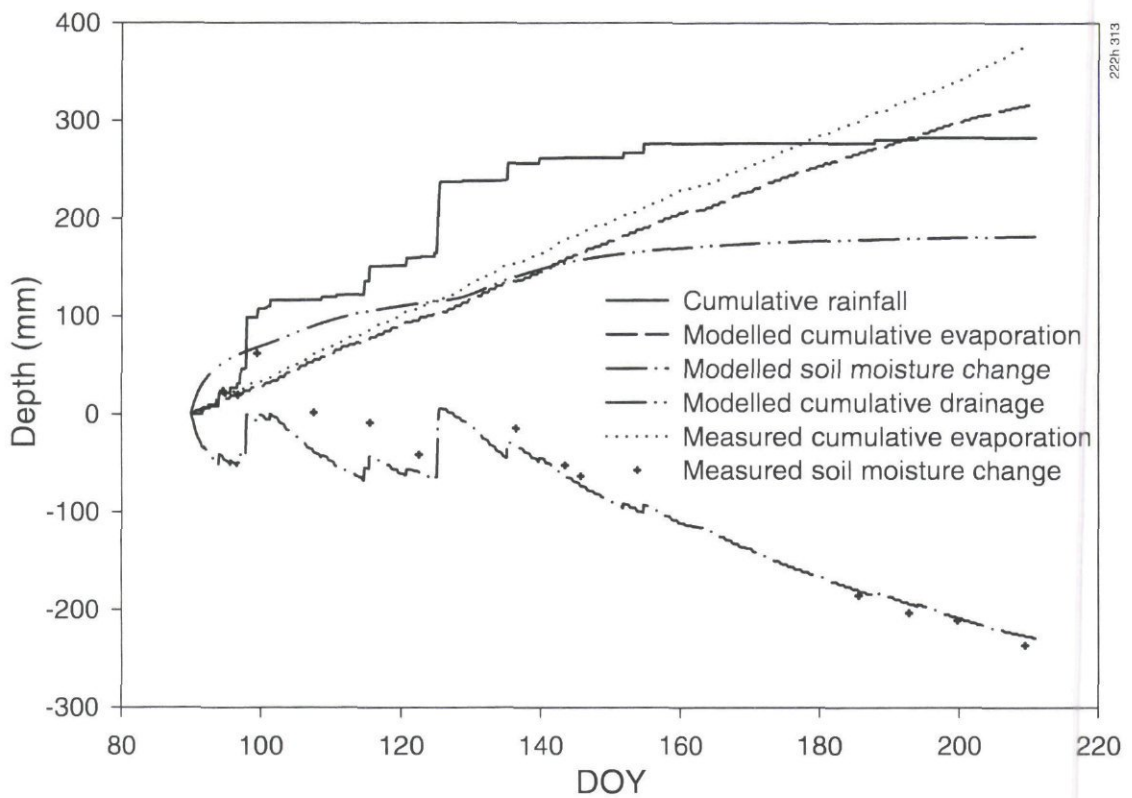


Fig. 3.13 MOSES-2S: cumulative gross precipitation, total evaporation (measured and simulated), total soil moisture change (measured and simulated), drainage (simulated) for NSP Mission 4 5.

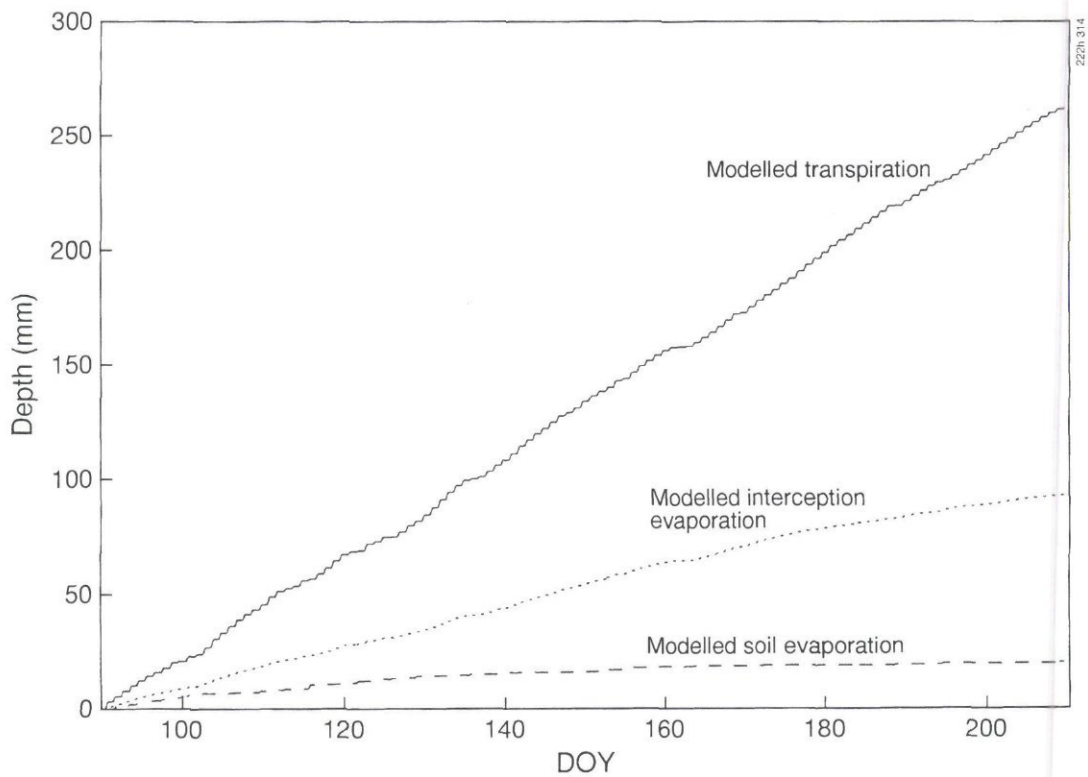


Fig. 3.14 ISBA: simulated cumulative transpiration, interception loss, bare soil evaporation for NSP Mission 4 5.

For ISBA Fig. 3.14 shows modelled cumulative transpiration, bare soil evaporation and interception loss. *Modelled* bare soil evaporation is significant, amounting to a cumulative value of 20 mm by the end of the mission. This is higher than that for the forest site (both absolute and as a percentage of the total evaporation). The modelled interception loss amounts to some 33% in this simulation. Fig. 3.15 shows the same cumulative variables for MOSES. Soil evaporation is again significant and amounts to 15mm. The larger soil evaporation predicted by ISBA may be explained by the force-restore method restoring the surface soil moisture to a value close to the total equilibrium value.

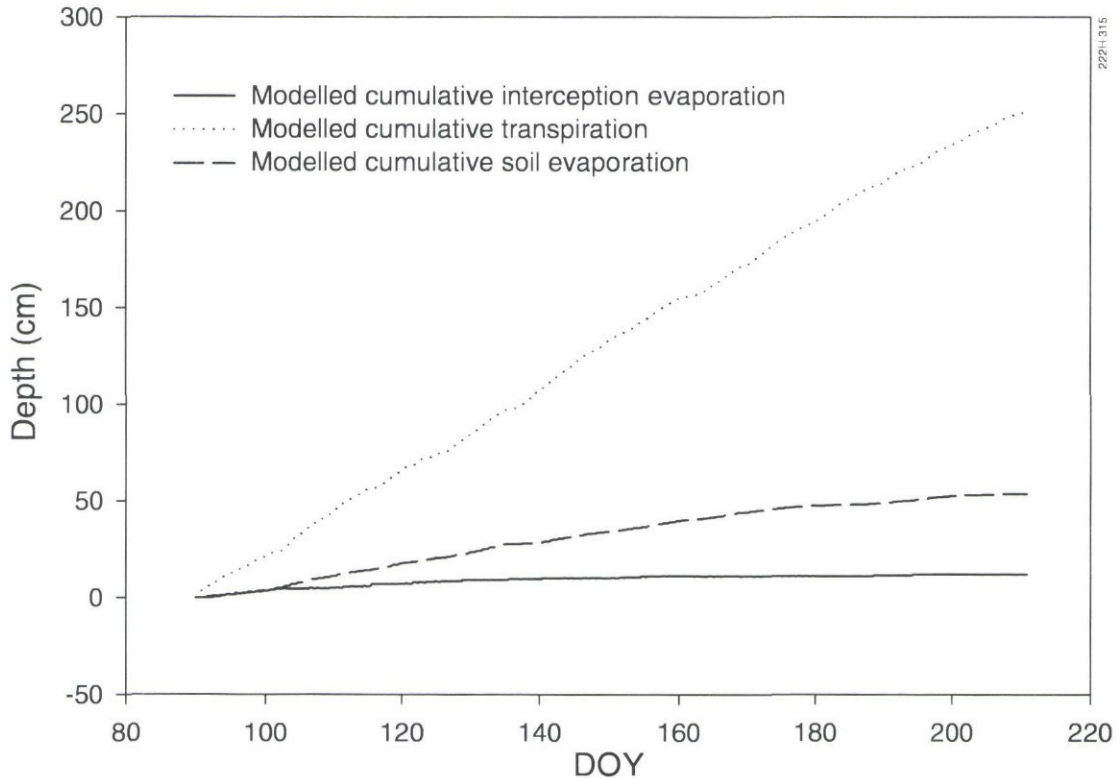


Fig. 3.15 MOSES-2S: simulated cumulative transpiration, interception loss, bare soil evaporation for NSP Mission 4/5.

All three models seem to predict the surface/in-canopy temperatures reasonably well, but again, like the forest simulation, underestimating the night-time values. Fig. 3.16 shows the in-canopy temperatures for MOSES simulated for a wet part of Mission 4/5. Note that generally for this mission the maximum 'surface' temperatures for the pasture are a few degrees higher than those for the forest.

Soil moisture at two depths is shown in Fig. 3.17 for ISBA. Spikes in the simulated surface moisture content correspond to rainfall inputs which are not shown in the soil moisture measurements. The depth of the modelled surface layer here is dependent on soil wetness and varies between 10 and 21 cm. As for the forest simulation the surface soil moisture is overpredicted because the force-restore method (see above).

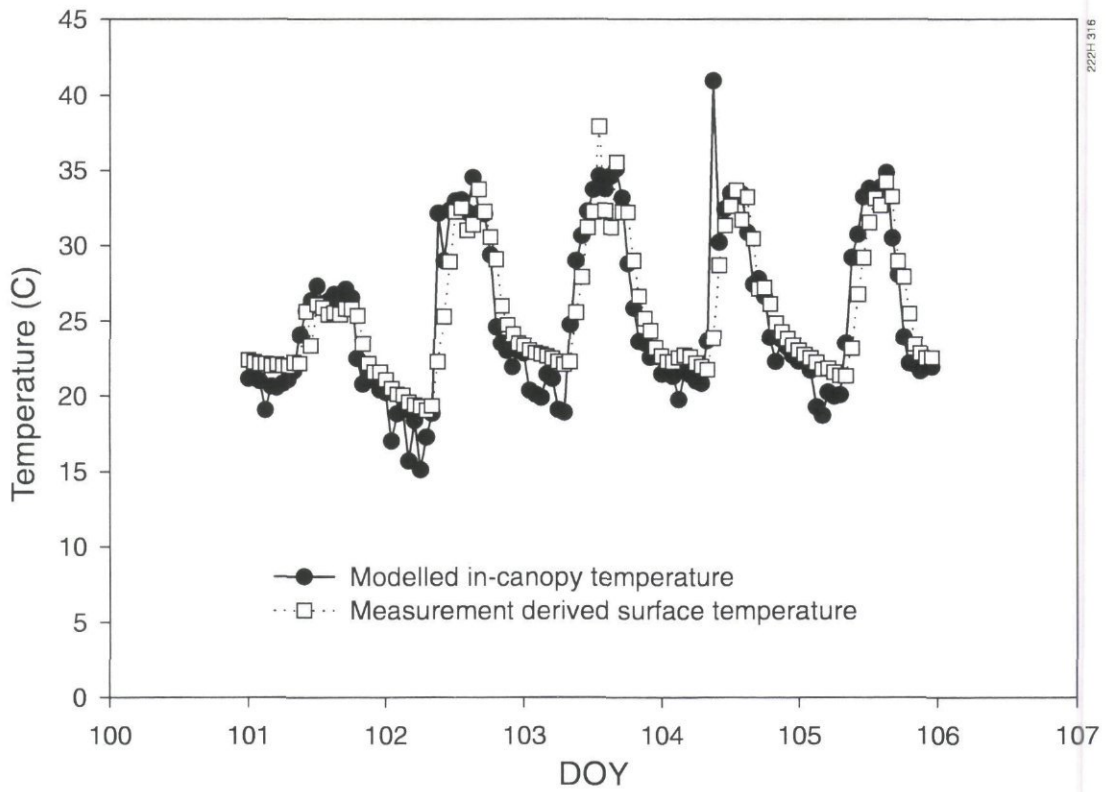


Fig. 3.16 MOSES-2S: simulated in-canopy and measurement derived surface temperature for NSP Mission 4/5 (wet part).

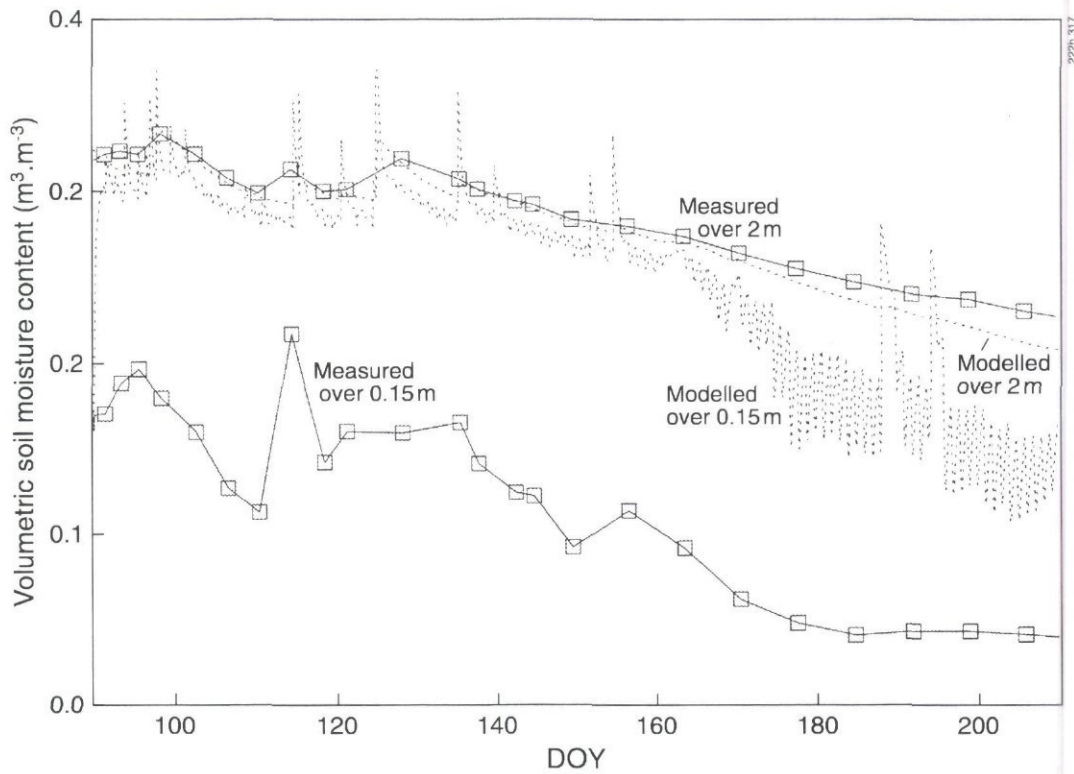


Fig. 3.17 ISBA: simulated and measured soil moisture to two depths for NSP Mission 4/5. Shallow depth is 15 cm for measurements, 10 - 21 cm (variable) for model; deep is 2 m for both model and measurements.

A direct comparison of total (mean) volumetric soil moisture with the measurements is valid here because in this simulation the soil and root profile was taken to a depth of 2 m. The model corresponds well to the measurements but with some increased drying towards the end off the mission.

Fig. 3.18 shows modelled and measured 'surface' and 'deep' volumetric soil moisture for MOSES. The model is designed for use in a GCM where the rainfall intensity is lower than a point measurement (possibly by a factor of 10), and assumes that soil moisture does not change rapidly with time. This is clearly not the case at the surface with measured rainfall, hence the spikes in the model results. Over long periods the effects of this are not significant. Generally the model significantly overpredicts the surface soil moisture and slightly underpredicts the deep soil moisture.

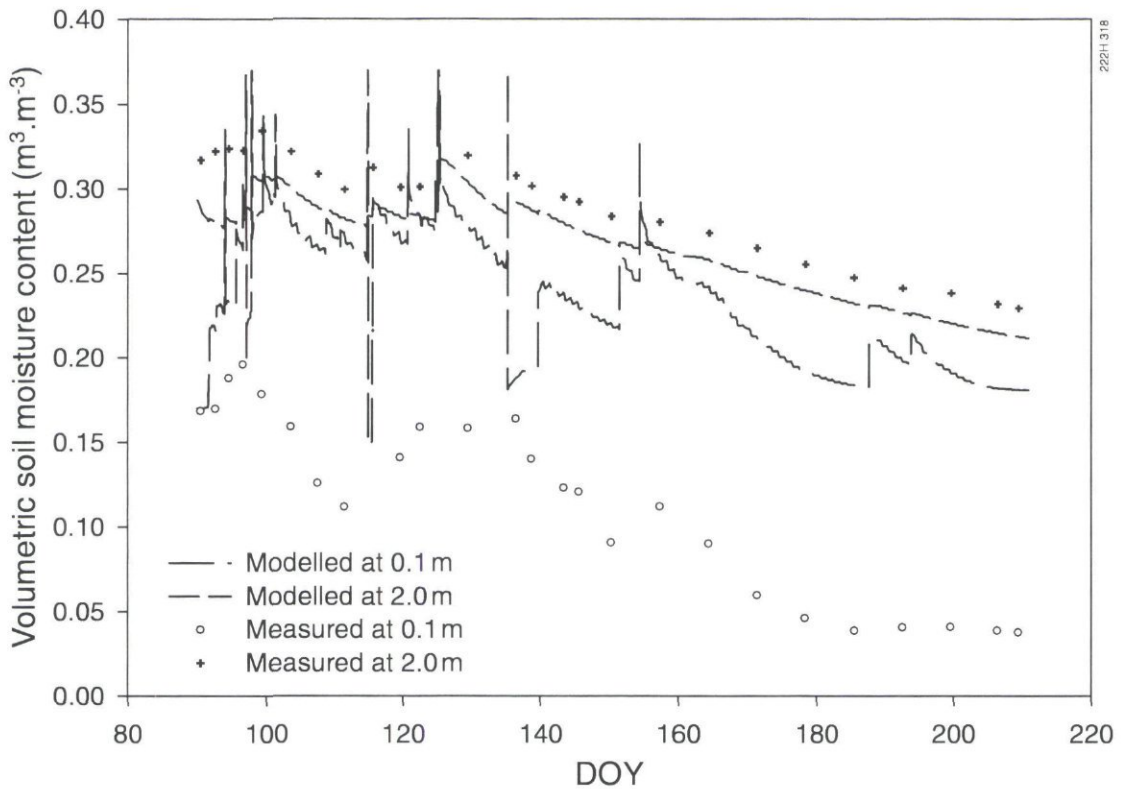


Fig. 3.18 MOSES-2S: simulated and measured volumetric soil moisture at two depths for NSP Mission 45.

Fig. 3.19 shows measured versus observed friction velocity for MOSES. There is some tendency to overpredict low friction velocities and slightly underpredict high values. For ISBA the same comments apply here as for the forest simulation for this mission, namely problems with night-time values of the friction velocity.

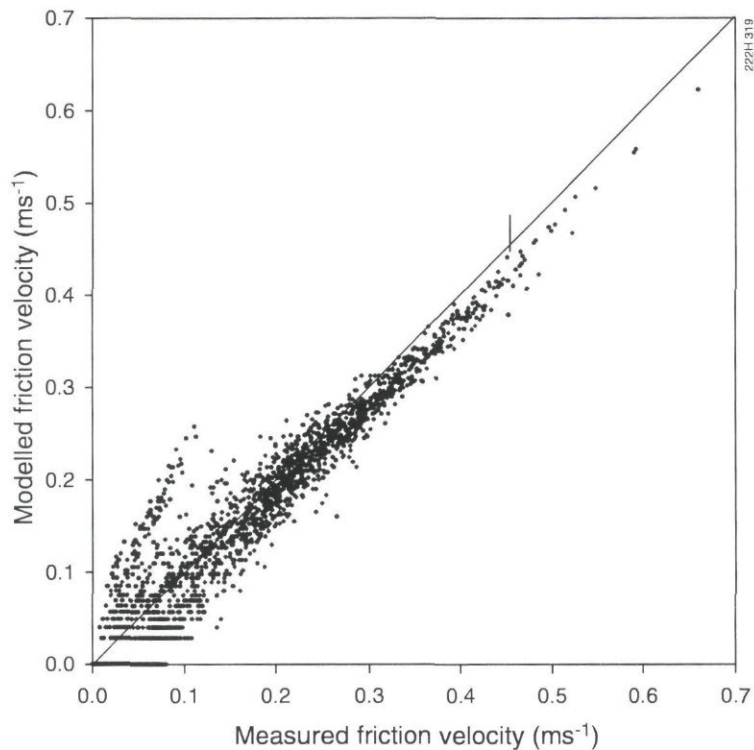


Fig. 3.19 MOSES-2S: simulated versus measured friction velocity for NSP Mission 4/5.

**Mission 7 - Reserva Jaru forest**

Fig 3.20 shows the cumulative water balance variables for forest produced by ISBA. There is a slight underprediction in total evaporation. Measured values of soil moisture change are not shown because measurements are only available at a single point in time during this mission . For SWAPS (not shown) a similar underprediction occurs for the total evaporation.

**Mission 7 - Nossa Senhora pasture**

Fig. 3.21 shows the following cumulative variables produced by SWAPS: total and soil evaporation, and transpiration. There is no modelled interception evaporation for this run. In the simulation the total evaporation is predominantly supplied by the transpiration component and soil evaporation is small. By the end of the mission the total evaporation is slightly underpredicted. This is also true for ISBA (not shown), although the soil evaporation component is greater than that for SWAPS.

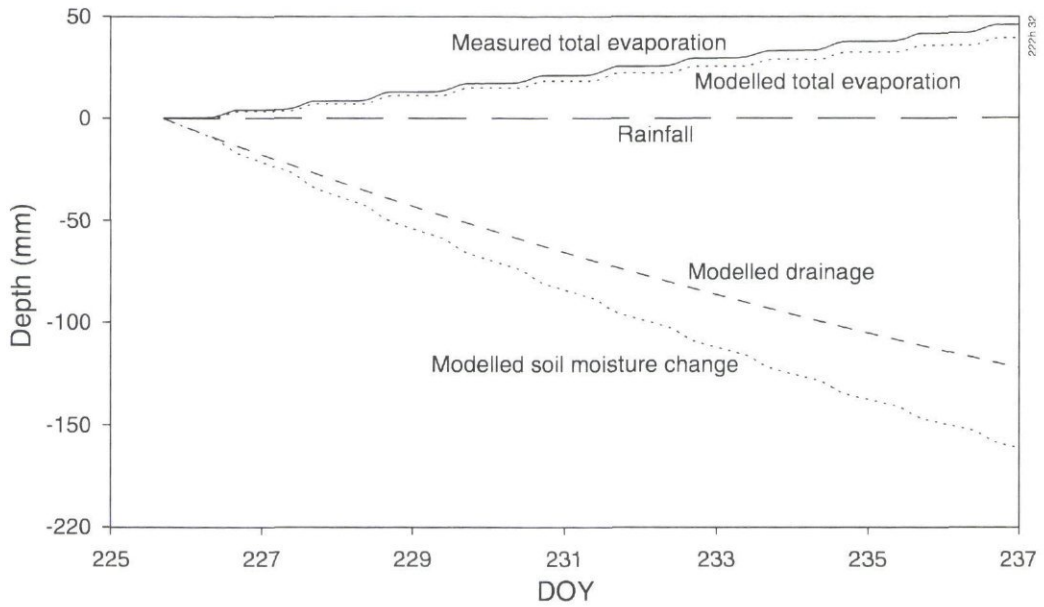


Fig. 3.20 ISBA: cumulative total evaporation (measured and simulated), and simulated total soil moisture change and drainage for R.J.F. Mission 7.

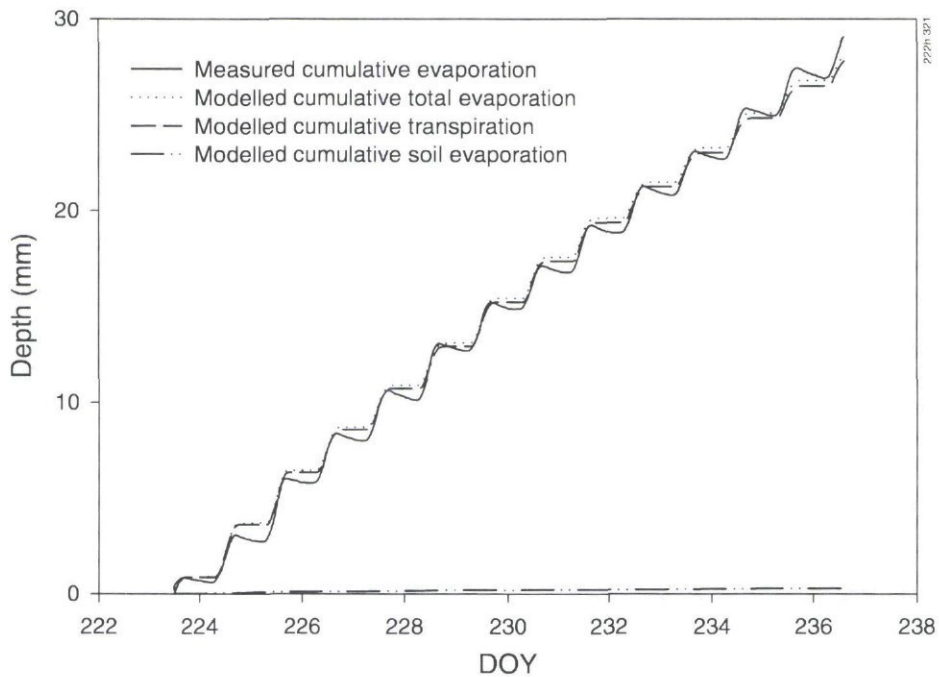


Fig. 3.21 SWAPS: simulated and measured cumulative total evaporation; simulated cumulative transpiration and bare soil evaporation for NSP Mission 7.

### 3.5 Discussion

Using the method of Culf and Gash to estimate incoming longwave radiation appears to work well and this is reflected in the plots of simulated versus measured net radiation. For high net radiation the spread appears to be less than for lower values. This may reflect that the models use a constant albedo with no account for the solar angle. In addition, some spread is to be expected due to rainfall modifying the albedo (in the wet season) which again is not accounted for in any of the models. For low values of net radiation the importance of simulating the surface temperature correctly becomes more important. However, despite the systematic underprediction of night-time surface temperatures by all models, there is no clear overprediction of net radiation at night.

All models are able to reproduce the latent heat fluxes for forest under both dry and wet conditions. This is in part due to the fact that there has been no observed water stress for forest and this has not been included as a stress function in the surface conductance model for the forest. During the wet season the water table at Reserva Jaru forest is within 2.0 m of the soil surface and this can considerably influence the soil moisture profile. It should be noted that this site is close to a river where ground water effects are important, but this will not be the case for all forest sites. For detailed soil moisture modelling a knowledge of the GWL may be important even though a model can reproduce the surface fluxes without necessarily reproducing the moisture distribution. Although the soil heat flux beneath forest is a relatively small part of the energy balance, the canopy storage for a rainforest is significant and can be of similar magnitude to the sensible heat flux.

The different models reproduce the latent heat fluxes over pasture with varying degrees of success. The cumulative total evaporation from ISBA agrees well with the measurements. For Mission 4/5 MOSES tends to underpredict the latent heat fluxes whereas SWAPS overpredicts. This highlights the need, particularly for pasture, in adequately predicting soil moisture, hence moisture stress in the surface conductance model; and the need for parameters that adequately describe the soil hydraulic properties. Note that rainfall input appears to cause problems for both SWAPS and MOSES for the pasture site, whereas SWAPS, at least, appears to perform well under dry conditions (Mission 7) at this site (MOSES has not yet been run for this site and mission). All models reproduce reduced evaporation (and increased sensible heat) for the pasture site compared to the forest and this is important when representing the different surface types in mesoscale models.

## 4 Mesoscale modelling

### 4.1 Introduction

Modelling studies with General Circulation Models have generally shown that large scale deforestation of the Amazon basin may result in increased surface temperatures and decreased rainfall (e.g. Lean and Rowntree, 1993). This result is obtained because the modelled deforestation reduces evaporation and increases long wave outgoing and sensible heat fluxes, and consequently induces a drying of the planetary boundary layer (Sud et al., 1996). Moreover, decreased large scale convergence of moisture through a reduced aerodynamic roughness of the pasture lands also acts to reduce precipitation. Typically decreases amount to 10 to 20% of the annual rainfall.

The GCM results suggest that the climatological and hydrological effects of deforestation are a mixture of meso scale (boundary layer) and continental through global processes. Experiments with meso scale models have shown that increased heating of the boundary layer may also trigger convection, if the initial moisture availability is sufficiently large (Avisar and Chen, 1995). Thus, according to this study, regional deforestation, leading to heat islands of pasture in an otherwise moist rainforest environment, may lead to enhanced rainfall. As deforestation does not as yet affect the whole of the Amazon basin, but is concentrated in regions such as Rondônia or Pará, there clearly is a need to understand the interplay between the local to meso scale and continental scale processes, particularly with regard to rainfall generation. The Large Scale Biosphere Atmosphere Experiment in Amazonia (Nobre et al., 1996) is designed to provide this knowledge. LBA aims to generate enhanced understanding of the way Amazonia functions as a regional entity and how this may change under global climate change and human induced land use changes.

The key questions to be addressed in the meso scale field campaigns of LBA (Nobre et al., 1996) are: what are the mesoscale mechanisms by which differences in surface characteristics translate into large scale weather anomalies and what is the role of dry and moist convection in transferring energy and how will this change with different land use patterns?

To prepare this experimental program a modelling program was initiated as part of the EU supported project to identify the main uncertainties in the current understanding of the effects of tropical deforestation at the mesoscale (Dolman et al., 1994). The program consisted of collection of available data and usage of this in combination with state of the art mesoscale models to bring out the major areas of uncertainty in the model predictions. These modelling deficiencies ideally would then be the focus of the experimental campaigns.

Experimental evidence from previous studies suggest that meso scale circulations caused by large water bodies such as the Amazonian rivers, may lead to significant small scale rainfall gradients (Martin et al., 1988). Furthermore, the Rondônia Boundary Layer Experiments II and III have provided the first experimental evidence



of large differences between the structure and growth of the boundary layer over forest and pasture (Fisch, 1996). During the dry season, simultaneous measurements of boundary layer temperature and humidity show that the boundary layer over the pasture is between 500 to 1000 m deeper and up to 2 K warmer. Although to a large extent these differences are related to differences in surface heating (see e.g. Wright et al., 1992), existing slab models of the boundary layer development fail to predict the correct growth when fed with observed surface heat fluxes (Nobre et al., 1996).

As the boundary layer plays a key role as mediator between the surface and large scale weather systems, it is of obvious importance to correctly model and understand the mechanisms involved in the boundary layer growth of the Amazonian dry season. This is even more so, as the GCM predicted drying will have the strongest ecological implications during the dry season, when rainfall is scarce, and most probably of local origin.

In this chapter we describe the modelling program initiated as preparation for the LBA meso scale field campaigns. Three models are used to integrate existing data and highlight deficiencies in the model parameterizations. They are the research version of the French operational forecast meso scale model PERIDOT (Bougeault et al., 1991), the Regional Atmospheric Modelling System (Pielke et al., 1992) and a 1-D version of the newly developed French non-hydrostatic meso scale model MESO-NH. The models are run in various configurations and at different resolutions to investigate surface atmosphere interaction at all relevant spatial scales. The models are run for periods during the 1994 dry season in Rondônia, a period during which the third Rondônia Boundary Layer Experiment took place and surface flux data were available from the joint Brazilian-UK ABRACOS experiment (Gash and Nobre, 1997).

## **4.2 Mesoscale models and data**

### **4.2.1 Model descriptions**

Two fully three-dimensional mesoscale models were used: the French hydrostatic PERIDOT model and the US developed RAMS model in operation at the Winand Staring Centre. A one-dimensional version of the new French non-hydrostatic mesoscale model MESO-NH was also used.

The MESO-NH model is a non-hydrostatic atmospheric model designed to simulate the phenomena occurring at scales ranging from a few ten-m to a few ten-km. The surface processes in MESO-NH are described by the ISBA scheme. In this study, the calibrated version of ISBA (Delire et al. 1997) is employed in MESO-NH to perform 1D simulations over RJF ( $\beta = 0$ , no deforestation) and NSP ( $\beta = 0.6$ , 60% deforestation) on August 18, 1994.

RAMS (the Regional Atmospheric Modelling System) has been developed at Colorado State University and the ASTER Division of the Mission Research Corporation. It has had widespread use in simulating and forecasting meteorological

phenomena. The two major components in RAMS are the data analysis and assimilation package and the atmospheric model. The former allows the use of meteorological observations and/or analyses from larger scale models for initialisation and model 'nudging'. The atmospheric model is based around the full set of primitive dynamical equations governing atmospheric motion. These equations are supplemented by optional parameterizations for long- and short-wave radiation, turbulent diffusion, moist processes, surface-atmosphere moisture and energy exchange, kinematic effects of terrain, and cumulus convection. The land surface scheme is based on the BATS model of heat and moisture exchange between the atmosphere, vegetation canopy, multiple soil layers and surface water. In principle there is no lower limit to the domain size or cell size of the finite difference grid, and the model can be configured to cover a planetary hemisphere. In addition, two-way interactive grid nesting allows simultaneous modelling of large scale and small scale phenomena.

The PERIDOT model has also been applied to the Amazon basin. The model has 30 levels in the vertical and operates at grid lengths greater than 10 km. Lateral boundary forcing is provided by a relaxation of the prognostic dynamic variables towards specified values on the boundaries of the domain. The radiation code distinguishes between clouded and clear sky conditions. Vertical diffusion is calculated using a turbulent kinetic energy system (Bougeault and Lacarriere, 1989). The model is initialised with data from the large scale analysis of ECMWF. Simulations have been performed over a large domain covering the Amazon basin (2000km×2000 km) and over a small domain (600km×600 km). The small domain covers Rondônia. It is centred on the RBLE III sites. The PERIDOT grid mesh is 58 and 10 km for the large and small domains, respectively. The meteorological synoptic analyses from the ECMWF model obtained for August 1994 serve as lateral boundary conditions for PERIDOT at the 58 km resolution. These low resolution results are then used as initial and lateral boundary conditions for the higher (10km) resolution model. The simulations with the 10 km resolution model are performed with the calibrated version of ISBA and the aggregated values of the surface parameters (Section 2.3) for several days during the RBLE III period.

#### **4.2.2 Data**

A data set consisting of forcing from large scale analysis, surface maps and boundary layer and flux data was assembled. ECMWF analyses were used at CNRM, NMC analyses at SC-DLO. The RBLE III radio soundings were obtained from our Brazilian colleagues. This campaign involved participants from IH (who also provided the radiosondes) and CNRM. The micro-meteorological measurements performed during RBLE III in the framework of the ABRACOS project were provided by IH. METEOSAT data (full spatial and temporal resolution) during RBLE III were provided by INPE (Brazil) to CNRM, also deforestation maps have been obtained from 1993-94 LANDSAT-TM data provided by INPE to CNRM. Soil and natural vegetation maps over Rondônia (600×600 km) at the 1 :1,000,000 scale were obtained in Brazil at IBGE. These maps are from the RADAMBRASIL 'Levantamento dos recursos naturais'. They are very well documented (the figures

from which the soil and vegetation maps were drawn are available in a set of comprehensive textbooks - in Portuguese). Also the topography is also available at both 1:1,000,000 and 1:250,000 scales. Vegetation, soils and topography data was digitised by CNRM to produce maps for use in the mesoscale models (see Chapter 1).

### 4.2.3 Aggregation of surface data for use in PERIDOT

More often than not, the PERIDOT grid points cover heterogeneous landscapes: in the deforested zones the proportion of pasture lands seldom exceeds 60% (Fig. 4.1), the soil characteristics may also vary a lot within the same grid box. Therefore, preliminary work consisted in producing 10km×10km physiographic maps adapted to the PERIDOT runs, from the high resolution digital maps proposed by Calvet et al. (1997) of soil and natural vegetation (1 to 2 km) and of the current (1993-1994) deforestation in Rondônia (120 m). The change in spatial resolution was made by applying simple aggregation rules.

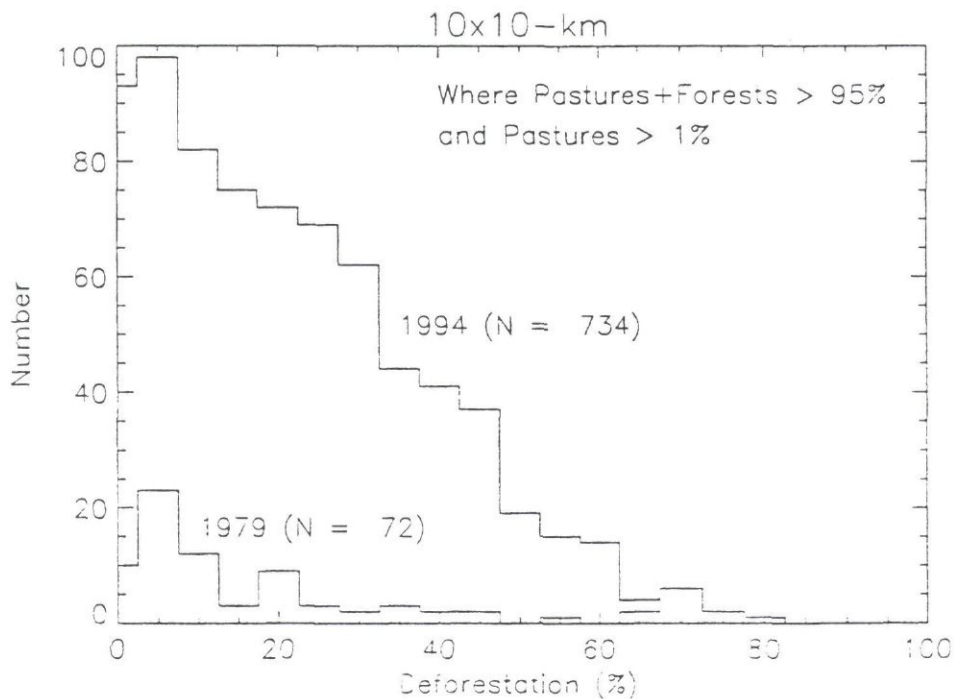


Fig. 4.1 Histogram of the deforestation rate in 1993-1994 as calculated for a 10km×10km grid from the 120-m resolution map produced over the 8-13 S, 60-65 W domain. The histogram obtained for 1979 from the RADAMBRASIL maps (Calvet et al. 1997) is also plotted.

The aggregation consists in determining, for each PERIDOT grid point, a set of values of the ISBA parameters which will produce surface fluxes equivalent to the sum of the fluxes produced by each individual pattern of the landscape. In the case of a forest-pasture land contact, the aggregation of the parameters of Table 4.1 is performed according to the proportion of pasture lands (i.e. the deforestation rate)  $\beta$ .

Table 4.1 The ISBA scheme soil and vegetation structure parameters over the Rondônia sites of ABRACOS during the dry season. The values are either prescribed, measured, calculated from continuous functions of the texture, or calibrated.

Symbol	Definition	RJF	NSP	Unit	Source
Soil parameters:					
$d_2$	Soil root depth	8	2	m	prescribed
CLAY	Clay fraction	24	30	%	measured
SAND	Sand fraction	63	60	%	measured
$w_{wilt}$	Wilting point	0.16	0.18	$m^3 m^{-3}$	continuous functions
$w_{fc}$	Field capacity	0.28	0.30	$m^3 m^{-3}$	calibrated functions
$w_{sat}$	Saturation	0.39	0.40	$m^3 m^{-3}$	continuous functions
Vegetation parameters:					
LAI	Leaf Area Index	4.6	1.5	$m^2 m^{-2}$	measured
Veg	Vegetation coverage	99	85	%	measured
	Albedo	0.14	0.20	-	measured
$\epsilon$	Emissivity	0.95	0.95	-	prescribed
$C_V$	Thermal coefficient	$1.2 \times 10^{-5}$	$5.0 \times 10^{-3}$	$Km^2 J^{-1}$	calibrated
$r_{smin}$	Minimum stomatal resistance	175	132	$sm^{-1}$	prescribed
	Vapor pressure deficit sensitivity	0.04	0.	$kg kg^{-1}$	prescribed
$R_{GL}$	Global radiation limit	30	100	$Wm^{-2}$	prescribed
$z_0$	Roughness length	2.6	0.06	m	calibrated
$z_0/z_{0h}$	Roughness length ratio	10	10	$m m^{-1}$	prescribed

Along with these parameters, the value of the initial soil moisture ( $w_2$ ) must also be aggregated. The  $\beta$  parameter can be estimated easily from the 120 m resolution deforestation map (Fig. 4.1). The manner in which the parameter concerning the forest characteristics ( $\varphi_F$ ) is combined with the parameter corresponding to the pasture land ( $\varphi_P$ ) to produce the aggregated value  $\varphi_A$ , depends on the parameter category:

$$\varphi_A = \beta \varphi_P + (1 - \beta) \varphi_F$$

for LAI, veg,  $\alpha$ , and  $d_2$ ,

$$\frac{1}{\varphi_A} = \frac{\beta}{\varphi_P} + \frac{(1 - \beta)}{\varphi_F}$$

for  $r_{smin}$ , and  $C_V$ ,

$$\frac{\varphi_A}{r_{smin}} = \beta \frac{\varphi_P}{r_{smin}} + (1 - \beta) \frac{\varphi_F}{r_{smin}}$$

$$\frac{LAI_A}{LAI_P} = \beta \frac{LAI_P}{LAI_P} + (1 - \beta) \frac{LAI_F}{LAI_P}$$

for  $\gamma$ ,  $R_{GL}$ , and the initial saturation fraction

$$\theta = \frac{(W_2 - W_{will})}{(W_{fc} - W_{will})}$$

Finally

$$\frac{1}{\ln^2 \left[ \frac{z_R}{\varphi_A} \right]} = \frac{\beta}{\ln^2 \left[ \frac{z_R}{\varphi_P} \right]} + \frac{(1-\beta)}{\ln^2 \left[ \frac{z_R}{\varphi_F} \right]}$$

for the roughness  $z_0$ . In this equation,  $z_R$  is a reference level. In practice,  $z_R$  is the first level of the atmospheric model.

The above equations have been used to produce aggregated maps for PERIDOT simulations. The aggregated ISBA parameters corresponding to the PERIDOT grid point covering NSP ( $\beta = 0.6$ ) have been employed to perform one-dimensional (1D) simulations with MESO-NH.

### 4.3 Calibration of the land surface schemes

The RAMS land surface scheme is based on that described by Avissar and Pielke (1989). For the runs with the mesoscale model in this part of the project it was decided not to change the land surface parameterization, but to calibrate the scheme so that it reproduced correctly the observed fluxes for the days of interest. This procedure is acceptable for simulation periods of the order of one to two days, but would become unreliable if longer runs were made and vegetation phenology and/or soil moisture changed.

The scheme allows for bare soil and vegetation to exist jointly. The latent heat flux is described as a function of the relative stomatal conductance, which is a function of global radiation, leaf temperature, vapour pressure difference between the leaf and air and soil water potential. In the present case the dependence of the relative stomatal conductance on soil water content was calibrated to obtain agreement with the observed fluxes for the two vegetation classes.

Fig 4.2 shows the comparison between observed and simulated shortwave, latent ( $\lambda E$ ) and sensible ( $H$ ) heat fluxes for 18-20 August for (a) the Reserva Jaru forest (RJF) and (b) Nossa Senhora pasture (NSP) sites. Initially the modelled shortwave radiation was too high. As the simulations were made for the dry season, when there is forest and pasture burning producing smoke, a considerable aerosol loading of the atmosphere was present at that time, but not accounted for in the model. The downward shortwave radiation flux was therefore calibrated by tuning the solar constant. This will give the correct radiation flux surface at the surface, but obviously does not account for scattering and absorption of radiation in the boundary layer. Given the correct downward shortwave, the fluxes of latent and sensible heat can be simulated to a level of acceptable accuracy. At the NSP site the latent and sensible heat fluxes are roughly of equal magnitude around  $200 \text{ Wm}^{-2}$ . This partitioning of

available energy is well captured by the scheme. For the RJF site the latent heat component is the larger term in the energy balance and again this is well simulated by the land surface scheme. Sensible heat is the smaller component of the energy balance at a value of  $100 \text{ Wm}^{-2}$ . Latent heat fluxes of about  $400 \text{ Wm}^{-2}$  are well simulated. In conclusion, the land surface scheme of RAMS is, after calibrating the relative stomatal conductance (particularly its dependence on soil moisture content) capable of simulating the correct partitioning of available energy between latent and sensible heat, both for the forest (RJF) and the pasture (NSF) sites. The parameters used in this study are given in Table 4.2.

The ABRACOS data have also been used to calibrate the surface sub-models (see Delire et al. 1997 in annex for the ISBA model - Noilhan and Planton 1989). Also, the hydraulic properties of the Amazonian soils have been accounted for in the calibration. The ISBA calibration results are presented in Table 4.1 for RJF and NSP.

## **4.4 Mesoscale modelling**

### **4.4.1 Data and model initialisation**

RAMS was run in non-hydrostatic mode over an area in Rondônia. The model was run with two nested grids in a larger domain. The grid length of the largest domain was 16 km, that of the smallest 1 km. A schematic of the model configuration indicating the areas of pasture and forest is shown in Fig. 4.3. The number of levels in the vertical was 28 and the top of the model was set at 16000 m. The top boundary condition was a rigid lid with no Rayleigh friction. The lateral boundary condition was of the Klemp-Wilhemson type. Nudging at the lateral and top boundaries took place at six and one hourly intervals respectively, and was obtained from the large scale analysis of NMC at  $2.5^{\circ}$  by  $2.5^{\circ}$ . This data was also used to initialise the model. In the RAMS simulation presented here RBLE III radiosonde data for RJF were also used in the initialisation. The model was integrated forward for 18, 19 and 20 August 1994.

The land surface data for RAMS was obtained from the CNRM classification (Alvalá et al., 1997 - see Chapter 2 and Appendix). This classification was downgraded to the required model resolution (16.4 and 1 km) by taking the predominant cover class.

This data set has been produced by CNRM in order to adapt the PERIDOT and MESO-NH mesoscale models to the study area. The 1:1,000,000 soil, vegetation and relief maps have been digitised at CNRM (see Calvet et al. 1997 given in the Appendix). Finally, the new version of ISBA was employed to perform mesoscale runs during RBLE III of the PERIDOT model at a resolution of  $10\text{km}\times 10\text{km}$ . Also, the French non-hydrostatic model MESO-NH has been used to perform a 1D sensitivity study also using the calibrated version of ISBA.

Table 4.2 The RAMS scheme soil and vegetation structure parameters over the Rondônia sites of ABRACOS during the dry season. The values are either prescribed, measured, calculated from continuous functions of the texture, or calibrated.

Symbol	Definition	RJF	NSP	Unit	Source
Soils parameters:					
	clay fraction	0.8	0.8		prescribed
	sand fraction	0.18	0.18		prescribed
B	Clapp and Hornberger b	10	10		prescribed
$k_s$	Thermal conductivity	$2.34 \cdot 10^{-7}$	$2.34 \cdot 10^{-7}$	$m^2/s$	measured
$k_{\theta s}$	Sat. hydraulic cond.	$2.6 \cdot 10^{-3}$	$2.6 \cdot 10^{-3}$	m/s	measured
$\sigma_{cp}$	Heat capacity of dry soil	$1344 \cdot 10^3$	$1344 \cdot 10^3$	J/m <sup>3</sup> /K	prescribed
$\sigma_s$	Density of wet soil	1600	1600	kg/m <sup>3</sup>	prescribed
$\theta_s$	Porosity	0.4	0.4	m <sup>3</sup> /m <sup>3</sup>	measured
$\psi_s$	Sat. moisture potential	-0.5	-0.5	m	measured
Vegetation parameters:					
LAI	Leaf Area Index	5.6	3	m <sup>2</sup> m <sup>-2</sup>	measured
$\alpha$	Vegetation coverage	95	85	%	measured
	Albedo	0.14	0.19	-	measured
$\epsilon$	Emissivity	0.95	0.95	-	prescribed
$Z_0$	Roughness length	2.35	0.053	m	measured

#### 4.4.2 MESO-NH 1D simulations (CNRM)

Over both sites, the clear sky boundary layer is simulated for 18 August 1994 from 0500 LST (the 0500 LST radio soundings are taken as the initial condition) to 1700 LST, with a time step of 60 s and a constant vertical resolution  $\Delta z = 35$  m. The simulations can be compared with the RBLE-3 measurements every three hours. The prescribed surface properties (i.e the ISBA parameters) are those obtained for the PERIDOT grid points covering RJF and NSP, following the aggregation equations. The average textural properties of the sites and the corresponding soil characteristics are presented in Table 4.3.

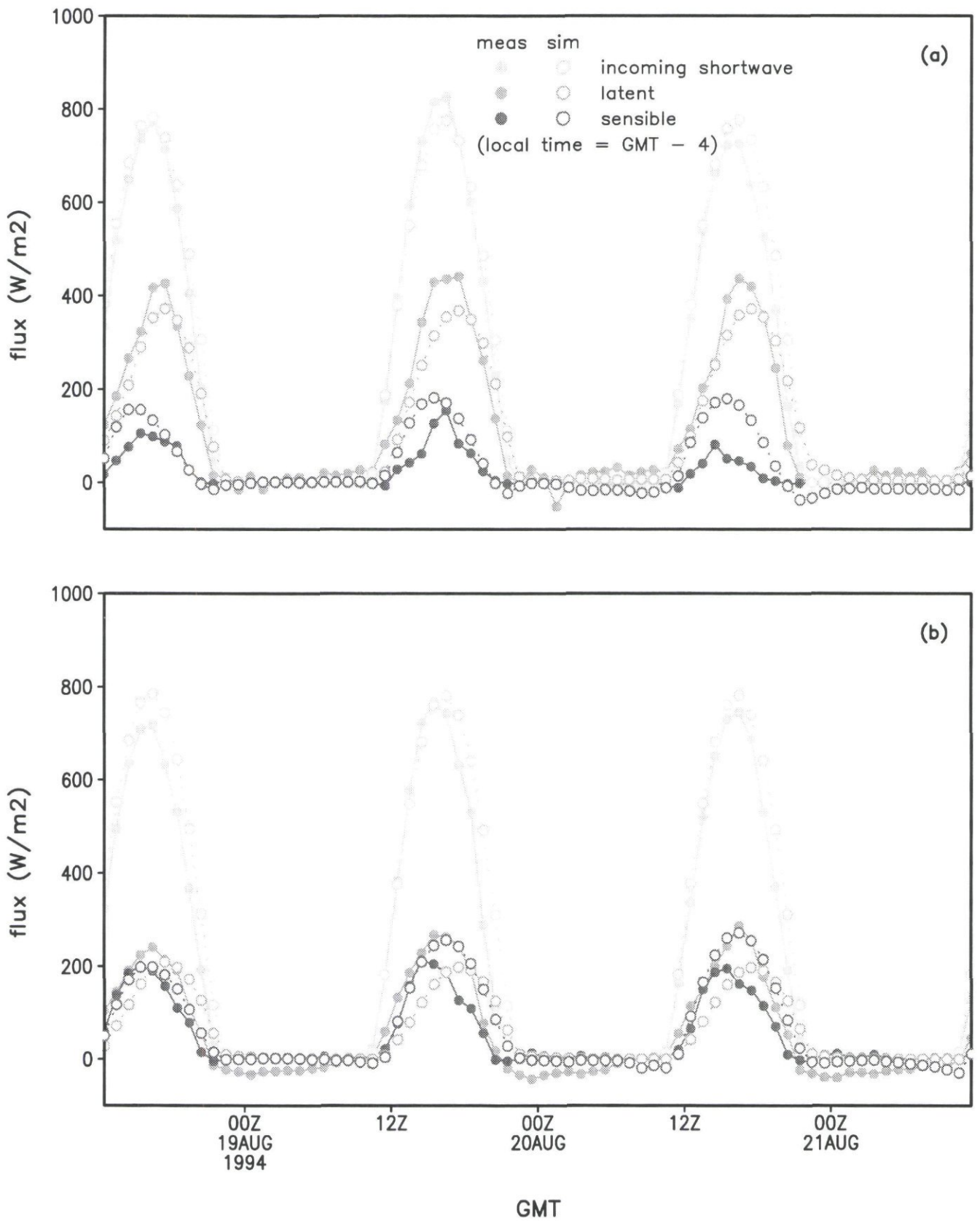
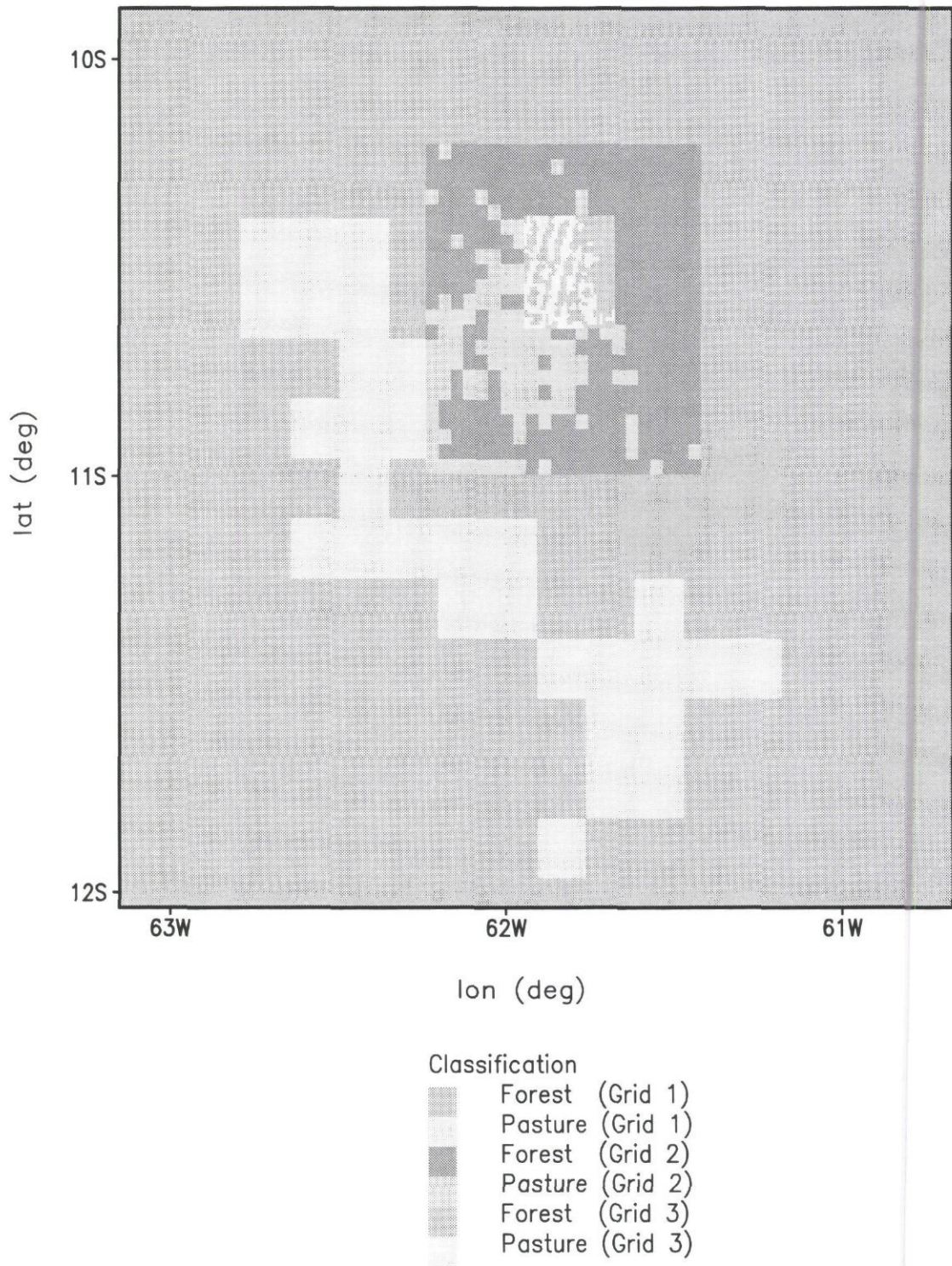


Figure 4.2 Comparison of modelled and observed incoming shortwave radiation, latent and sensible heat flux for (a) Reserva Jaru forest (RJF) and (b) Nossa Senhora pasture (NSP) for the RAMS land surface model.





*Figure 4.3*      *Nested simulation domains for the RAMS model.*

GrADS: COLA/IGES

Table 4.3 Average textural properties of the 10km×10km areas covering RJF and NSP and the corresponding soil characteristics (field capacity water content  $w_{fc}$ , wilting point  $w_{wilt}$ ) together with the observed or assumed local saturation fraction on August 18, 1994 ( $\theta$ ) and the estimated aggregated value according to the pasture proportion ( $\beta$ ).

10 km × 10 km site	Clay	Sand	$w_{fc}$	$w_{wilt}$		on August 18, 1994	$w_s$ on August 18, 1994
RJF	42%	42%	0.34	0.22	0%	100% (forest)	0.34 (forest)
NSP	29%	47%	0.30	0.18	60%	27% (pasture)	0.21 (pasture)
						100% (forest)	0.30 (forest)
						66% (aggregated)	0.26 (aggregated)

From the surface solar radiation ( $R_g$ ) measurements and preliminary simulations with MESO-NH, it appears that a large part of the solar radiation is absorbed by the aerosols. From these simulations, the estimated optical thickness of the aerosols on August 18, 1994 is 0.20 for RJF and 0.25 for NSP at 1200 LST. In the simulations presented here, it is assumed that the aerosol profile grows with the boundary layer. The aerosol optical thickness at the altitude  $z$  is expressed as:

$$\tau_{aer}(t, z) = a q_a(t, z) \delta z$$

where  $q_a$  is the simulated specific humidity at time  $t$  and level  $z$ , and  $a$  a tuned coefficient. In the simulations, the aerosol properties (single scattering albedo and extinction coefficient) correspond to a standard continental aerosol class. The estimated value of  $a$  on August 18, 1994 is 0.0429 and 0.0543  $m^{-1}$  for RJF and NSP, respectively.

Fig. 4.4 presents the simulated and observed humidity and temperature profiles over the two sites at 1700 LST. Over RJF (Fig. 4.4A and 4.4B), the boundary layer height ( $BLH$ ) of about 1000 m is well simulated, although the air humidity is slightly overestimated. On the other hand, the  $BLH$  of NSP is significantly underestimated (the model predicts a  $BLH$  of 1600 m whereas the observed value is about 2200 m). Again, the air humidity within the boundary layer is slightly overestimated. Figs. 4.5 and 4.6 show more details about the simulations. Also, the surface fluxes are compared with the in situ measurements. The agreement between the measured and simulated surface fluxes is good for RJF (Fig. 4.5B). For NSP (Fig. 4.6B), the simulated aggregated  $H$  is lower than the measured value because the aggregated value represents the combined effect of the pasture and forest stripes, whereas the measured value represents what occurs within the pasture.

The impact of deforestation at several rates, as simulated by MESO-NH, is presented in Fig. 4.7. It is assumed that the RBLE radio soundings are representative of what occurs at the regional scale (i.e.  $\beta = 0.6$  at NSP), whereas the measured in situ fluxes correspond to local properties (i.e.  $\beta = 1$  at NSP and  $\beta = 0$  at RJF). Fig. 4.7A shows, again, that the measured  $BLH$  at NSP is much higher than the simulated value at  $\beta = 0.6$ .

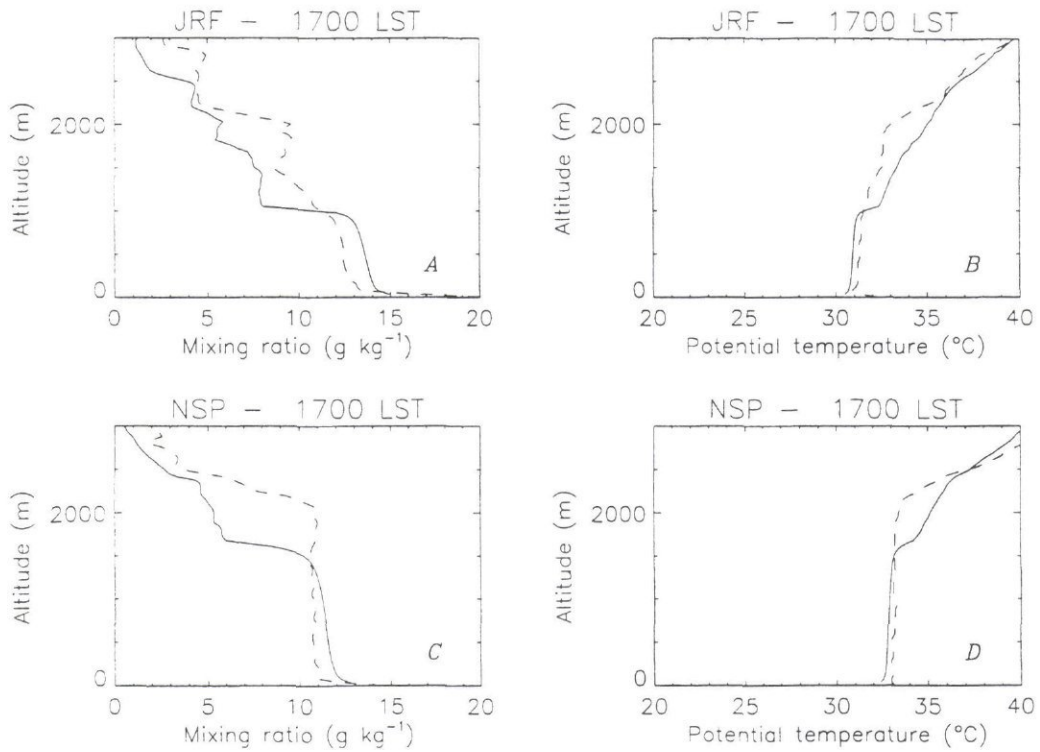


Fig. 4.4 Simulated (solid line) and observed (dashed line) vertical profiles of (A,C) humidity mixing ratio, and (B,D) potential temperature at 1700 LST, over (A,B) natural forest and (C,D) 60% deforested sites of Rondônia for August 18, 1994 from MESO-NH

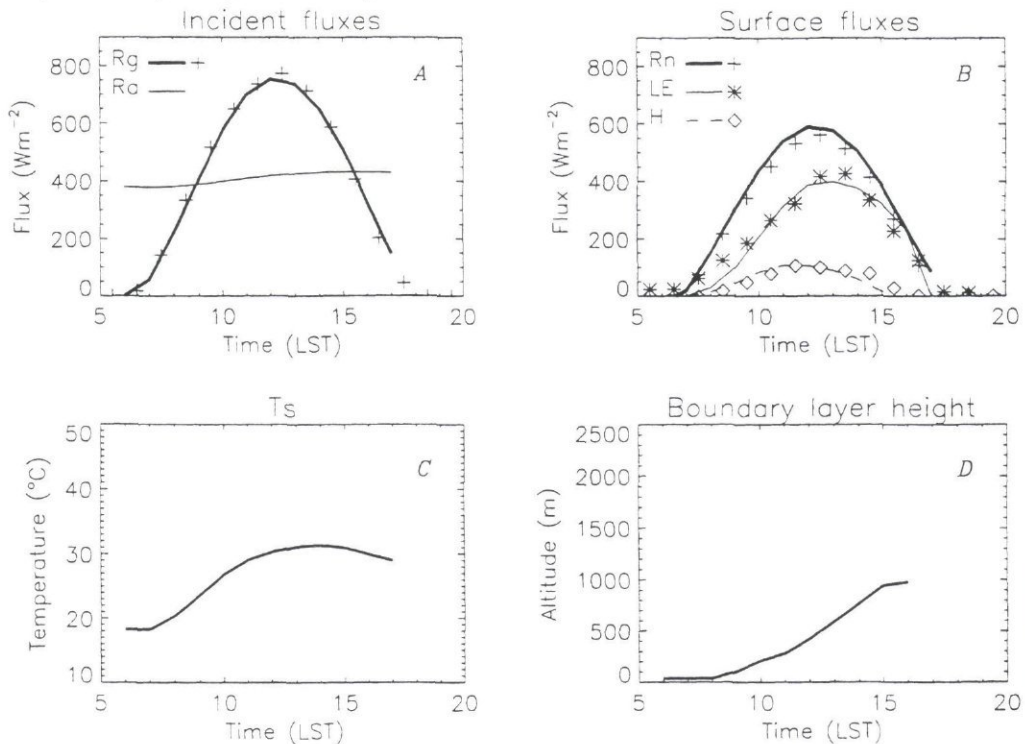


Fig. 4.5 Simulated parameters over the forest site: (A) incident solar ( $R_g$ ) and atmospheric ( $R_a$ ) radiation, (B) surface net radiation ( $R_n$ ), evapotranspiration ( $LE$ ), and heat flux ( $H$ ), (C) surface temperature, and (D) boundary layer height from MESO-NH. The observed values are indicated by points (A,B)

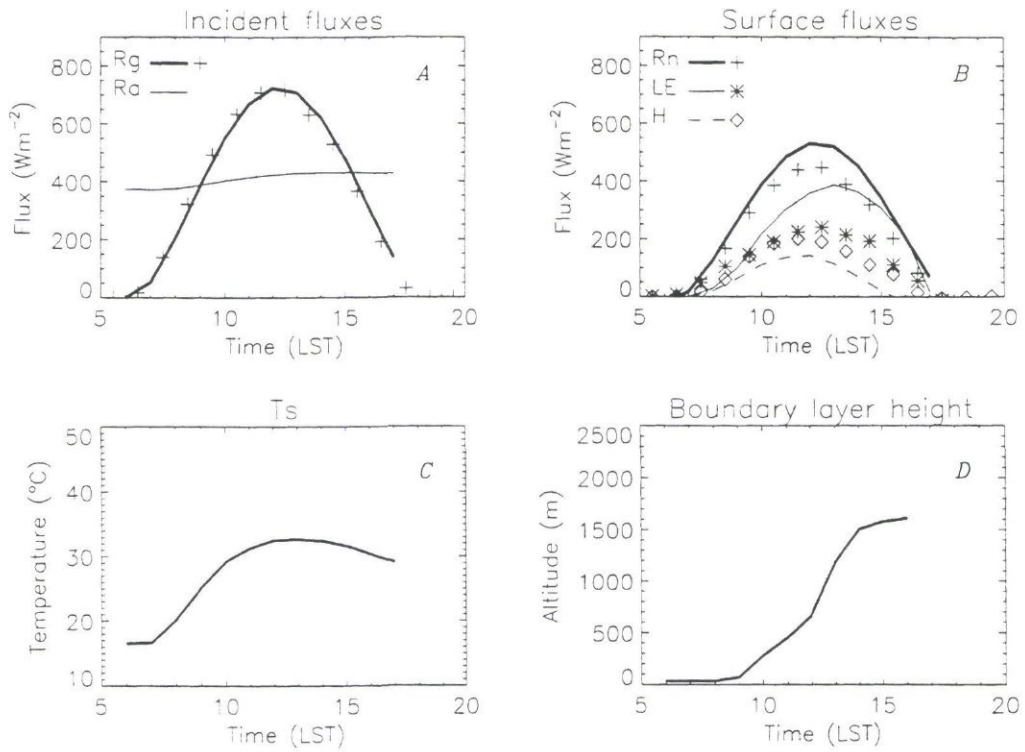


Fig. 4.6 As in Fig. 4.3, except for the 60% deforested site

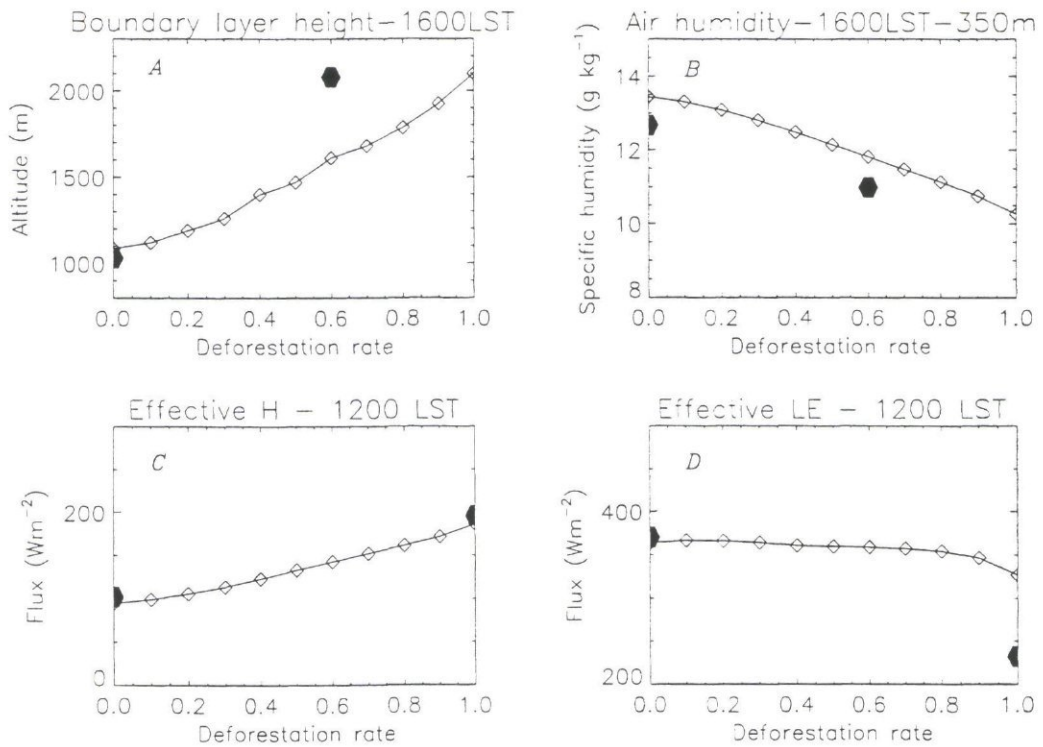


Fig. 4.7 Simulated deforestation impact on (A) boundary layer height, and (B) air humidity at 350 m, at 16 LST, and on the regional surface (C) heat flux, and (D) evapotranspiration from MESO-NH. The dark points represent the observed values

Table 4.4 Simulated impact of 100% deforestation using the MESO-NH model. The differences in boundary layer height (BLH), air specific humidity ( $q_a$ ), surface heat flux ( $H$ ), surface latent heat flux ( $LE$ ), and surface temperature ( $T_s$ ), are obtained by replacing the surface parameters of the natural forest by those of the pasture. The impact of each parameter is also assessed.

Modified surface parameter	BLH at 1600 LST (m)	$q_a$ at 350 m, 1600 LST ( $g\ kg^{-1}$ )	$H$ at 1200 LST ( $Wm^{-2}$ )	$LE$ at 1200 LST ( $Wm^{-2}$ )	$T_s$ at 1200 LST ( $^{\circ}C$ )
All parameters	+1015	-3.1	+90.9	-36.8	+8.5
w2	+980	-3.8	+128.6	-185.1	+3.2
LAI	+840	-3.3	+98.8	-149.5	+2.6
Veg	-35	+0.2	-3.6	-3.4	-0.1
Vis	-35	+0.1	-5.3	-9.0	-0.2
Nir	-35	+0.1	-6.1	-10.5	-0.2
CV	+700	-1.8	+39.7	+78.4	+1.9
Rsmin	-140	+0.9	-18	+30.7	-0.6
	-210	+1.3	-21.9	+43.8	-0.6
RGL	+280	-1.1	+22.8	-37.0	+0.7
z0	0	0	-2.9	-10.1	+0.9
z0h	+35	-0.2	-1.7	-8.9	+2.2

Finally, Table 4.4 presents the simulated impact of a 100% deforestation over surface and boundary layer parameters. Replacing, one by one, the ISBA parameters by their pasture value enables one to assess the effect of each canopy's characteristics. Table 4.4 shows that the most important variable in terms of  $BLH$  is the soil water content. Vegetation parameters such as  $LAI$  or  $C_v$  also have a very significant impact on  $BLH$  and surface temperature.

#### 4.4.3 RAMS 3-D small-scale simulations (SC-DLO)

The simulation of the surface fluxes of latent and sensible heat of the RAMS land surface model has been dealt with above. Here it is sufficient to note that they are sufficiently close to the observations to assume that the input from the homogeneous surface to the atmospheric boundary layer is simulated correctly.

Earlier work (Fisch, 1995) has shown that a marked difference can exist between the growth characteristics of the boundary layer over forest and pasture. The structure and time evolution of the Amazonian ABL at Ji-Paraná has been measured during the RBLE-II (Nobre et al., 1996). Observations showed that over forest the convective ABL grows up to a height of 1000-1200 m, whilst, over the pasture the final depth could be 2000 m. It is to be expected that this change in final depth is primarily the result of differences in sensible heat fluxes from surface. The measurements of RBLE II and III (Fisch, 1995) can thus be used to assess the quality of the model simulations. Figs. 4.8 and 4.9 show the boundary layer development for 18 and 19 August respectively. The observed and simulated potential temperature is shown over the RJF (b) and NSP (d) sites. In this simulation the nudging was applied only at the outer three points of the coarse domain, but not domain-wide. RBLE III radiosonde data for forest were also used to initialise the simulation.

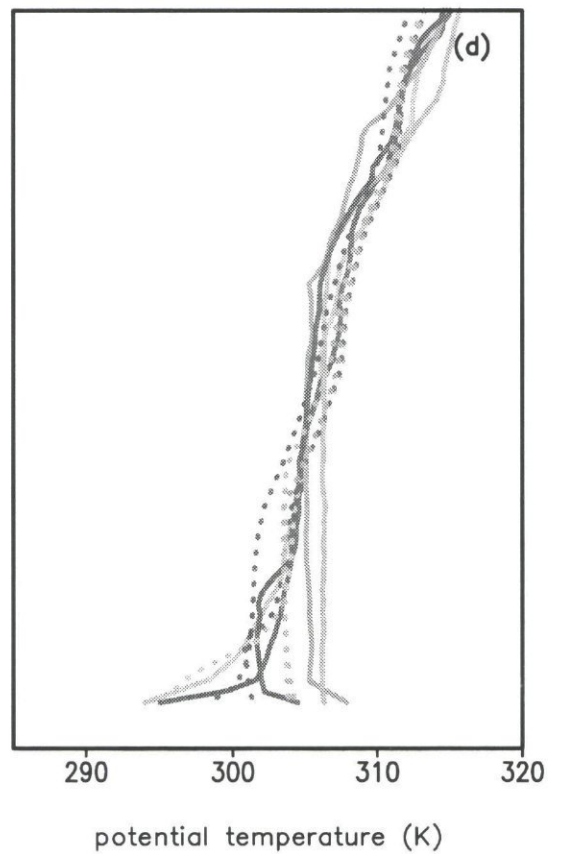
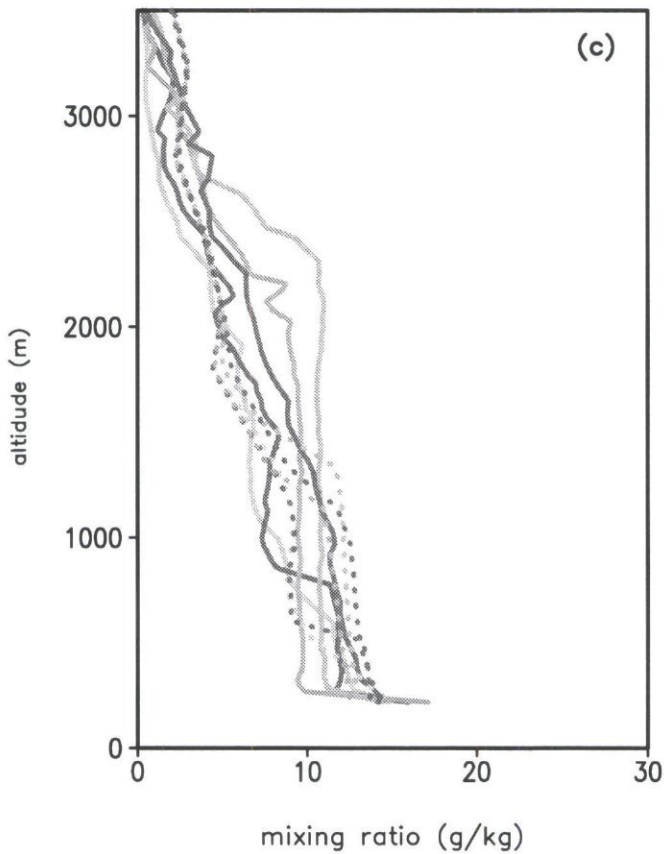
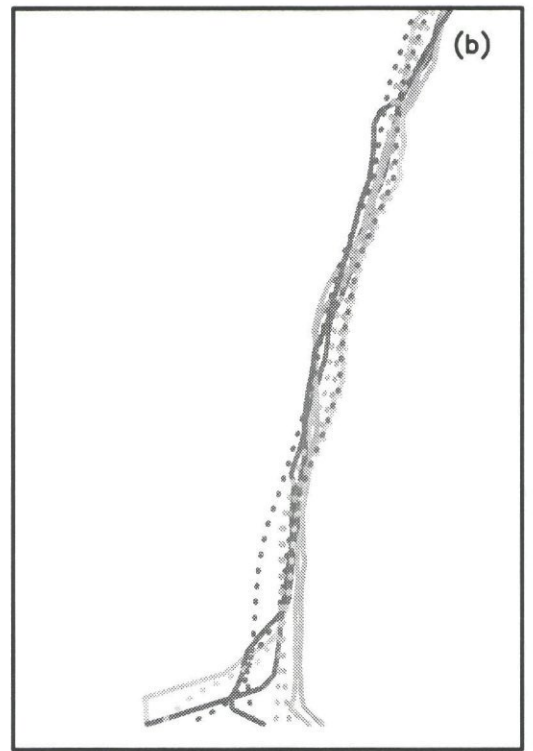
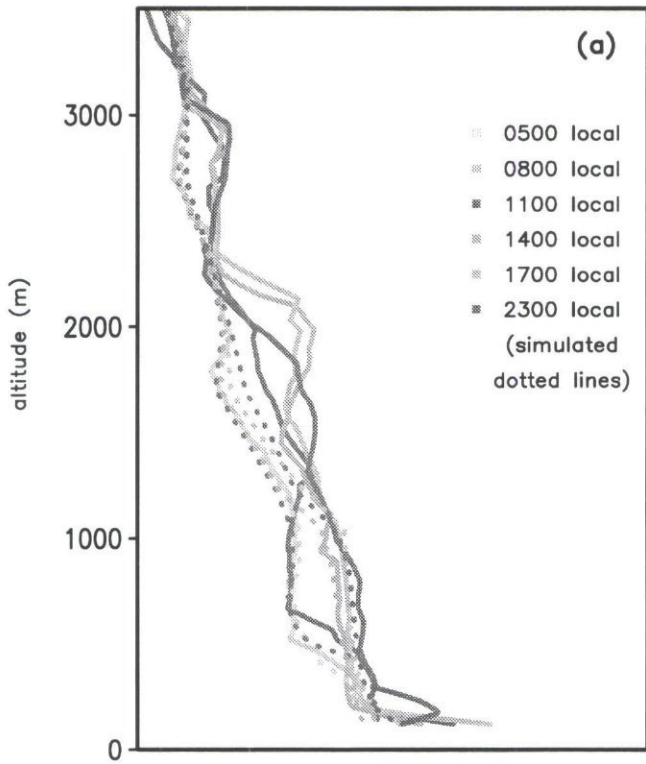


**Figure 4.8** RAMS simulated (dotted Lines) and observed (solid lines) profiles for 18 August: RJF mixing ratio (a) and potential temperature (b); NSP mixing ratio (c) and potential temperature (d).

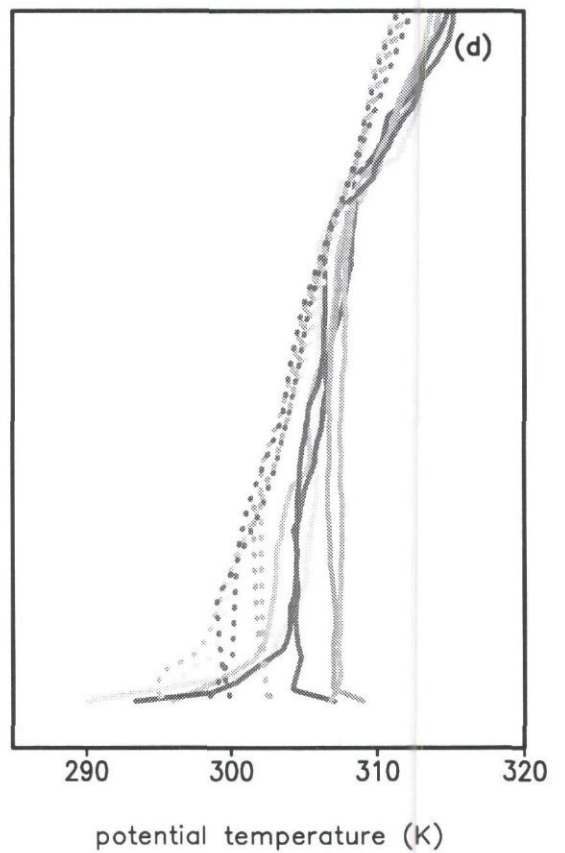
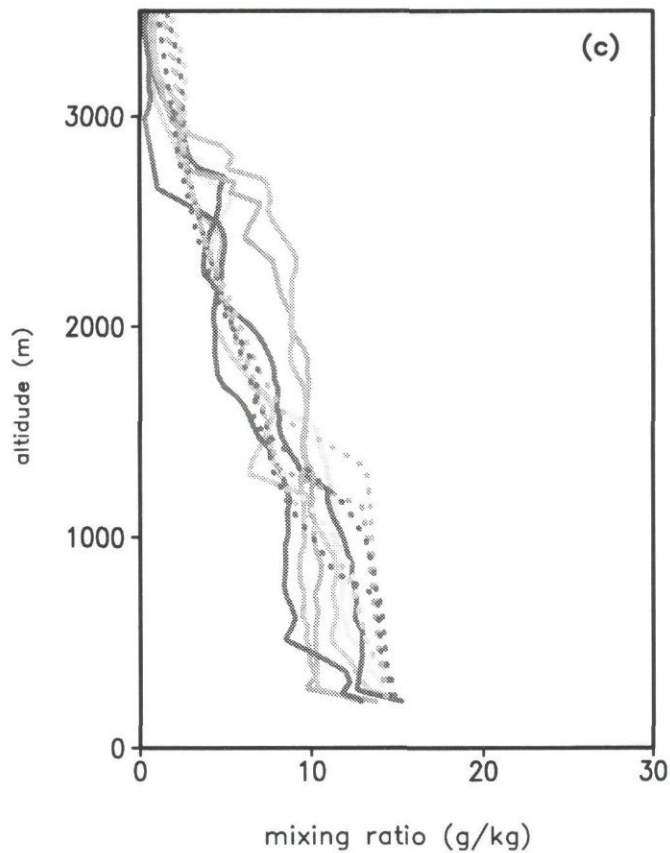
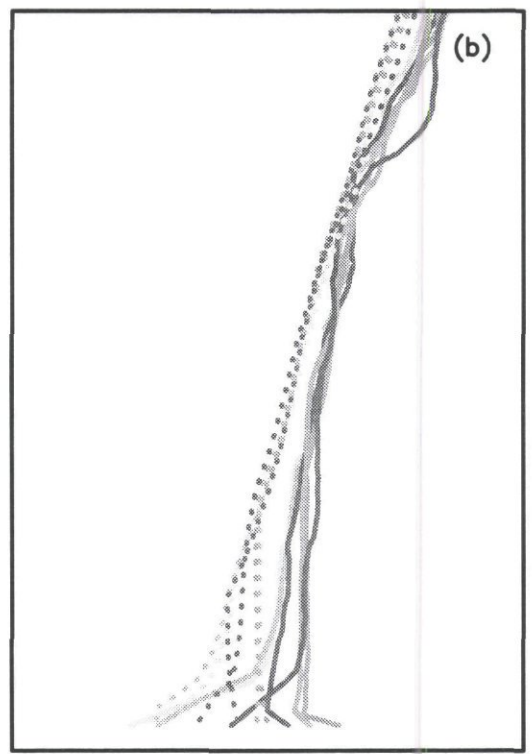
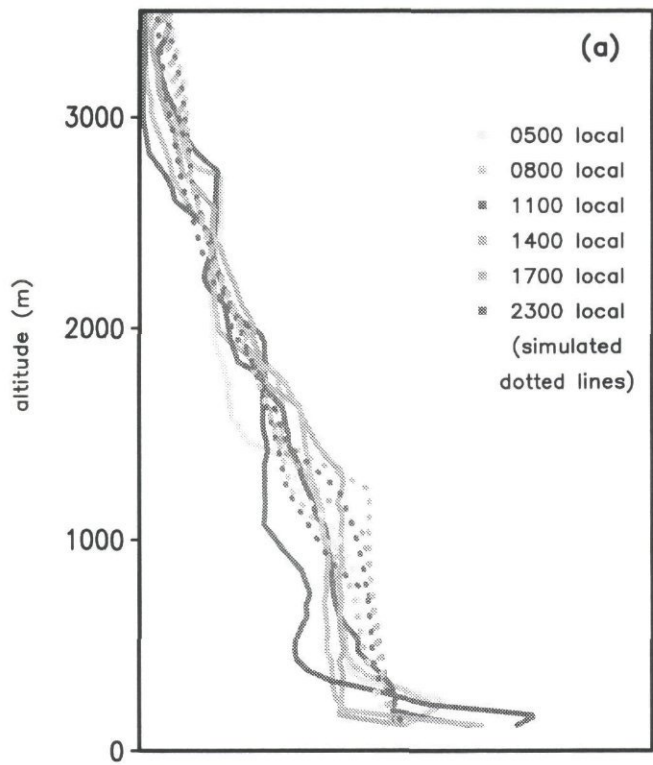


**Figure 4.9** RAMS simulated (dotted Lines) and observed (solid lines) profiles for 19 August: RfJ mixing ratio (a) and potential temperature (b); NSP mixing ratio (c) and potential temperature (d).

For both RJF and NSP sites the model underpredicts the boundary layer heating. At the RJF site the results are reasonable for 18 August and less so for 19 August. The results for the pasture site are worse: simulated values are too cold in the morning, also in the afternoon by up to 5 K, and the final boundary layer depth underestimated.

Given that the sensible heat input from the surface is close to observations, this implies that the model does not provide enough extra heat input for the boundary layer from other processes, such as possible radiative absorption through aerosols. In the simulations by the 1-D MESO-NH model, similar problems were encountered. During the dry season forest burning produces large amounts of aerosols in the area of Rondônia and it is likely that the absence of a parameterization of the absorption of radiation explains the high growth of the observed boundary layer compared to the modelled one. This would also explain why initially the modelled downwards shortwave radiation was too high compared to surface observations.

For simulations where domain-wide nudging is applied and measurements are not used in the initialisation (not shown), profiles of potential temperature are good for the forest. The profiles over pasture are better than those presented here, but still significantly underestimate the boundary layer warming and depth. This indicates that the large scale analysis of the NMC model used for initialising and nudging is probably representative of the forest boundary layer for this field.

Figs. 4.8 and 4.9 show modelled and observed humidity profiles for 18 and 19 August respectively for RJF (a) and NSP (c). In this case agreement between observed and simulated profiles is reasonable and again generally better for the forest, recalling that a sounding over the forest was used in the initialisation. When domain-wide nudging is applied and measurements are not used in the initialisation (not shown), the humidity profiles for both sites are worse than those presented here. This may be caused by the representation of the humidity field in the large scale analysis, where nudging and initialisation in the mesoscale simulations would tend to amplify errors in the humidity field.

The differential heating due to the surface transition of forest and pasture is also shown in Fig. 4.10 where contours are drawn for sensible and latent heat at 13:00 local time. The pattern follows the typical fishbone pattern of vegetation closely.

The differential heating produces an effect in the distribution of the vertical velocity. Fig. 4.11 show cross sections of vertical velocity for 20 August 13:00 and 17:00 local time. These are for the fine grid at 10.39S. At low levels air is seen to be rising preferentially over the pasture and sinking over the forest. The largest values of vertical velocity are found at midday to mid-afternoon. For this simulation no thermal circulations are evident at this or the larger scale. This may be due to the relatively strong background wind. The scale at which this is happening is relatively small and of the order of a few kilometres rather than tens of kilometres and may result in more effective turbulence in the region rather than well defined thermal circulations.



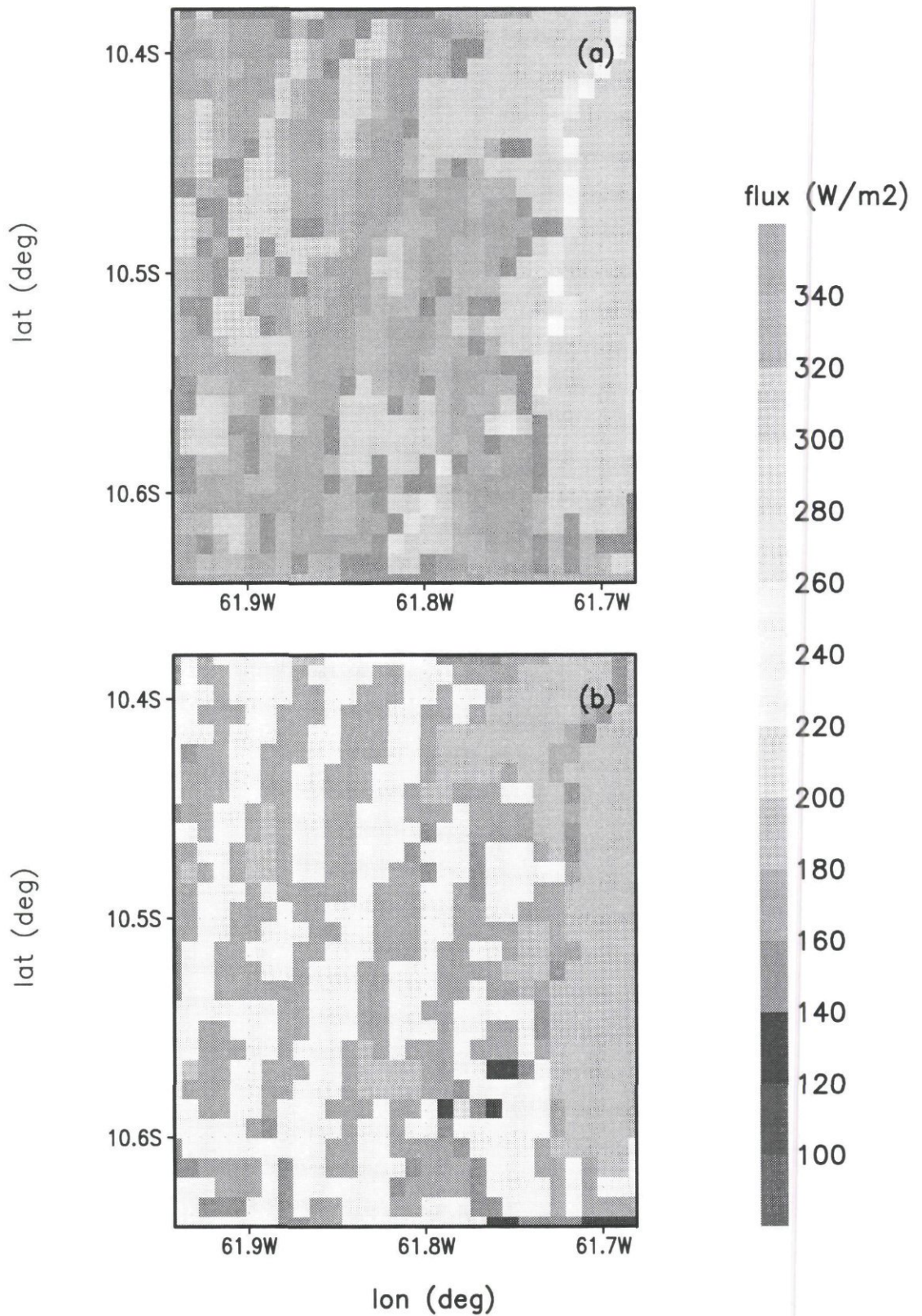


*Figure 4.10* RAMS (a) latent and (b) sensible heat fluxes for the fine grid (see Figure 4.3) at 13:00 local time, 19 August.

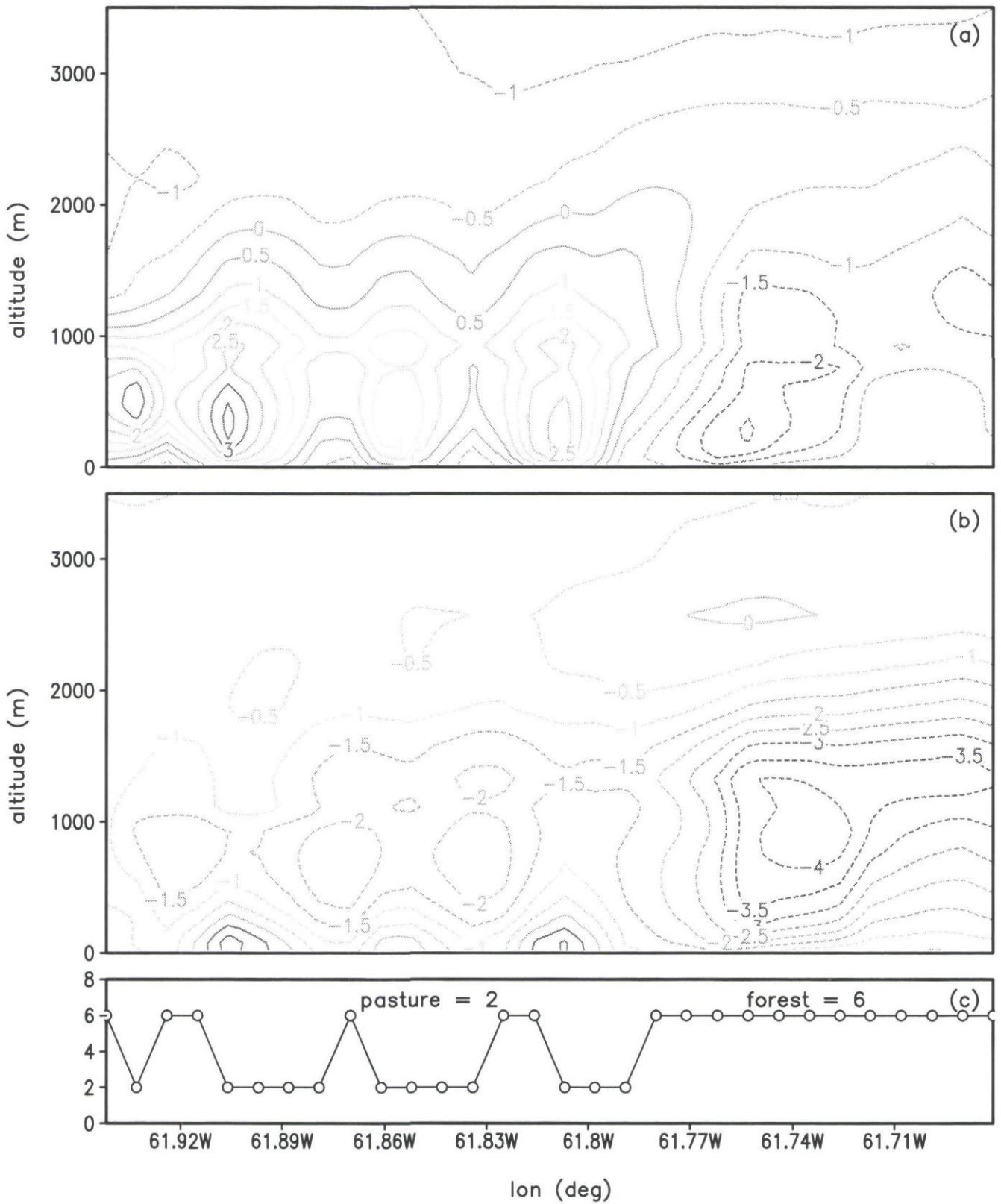
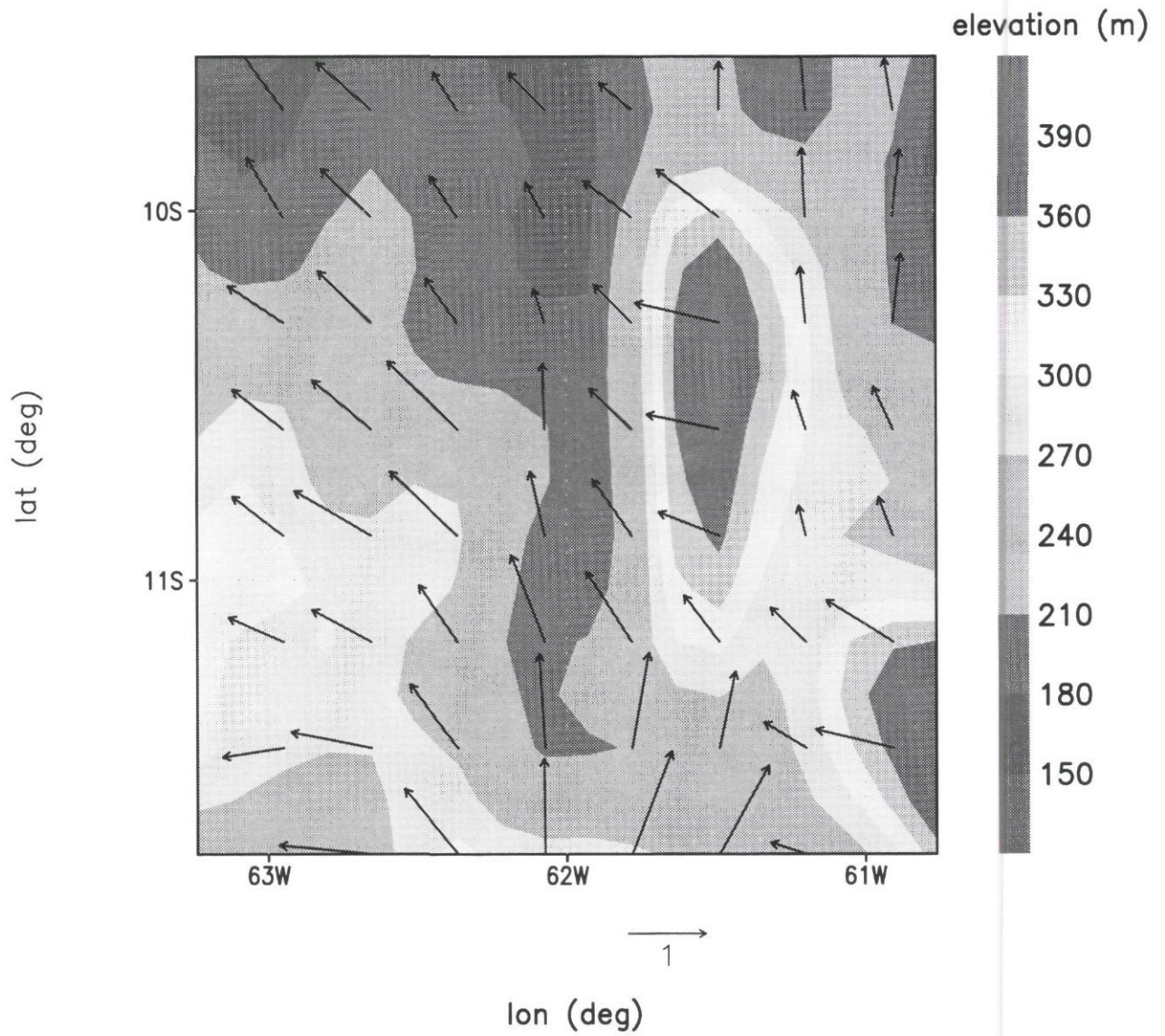


Figure 4.11 Cross section of vertical velocity (cm/s) at 10.39 S for the RAMS fine grid (see Figure 4.3) on 20 August at (a) 13:00 and (b) 17:00 local time, with (c) corresponding surface type.



*Figure 4.12 Wind field generated by RAMS for 19 August at 11:00 local time showing channelling through valley bottoms.*

The RAMS mesoscale model was also run non-hydrostatically. The model was initialized for 19 August 1994, with a single radio sounding over RJF obtained from the Rondônia boundary layer experiment (RBLE III) and then allowed to run without nudging. The land surface cover used in this simulation was based on data from the land surface cover classification produced by the University of New Hampshire (Skole and Tucker, 1993). The model domain for the experiment was approximately 290 by 250 km. As before and not shown here, the grids covered with pasture have a higher sensible heat flux than the forest. The values agree well with the observations from flux towers. The marked topography and higher sensible heat fluxes over the pasture give rise to a complicated pattern of circulation in the area. Both thermally induced flows and channelling are apparent in this simulation. Fig. 4.12 shows how at 11.00 local time channelling through the valley bottoms occurs. As these results were obtained using observed deforestation patterns, these results enforce the evidence obtained from theoretical studies that regional deforestation may affect regional climate.

#### 4.4.4 PERIDOT 3-D large-scale simulations (CNRM)

Simulated surface fluxes and vertical profiles of temperature and humidity have been compared with the local measurements at the NSP and RJF sites. Mainly, the results obtained with the 3-D PERIDOT model on these two sites are similar to those obtained with the 1-D version of MESO-NH. At RJF, simulated *BLH* and surface fluxes are in good agreement with the measurements but the model underestimates *BLH* at the NSP site.

Fig. 4.13 shows the simulated sensible heat flux at 1300 LST over the 600km×600km domain (60-65°W, 8-13°S). The highest values of the sensible heat flux (more than 200 Wm<sup>-2</sup>) are found over the savannah regions at the North-East of the domain and South-West of NSP (Calvet et al., 1997). The effect of the deforestation can be seen on Fig. 4.13 through the 100 Wm<sup>-2</sup> isoline around NSP. The aggregated sensible heat flux over the deforested zones reaches 110 W m<sup>-2</sup> while it does not exceed 60 Wm<sup>-2</sup> over the forest on August 15, 1994 at 1300 LST. However, this behaviour could only be observed until 1300 LST because the model simulates the development of clouds over most of the domain in the afternoon.

Fig. 4.14 presents the vertical cross section of the wind speed and the potential temperature over NSP and RJF at the same time. The surface characteristics along this cross section vary from natural forest (A to RJF) to partly deforested areas (NSP) and savannahs over the hills between NSP and B. Although the synoptic situation is rather complex, it is clear that *BLH* grows with the flow as it moves from forest to pastures and savannahs. At the South-West of the domain (near point B), PERIDOT simulates unrealistic clouds (low values of *H* in Fig. 4.12). Fig. 4.14 shows that the wind pattern is related to the boundary layer development.

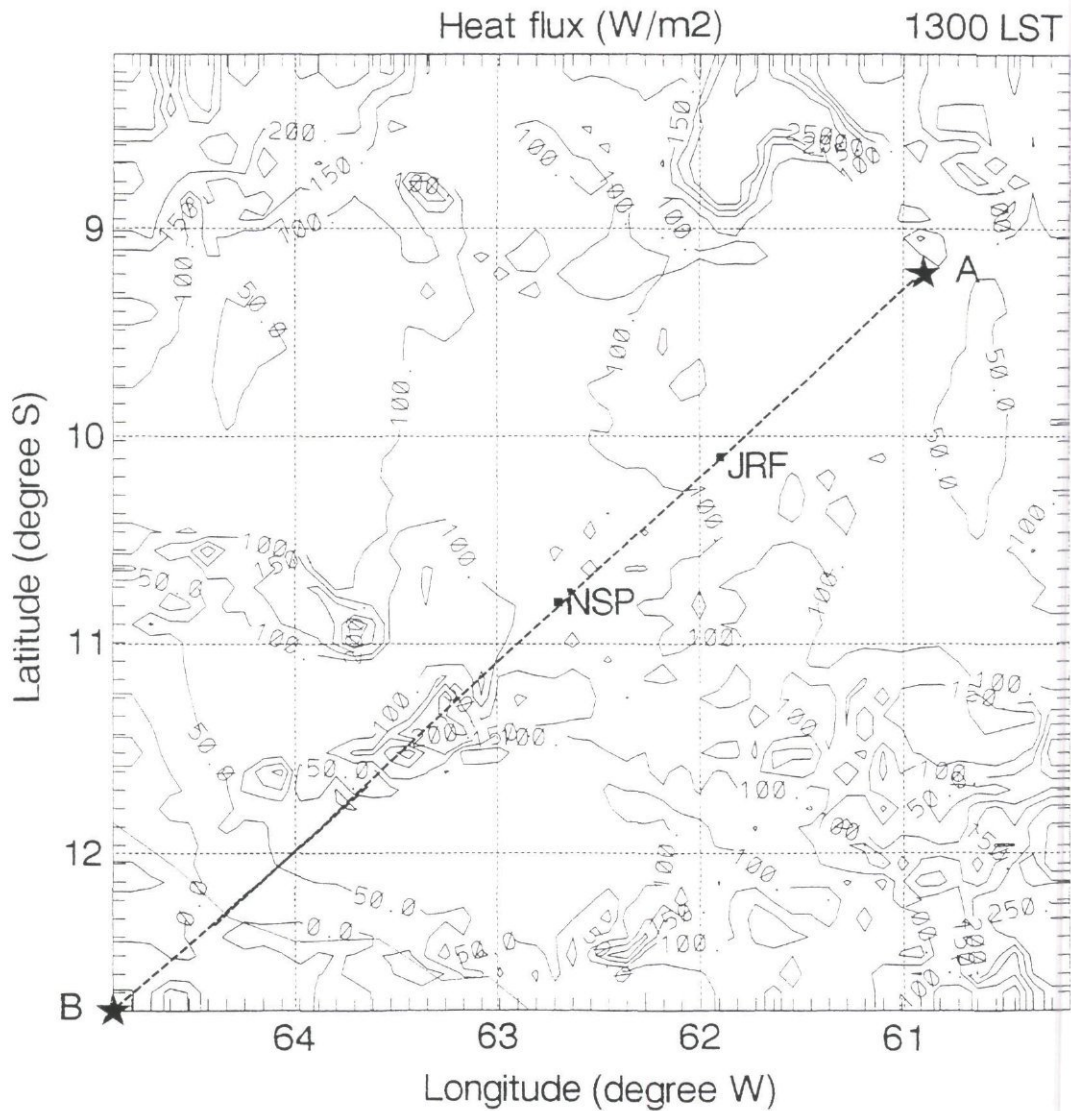


Fig. 4.13 Sensible heat flux simulated by PERIDOT on August 15, 1994 at 1300 LST over the studied domain

Fig. 4.15 shows the same variables simulated by PERIDOT with higher prescribed deforestation rates: the PERIDOT grid points with a deforestation rate higher than 30% are assumed to be totally deforested. In this case, *BLH* is higher around NSP, with a maximum value between NSP and RJF. Also, the wind pattern is significantly modified. This shows that the wind field is affected by the surface properties.

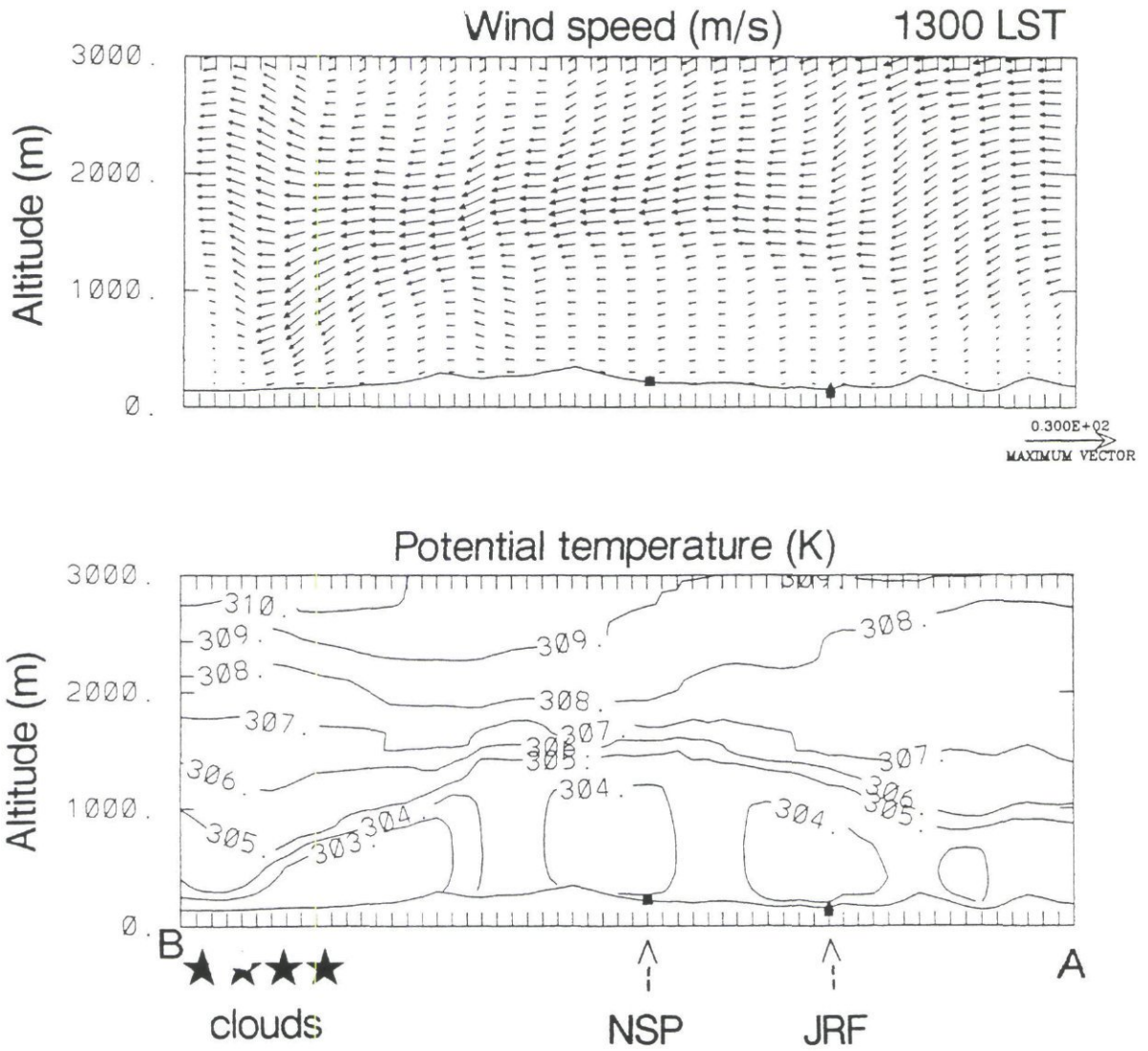


Fig. 4.14 Vertical A-B (Figure 4.13) cross section through RJF and NSP of wind speed and potential temperature on August 15, 1994 at 1300 LST.

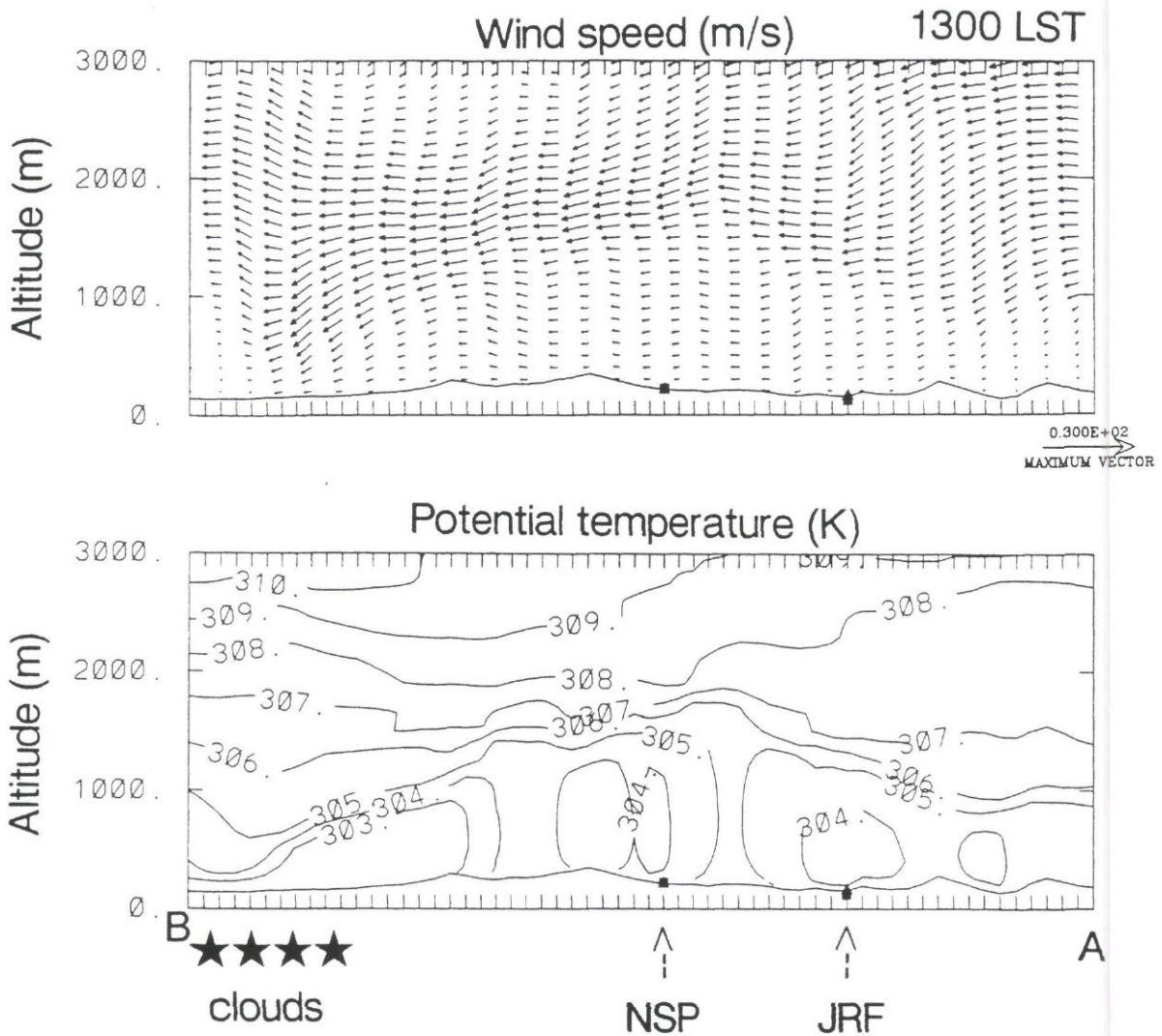


Fig. 4.15 As in Figure 4.14, except for higher prescribed deforestation (see text)

**4.4.5 RAMS 3-D large-scale simulations - The effect of the Andes Mountains on the atmosphere over Rondônia**  
(USP, M.A. da Sylva Dias)

The RAMS model has also been run with 2 grids centred at 15°S and 63°W, in central Rondônia. The first grid has grid spacing of 60 km and the second of 20 km. The first grid covers the Amazon Basin plus the Andes Mountains the second covers Rondônia state. Simulations have been run for the 15 to 20 August 1994 inclusive, in the dry season using NMC's analysis as the initial condition and as boundary conditions updated every 12 hours. The vertical resolution starts at 300 m close to the surface, and gradually decreases to 1000 m and remains fixed at this value up to the model top at almost 20 km above sea level, using a total of 25 vertical levels. The land surface in this case is covered by evergreen forest.

From the simulations performed, two examples will be used here to indicate the possible impact of the Andes mountains in the atmosphere over Rondônia in the dry season. Note that even if the convection parameterization was turned on, no modelled convection was triggered over Rondônia, in accordance with the satellite images for the period which showed a general absence of cloudiness over the region. Some cloud was observed, in the model simulations and in the satellite images, in the northern part of the Amazon Basin.

Simulations of the circulation in a zonal cross section, in grid 1, for August 17 1994, at 1800 UTC can be seen in Fig. 4.16a (u component) and 4.16b (vertical component). Local time is 14:00. The outline of the Andes may be seen in these figures, while the centre of the domain is at  $x = 0$  km corresponding to  $15^{\circ}\text{S}$  and  $63^{\circ}\text{W}$ .

It can be seen that the circulation due to the Andes is quite strong, generating vertical velocities of the order of almost  $30 \text{ cm s}^{-1}$  close to the eastern slopes. The return circulation may be seen to reach a few hundreds of km to the east of the eastern mountain top in Fig. 4.16a and the induced subsidence even further east. The region over central Rondônia experiences a (downward) vertical velocity of  $5 \text{ cm s}^{-1}$  at about 1500 m above sea level. This Andes induced subsidence (roughly  $50 \text{ hPa day}^{-1}$ ) is important in suppressing the growth of the mixed layer over Rondônia and in maintaining the inversion strength in conjunction with the large scale subsidence associated to the subtropical high pressure area.

Another example of the Andes effect is the generation of mountain waves. Fig. 4.17a and 4.17b show the simulation for August 19, at 1800 UTC and 600 UTC, for grid 2. While the afternoon simulation shows widespread subsidence over Rondônia in the lower and middle levels, the night time situation shows a pattern of gravity waves with a vertical wavelength of about 6 km. The horizontal wavelength is of the order of 250 km. Theoretically those would be classified as inertia-gravity waves with almost horizontal propagation. The implications of the existence of these waves for the vertical transport of atmospheric constituents is not certain. Maximum vertical speeds are of the order of  $8 \text{ cm s}^{-1}$ . Acting over 4 hours, these would mean a vertical displacement of air parcels of about 1000 m, upward or downward.

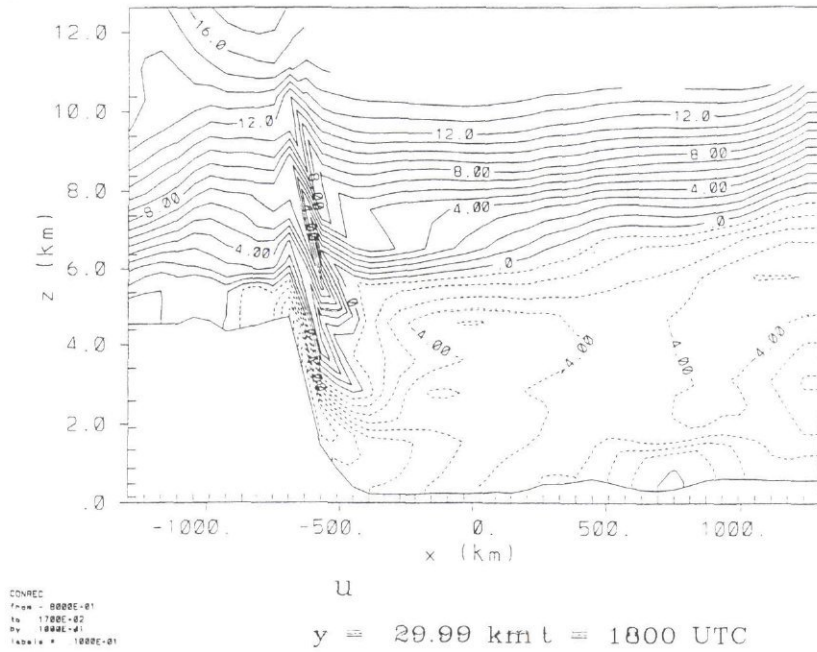
Other effects are also important and have been reported elsewhere. Figueiroa et al. (1995) and Gandu and Geisler (1992) have shown that during the wet season the effect of the Andes is to channel the low level flow, producing a southward current in low levels which transports moisture from the Amazon Basin towards mid-latitude South America.

In the dry season, the climatological flow in Rondônia has a stronger eastern component, and meridional transport is not well defined. The incursion of mid latitude frontal boundaries may reverse the wind direction. Nobre et al. (1996) show two periods within the dry season where the meridional wind in low levels over Rondônia is between  $-2$  and  $2 \text{ m s}^{-1}$ .



Rondonia - Aug. 1994

Grid 1



Rondonia - Aug. 1994

Grid 1

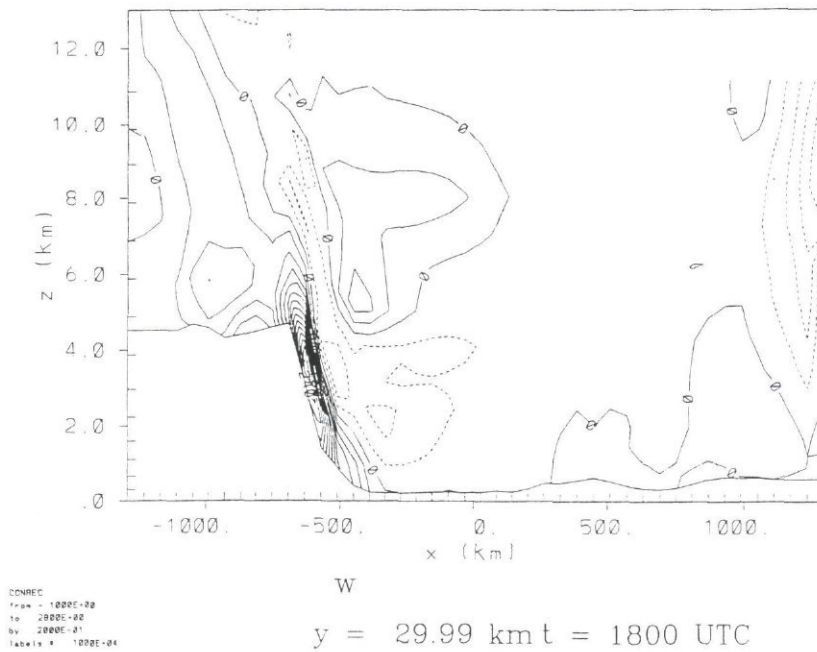


Fig. 4.16 Zonal component (a) and vertical component (b) of the wind field in a vertical cross section, for August 17, 1994, 1800 UTC. Topography outline at the bottom. Dashed lines indicate negative values. Isolines at every  $1 \text{ m.s}^{-1}$ . Simulation started on August 15, 1994, 12 UTC

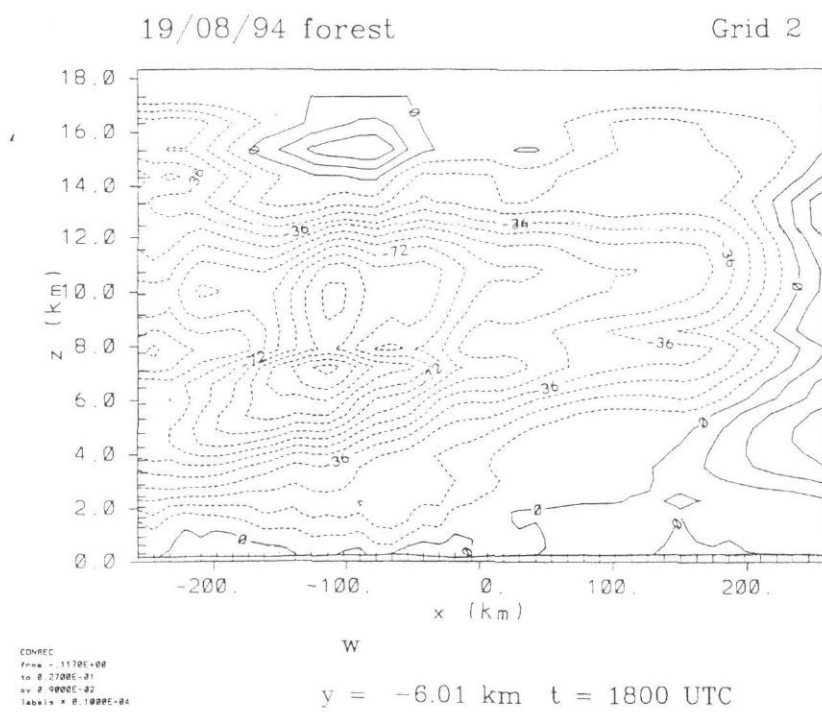
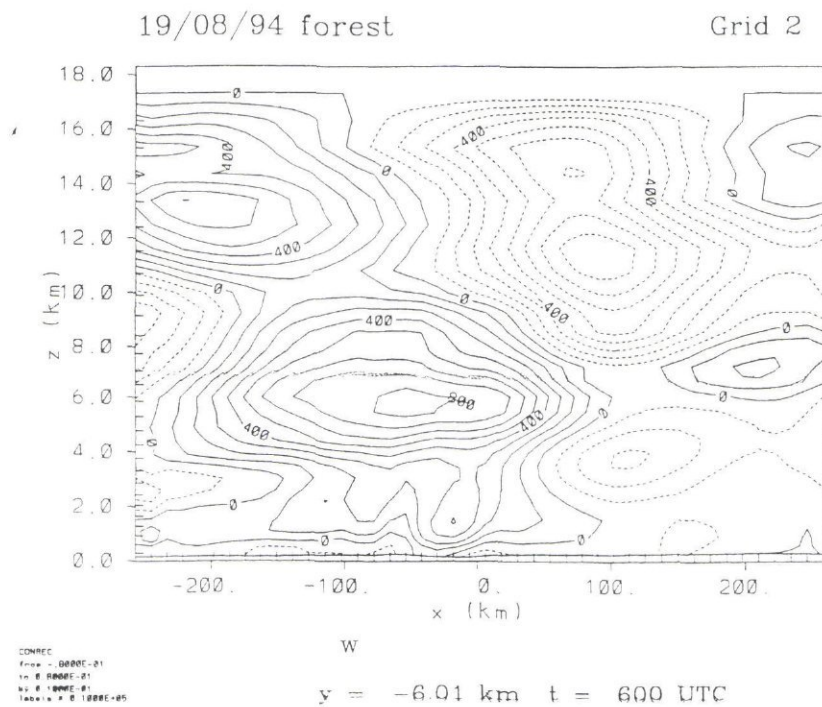


Fig. 4.17 Vertical velocity in a vertical cross section, for August 19, 1994, at 1800 UTC (a) and 600 UTC (b). Topography outline at the bottom. Dashed lines indicate negative values. Isolines at every  $1 \text{ cm.s}^{-1}$ . Maximum value  $8 \text{ cm.s}^{-1}$ , minimum value  $-8 \text{ cm.s}^{-1}$ . Simulation started on August 17, 1994, 12 UTC

#### 4.5 Discussion and conclusions

The land surface models, ISBA and that of RAMS are capable of adequately describing the partitioning of surface fluxes. This is slightly better for forest than for pasture, where soil moisture stress needs to be calibrated. The modelling of the development of the boundary layer is good-to-reasonable for forest areas. For pasture areas, where the ABL is observed to be up to 800 m deeper than over the forest, the model boundary layers are too cold and the final depths too low. The models are thus not able to reproduce the observed differences in temperature and depth of the ABL between forest and pasture.

Given the importance of the boundary layer in transferring energy away from the surface into regions where it can be used to sustain convection, the disability of the models to predict the correct boundary layer growth and structure over pasture is particularly worrisome. This failure of the models inhibits realistic simulations of the effect of regional deforestation on the precipitation, both in the dry and the wet season. Furthermore, it is noteworthy that both the simple slab models as well as the more developed mesoscale models do not perform well over the pasture. Simultaneous measurements of aerosol content and boundary layer structure during the dry season campaign is the most important experimental requirement.

Three possible reasons may explain this missing heat source. The models currently do not prescribe boundary layer heating through enhanced radiation absorption by aerosols, and also do not have sufficient extinction of short wave radiation to predict the correct surface radiation budget. At present the effect of aerosols is taken into account by empirically adjusting the solar constant for RAMS, or in MESO-NH by assuming a boundary layer profile similarity with humidity. It is not known whether the smoke aerosols act only as reflecting particles or as absorbing particles. In the latter case they may contribute to boundary layer heating. Indeed, the study area in Rondônia is affected by biomass burning at the end of the dry season, and a large part of the aerosols comprises soots, whose properties may differ significantly from standard continental aerosols. Therefore, future measurements should include a precise characterisation of the aerosols.

Biomass burning generally takes place in existing pasture or recently deforested areas within the mixed forest/pasture landscape. The fact that the forest boundary layer heating is better described than that of the pasture may then be consistent with this if the radiative effects of aerosols are important. Nevertheless the lateral and vertical distribution and spread of aerosols need to be known to be able to make realistic mesoscale simulations

Secondly, the areas of pasture in the mesoscale model grids are in reality combinations of pasture and forest. The French PERIDOT simulation used high resolution land cover classification data to produce aggregated parameters at the 10 km scale. This will increase the area grid box roughness length, but may reduce the sensible heat input because of the lower surface resistance of the forest. The combined effect does still not produce enough warming.

However, the turbulence structure over pasture areas also needs further study. An under prediction of the turbulence intensity may, if it affects entrainment at the boundary layer top, also contribute to extra heating. The mechanism of this would have to be sought in the interplay between partly dissolved thermal circulations, and the increased non linear contribution to the overall roughness of pasture areas by remaining patches of forest. Momentum transport could well be substantially increased at the edges of the remaining forests, an effect which is not well parameterized in current models; and also was not accounted for in the simulations with the French models, which did account for some form of sub-grid variability. This aspect needs to be further investigated by using a combination of boundary layer, tethered balloon, RASS and Sodar measurements at and around the forest-pasture interfaces. Using the 1D simulations, it has however been shown that an increase of the roughness length does not increase the height of the boundary layer. Low flying flux aircraft will be needed to assess the lateral and vertical variation in momentum, and possibly sensible heat flux.

The model difficulties in simulating the correct boundary layer over NSP may be related to other errors in the assumptions of the models. For instance the prescribed aerosol properties may differ from reality, or the assumption that the soil water content of the forest stripes is at field capacity (like the undisturbed forest) may be wrong. Also, the forest stripes in the partly deforested zones may differ from natural forests. The deforestation map used was obtained by a simple forest/non-forest classification. In reality, a significant part of the forest stripes may correspond to regrown vegetation. Also, the air is warmer and dryer over the deforested areas than over the natural forest, and therefore the transpiration from the forest stripes may be enhanced compared with the natural forest. In this case, the soil water content may be lower than field capacity because of increased root extraction during the dry season. Measurements are needed to better characterise the hydrology of forest stripe behaviour.

Topography influences the flows at both large and mesoscale, as shown by the RAMS and PERIDOT simulations. At the meso  $\gamma$  scale a clear channelling effect was simulated. This needs to be taken into account generally when selecting sites and more specifically when setting up balloon stations and automatic weather stations for budget studies. At low resolution, this effect may need to be parameterized.

At the larger scale the influence of the Andes becomes important as shown by the large scale RAMS runs. Not only is large scale subsidence in the dry reason a result from circulations induced by the Andes, the mountain range also generates gravity waves, which may have implications for transport of atmospheric constituents. The subsidence induced by the Andes circulations may be important in suppressing boundary layer growth and convection in the dry season. Indeed, a model comparison with convection switched on, showed no events where convection was triggered in the model.

This is likely to be different for convection in the wet season. As a matter of fact, the ability of meso scale models to simulate wet season conditions in the Rondônia area has not yet been adequately tested, largely because of the lack of observations of the

boundary layer. The mismatch between observed and modelled humidity (e.g. when observations are not used to initialise simulations) is therefore not too encouraging. Initial model studies are required to investigate the effect of the surface on convection, in particular the effect of the effective aerodynamic roughness or enhanced turbulence of the surface coupled with the rapid recycling of intercepted water.

The model studies presented in the current project are attempts to show where our understanding of the interplay of local and continental scale mechanisms is not quite adequate. Most of all they show that the picture presented by GCM modelling studies needs to be balanced by an increased understanding of what happens at the meso scale. LBA can provide this much needed understanding.

## **5 Implications for design of the LBA mesoscale field experiments**

### **5.1 Introduction**

The aim of the CABARE project was to identify gaps in our current understanding of the interaction of tropical rainforest in Amazonia with the atmosphere. Identifying these gaps could then lead to a well designed and focused programme of experiments and field work. The two questions to be addressed by the land surface-atmosphere mesoscale experiment of the Large Scale Biosphere Atmosphere Experiment in Amazonia (LBA, Nobre et al., 1996) are the following: what are the mesoscale mechanisms by which differences in surface characteristics translate into large scale weather anomalies and what is the role of dry and moist convection in transferring energy and how will it change with different land use patterns?

The availability and use of existing data, such as that from ABRACOS (Gash and Nobre, 1997) and the Rondonia Boundary Layer Experiment (Fisch, 1996) was therefore essential to the success of this project. In essence the project concentrated on three areas: ongoing collection of field data, mesoscale and 1-D modelling and remote sensing. The implications of the modelling program are discussed first.

#### **5.2 1-D site based measurements**

Using the method of Culf and Gash to estimate incoming longwave radiation appears to work well in the SVAT models. However, for high net radiation the scatter in the results appears to be less than for lower values. For low values of net radiation the importance of simulating the surface temperature correctly becomes more important. Accurate measurements of surface temperature are therefore needed to reduce the number of degrees of freedom in the calibration of the SVAT models and as a further check on their performance.

All SVAT models used in current project are able to reproduce the latent heat fluxes for forest under both dry and wet conditions. This is in part due to the fact that there has been no observed water stress for forest, and this has not therefore been included as a stress function in the surface conductance models for the forest. During the wet season the water table at Reserva Jaru forest is within 2.0 m of the soil surface and this can considerably influence the soil moisture profile. For detailed soil moisture modelling a knowledge of the ground water level (GWL) is important and accurate measurements are therefore needed.

Although the soil heat flux beneath forest is a relatively small part of the energy balance, the canopy storage for a rainforest is significant and can be of similar magnitude to the sensible heat flux. In canopy measurements of temperature are therefore required to estimate this component.

The SVAT inter-comparison study highlights the need, particularly for pasture, to make adequate predictions of soil moisture, and more specifically moisture stress in the surface conductance model. This goes alongside the need for accurate measurements of those parameters that describe the soil hydraulic properties. Note that a good estimate of soil moisture and rooting depth is vital for comparison of modelled with observed values. There may be a need to work out a more spatially based soil moisture sampling scheme. Specific measurement programme should be design to estimate and parameterise soil hydraulic properties of the Amazonian soils, which demonstrate a different hydraulic behaviour from the temperate soils. Especially needed are a proper estimation of the saturated hydraulic conductivity and the measurements of moisture movement and the composition of the soil to generate the thermal properties of the top layer. Other required observations are, the deep (at diurnal damping depth) soil temperature, LAI and the measurement of the pressure heads at a depth to determine the deep soil moisture fluxes. A crucial parameter remains the rooting depth for both the forest and the pasture.

### **5.3 Boundary layer and mesoscale measurements**

Given the importance of the boundary layer in transferring energy away from the surface into regions where it can be used to sustain convection, the inability of the models to predict the correct boundary layer growth and temperature and humidity structure over pasture is particularly worrisome. This failure of the models inhibits realistic simulations of the effect of regional deforestation on the precipitation, both in the dry and the wet season. Furthermore, it is noteworthy that both the simple slab models as well as the more developed mesoscale models do not perform well over the pasture. Simultaneous measurements of aerosol content and boundary layer structure during the dry season campaign is the most important experimental requirement.

The study area in Rondonia is affected by biomass burning at the end of the dry season, and a large part of the aerosols comprises soots, whose properties may differ significantly from standard continental aerosols. Therefore, future measurements should include a precise characterisation of the aerosols.

Biomass burning generally takes place over pasture areas and new forest land. The fact that the forest boundary layer heating is reasonably well described, suggests that the RJF was either sufficiently far away from the burning areas, so as not be affected, or that the lateral dispersion of the aerosols is sufficiently strong not to affect the forest. Nevertheless, the lateral and vertical distribution and spread of aerosols needs to be known to be able to make realistic mesoscale simulations

In view of the under prediction of boundary layer warming, the turbulence structure over pasture areas also needs further study. An under prediction of the turbulence intensity may, if it affects entrainment at the boundary layer top, also contribute to a loss in heating at the inversion height. The mechanism of this would have to be sought in the interplay between, partly dissolved thermal circulations and the increased non linear contribution to the overall roughness of pasture areas by remaining patches of forests. Momentum transport could well be substantially

increased at the edges of the remaining forests. This aspect needs to be further investigated by using a combination of boundary layer, tethered balloon, RASS and Sodar measurements at and around the forest/pasture interfaces. Using the 1D simulations, it has however been shown that an increase of the roughness length does not increase the height of the boundary layer. Low flying flux aircraft will be needed to assess the lateral and vertical variation in momentum, and possibly sensible heat flux.

The deforestation map used was obtained by a simple forest/non forest classification. In reality, a significant part of the forest stripes may correspond to regrown vegetation. A more accurate classification, perhaps based on radar would be useful to identify these regrowth areas.

Topography influences the flows at both large and mesoscale, as shown by the RAMS and PERIDOT simulations. At the meso  $\gamma$  scale a clear channelling effect was simulated. This needs to be taken into account generally when selecting sites and more specifically when setting up balloon stations and automatic weather stations for budget studies and initially, if the locations are chosen, simulations may be performed to assesses the possibility of deriving physically meaningful budgets.

The validation plans for the Tropical Rainfall Measuring Mission (TRMM) play an important role here as the objectives of the LBA mesoscale field campaigns and TRMM validation are very complementary. The TRMM field campaigns need to measure vertical air motion to a high resolution and will require surface and airborne radar, 4 to 5 radio sounding sites with more than 4 soundings per day for the duration of the campaign, and a network of surface raingauges. The radar has a quantitative range of about 150 km; the spatial scale of the required experimental domain should be the 150 km radius circle centred on the radar. Thus, at the larger scale a set-up of 4-5 radiosonde stations (three is the minimum, but some redundancy is required) is needed, complemented by tethered balloons for measuring the surface and lower boundary layer. The importance of these for adequate initialisation and validation of mesoscale models cannot be stressed enough. For the wet season AMC, the soundings should be near the perimeter of the 150 km circle centred on the radar. Preliminary sites of the radar are given in Fig. 5.1

TRMM will also involve the NASA ER-2 high altitude aircraft, equipped with Doppler radar, multi-frequency passive microwave sensors, electric field sensors, visible/infrared sensors (and more) for 12 -15 flights. The TRMM mission requires overflying major convective clouds and organised mesoscale precipitation systems. The aircraft's most likely base would be Brasilia. Efficient utilisation of the aircraft requires accurate six-hour forecasts of the existence of precipitation systems over the AMC domain from CPTEC.



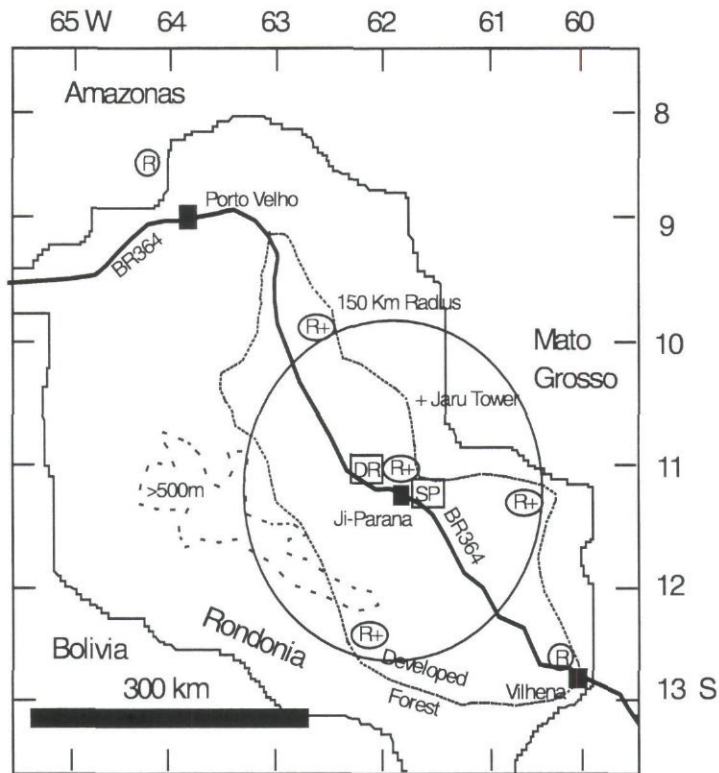


Fig. 5.1 Possible distribution of certain observing capabilities for LBA/TRMM Atmospheric Mesoscale Campaign (wet season). The candidate site for the S-POL radar (SP) is at Ji-Parana with the 2nd Doppler radar (DR) 40 km to the north west. Augmented rawinsonde launches (R) would take place at the operational sites at Porto Velho and Vilhena. Special rawinsonde sites, supplemented with tethersondes (R+) would be placed near the periphery of the quantitative radar coverage. A 4th peripheral site is highly desirable if practical. The "developed area" is, in fact, partially deforested, while the forested area is largely just that. Not shown are sites for 8 pilot balloons, 30 rain gauges, lightning sensors, 10 automatic weather stations, LIDAR, RASS, SODARS, flux balloon, two pasture towers, and a second forest tower. For reasons of accessibility most facilities will be located in the "developed area"

To estimate rainfall and windspeed US scientists propose bringing NCAR's S-POL radar, a state-of-the-art 10 cm radar with polarisation diversity. A second Doppler radar would be sited 30-50 km from the S-POL. This dual Doppler capability would be used to obtain 3-dimensional wind fields at the convective and meso- scale. The two radars would come in a total of 6-8 standard sea containers. Each requires a site with a clear field of view above half degree elevation for 360 degrees around the site. These radars would be of great use to check the modelled wind and rainfall fields.

At the larger scale the influence of the Andes becomes important as shown by the large scale RAMS runs. Not only is large scale subsidence in the dry season a result from circulations induced by the Andes, the mountain range also generates gravity waves, which may have implications for transport of atmospheric constituents. The subsidence induced by the Andes circulations may be important in suppressing

boundary layer growth and convection in the dry season. This calls for the need to improve the 4DDA system of CPTEC with additional sounding locations over the whole LBA domain.

The ability of mesoscale models to simulate wet season conditions in the Rondonia area has not yet been adequately tested, largely because of the lack of observations of the boundary layer. Furthermore, the poor representation of the humidity profiles (e.g. when measured profiles are not used to initialise simulations) is alarming, and could be potentially disastrous for simulations of the wet season. Initial model studies are required to investigate the effect of the surface on boundary layer growth and convection, in particular the effect of the effective aerodynamic roughness or enhanced turbulence of the surface coupled with the rapid recycling of intercepted water.

#### 5.4 Experimental strategy

The experimental strategy of the AMC reflects the deficiencies found in the current mesoscale models. These appear to be in the neglect of aerosols in the radiation and thermal budget equations, the possibility of enhanced turbulence over the pasture areas, and the interaction of the land surface with convective processes. The AMC should aim to provide the data needed to initialise, calibrate and validate the models. The following set-up was proposed and accepted for the *wet season* (Fig. 5.2).

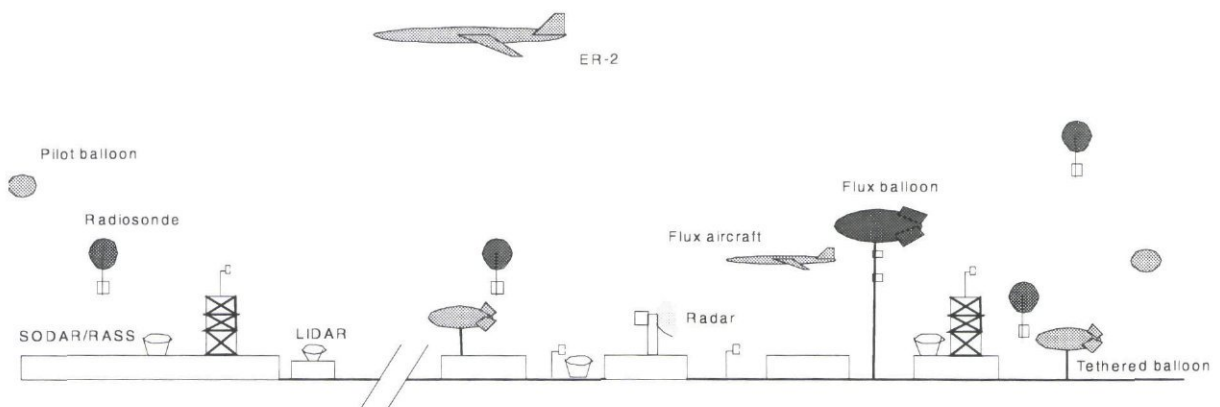


Fig. 5.2 Schematic of the proposed wet season AMC

To understand the boundary layer dynamics and turbulence of the pasture area, an array of RASS/Sodar systems is needed. Low flying flux aircraft are needed to sample area average flux, and a fixed tethered balloon system is needed to measure fluxes at two heights to sample the time variation of fluxes. Fully equipped tower sites are needed at undisturbed forest, at pasture and above the strips in pasture and

forest. A Doppler lidar system should be available at the boundary of forest and pasture. Sun photometers are needed to sample biogenic aerosols. A quantitative Doppler radar such as the S-POL is needed for TRMM rainfall validation, with a second Doppler radar 30 - 50 km distant to provide 3-D wind fields. The vertical velocities from these wind fields will be used to validate TRMM's algorithms for separation of convective from stratiform rainfall. This needs complementing with a network of tipping bucket rainfall gauges. For TRMM purposes the ER-2 will be available, a microphysics plane is also needed. Lightning detectors (3) are needed to correlate rainfall with lightning. Table 5.1 gives the optimum instrument deployment; an assessment of the likelihood of obtaining the instruments for LBA is also given.

*Table 5.1 The optimum instrument deployment and an assessment of the likelihood of obtaining the instruments for LBA*

Instrument	No	Avail-ability	Comments
dual Doppler radar	2	+	available wet season only
tower site grass	2	+	
tower site forest	2	+	
Radiosonde station	4/5	+	2 exist in Brazil
Tethersonde	4/5	+	systems need uprating with larger balloons
flux balloon	1	+	
RASS	3	+	or 1 RASS & 2 SODARS
LIDAR	1	+/-	primarily for wind (CNRM not available 1999)
Raingauges	30	+	
sun photometers	3/4	+	
surface AWS	10	+/-	number includes tower flux sites
pilot balloons	8	+	
drop-size disdrometer	1	+	wet season only
low flying flux aircraft	2	-	preference for Long E-Z, INPE a possibility
lightning sensors	3	+/-	wet season only (but once installed should remain for many years)
ER-2	1	+	wet season only
cloud microphysics (Learjet)	1	+/-	wet season only
DC-8 with LIDAR	1	+	wet season only
NOAA P-3/Electra	1	-	wet season only
NCAR Aster surface flux network	1	-	

A *dry season* campaign will need a similar set-up (except for the measurements required specifically for rainfall detection and TRMM). The AMC dry season campaign should address the issues related to the failure of the models to predict the observed boundary layer structure, in an effort to understand what is happening at the scale of the pasture/forest strips. This information can then lead to new parameterizations where the effects of mesoscale flows and circulation at the scale of 20-200 km can be studied. In the dry season campaign aerosol detection from aircraft will be critical.

The timing of the wet and dry season campaigns depends to a large extent on the other components of LBA. It is essential that the wet season campaign links up with the TRMM validation effort. The timing of funding constrains the choice - a wet season campaign in Jan-February 1999 and a dry season campaign in July-August 2000 is the current plan.

## 5.5 Surface flux measurements and small hydrological catchments in LBA

The evaporation from the pasture, both measured and modelled, is systematically less than that from forest. Over tested sites the average total difference is 323 mm per year. During the wet season this will mainly be the result of the higher albedo of the grass reflecting more solar energy and resulting in less net radiation available for evaporation. No reduction in dry season evaporation from the forest has been observed in the measurements *available so far*. More long term measurements at several LBA sites, covering a wider range of the climatic and soil conditions are needed to support or reject this conclusion.

The modelled reduction in pasture evaporation during the dry season is smaller than expected but the estimated amounts of water extracted from the soil during the dry season are consistent with the variations in soil moisture observed by Hodnett et al. (1996). Additional measurements at several pasture sites covering wider a variety of climatic and soil regimes need to be made in LBA to assess the susceptibility of grasslands to the drought stress.

The differences in evaporation between primary forest and pasture will have an effect on surface runoff and river flows which will be relatively larger in the lower rainfall areas, such as around Ji-Paraná and Marabá. In these areas the use of long term rainfall records and the estimated average reduction in evaporation (323 mm in the present study) results in predicted increases in runoff of 48 and 41% respectively. These preliminary estimates do not allow for any decrease in rainfall which might accompany the deforestation. In Central Amazon (Manaus) the predicted increase in runoff was 29%. These increases are large and it should certainly be possible to observe such changes by using conventional catchment experiment techniques which are planned in the hydrology part of LBA.

LBA calls for measurements over a sample of five land covers associated with deforestation and re-growth: primary forest, freshly burnt and established pastures, and two types of re-growth forests. In terms of surface flux measurements the current modelling results show that this basic stratification would be adequate.

## 5.6 Land cover change mapping

The current project has shown the crucial importance of a *combined* strategy to map and monitor the land surface and its change in the Amazon basin. Ideally, this combined strategy would employ geographical information comprising both existing (paper) maps for the natural landscape structures, the multi-resolution satellite data for current alterations and ground truth collection for verification of the inversion algorithm.

Optical satellite data have been shown to be highly accurate and valuable for the cartography of tropical areas. Nevertheless monitoring of these areas is somewhat impeded by the poor availability of optical data, due to weather conditions (cloudiness). Furthermore the ability to estimate biomass from optical data is limited.

Biomass estimation in the near infrared is possible but works only in the earliest stages of regrowth, due to rapidly increasing leaf biomass and the resulting saturation in the wavelength. Also, optical data do not detect sub-canopy floodings, a land-cover class of great interest in climate modelling, due to its functions as a CO<sub>2</sub> source.

Radar sensors (SAR) have a different information quality and content depending on the frequencies and polarisations employed. C-band SAR, as available from ERS-1/ERS-2 and SIR-C, offers acceptable forest/non-forest discrimination. ERS-1/2 data can be combined to multi-seasonal or multi-temporal products to further enhance the information content. C-band data show stages of pasture degradation and different biomass levels of pastures in HV, VV and HH polarisations. Furthermore ERS-1/2 data are well suited for monitoring areas because of their 35 days repetition rate in the tropics.

The combination of optical and SAR data also gives good results in mapping land use patterns. In the current project, a combined product of TM and ERS-1 is presented and classified. However, an improvement in the automatic classification could not be achieved by this method. More classes could not be detected compared to an optical data set alone. Nevertheless, the visual interpretability was highly improved by imbedding the relief information from the SAR data in the combination product.

In L-band SAR discrimination of forest and non-forest classes is particularly good. L-HH is sensitive to sub-canopy floodings which are clearly distinguished. The Japanese JERS sensor delivers good results in detecting and mapping these areas. The correlation of biomass in HV polarisations is high and increases when data of two frequencies are used. The saturation level is about 100 to 150 tons/hectare. Thus, early to middle stages of regeneration areas not older than ten years are detectable. In L-HH the correlation for biomass is not particularly high, due to double bounce scattering on tree trunks. Different pasture stages are detectable. The use of biomass ratios improves separability of pasture classes.

Using SIR-C/X-SAR data, discrimination of the following classes has been shown to be feasible in the current project: primary rainforest; sub-canopy flooding (flooded rainforest along rivers); pastures; degraded pastures (< 40% ground cover); overgrown pastures (with trees, palms or dead trunks, up to 10% ground cover); initial regrowth (1-4 years of age); intermediate regrowth (5-10 years); bare soils (dirt roads, badlands); and fresh clear-cuts (newly burned areas without vegetation cover).

The high quality and high resolution land cover and land use data are crucial to the success of almost every single study within LBA. Each of the classification methods, either satellite or map-based, has its limitations. It is therefore a strong recommendation of the current project to focus on a combined strategy within LBA to classify the land cover and its change, rather than on one based on single, isolated data sources.

## 5.7 Spatial distribution of LBA measurement sites

The satellite data, vegetation maps and other model-derived products and a regression tree technique presented in current project (Section 2.4.) may be applied to the selection of regions that should be represented with LBA field measurement sites. Moreover the status of regions with existing field sites can be determined, perhaps with a view to augmenting certain types of measurements.

The existing field study sites that have been identified as potential LBA sites are marked on the RTA maps as white rectangles (Figs. 2.35 and 2.37 in Chapter 2). It is clear that an additional site in the high productivity region of Guyana (red) would be useful; possibly located midway between Santarem and Boa Vista, since the currently proposed site on Brazilian-Venezuelan border appears to be in a vegetation transition area. The transition from evergreen to semi-deciduous forest class (pink, yellow, light green) in the south west of the basin in Rondônia - Santa Cruz was distinct from that in Pará and should also be sampled; NE Santa Cruz province in Bolivia would be a possible location. The west Brazilian Amazon site near Tabatinga is also in an area of vegetation transition and may be better placed near Iquitos, Peru.

LBA has a major interest in the sustainability of various types of forest conversion, such as total clearance, selective logging, and traditional shifting agriculture. These human-induced transformations have affected a relatively small proportion of the total basin area at the present time and seem only to have influenced the current RTA classifications in areas of concentrated land conversion, such as in central Rondônia. *Thus stratification for measurement design purposes at smaller scales (meso-scale) should be undertaken next at a more local scale using higher resolution data sets, such as Landsat.*

The need to stratify at multiple spatial scales is inevitable when dealing with such a large area as the entire Amazon basin. The stratifications presented in the current project used  $8 \times 8$  km data at the highest resolution, but several data sets were at  $1^\circ \times 1^\circ$ . Hence regional differences have been emphasized and not variation at finer spatial resolutions. Equatorial lowland forest is well known to exhibit much stronger  $\alpha$ -diversity than  $\beta$ -diversity, unlike temperate and arid regions, therefore much of the fine-scale variation may be lost at the scales explored here. The stratifications presented here are relevant to the  $1^\circ$  scale and they indicate which entire  $1^\circ$  area would give the optimal sampling of the basin-wide variation. *Further stratification within each selected  $1^\circ$ , perhaps using similar techniques, is necessary to determine the optimal location of individual, point, field measurement locations.*

These finer scale stratifications should be explicitly linked with the coarser, basin scale to ensure continuity in scaling up. At the basin scale, the RTA identified annual and monthly minimum PAR, minimum rain fall, and the number of months with less than 150 mm of rain fall, as critical variables that determine  $R_n$ . These same variables are identified as critical for LE, although the first division of LE was on annual rainfall. Minimum NDVI, annual PAR, and the number of months with less than 150 mm rain fall were the most important variables in the tree model of NPP. Annual NDVI and rainfall were also important in the dryer, low NPP areas, while the

monthly minimums of NDVI, PAR and temperature were important in the more humid, high NPP areas. The field measurement design should therefore emphasize measurement of these variables at the  $1^{\circ} \times 1^{\circ}$  scale.

The stratifications of the Amazon presented here were almost entirely based on climate data and, consequently, there were many seemingly obvious surface and vegetation features which have not been captured. Some vegetation classes which we would have liked to be able to distinguish include liana forests, particularly in Pará and Bolivia; bamboo forests, especially in southeastern Peru and Acre; palm swamps; and white sand vegetation such as that of the upper Rio Negro. There are no maps available which delineate these vegetation types. Furthermore, all of these formations probably exist as mosaics with dense evergreen forest, and thus may not significantly influence bioclimate at the scale of the data used in this study. Stratification of only the Rondônia window did not successfully represent such classes as liana forest, seasonally inundated forest and palm swamp which are known to cover large portions of that area. This is more an issue of data scale and availability rather than a failure of the RTA technique. RTA could be undertaken using finer resolution data, such as 1 km AVHRR data.

## 6 Planning and coordination activities

### 6.1 LBA planning activities

The design of LBA has evolved over a series of workshops and meetings held over the past three years. The results of the current project, together with the experience of the current project participants in organising international experiments, makes this project uniquely placed to play a major role in establishing LBA. Current project participants have been actively involved in the design, planning and preparation activities, not just by organising and attending meetings, but also in the writing and preparation of the documentation. Some of the key events are summarised below:

#### 1994

November Piracicaba, LBA Hydrology planning workshop (H. Dolman, J. Gash)

December Cachoeira Paulista, LBA Atmospheric Mesoscale Campaign preliminary planning meeting (H. Dolman, J. Gash)

#### 1995

February Cachoeira Paulista, LBA Atmospheric Mesoscale Campaign planning workshop (H. Dolman & J. Gash, P. Kabat, P. Bessemoulin, J.C. Calvet, M. Inclan)

May Manaus, LBA ecology planning workshop (P. Kabat, J. Gash)

September São José dos Campos, LBA writing workshop for Integrated Science Plan (H. Dolman, J. Gash)

November Brasilia, workshop on Interdisciplinary Research on the Conservation and Sustainable Use of the Amazon Rain Forest and its Information Requirements (J. Gash, P. Kabat)

November Preparation of first draft of LBA Concise Experimental Plan (J. Gash, P. Kabat)

#### 1996

May Publication of LBA Concise Experimental Plan (P. Kabat, H. Dolman, R. Hutjes)

July São José dos Campos, LBA Science Meeting (P. Kabat, J. Gash, R. Hutjes)

July Brasilia, EU-delegation, Meeting on EU-contribution to LBA 1998-2003 (P. Kabat, H. Dolman)



September Pan-Amazonia LBA site reconnaissance flight (J. Gash, P. Kabat)

October Cachoeira Paulista, LBA Atmospheric Mesoscale Campaign planning meeting (H. Dolman, J. Gash, J.C. Calvet)

## **6.2 European co-ordination**

One objective of the project was to prepare a co-ordinated proposal for the European participation in LBA. Work towards this objective was initially concentrated on a co-ordinated bid in the European Union Framework IV Environment and Climate programme. Following a meeting at the Staring Centre, Wageningen in March 1995 a proposal with 21 participants was prepared and submitted. This bid was not successful. Subsequently, two new projects have been prepared (LBA-EUSTACH and LBA-ERACO/ENRICH) and were submitted to the EU-DG XII Environment and Climate Programme in January 1997. The LBA-EUSTACH and ERACO projects build to a large extent on the results of the current project. Both projects have been proposed by the European Commission for funding.

Independent from these activities, the co-ordinator and the collaborators in the current project have been leading an effort to prepare European contribution to the main phase of LBA over 1998 - 2002, which is to be supported by several EU - Directorates (see Attachment 4: Background note on European involvement in LBA). In the course of the current project, a European LBA - co-ordination office has been established at the SC-DLO in Wageningen, the Netherlands. A European LBA co-ordination workshop, supported by DG XI and DG XII was organised in June 1997 in Wageningen and attended by more than 150 participants from Europe, South America and USA.

## **6.3 Collaboration with Brazilian and other institutions**

Though the current project did not include any formal non-European partners or exchange of funds outside Europe, collaboration with Brazilian institutions was a major aspect of the present project. The help of Brazilian scientists contributed to making the different studies carried out in this project successful. All the aspects of the present scientific work have been carried out in collaboration with Brazilian institutions: field measurements, data collection, and modelling.

The ABRACOS measurement network was operated as a continuing collaboration between IH and CPTEC/INPE, INPA, INCRA and the Federal Universities of Pará and Rondônia. The new site near Brasilia is operated in collaboration with the National University of Brasilia. The Brazilian RBLE III experiment provided the opportunity to combine the efforts of both European and Brazilian teams (from several institutions, including INPE, CTA, the University of São Paulo (USP), the Federal Universities of Alagoas and Pará and FUNCEME) during the field campaign.

The physiographic data collection (topography, soils, vegetation) was also a common effort: INPE/CPTEC provided Landsat data and INPE/DSM provided METEOSAT data and helped in classifying the satellite data and interpreting the RADAMBRASIL maps. This latter work was an opportunity for both European and Brazilian teams involved to gain experience in the use of geographical information systems.

USP and CPTEC/INPE joined EU teams in the modelling effort. Their help was fundamental since they have long term experience in mesoscale modelling over Rondônia.

Based on a long term co-operation in previous projects (e.g. HAPEX-Sahel), University of Maryland, College Park, MD, USA collaborated with DLR and SC-DLO in producing the Biophysical stratification of the Amazon basin (Section 2.4).

## References

- Agbu, P.A. & James, M.E., 1994. *The NOAA/NASA Pathfinder AVHRR Land Data Set User's Manual*. Goddard Distributed Active Archive Center, NASA, Goddard Space Flight Center, Greenbelt.
- Alvalá, Santos, R.C., Calvet, J.-C., Jaubert, G., Noilhan, J. and Wright, I.R., 1996. Mapping surface parameters for mesoscale modelling in forested and deforested South western Amazonia. Note du travail GMME, Météo France, CNRM, Toulouse.
- Alvalá, Santos, R. C., Gielow, R., Wright, I. R. & Hodnett, M. G., 1996. Thermal diffusivity of Amazonian Soils. In: Gash, J.H.C., Nobre, C.A., Roberts, J.M. & Victoria, R.L. (eds.), *Amazonian Deforestation and Climate*. John Wiley & Sons, Chichester. pp. 139-150.
- Ashby, M.J., Dolman, A.J., Kabat, P., Moors, E.J. & Ogink-Hendriks, M.J. *SWAPS Version 1.0 Technical Reference Manual*. Technical Document 42, DLO-Staring Centrum, Wageningen, 1996.
- Avisar, R. & Pielke, R.A., 1989. A parameterization of heterogeneous land surfaces for atmospheric numerical models and its impact on regional meteorology. *Mon. Wea. Rev.*, 117: 2113-2136.
- Bastianssen, W.G.M., 1995. *Regionalization of surface flux densities and moisture indicators in composite terrain: A remote sensing approach under clear skies in Mediterranean climates*. Thesis Landbouwniversiteit Wageningen.
- Becker, R.A., Chambers, J.M. & Wilks, A.R., 1988. *The New S Language*. Wadsworth & Brooks, Pacific Grove, California, 702 pp.
- Bhumralkar, C.M., 1975. Numerical experiments on the computation of ground surface temperature in an atmospheric circulation model. *J. Appl. Meteorol.*, 14: 1246-1258.
- Bougeault, P. & Lacarre, P., 1989. Parameterisation of orography-induced turbulence in a meso- $\beta$ -scale model. *Mon. Wea. Rev.*, 117, 1872-1890.
- Bougeault, P., Noilhan, J., Lacarere, P. & Mascart, P., 1991. An experiment with an advanced land surface parameterisation in a mesobetascale model. Part I: Implimentation. *Mon. Wea. Rev.*, 119: 2358-2373.
- Breiman, L., Friedman, J., Olshen R. & Stone, C., 1984. *Classification and regression trees*. Wadsworth, Belmont, CA.
- Brown, J.H., 1995. *Macroecology*. University of Chicago Press, Chicago, 269 pp.

Cialella AT, Dubayah R, Lawrence W, Levine E (1997) Predicting soil drainage class using remotely sensed and digital elevation data. *Photogrammetric Engineering and Remote Sensing*, 63: 171-178.

Calvet J.-C., Santos-Alvalá R., Jaubert, G., Delire, C., Nobre, C., Wright, I.R. & Noilhan, J., 1997: Mapping surface parameters for mesoscale modelling in forested and deforested south-western Amazonia. *Bulletin of the American Meteorological Society*, in press.

Clapp, R.B. & Hornberger, G.M., 1978. Empirical equations for some hydraulic properties. *Water Resour. Res.*, 14: 601-604.

Cox, P.M., Essery, R., et al. 1997. MOSES-1 - the SVAT used in the Unified Model.

Crist, E. P. & Cicone, R. C., 1984. A Physically-based transformation of thematic mapper data - The TM tasseled cap. *IEEE Trans. on Geosci. and Remote Sens.*, GE-22, 256-263.

Culf, A.D., Fisch, G.F. & Hodnett, M.G., 1995. The albedo of Amazonian Forest and Ranch Land. *J. Climate*. In Press.

Culf, A.D. & Gash, J.H.C., 1992. Longwave radiation from clear skies in Niger: A comparison of observations with simple formulas. *J. Appl. Meteorol.*, 32 (3): 540-547.

Davis, F.W., Michaelson, J., Dubayah, R. & Dozier, J., 1990. Optimal terrain stratification for integrating ground data from FIFE. *Symposium on FIFE, First ISLSCP Field Experiment*. American Meteorological Society, Anaheim, California, pp.11-15.

Delire, C., Calvet, J.-C., Noilhan, J., Wright, I.R., Manzi, A. & Nobre, C. 1997. Physical properties of Amazonian soil - a modelling study using the ABRACOS data. *Journal of Geophysical Research*, submitted.

De Fries, R., Hansen, M., Steininger, M., Dubayah, R., Sohlberg, R. & Townshend, J., in press. Subpixel forest cover in Central Africa from multisensor, multitemporal data. *Remote Sensing of Environment*.

Dickinson, R.E., Henderson-Sellers, A., Kennedy, P.J. & Wilson, M.F., 1986. Biosphere-atmosphere transfer scheme (BATS) for the NCAR community climate 3p model. NCAR Tech. Note. NCAR/TN-275+STR, 69 pp.

Dickinson, R.E. & Henderson-Sellers, A., 1988. Modeling tropical deforestation: A study of GCM land-surface parameterizations. *Quart. J. R. Meteorol. Soc.*, 114, 439-462.

Dinerstein, E., Olson, D., Graham, A., Webster, A., Primms, S., Bookbinder, M., Ledec, G., 1995. A Conservation Assessment of the Terrestrial Ecoregions of Latin America and the Caribbean. The World Bank, Washington, D.C.

Dolman, A.J., 1993. A multiple-source land surface energy balance model for use in general circulation models. *Agric. For. Meteorol.*, 65: 21-45.

Dolman, A.J., Gash, J.H.C., Roberts, J. & Shuttleworth, W.J., 1990. Stomatal and surface conductance of tropical rainforest. *Agric. For. Meteorol.*, 54: 303-318.

Dolman, A.J. & Gregory, D., 1992. The parameterization of rainfall interception in GCMs. *Q. J. R. Meteorol. Soc.*, 118: 455-467.

Dolman, A.J., Silva Dias, M.A., Calvet, J-C., Ashby, M., Tahara, A.S., Delire, C., Kabat, P., Fisch, G.A. & Nobre, C.A., 1997. Meso scale effects of tropical deforestation in Amazonia: preparatory LBA modelling studies. *Journal of Geophysical Research*, submitted.

Dye, D., 1992. Satellite estimation of the global distribution and interannual variability of photosynthetically active radiation. Ph.D. dissertation, University of Maryland, College Park, 178 pp.

Dye, D.G., Ryosuke, Shibaki, 1995. Intercomparison of global PAR data sets. *Geophysical Research Letters*, 22: 2013-2016.

Eck, T.F. & Dye, D.G., 1991. Satellite estimation of incident photosynthetically active radiation from ultraviolet reflectance. *Remote Sensing of Environment*, 38: 135-146.

Fisher, R.A., 1950. *The design of experiments*. Oliver & Boyd, Edinburgh.

Figueiroa, N.F., Satyamurty, P. & Silva Dias, P.L., 1995. Simulations of the summer circulation over the South American region with an eta coordinate model. *J. Atmos. Sci.*, 52, 1573-1584.

Fisch, G., 1996. Camada limite Amazonica: aspectos observacionais e de modelagem. PhD Thesis, INPE/USP, Sao Jose dos Campos, Brazil.

Gandú, A.W. & Geisler, J.E., 1992: A primitive equation model study of the effect of topography on the summer circulation over tropical South America. *J. Atmos. Sci.*, 48, 1822-1836.

Gash, J.H.C. & Nobre, C.A., 1997. Climatic effects of Amazonian deforestation: some results from ABRACOS. *Bulletin of the American Meteorological Society*, in press.

Gash, J.H.C., Nobre, C.A., Roberts, J.M. & Victoria, R.L., 1996. An overview of ABRACOS. In: Gash, J.H.C., Nobre, C.A., Roberts, J.M. & Victoria, R.L. (eds.), *Amazonian Deforestation and Climate*. John Wiley & Sons, Chichester. pp. 1-14.

Genuchten, M.T. van, 1980. A closed form equation for predicting the hydraulic conductivity of unsaturated soils. *Soil Sc. Soc. Am. J.*, 44: 892-898.

Giddings, L. & Choudhury, B.J., 1989. Observation of hydrologic features with Nimbus 7 37GHz data, applied to South America. *International Journal of Remote Sensing*, 10: 1673-1686.

Goutorbe, J.-P., Lebel, T., Tinga, A., Bessemoulin, P., Brouwer, J., Dolman, A.J., Engman, E.T., Gash, J.H.C., *et al.*, 1994. HAPEX-SAHÉL: A large scale study of land-atmosphere interactions in the semi-arid tropics. *Annales Geophysicae*, 12: 53-64.

Grace, J., Lloyd, J. & Gash, J., 1995. Carbon dioxide uptake by an undisturbed tropical rain forest in southwest Amazonia, 1992 to 1993. *Science*, 270: 778.

GRASS (Geographic Resources Analysis Support System), 1995. Environmental Division of the US Army, USACERL-EN, Champaign, USA.

Hansen, M., Dubayah, R. & De Fries, R., 1996. Classification trees: an alternative to traditional land cover classifiers. *International Journal of Remote Sensing*, 17: 1075-1081.

Hodnett, M.G., Oyama, M.D., Tomasella, J. & Marques, A. de O Comparisons of long-term soil water storage behaviour under pasture and forest in three areas of Amazonia. In: Gash, J.H.C., Nobre, C.A., Roberts, J.M. & Victoria, R.L. (eds.). *Amazonian Deforestation and Climate*. John Wiley & Sons, Chichester. pp. 57-77.

Huber, O., 1995. Vegetation map of the Venezuelan Guyana. In: Berry, P.E., Holst, B.K. & Yatskievych K. (eds.). *Flora of the Venezuelan Guyana Vol. 1*. Missouri Botanic Garden, St. Louis, Missouri. 320 pp.

Huntingford, C., Allen, S.J. & Harding, R.J., 1995. An intercomparison of single and dual-source vegetation-atmosphere transfer models applied to transpiration from Sahelian Savannah. *Boundary Layer Meteorol.*, 74: 397-418.

IBGE - Instituto Brasileiro de Geografia e Estatística, 1979. International map of the world on the millionth scale, Porto Velho (SC-20), Guapore (SD-20). Rio de Janeiro.

Jarvis, P.G., 1976. The interpretation of the variations of leaf water potential and stomatal conductance found in canopies in the field. *Philosophical Transactions of the Royal Society, London, B* 273: 593-610.

Jeffers, J.N.R. *Sampling*. Natural Environment Research Council, U.K., Grange-over-Sands, Cumbria, U.K.

Kabat, P., van den Broek, B.J. & Feddes, R.A., 1992. SWACROP: a water management and crop production simulation model. *ICID Bulletin* 41 (2): 61-83.

Kabat, P. et al., 1996. Combined Atmosphere-Biosphere Amazon Region Experiment (CABARE). Use of integrated modeling for experimental design. Interim report of CEC Environment programme project no. PL-931938 contract EV5V-CT94-0456.

Keil, M., Scales, D., Winter, R., Kux, H. & Dos Santos, J.R., 1996. Tropical Rainforest Investigation in Brazil using Multitemporal ERS-1 SAR Data, Proceedings of the Second ERS Application Workshop, London, 6-8 Dec. 1995. (ESA SP-383, February 1996).

Killeen, T., Steininger, M. & Tucker, C.J., 1974. Formaciones Vegetales del Parque Nacional Noel Kempff Mercado (Santa Cruz, Bolivia) y las Zonas Colindantes de Bolivia y Brasil. In *Rapid Ecological Assessment of Noel Kempff Mercado Park, Bolivia*. Conservation International, *in press*.

Lawrence, W., Chomentowski, W., 1992. Data base project to use nearly 3.000 satellite scenes. *Earth Observation Magazine*, 12: 28-30.

Lean, J. & Rowntree, P., 1993. A GCM simulation of the impact of deforestation on climate using an improved canopy representation. *Quart. J. Roy. Meteorol. Soc.*, 119: 509-530.

Leemans, R. & Cramer, W.P., 1991. *The IIASA Database for Mean Monthly Values of Temperature, Precipitation, and Cloudiness on a Global Terrestrial Grid*. International Institute for Applied Systems Analysis, Laxenburg, Austria.

Lohmann, G., 1991. An Evidential Reasoning Approach to the Classification of Satellite Images. DLRResearch Report 91-29. Deutsche Forschungsanstalt für Luft- und Raumfahrt, Köln.

Lohmann, G., 1994. Co-occurrence based Analysis and Synthesis of Textures, International Conference on Pattern Recognition, Jerusalem, Israel (October 1994).

Louis, J., 1979. A parametric model of vertical eddy fluxes in the atmosphere. *Boundary Layer Meteorol.*, 17: 187-202.

Lloyd, C.R., Gash, J.H.C., Shuttleworth, W.J. & Marques, A. de O., 1988. The measurement and modelling of rainfall interception by Amazonian rain forest. *Agric. For. Meteorol.*, 43: 277-294.

Mahfouf, J.F., Richard, E. & Mascart, P., 1987. The influence of soil and vegetation on the development of mesoscale circulations. *J. Climate Appl. Meteorol.*, 26, 1483-1495.

Malingreau, J.-P., Aschbacher, J., Achard, F., Conway, J., De Grandi, F. & Leysen, M., 1994. TREES ERS-1 Study '94: Assessment of the Usefulness and Relevance of ERS-1 for TREES, Proceedings of the First ERS-1 Pilot Project Workshop, Toledo, Spain, 22-24 June 1994 (ESA SP-365, October 1994).

Manzi, A.O., 1994. INPE, personal communication.

Manzi, A.O. & Planton, S., 1994. Implementation of the ISBA parameterization scheme for land surface processes in a GCM - an annual cycle experiment. *J. Hydrol.*, 155, 353-387.

Martin, C.L., Fitzjerrald, D., et. al., 1988 Structure and growth of the mixing layer over Amazonian rain forest. *Journal of Geophysical Research*, 93 D: 1361-1375.

Meeson, B.W., Corprew, F.E., McManus, J.M.P., Closs, J.W., Sun K.-J., Sunday, D.J. & Sellers, P.J., 1995. ISLSCP Initiative I- Global data sets for land-atmosphere models, 1987-1988. Published on CD by NASA, Greenbelt, MD.

Michaelson, J., Schimel, D.S., Friedl, M.A., Davis, F.W. & Dubayah, R.C., 1994. Regression tree analysis of satellite and terrain data to guide vegetation sampling and surveys. *Journal of Vegetation Science*, 5: 673-686.

Nobre, C.A., 1995. INPE, personal communication.

Nobre, C. A., Sellers, P. J. & Shukla, J., 1991. Amazonian deforestation and regional climate change. *J. Climate*, 4, 957-988. |

Nobre, C.A., et al., 1996. The large scale biosphere atmosphere experiment in Amazonia (LBA). Concise Experimental plan. CPTEC, Cachoeira Paulista, SC-DLO, Wageningen.

Nobre, C.A., Fisch, G., Rocha, H.R., Lyra, R.F., Rocha, E.P., Costa, A.C.L. & Ubarana, V.N., 1996: Observations of the atmospheric boundary layer in Rondonia. In: Gash, J.H.C., Nobre, C.A., Roberts, J.M. & Victoria, R.L. (eds.). *Amazonian Deforestation and Climate*. John Wiley & Sons, Chichester. pp. 413-424.

Noilhan, J., Lacarrere, P. & Bougeault, P., 1991. An experiment with an advanced surface parameterization in a meso-beta-scale model. Part III: Comparison with the HAPEX-MOBILHY data set. *Mon. Wea. Rev.*, 119, 2393-2413.

Noilhan, J. & Mahfouf, J.-F., 1996. The ISBA land surface parameterization scheme. *Gl. Plan. Change*, 35: 987-992.

Noilhan, J. & Planton, S., 1989: A simple parameterization of land surface processes for meteorological models. *Mon. Wea. Rev.*, 117: 536-549.

Polcher, J. & Laval, K., 1994. The impact of African and Amazonian deforestations GCM on tropical climate. *J. Hydrol.*, 155, 389405.

Prince, S.D. & Goward, S.N., 1995. Global primary production: a remote sensing approach. *Journal of Biogeography*, 22: 815-835.

PV-WAVE Advantage, 1993. Visual Numerics, Inc., Houston, USA.



RADAMBRASIL, 1978. Levantamento dos Recursos Naturais. Porto Velho, 16:SC 20, Rio de Janeiro, Brazil. 668 pp.

RADAMBRASIL, 1979. Levantamento dos Recursos Naturais. Guapore, 19:SD-20, Rio de Janeiro, Brazil. 378 pp.

Roberts, J.M., Cabral, O.M.R., da Costa, J.P., McWilliam, A.-L.C. & Sa, T.D.A., 1996. Leaf area index, biomass and physiological responses in Amazonian forest and pasture: an overview. In: Gash, J.H.C., Nobre, C.A., Roberts, J.M. & Victoria, R.L. (eds.). *Amazonian Deforestation and Climate*. John Wiley & Sons, Chichester. pp. 287-306.

Rocha, H. da, Nobre, C., Bonatti, J. & Sellers, P., 1996. A vegetation-atmosphere interaction study for Amazonian deforestation using field data and a single column model. *Q. J. R. Meteorol. Soc.*, 122: 567-594.

Rutter, A.J., Kershaw, K.A., Robins, P.C. & Morton, A.J., 1971. A predictive model of rainfall interception in forests: 1 Derivation of the model from observations in a plantation of Corsican pine. *Agric. Meteorol.*, 9: 367-384.

Sellers, P.J., Hall, F.G., Asrar, G., Strebel, D.E. & Murphy, R.E., 1992. An overview of the First International Satellite Land Surface Climatology Project (ISLSCP) Field Experiment (FIFE). *Journal of Geophysical Research*, 97: 18345-18371.

Sellers, P., Hall, F., Margolis, H., Kelly, B., Baldocchi, D., den Hartog, J., Cihlar, J., Ryan, M., *et al.*, 1995a. The Boreal Ecosystem-Atmosphere Study (BOREAS): an overview and early results from the 1994 field year. *Bulletin of the American Meteorological Society*, 76: 1549-1577.

Sellers, P.J., Meeson, B.W., Closs, J., Collatz, J., Coprew, F., Dazlich, D., Hall, F.G., Kerr, Y., *et al.*, 1995b. An overview of the ISLSCP Initiative I Global Data Sets. On: ISLSCP Initiative I-Global Data Sets for Land Surface Models, 1987-1988. Volumes 1-5. Published on CD by NASA, Greenbelt, MD.

Sellers, P.J., Mintz, Y., Sud, Y.C. & Dalcher, A., 1986. A simple biosphere model (SiB) for use within general circulation models. *J. Atmos. Sci.*, 43, 505-531.

Shuttleworth, W.J., 1988. Evaporation from Amazonian rain forest. *Proc. Roy. Soc. (Lond.) B*, 233: 321-346.

Shuttleworth, W. J., 1989. Micrometeorology of temperate and tropical forest. *Phil. Trans. R. Soc. (Lond.)*, B 324: 299-334.

Shuttleworth, W.J. & Wallace, J.S., 1985. Evaporation from sparse crops - an energy combination theory. *Quart. J.R. Meteorol. Soc.*, 111: 839-855.

Skole D. & Tucker, C., 1993. Tropical deforestation and habitat fragmentation in the Amazon: satellite data from 1978-1988. *Science*, 260: 1905-1910.

Stewart, J.B., 1988. Modelling surface conductance of pine forest. *Agric. For. Meteorol.*, 43: 19-35.

Sud Y.C., Walker, G.K., Kim, J.H., Liston, G.E., Sellers, P.J. & Lau, W., 1996. Biogeophysical consequences of a tropical deforestation scenario: a GCM simulation study. *J. Climate*, 9: 3225-3247.

Tomasella, J. & Hodnett, M.G., 1996. Soil hydraulic properties and van Genuchten parameters an oxisol under pasture in central Amazonia. In: Gash, J.H.C., Nobre, C.A., Roberts, J.M. & Victoria, R.L. (eds.). *Amazonian Deforestation and Climate*. John Wiley & Sons, Chichester. pp. 101-124.

Ubarana, V.N. Observation and modelling of rainfall interception loss in two experimental sites in Amazonian forest. In: Gash, J.H.C., Nobre, C.A., Roberts, J.M. & Victoria, R.L. (eds.). *Amazonian Deforestation and Climate*. John Wiley & Sons, Chichester. pp. 151-162.

USDA (US Department of Agriculture), 1970. Soil Taxonomy of the National Cooperative Soil Survey. USDA Soil Conservation Service. Washington DC, 510 pp.

USDC-NOM (US Department of Commerce - National Oceanic and Atmospheric Administration), 1995. TerrainBase - Worldwide digital terrain data, CD-ROM release 1.0, Documentation manual, Boulder, 168 pp.

Venables, W.N. & Ripley, B.D., 1994. *Modern Applied Statistics with S-Plus*. Springer-Verlag, New York, 462 pp.

Vries, D.A. de, 1963. Thermal properties of soils. In Wijk, W.R., (ed.). *Physics of plant environment*. North-Holland Publishing Company, Amsterdam, pp. 210-235.

Walker, R., (ed.), 1996. Land Use Dynamics in the Brazilian Amazon. In: Ecological Economics, Special Issue No. 18, Elsevier.

Wetzel, P.J. & Chang, J.T., 1987. Concerning the relationship between evapotranspiration and soil moisture. *J. Climate Appl. Meteorol.*, 26, 18-27.

Wright, I.R., Gash, J.H.C., da Rocha, H.R., Shuttleworth, W.J., Nobre, C.A., Maitelli, G.T., Zamparoni, C.A.G.P and Carvalho, P.R.A., 1992. Dry season micrometeorology of central Amazonian ranchland. *Quart. J. Roy. Meteorol. Soc.*, 118: 1083-1099.

Wright, I.R., Gash, J.H.C., Rocha, H.R. da & Roberst, J.M., 1996a. Modelling surface conductance for Amazonian pasture and forest. In: Gash, J.H.C., Nobre, C.A., Roberts, J.M. & Victoria, R.L. (eds.). *Amazonian Deforestation and Climate*. John Wiley & Sons, Chichester. pp. 437-458.

Wright, I.R., Nobre, C.A., Tomasella, J., Rocha, H.R. da, Roberts, J.M, Vertamatti, E., Culf, A.D., Alvalá, R.C.S., Hodnett, M.G. & Ubarana, V.N., 1996b. Towards a

GCM surface parameterization for Amazonia. In: Gash, J.H.C., Nobre, C.A., Roberts, J.M. & Victoria, R.L. (eds.). *Amazonian Deforestation and Climate*. John Wiley & Sons, Chichester. pp. 473-504.

## **Attachment 1**

ABRACOS electronic data base to which completion the current project contributed. Examples of data pages for micrometeorology and soil moisture. The data are in the public domain.

Access: <http://yabae.cptec.inpe.br/lba> or <http://www.nwl.ac.uk/ih>





# **ABRACOS**

**Anglo-Brazilian Amazonian  
Climate Observation Study**



[Introduction](#) [Climate Micrometeorology](#)  
[and evaporation](#) [Physiology](#) [Carbon](#)  
[dioxide fluxes](#) [Soil physics](#) [References](#)  
[Available Data \(FTP\)](#)



MINISTÉRIO DA CIÊNCIA E TECNOLOGIA  
INSTITUTO NACIONAL DE PESQUISAS ESPACIAIS



Centro de Previsão de Tempo  
e Estudos Climáticos



Institute of  
Hydrology

**ODA**

Accesses to this page since August 23, 1996 : **000508**



E-mail: [javier@cptec.inpe.br](mailto:javier@cptec.inpe.br) or [maura@cptec.inpe.br](mailto:maura@cptec.inpe.br)

# MICROMETEOROLOGY

Hourly estimates of evaporation, heat flux and conductances supported by climate data and calibrated estimates of the hourly momentum flux and atmospheric stability. The data were recorded during the intensive study periods at 5 of the 6 ABRACOS sites and range in duration from 3 weeks to 3 months.

The micrometeorology disk files are as follows:  
PASTURE (compressed into PAST.EXE)

File NAME	Mission NUMBER	Site Code	Year	Local Time/Date	
				Initial	Final
PASTM1.PRN	1	FD	1990	01hr, 18 Sep.	24hr, 2 Nov.
PASTM2.PRN	2	FD	1991	01hr, 29 June	12hr, 11 Sep.
PASTM3.PRN	3	NS	1992	01hr, 06 Aug.	12hr, 7 Oct.
PASTM45.PRN	4/5	NS	1993	01hr, 31 Mar.	12hr, 28 Jul.
PASTM6.PRN	6	BS	1993	18hr, 05 Oct.	09hr, 26 Oct.
PASTM7.PRN	7	NS	1994	12hr, 11 Aug.	15hr, 24 Aug.

FOREST (compressed into FORST.EXE)

File NAME	Mission NUMBER	Site Code	Year	Local Time/Date	
				Initial	Final
FORSTM3.PRN	3	RJ	1992	16hr, 08 Aug.	10hr, 05 Oct.
FORSTM45.PRN	4/5	RJ	1993	01hr, 04 Apr.	24hr, 26 July
FORSTM6.PRN	6	RV	1993	11hr, 18 Oct.	10hr, 27 Oct.
FORSTM7.PRN	7	RJ	1994	17hr, 13 Aug.	15hr, 25 Aug.

where the site codes are as follows,

FD	Fazenda Dimona, near Manaus, Amazonas
NS	Fazenda Nossa Senhora, near Ji-Parana, Rondonia
BS	Fazenda Boa Sorte, near Maraba, Para
RJ	Reserva Jarú, near Ji-Parana, Rondonia
RV	Reserva Vale, near Maraba, Para

Site details are given in the climate text file AB-AWS.TXT

Within each file each datum is in free format, in seven character columns and space delineated. Missing data are indicated by a value of -99. In summary the columns are follows:

Col.	
1	Julian day number
2	Hour(local)
3	Total incoming short-wave. W/m <sup>2</sup>
4	Reflected short-wave. W/m <sup>2</sup>
5	Net radiation. W/m <sup>2</sup>
6	Soil heat flux. W/m <sup>2</sup>
7	Air temperature oC
8	Specific humidity g/kg
9	Wind speed m/s
10	Wind direction (degrees arc, clock-wise from North)
11	Friction velocity m/s
12	Stability parameter, z/L, where L is Monin-Obukhov length
13	Integrated stability correction parameter for sensible heat flux
14	Integrated stability correction parameter for momentum flux
15	Aerodynamic conductance for heat fluxes mm/s
16	Bulk surface conductance. mm/s
17	Latent Heat Flux. W/m <sup>2</sup>
18	Sensible Heat Flux. W/m <sup>2</sup>
19	EITHER Pasture: soil moisture in the root zone m <sup>3</sup> /m <sup>3</sup>
19	OR Forest: change in biomass heat storage W/m <sup>2</sup>
20	Rainfall. mm
21	Soil temperature at 10cm (some pasture sites only) oC
22	Soil temperature at 20cm (some pasture sites only) oC
23	Soil temperature at 40cm (some pasture sites only) oC

## DATA FILE DETAILS AND NOTES

The following is a more detailed description of each column giving:

Instrument type details (AWS refers to the collocated Automatic Weather Station)



Instrument location details  
 Derivation of analyzed figures  
 Quality control information  
 Cautionary notes where problems arise

General information concerning groups of missions is given first, followed by notes specific to individual missions indicated by the site code and mission number (e.g. FD-2)

### 1. JULIAN DAY NUMBER

All data files contain a continuous time series of hourly information, although some files have gaps in individual channels.

### 2. HOUR

Time is local and gives the end time of the hourly period for which the total or average is given.

### 3. TOTAL INCOMING SHORT-WAVE (W/m<sup>2</sup>)

AWS - Recorded by Kipp and Zonen solarimeter

FD-1	## GAP ##	>	217 14:00 (first 10 days)
FD-2	## GAP ##	190 10:00	93 19:00 (small gap 10th - 13th day)

### 4. REFLECTED SHORT-WAVE (W/m<sup>2</sup>)

AWS - Recorded by Kipp and Zonen solarimeter

FD-1	## GAP ##	>	217 14:00 (first 10 days)
		>	101 06:00
NS-45	## GAPS ##	129 21:00	130 20:00
		144 19:00	145 20:00
		146 21:00	157 20:00

### 5. NET RADIATION (W/m<sup>2</sup>)

AWS - REBS net all-wave radiometer

### 6. SOIL HEAT FLUX (W/m<sup>2</sup>)

This is a larger and more important component of the energy balance at pasture sites than forest. Each AWS has two sensors placed at 5mm in the soil which is an adequate sample for forests but less so for pasture. During most pasture missions 9

sensors were used at 5mm depth. Some gaps have been filled using regressions against either net radiation in the pasture or air temperature in the forests.

NS-3 During the dry start to this mission evaporation could be occurring below the sensors creating a small underestimation in the heat or vapour flux. Compensation for this could be derived from the following years analysis. (see below)

NS-45 During the driest part of this mission evaporation below the shallow sensors was identified. The evaporation front passed below the 5mm sensors on about day 271. After this SHF in the data base is derived from the deeper sensors (15cm) to give the overall heat energy leaving the system, and diurnally adjusted for soil heat storage above the sensors using the soil temperature measurement.

BS-6 Record based upon only two sensors.

BS-6 10% patched using regression with net radiation

RJ-3 ## GAP ## 8 days (266-234) filled by regression with air temperature

7. AIR TEMPERATURE (oC)

AWS - Platinum resistance thermometer except FD-M1, FD-M2 and other instances where it was necessary to the micromet. channel.

FD-1	## GAPS ##	269 03:00 - 269 10:00
		270 01:00 - 270 10:00
		270 20:00 - 271 11:00
		(small gaps 8th to 10th day)

8. SPECIFIC HUMIDITY (g/kg)

AWS - Platinum resistance wet-bulb thermometer except FD-M1, FD-M2 and other instances where it was necessary to the micromet. channel.

FD-1	## GAPS ##	269 03:00 - 269 10:00
		270 01:00 - 270 10:00
		270 20:00 - 271 11:00
		(small gaps 8th to 10th day)
RV-6	## GAPS ##	283 22:00 - 285 13:00
		286 01:00 - 291 11:00

9. WIND SPEED (m/s)

AWS - Didcot Instruments, UK

10. WIND DIRECTION (degrees arc, clock-wise from North)

AWS - Didcot Instruments, UK

FD-1	## GAP ##	}	271 14:00 (first 10 days)
FD-2	## GAP ##		190 10:00 - 193 19:00

11-15. MOMENTUM FLUX VARIABLES

Friction velocity (m/s)

Stability parameter,  $z/L$

Integrated stability correction for sensible heat flux

Integrated stability correction for momentum flux

Aerodynamic conductance for heat fluxes (mm/s)

All momentum flux and stability variables are calculated using the best possible roughness calibration for each site (see Wright et al 1992, Wright et al 1996b) as follows:

Mission	z	d	z0
FD-1	3.5	0.17	0.026
FD-2	3.5	0.19	0.026
NS-3	5.5	0.38	0.064
NS-45	5.5	0.40	0.064
NS-7	3.8	0.20	0.030
BS-6	4.0	0.46	0.076
RJ-3 & 45	53.5	5.8	2.60
RV-6	53.5	30.1	2.35

Data base columns 11-14 were then calculated by iteration of the wind profile and stability correction formulae based on the Monin-Obukhov length,  $L$ , and similarity theory (Arya 1988). The aerodynamic conductance given in column 15 is then calculated from the friction velocity and stability corrections, and is the conductance applicable for heat and water vapour. This application includes a correction for the different source/sink heights for heat and momentum and gives  $\ln(z_{0m}/z_{0h})$  the value 2.0 for pasture and 1.5 for forest (Brutsaert, 1984). When heat flux data is missing the variables are given for neutral conditions

16. BULK SURFACE CONDUCTANCE (mm/s)

Calculated from a rearrangement of the Penman-Monteith equation. The value is set to -99 either at night or when the calculated values is very high or negative. (Wright et al. 1995,1996a)

17. LATENT HEAT FLUX (W/m<sup>2</sup>)

Pasture and forest fluxes were frequently verified against other independent Bowen ratio and eddy-correlation devices

Pasture - evaporation calculated from estimates of Bowen ratio (9m profile tower), directly from an eddy-correlation device or as a residual of the energy balance when the two former sources are unavailable. A few gaps of not more than 2 daylight hours were filled using a detailed time-series model of Bowen ratio.

Forest - the same as for pasture but without the use of psychrometer profiles. Changes in biomass heat storage were include in the residual energy balance method (Moore and Fisch,1986)

FD-1	## GAPS ##	269 03:00 - 269 10:00
		270 01:00 - 270 10:00
		270 20:00 - 271 11:00
		(small gaps 8th to 10th day)
FD-2	## GAP ##	180 00:00 - 180 17:00
		(first day)
RV-6	## GAPS ##	283 22:00 - 285 13:00
		286 01:00 - 291 11:00
		293 10:00 - 294 10:00

18. SENSIBLE HEAT FLUX (W/m<sup>2</sup>)

Pasture and forest fluxes were frequently verified against other independent Bowen ration and eddy-correlation devices

**Pasture** - heat flux calculated from estimates of Bowen ratio (9m profile tower), directly from an eddy-correlation device. A few gaps of not more than 2 daylight hours were filled using a detailed time-series model of Bowen ratio.

**Forest** - the same as for pasture but without the use of psychrometer profiles.

FD-1	## GAPS ##	269 03:00 - 269 10:00
		270 01:00 - 270 10:00
		270 20:00 - 271 11:00
		(small gaps 8th to 10th day)
FD-2	## GAP ##	180 00:00 - 180 17:00
		(first day)
RV-6	## GAPS ##	283 22:00 - 285 13:00
		286 01:00 - 291 11:00
		293 10:00 - 294 10:00

19. EITHER PASTURE: SOIL MOISTURE IN THE ROOT ZONE ( $m^3/m^3$ )  
Mean moisture storage in the top 1.5 m (FD) or 2.0 m (NS & BS) of soil, derived from between 5 and 8 neutron access tubes with 10-20 cm measurement depth increments. (Wright 1995, 1996a)

Or FOREST: CHANGE IN BIOMASS HEAT STORAGE ( $W/m^2$ )

Calculated using the AWS air temperature and humidity in the equations of Moore and Fisch (1986) and best estimates of forest structure parameters from Reserva Jaru.

FD-2	## GAP ##	180 00:00 - 180 23:00 (first day)
------	-----------	--------------------------------------

20. RAINFALL (mm)

AWS - Didcot Instruments, UK. 0.1-0.2mm tipping bucket device.

FD-1	## GAPS ##	>	- 277 19:00 278 21:00 - 281 19:00
------	------------	---	--------------------------------------

A Manual raingauge showed little significant rain fall up to day 277, except for 27mm during the afternoon of day 270.

21-23. SOIL TEMPERATURE AT 10cm (pasture only) (oC)

SOIL TEMPERATURE AT 20cm (pasture only)(oC)

SOIL TEMPERATURE AT 40cm (pasture only)(oC)

Mean of three thermistors at 10 cm and a single thermistor at the other two depths.

FD-1	## GAPS ##	>	267 13:00 (10cm and 20cm)
		>	271 16:00 (40cm)
		279 17:00 -	281 16:00 (all)
		283 12:00 -	287 06:00 (all)
		289 16:00 -	302 10:00 (40cm)
		306 11:00 >	271 16:00 (40cm)
FD-2	## GAP ##	180 00:00	180 17:00
		(first day)	
FD-2	No data for 40 cm		
NS-3	## GAP ##	>	225 11:00 (all)
		270 10:00 -	>
NS-45	## GAPS ##	>	111 24:00
		114 10:00 -	114 16:00
		185 00:00 -	186 14:00

## REFERENCES

Arya, S.P., 1988. Introduction to micrometeorology. Academic Press (London). pp 307.

Brutsaert, W. 1984. Evaporation into the atmosphere. D. Riedel Publ. Co., Dordrecht.

Moore, C.J. and Fisch, G., 1986. Estimating heat storage in Amazonian tropical forests. Agric. For. Meteorol., 38: 147-169.

Wright, I.R., Gash, J.H.C., da Rocha, H.R., Shuttleworth, W.J., Nobre, C.A., Maitelli, G.T., Zamparoni, C.A.G.P. and Carvalho, P.R.A., 1992. Dry season micrometeorology of central Amazonian ranchland. Quart. J. R. Meteorol. Soc., 118: 1083-1099.

Wright, I.R., Manzi, A.O. and da Rocha, H.R., 1995. Surface conductance of Amazonian pasture: model application and calibration for canopy climate. Agric. For. Meteorol., 75: 51- 70.

Wright, I.R., Gash, J.H.C.G. and da Rocha, H.R., 1996b. Modelling surface conductance for Amazonian pasture and forest. In Amazon Deforestation and Climate (Eds. J.H.C. Gash, C.A. Nobre, J.M. Roberts and R.L. Victoria), In Press. John Wiley, Chichester. pp 437-458.

Wright, I.R., Nobre, C.A., Tomasella, J, da Rocha, H.R., Roberts, J.M., Vertamatti, E., Culf, A.D., Alval , R.C.S., Hodnett, M.G. and Ubarana, V., 1996b. Towards a GCM surface parameterisation for Amazonia. In *Amazon Deforestation and Climate* (Eds. J.H.C. Gash, C.A. Nobre, J.M. Roberts and R.L. Victoria), In Press. John Wiley, Chichester. pp 473-504.

Yang, Z.L., Dickinson, R.E. and Shuttleworth, W.J., 1996. Treatment of Soil, Vegetation and Snow in Land-surface Models: A Test of the Biosphere-Atmosphere Transfer Scheme with the HAPEX-MOBILHY, ABRACOS and Russian Data, invited to a BAHC Special Issue of *Journal of Hydrology*. (in revision)



## SOIL MOISTURE

### GENERAL

The soil moisture file format is

SOIL[site code].DAT

and is compressed into a single file AB\_SOIL.EXE.

The first three columns of each file give the year, day number and time (decimal hour) of measurement. Thereafter, the remaining columns contain the mean soil moisture, at various depths, in units of moisture volume fraction (m<sup>3</sup>/m<sup>3</sup>). The means are calculated as the linear average of all access tubes at each site, with the exception of Reserva Jaru (see below).

Soil moisture was measured close to the automatic weather station (AWS) using a neutron probe soil moisture meter. The only exception to this was the 'Manaus forest' data which was recorded in primary forest close to the pasture site (FD) rather than at the Manaus forest AWS site (RD), see Hodnett et al. (1995). For this reason an extra code is introduced, FDF, for forest at Fazenda Dimona. Further details of all sites are given in AB-AWS.TXT. The soil moisture at each access tube was read approximately every 7 days and with increased frequency during the intensive data missions (see AB-MMET.TXT).

Measurement access tubes were permanently installed at random positions at each site. Details are as follows:

PASTURE SITES	FD	NS	BS
Tubes	8	6	6
Depth Code	a	c	d
Starting	18/09/90	05/11/91	25/08/91
Ending(*)	02/12/93	20/12/93	29/10/93

### SOIL TYPE

Brazilian	Yellow		Red-yellow
	latosol		podsol
FOA	Xanthic	Orthic	Orthic
	ferralsol	acrisol	acrisol
US	Haplic	Typic	Typic
	acrorthox	paleudult	haplustult

FOREST SITES	FDF	RJ	RV
--------------	-----	----	----



Tubes	5	8	6
Depth Code	b	c	d
Starting	18/09/90	30/10/91	17/08/91
Ending(*)	02/12/93	29/12/93	27/10/93

## SOIL TYPE

Brazilian	Yellow latosol		
FOA	Xanthic ferralsol	Orthic acrisol	Humic cambisol
US	Haplic acrorthox	Typic paleudult	Typic dystrochrept

Where the depth codes, in metres, are as follows

a	0.1, 0.2 then every 0.2 to a depth of 2.0
b	until 17/10/91 as (a) then as (c)
c	0.1, 0.2 then every 0.2 to 3.6 (see also NOTES for RJ below)
d	0.1, 0.2 then every 0.2 to 1.2, and then every 0.3 to 3.6

In each file the depths appear as a header (in the first line) and therefore may be read in as required by any software.

(\*) The soil moisture measurement network was not dismantled in December 1993, and measurement continued beyond this date. These subsequent data are managed by CPTEC/INPE at Cachoeira Paulista, SP, Brazil.

## NOTES SPECIFIC TO EACH SITE

## FD FAZENDA DIMONA (Pasture)

1. Specific calibration derived and used for 0.1 m depth

## FDF FAZENDA DIMONA (Forest)

1. Specific calibration derived and used for 0.1 m measurements.
2. Installation of 3.6 m tubes, 17 October 1991. Two sets of data are shown for this date. The first was made in the original (max depth 2 m) tubes, the second was made in the new tubes. There is a difference in water content due to spatial variability, but the two sets of observations on the same day (effectively at the same time) allow the data sets for the 2 m and 3.6 m tubes to be linked.

## NS FAZENDA NOSSA SENHORA

1. A specific calibration for the surface layer was not derived. The absolute water contents will be under-estimated and it is likely that the under-estimation will increase as the water content decreases. Overall this is expected to lead to an under-estimation of the changes of water content at 0.1 m and, to a lesser extent, at 0.2 m.
2. Between 9 February and 1 August 1992 the data are not reliable because of inconsistencies in depth location of the probe. However, they give a good general

indication of the soil water behaviour. From 8 August to 1 October 1992 (inclusive), the data are very unreliable and should not be used. On 7 October 1992 the depth location problem was eliminated and the subsequent the data are good (including 7/10/92).

3. In the wet season, the water content in the profile is influenced by the presence of the water table which can reach to within 2.0 m of the soil surface during the wet season.

#### RJ RESERVA JARU

1. The depth of 6 of the 8 tubes was limited by the depth to bedrock. The maximum depth in the 6 tubes ranged from 2.0 to 3.2m. Therefore the mean moisture content at each depth from the 0.1 to 2.0m uses all 8 tubes: then the mean of 7 tubes at 2.2 m, 6 at 2.4, 5 at 2.6, 4 at 2.8, 3 at 3.0 and 3.2 and the mean of 2 tubes at 3.4 and 3.6.

2. A specific calibration for the surface layer was not derived. The absolute water contents will be under-estimated and it is likely that the under-estimation will increase as the water content decreases. Overall this is expected to lead to an under-estimation of the changes of water content at 0.1 m and, to a lesser extent, at 0.2 m.

3. Between 9 February and 10 October 1992 the data are not reliable because of inconsistencies in depth location of the probe. However, they give a good general indication of the soil water behaviour.

4. In the wet season, the water content in the profile is strongly influenced by the presence of the water table which can reach to within 1.0 m of the soil surface during the wet season.

#### BS FAZENDA BOA SORTE

1. A specific calibration for the surface layer was not derived. The absolute water contents will be under-estimated and it is likely that the under-estimation will increase as the water content decreases. Overall this is expected to lead to an under-estimation of the changes of water content at 0.1 m and, to a lesser extent, at 0.2 m.

#### RV RESERVA VALE DO RIO DOCE

1. A specific calibration for the surface layer was not derived. The absolute water contents will be under-estimated and it is likely that the under-estimation will increase as the water content decreases. Overall this is expected to lead to an under-estimation of the changes of water content at 0.1 m and, to a lesser extent, at 0.2 m.

#### REFERENCES

Hodnett, M.G., da Silva, L.P., da Rocha, H.R. and Cruz Senna, R.C., 1995.  
Seasonal soil water storage changes beneath central Amazonian rainforest and

pasture. J. Hydrol., 170, 233-254.



## **Attachment 2**

Pre - LBA data set initiative to which the current project contributed. The data are also included on a CD-ROM, which is being produced with contribution of the current project and under the auspices of the IGBP-BAHC and WCRP- GEWEX/ISLSCP.

Access and more information: **<http://yabae.cptec.inpe.br/lba>**

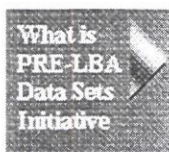




## PRE-LBA Questionnaire

# LBA

## PRE-LBA Data Sets Initiative



A PRE-LBA Data Sets CDROM is currently being implemented. The goals of this activity are:

- Quick overview of available data for Amazonia
- Quick access to available data and data products



In the presentation of the working groups during the First LBA Open Science Meeting, held in June 27-July 2 1996, in Sao Jose dos Campos, SP, Brazil, it was very clear that the PRE-LBA initiative lead by CPTEC/INPE is a very important effort in data location and collection. The LBA data and information group intends to be involved in this task as much as possible, to use this experience in the design of the data management system for LBA and the primary data layers to be used commonly by several science themes.

The data group would like to contribute to the selection of the data to be put onto the CDROM, based on the relevance of the science agenda. All other data sets that are not included in the PRE-LBA CDROM will be referenced as metadata pointers in the WWW.

To locate and compile all the information on Amazonian data sets of interest to the LBA effort, we have prepared a questionnaire that will be sent out to all scientists interested in LBA. Please, find the questionnaire and explanations right above.

Access to this page since September, 1996: **01046**

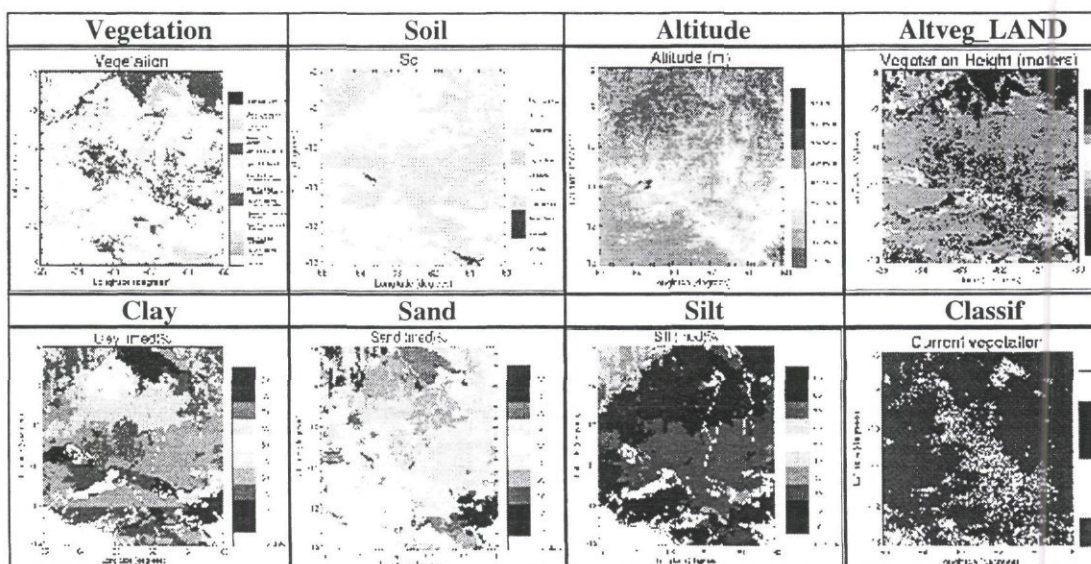
[e-mail:lba@cptec.inpe.br](mailto:lba@cptec.inpe.br)

<http://www.cptec.inpe.br/lba/prelba/prelba.html>

21-07-97

# Mapping Surface Parameters in Forested and Deforested South-Western Amazonia

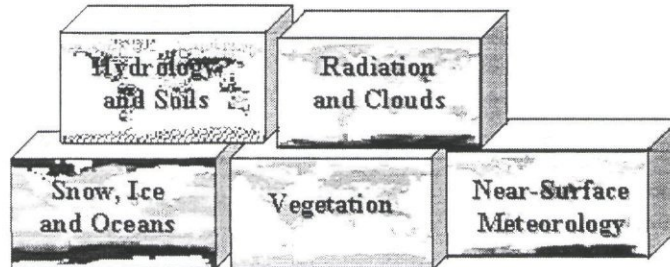
Surface parameter digital maps of vegetation, soil, and topography are obtained for Rondonia, Brazil, covering the 5x5° region 8-13°S, 65-60°W. Numerical maps of the natural landscape structure have been achieved by digitizing existing 1:1,000,000 maps. Satellite data give information about the most recent modifications of the surface due to human activities. This mapping work is the first step of a mesoscale meteorological modeling program.



Santos Alvalá, R.C., J. C. Calvet, G. Jaubert, J. Noilhan, I. R. Wright, 1996: Mapping surface parameters for mesoscale modeling in forested and deforested South-Western Amazonia. Note de Centre, No. 40, Janvier 1996, Centre National de Recherches Meteorologiques - CNRM, METEO FRANCE, TOULOUSE CEDEX, France.

Calvet, J.C., Regina C. Santos Alvalá, Genevieve Jaubert, Christine Delire, Carlos A. Nobre, Ivan Wright and Joel Noilhan, 1996: Mapping surface parameters for mesoscale modeling in forested and deforested South-Western Amazonia. Bulletin of the American Meteorological Society. In Press.

# *ISLSCP Initiative I*



The International Satellite Land Surface Climatology Project (ISLSCP) Initiative I data collection described here was borne out of a workshop organized by the ISLSCP scientific community in 1992. This workshop brought modelers, algorithm developers, and field experiment scientists together to discuss future steps for applying and translating current research findings into useful global data sets for land-atmosphere models. The data sets contained within this CD set are a direct response to the recommendations of that workshop. The intent here was to produce, as quickly as possible, a consistent collection of high priority global data sets using existing data sources and algorithms, designed to satisfy the needs of those modelers. The workshop recommendations specified that global data sets at a consistent spatial and temporal resolution be compiled in four key areas: land cover, hydrometeorology, radiation, and soils.

[ *Hydrology* | *Vegetation* | *Radiation* | *Snow, Ice and Oceans* | *Near-Surface Meteorology* ]

## **Information on *ISLSCP Initiative I* CD-ROM**







### **Attachment 3**

The soil and natural vegetation categories obtained from the RADAMBRASIL (1978, 1979) Porto Velho and Guapore maps. For each soil and vegetation class, the measured median proportion of clay and sand (%) and estimated vegetation height (m) respectively, are indicated (see Chapter 2.2)



SOIL CATEGORIES

COVER	CAT	CLAY	SAND	ABREV	DESCRIPTION
sol	1	58	36	LAa1	PORTO-VELHO LATOSSOLO AMARELO ALICO text. m. arg. e Latossolo Amarelo Alico text. arg. fl. aberta rel. pl. e s. ond.
sol	2	32	58	LAa2	PORTO-VELHO LATOSSOLO AMARELO ALICO text. med. e Latossolo Amarelo Alico text. arg. fl. aberta rel. pl.
sol	3	15	77	LAa3	PORTO-VELHO LATOSSOLO AMARELO ALICO text. med., Latossolo Amarelo Alico text. arg. e Areias Quartzosas Alicas fl. densa rel. pl. e s. ond.
sol	4	-999	-999	LVa1	PORTO-VELHO LATOSSOLO VERMELHO AMARELO ALICO text. m. arg. fl. aberta e Latossolo Vermelho Escuro Alico text. m. arg. fl. densa rel. pl. e s. ond.
sol	5	48	37	LVa2	PORTO-VELHO LATOSSOLO VERMELHO AMARELO ALICO text. m. arg. e Latossolo Vermelho Amarelo Alico text. arg. fl. aberta e fl. densa rel. pl. e s. ond.
sol	6	-999	-999	LVa3	PORTO-VELHO LATOSSOLO VERMELHO AMARELO ALICO text. arg. e Latossolo Vermelho Amarelo Alico concrecionario text. arg. fl. densa rel. pl.
sol	7	44	41	LVa4	PORTO-VELHO LATOSSOLO VERMELHO AMARELO ALICO text. arg. rel. pl. e s. ond. e Podzolico Vermelho Amarelo Alico at. baixa text. arg. fl. aberta rel. s. ond.
sol	8	28	65	LVa5	PORTO-VELHO LATOSSOLO VERMELHO AMARELO ALICO text. arg. rel. pl. e s. ond. e Latossolo Vermelho Amarelo Alico text. med. fl. aberta e fl. densa rel. pl.
sol	9	22	67	LVa6	PORTO-VELHO LATOSSOLO VERMELHO AMARELO ALICO text. med. e Podzolico Vermelho Amarelo Alico at. baixa text. med. fl. aberta rel. pl. e s. ond.
sol	10	26	57	LVa7	PORTO-VELHO LATOSSOLO VERMELHO AMARELO ALICO text. med. e Areias Quartzosas Alicas fl. aberta rel. pl. e s. ond.
sol	11	35	59	LVa8	PORTO-VELHO LATOSSOLO VERMELHO AMARELO ALICO text. arg., Latossolo Vermelho Amarelo Alico text. m. arg. rel. pl. e s. ond. e Podzolico Vermelho Amarelo Alico at. baixa text. arg. fl. aberta rel. s. ond.
sol	12	49	42	LVa9	PORTO-VELHO LATOSSOLO VERMELHO AMARELO text. arg. rel. pl. e s. ond., Podzolico Vermelho Amarelo Alico at. baixa text. arg. e Podzolico Vermelho Amarelo Alico concrecionario at. baixa text. arg. fl. aberta rel. s. ond.
sol	13	60	33	LVa10	PORTO-VELHO LATOSSOLO VERMELHO AMARELO ALICO text. arg., Podzolico Vermelho Amarelo Alico concrecionario at. baixa text. arg. e Solos Concrecionarios Lateriticos indiscriminados Alicos at. baixa text. arg. fl. aberta rel. s. ond.
sol	14	-999	-999	LVa11	PORTO-VELHO LATOSSOLO VERMELHO AMARELO ALICO text. arg. rel. s. ond., Podzolico Vermelho Amarelo Alico at. baixa text. arg. rel. ond. e Solos Concrecionarios Lateriticos Indiscriminados Alicos at. baixa text. m. arg. fl. aberta rel. s. ond.
sol	15	68	24	LVa12	PORTO-VELHO LATOSSOLO VERMELHO AMARELO ALICO text. arg. Latossolo Vermelho Amarelo Alico text. m. arg. rel. s. ond. e ond. e Podzolico Vermelho Amarelo Alico at. baixa text. arg. fl. aberta rel. ond.
sol	16	62	25	TRd1	PORTO-VELHO TERRA ROXA ESTRUTURADA DISTROFICA text. arg. fl. aberta rel. s. ond. e ond.
sol	17	61	8	TRd2	PORTO-VELHO TERRA ROXA ESTRUTURADA DISTROFICA text. arg. e Latossolo Roxo Alico text. arg. fl.

aberta rel. f. ond. e mont.

sol	18	28	49	PE1	PORTO-VELHO PODZOLICO VERMELHO AMARELO EUTROFICO at. baixa text. arg. e Terra Roxa Estruturada Eutrofica text. arg. fl. aberta rel. s. ond.
sol	19	-999	-999	PE2	PORTO-VELHO PODZOLICO VERMELHO AMARELO EUTROFICO at. baixa text. arg. e Podzolico Vermelho Amarelo Eutrofico raso at. baixa text. arg. fl. aberta rel. ond. e f. ond.
sol	20	30	48	PE3	PORTO-VELHO PODZOLICO VERMELHO AMARELO EUTROFICO at. baixa text. arg., Podzolico Vermelho Amarelo Distrofico at. baixa text. arg. e Terra Roxa Estruturada Eutrofica text. arg. fl. aberta rel. pl. e s. ond.
sol	21	45	26	PE4	PORTO-VELHO PODZOLICO VERMELHO AMARELO EUTROFICO at. baixa text. arg., Terra Roxa Estruturada Eutrofica text. arg. e Solos Litolicos Eutroficados at. baixa text. arg. fl. aberta rel. f. ond.
sol	22	27	52	PVd1	PORTO-VELHO PODZOLICO VERMELHO AMARELO DISTROFICO at. baixa text. arg. e Podzolico Vermelho Amarelo Eutrofico at. baixa text. arg. fl. aberta e fl. densa rel. s. ond. com testemunhos esparsos
sol	23	31	50	PVd2	PORTO-VELHO PODZOLICO VERMELHO AMARELO DISTROFICO at. baixa text. arg. e Podzolico Vermelho Amarelo Distrofico cascalhento at. baixa text. arg. fl. aberta e fl. densa rel. s. ond.
sol	24	30	48	PVd3	PORTO-VELHO PODZOLICO VERMELHO AMARELO DISTROFICO at. baixa text. arg. e Podzolico Vermelho Amarelo Alico at. baixa text. arg. fl. aberta e fl. densa rel. s. ond.
sol	25	-999	-999	PVd4	PORTO-VELHO PODZOLICO VERMELHO AMARELO DISTROFICO at. baixa text. arg. e Podzolico Vermelho Amarelo Distrofico cascalhento at. baixa text. arg. fl. aberta rel. ond. e s. ond.
sol	26	8	79	PVd5	PORTO-VELHO PODZOLICO VERMELHO AMARELO DISTROFICO at. baixa text. arg. e Podzolico Vermelho Amarelo Distrofico raso at. baixa text. arg. fl. aberta e fl. densa rel. ond. com testemunhos esparsos
sol	27	-999	-999	PVd6	PORTO-VELHO PODZOLICO VERMELHO AMARELO DISTROFICO at. baixa text. arg., Podzolico Vermelho Amarelo Eutrofico at. baixa text. arg. rel. pl. e s. ond. e Podzolico Vermelho Amarelo Alico concrecionario at. baixa text. arg. fl. aberta rel. s. ond.
sol	28	-999	-999	PVd7	PORTO-VELHO PODZOLICO VERMELHO AMARELO DISTROFICO at. baixa text. arg., Podzolico Vermelho Amarelo Distrofico raso at. baixa text. arg. e Solos Litolicos Distroficados at. baixa text. arg. fl. aberta rel. f. ond. e ond.
sol	29	-999	-999	PVa1	PORTO-VELHO PODZOLICO VERMELHO AMARELO ALICO at. baixa text. arg. e Podzolico Vermelho Amarelo Alico plintico at. baixa text. arg. fl. aberta rel. pl. e s. ond.
sol	30	29	56	PVa2	PORTO-VELHO PODZOLICO VERMELHO AMARELO ALICO at. baixa text. arg. e Latossolo Vermelho Amarelo Alico text. arg. fl. aberta rel. s. ond.
sol	31	-999	-999	PVa3	PORTO-VELHO PODZOLICO VERMELHO AMARELO ALICO at. baixa text. arg. e Podzolico Vermelho Amarelo Alico abruptico at. baixa text. med. fl. densa rel. s. ond.
sol	32	43	31	PVa4	PORTO-VELHO PODZOLICO VERMELHO AMARELO ALICO at. baixa text. arg. e Podzolico Vermelho Amarelo Alico plintico at. baixa text. arg. fl. aberta rel. s. ond.
sol	33	46	4	PVa5	PORTO-VELHO PODZOLICO VERMELHO AMARELO ALICO at. baixa text. arg. fl. aberta rel. ond. e Latossolo Vermelho Amarelo Alico text. arg. fl. densa rel. s. ond.

sol	34	42	43	PVa6	PORTO-VELHO PODZOLICO VERMELHO AMARELO ALICO at. baixa text. arg. e Latossolo Vermelho Amarelo Alico text. arg. fl. aberta e fl. densa rel. ond.
sol	35	17	59	PVa7	PORTO-VELHO PODZOLICO VERMELHO AMARELO ALICO abruptico at. baixa text. med. fl. densa e Cambissolo Tropical Alico at. baixa text. med. fl. aberta rel. pl.
sol	36	22	47	PVa8	PORTO-VELHO PODZOLICO VERMELHO AMARELO ALICO at. baixa text. med. e Podzolico Vermelho Amarelo Alico at. baixa text. arg. fl. aberta rel. pl. e s. ond.
sol	37	27	54	PVa9	PORTO-VELHO PODZOLICO VERMELHO AMARELO ALICO at. baixa text. med. rel. pl. e s. ond. e Areias Quartzosas Alicas fl. aberta rel. pl.
sol	38	40	15	PVa10	PORTO-VELHO PODZOLICO VERMELHO AMARELO ALICO plintico at. baixa text. arg. e Laterita Hidromorfica Alica de elevacao at. baixa text. arg. cont. savana/fl. aberta rel. pl.
sol	39	23	47	PVa11	PORTO-VELHO PODZOLICO VERMELHO AMARELO ALICO plintico at. baixa text. arg. cont. savana/fl. aberta e Podzolico Vermelho Amarelo Alico at. baixa text. arg. fl. aberta rel. pl.
sol	40	43	12	PVa12	PORTO-VELHO PODZOLICO VERMELHO AMARELO ALICO plintico at. baixa text. arg. cont. savana/fl. aberta rel. pl. e s. ond. e Podzolico Vermelho Amarelo Alico at. baixa text. arg. fl. aberta rel. s. ond.
sol	41	31	45	PVa13	PORTO-VELHO PODZOLICO VERMELHO AMARELO ALICO at. baixa text. arg., Podzolico Vermelho Amarelo Alico cascalhento at. baixa text. arg. rel. pl. e s. ond. e Latossolo Vermelho Amarelo Alico text. arg. fl. aberta rel. pl.
sol	42	24	52	PVa14	PORTO-VELHO PODZOLICO VERMELHO AMARELO ALICO at. baixa text. arg., Podzolico Vermelho Amarelo Alico cascalhento at. baixa text. indisc. e Podzolico Vermelho Amarelo Eutrofico at. baixa text. arg. fl. aberta rel. pl. e s. ond.
sol	43	53	23	PVa15	PORTO-VELHO PODZOLICO VERMELHO AMARELO ALICO concrecionario at. baixa text. arg., Podzolico Vermelho Amarelo Alico at. baixa text. arg. rel. ond. e s. ond. e Solos Concrecionarios Lateriticos Indiscriminados Alicos at. baixa text. arg. fl. aberta rel. ond.
sol	44	21	58	PVa16	PORTO-VELHO PODZOLICO VERMELHO AMARELO ALICO concrecionario at. baixa text. med., Areias Quartzosas Alicas e Cambissolo Tropical Eutrofico at. alta text. arg. cont. savana/fl. aberta rel. pl.
sol	45	-999	-999	HLa	PORTO-VELHO LATERITA HIDROMORFICA ALICA at. baixa text. arg. e Podzolico Vermelho Amarelo Alico plintico at. baixa text. arg. fl. aberta aluvial rel. pl.
sol	46	25	30	HLra1	PORTO-VELHO LATERITA HIDROMORFICA ALICA DE ELEVACAO at. baixa text. arg. e Podzolico Vermelho Amarelo Alico plintico at. baixa text. arg. savana rel. pl.
sol	47	29	34	HLra2	PORTO-VELHO LATERITA HIDROMORFICA ALICA DE ELEVACAO at. baixa text. arg. e Podzolico Vermelho Amarelo Alico plintico at. baixa text. arg. cont. savana/fl. aberta rel. pl.
sol	48	8	81	HLra3	PORTO-VELHO LATERITA HIDROMORFICA ALICA DE ELEVACAO abruptica at. alta text. med. e Podzolico Vermelho Amarelo Alico plintico at. baixa text. arg. cont. savana/fl. aberta rel. pl.
sol	49	9	76	HLra4	PORTO-VELHO LATERITA HIDROMORFICA ALICA DE ELEVACAO abruptica at. alta text. med. e Areias

					Quartzosas Hidromorficas Alicas savana rel. pl.
sol	50	10	82 HP1	PORTO-VELHO PODZOL HODROMORFICO e Areias Quartzosas Alicas cont. savana/fl. aberta e fl. aberta rel. pl.	
sol	51	1	95 HP2	PORTO-VELHO PODZOL HODROMORFICO e Areias Quartzosas Alicas cont. formacoes pioneiras/fl. aberta rel. pl.	
sol	52	3	84 HP3	PORTO-VELHO PODZOL HODROMORFICO e Areias Quartzosas Alicas e Solos Litolicos Alicos at. baixa text. aren. savana e cont. savana/fl. aberta rel. pl.	
sol	53	47	16 Cte1	PORTO-VELHO CAMBISSOLO TROPICAL EUTROFICO at. alta text. m. arg. cont. savana/fl. aberta rel. pl.	
sol	54	-999	-999 Cte2	PORTO-VELHO CAMBISSOLO TROPICAL EUTROFICO at. alta text. m. arg. e Areias Quartzosas Alicas savana rel. pl.	
sol	55	-999	-999 Cte3	PORTO-VELHO CAMBISSOLO TROPICAL EUTROFICO at. alta text. m. arg. e Podzolico Vermelho Amarelo Distrofico at. baixa text. arg. fl. aberta rel. pl. e s. ond.	
sol	56	-999	-999 Cte4	PORTO-VELHO CAMBISSOLO TROPICAL EUTROFICO at. alta text. m. arg. rel. s. ond. e ond. e Areias Quartzosas Alicas cont. savana/fl. aberta rel. s. ond.	
sol	57	11	69 Cte5	PORTO-VELHO CAMBISSOLO TROPICAL EUTROFICO at. alta text. m. arg., Areias Quartzosas Alicas cont. savana/fl. aberta e Podzolico Vermelho Amarelo Alico at. baixa text. med. fl. aberta rel. pl.	
sol	58	42	30 Cta	PORTO-VELHO CAMBISSOLO TROPICAL ALICO at. baixa text. arg. fl. densa e fl. aberta e Solos Litolicos at. baixa text. arg. fl. densa rel. f. ond. e mont.	
sol	59	25	64 HGPa1	PORTO-VELHO GLEY POUCO HUMICO ALICO at. baixa text. arg. e Solos Aluviais Distroficos at. baixa text. indisc. fl. aberta aluvial rel. pl.	
sol	60	-999	-999 HGPa2	PORTO-VELHO GLEY POUCO HUMICO ALICO at. baixa text. arg., Solos Aluviais Distroficos at. baixa text. indisc. e Laterita Hidromorfica Alica at. baixa text. arg. fl. densa aluvial rel. pl.	
sol	61	7	90 AQa1	PORTO-VELHO AREIAS QUARTZOSAS ALICAS cont. savana/fl. rel. pl. e s. ond.	
sol	62	-999	-999 AQa2	PORTO-VELHO AREIAS QUARTZOSAS ALICAS e Areias Quartzosas Hidromorficas Alicas savana rel. pl.	
sol	63	8	82 AQa3	PORTO-VELHO AREIAS QUARTZOSAS ALICAS, Solos Litolicos Alicos at. baixa text. aren. cont. savana/fl. aberta e Afloramentos Rochosos rel. pl. e s. ond.	
sol	64	8	78 HAQa1	PORTO-VELHO AREIAS QUARTZOSAS HIDROMORFICAS ALICAS e Podzol Hidromorfico savana rel. pl.	
sol	65	19	71 HAQa2	PORTO-VELHO AREIAS QUARTZOSAS HIDROMORFICAS ALICAS e Podzolico Vermelho Amarelo Alico at. baixa text. med. formacoes pioneiras e fl. aberta rel. pl.	
sol	66	33	37 Ad	PORTO-VELHO SOLOS ALUVIAIS DISTROFICOS at. baixa text. indisc. e Solos Hidromorficos Gleyzados Eutroficos e Distroficos at. baixa text. indisc. fl. densa aluvial rel. pl.	
sol	67	37	37 Re	PORTO-VELHO SOLOS LITOLICOS EUTROFICOS at. baixa text. arg. rel. f. ond. e mont., Podzolico Vermelho Amarelo Eutrofico raso at. baixa text. arg. fl. densa rel. f. ond. e Afloramentos Rochosos rel. f. ond. e mont.	
sol	68	-999	-999 Rd1	PORTO-VELHO SOLOS LITOLICOS DISTROFICOS at. baixa text. aren. cont. savana/fl. aberta e Afloramentos	

Rochosos rel. s. ond. e ond.

sol	69	28	37	Rd2	PORTO-VELHO SOLOS LITOLICOS DISTROFICOS at. baixa text. med. rel. ond. e f. ond., Podzolico Vermelho Amarelo Alico at. baixa text. med. fl. densa e fl. aberta rel. ond. e Afloramentos Rochosos rel. f. ond. e mont.
sol	70	32	41	Rd3	PORTO-VELHO SOLOS LITOLICOS DISTROFICOS at. baixa text. indisc., Podzolico Vermelho Amarelo Alico raso at. baixa text. arg. fl. densa e Afloramentos Rochosos rel. f. ond. e mont.
sol	71	8	69	AR1	PORTO-VELHO AFLORAMENTOS ROCHOSOS e Solos Litolicos Distroficos at. baixa text. aren. savana rel. pl. e s. ond.
sol	72	-999	-999	AR2	PORTO-VELHO AFLORAMENTOS ROCHOSOS rel. f. ond. e mont. e Solos Litolicos Distroficos at. baixa text. indisc. savana rel. f. ond.
sol	73	22	59	LAa1	GUAPORE LATOSSOLO AMARELO ALICO text. med. e Latossolo Amarelo alico text. arg. fl. rel. pl.
sol	74	24	58	LAa2	GUAPORE LATOSSOLO AMARELO ALICO text. med. rel. pl. e Latossolo Amarelo distrofico text. med. fl. rel. s. ond.
sol	75	28	52	LAa3	GUAPORE LATOSSOLO AMARELO ALICO text. med. e Laterita Hidromorfica alica at. baixa e text. arg. e med. fl. rel. pl.
sol	76	-999	-999	LAa4	GUAPORE LATOSSOLO AMARELO ALICO text. med. e Areias Quartzosas alicas fl. rel. pl.
sol	77	30	61	LAa5	GUAPORE LATOSSOLO AMARELO ALICO text. med. rel. s. ond., Laterita Hidromorfica alica at. baixa text. med. fl. e Areias Quartzosas Hidromorficas alicas form. pion. rel. pl.
sol	78	-999	-999	LVa	GUAPORE LATOSSOLO VERMELHO AMARELO ALICO text. arg., Latossolo Vermelho Amarelo Alico text. m. arg. rel. pl. e s. ond. e Podzolico Vermelho Amarelo Alico at. baixa text. arg. fl. rel. s. ond.
sol	79	0	0	LEd1	GUAPORE LATOSSOLO VERMELHO-SCURO DISTROFICO text. m. arg. sav. rel. pl.
sol	80	0	0	LEd2	GUAPORE LATOSSOLO VERMELHO-SCURO DISTROFICO text. med. rel. pl., Latossolo Vermelho Amarelo Alico text. arg. rel. s. ond. e Latossolo Vermelho-Escuro distrofico text. arg. sav. rel. pl.
sol	81	28	30	BV1	GUAPORE BRUNIZEM AVERMELHADO text. arg. e Brunizem Avermelhado text. med. fl. rel. ond.
sol	82	21	54	BV2	GUAPORE BRUNIZEM AVERMELHADO text. arg. e med. rel. ond. e f. ond., Terra Roxa Estruturada eutrofica text. arg. e Podzolico Vermelho-Amarelo Eutrofico cascalhento at. baixa text. med. fl. rel. ond.
sol	83	35	39	TRe	GUAPORE TERRA ROXA ESTRUTURADA EUTROFICA text. arg., Brunizem Avermelhado text. arg. rel. ond. e Podzolico Vermelho-Amarelo Eutrofico at. baixa text. arg. fl. rel. s. ond.
sol	84	17	50	PE1	GUAPORE PODZOLICO VERMELHO-AMARELO EUTROFICO at. alta text. med. rel. s. ond. e Brunizem Avermelhado text. arg. fl. rel. ond.
sol	85	12	79	PE2	GUAPORE PODZOLICO VERMELHO-AMARELO EUTROFICO at. baixa text. med. rel. s. ond. e Areias Quartzosas distroficas fl. rel. pl.
sol	86	30	59	PE3	GUAPORE PODZOLICO VERMELHO-AMARELO EUTROFICO at. baixa text. arg. e Podzolico Vermelho-Amarelo distrofico at. baixa text. arg. fl. rel. s. ond.
sol	87	29	42	PE4	GUAPORE PODZOLICO VERMELHO-AMARELO EUTROFICO at.



					baixa text. arg. e Podzolico Vermelho-Amarelo distrofico at. baixa text. arg. e Terra Roxa Estruturada eutrofica text. arg. fl. rel. pl. e s. ond.
sol	88	38	35	PE5	GUAPORE PODZOLICO VERMELHO-AMARELO EUTROFICO at. baixa text. arg. rel. s. ond., Terra Roxa Estruturada eutrofica text. arg. e Podzolico Vermelho-Amarelo Eutrofico at. baixa text. med. fl. rel. ond.
sol	89	-999	-999	PE6	GUAPORE PODZOLICO VERMELHO-AMARELO EUTROFICO at. baixa text. arg., Podzolico Vermelho-Amarelo Distrofico at. baixa text. arg. e Latossolo Vermelho-Escuro distrofico text. arg. fl. rel. s. ond.
sol	90	44	25	PE7	GUAPORE PODZOLICO VERMELHO-AMARELO EUTROFICO at. baixa text. arg., Terra Roxa Estruturada eutrofica text. m. arg. rel. ond. e Solos Litolicos eutroficos at. baixa text. arg. fl. rel. f. ond.
sol	91	43	40	PVd1	GUAPORE PODZOLICO VERMELHO-AMARELO DISTROFICO at. baixa text. arg. e Podzolico Vermelho-Amarelo Eutrofico at. baixa text. arg. fl. rel. s. ond.
sol	92	21	59	PVd2	GUAPORE PODZOLICO VERMELHO-AMARELO DISTROFICO at. baixa text. arg. e Latossolo Vermelho-Amarelo alico text. arg. fl. rel. s. ond.
sol	93	5	91	PVd3	GUAPORE PODZOLICO VERMELHO-AMARELO DISTROFICO at. baixa text. med. fl. rel. s. ond. a ond. e Areias Quartzosas distroficas sav. rel. s. ond.
sol	94	30	36	PVd4	GUAPORE PODZOLICO VERMELHO-AMARELO DISTROFICO at. baixa text. med. fl. e Cambissolo Tropical distrofico at. alta text. med. sav. rel. ond.
sol	95	-999	-999	PVd5	GUAPORE PODZOLICO VERMELHO-AMARELO DISTROFICO at. baixa text. med. rel. s. ond. e Laterita Hidromorfica alica at. baixa text. med. fl. rel. pl.
sol	96	-999	-999	PVd6	GUAPORE PODZOLICO VERMELHO-AMARELO DISTROFICO at. baixa text. arg. fl. Latossolo Vermelho-Escuro distrofico text. arg. sav. e Podzolico Vermelho-Amarelo distrofico at. baixa text. med. fl. rel. s. ond.
sol	97	-999	-999	PVd7	GUAPORE PODZOLICO VERMELHO-AMARELO DISTROFICO at. baixa text. med., Podzolico Vermelho-Amarelo Eutrofico at. baixa text. arg. rel. s. ond. e Podzolico Vermelho-Amarelo alico plintico at. baixa text. arg. fl. rel. pl.
sol	98	56	25	PVd8	GUAPORE PODZOLICO VERMELHO-AMARELO DISTROFICO at. baixa text. med. fl., Areias Quartzosas distroficas sav. e Podzolico Vermelho-Amarelo Eutrofico at. baixa text. arg. fl. rel. s. ond.
sol	99	-999	-999	PVd9	GUAPORE PODZOLICO VERMELHO-AMARELO DISTROFICO at. baixa text. med. rel. ond., Solos Litolicos distroficos concrecionarios at. baixa text. med. fl. rel. f. ond. e Areias Quartzosas distroficas sav. rel. s. ond.
sol	100	56	8	HLa1	GUAPORE LATERITA HIDROMORFICA ALICA at. baixa text. arg. e med. fl. e Planossolo alico at. baixa text. arg. e med. form. pion. rel. pl.
sol	101	24	39	HLa2	GUAPORE LATERITA HIDROMORFICA ALICA at. baixa text. med. e Areias Quartzosas Hidromorficas alicas form. pion. rel. pl.
sol	102	-999	-999	HLa3	GUAPORE LATERITA HIDROMORFICA ALICA at. baixa text. arg. e med. form. pion., Planossolo alico at. baixa text. arg. sav. e Gley Pouco Humico alico at. baixa text. indisc. form. pion. rel. pl.
sol	103	-999	-999	HLa4	GUAPORE LATERITA HIDROMORFICA ALICA at. baixa text. arg. e med., Planossolo alico at. baixa text. media e arg. e Areias Quartzosas

Hidromorficas distroficas sav. rel. pl.

sol	104	35	48	HLa5	GUAPORE LATERITA HIDROMORFICA ALICA at. baixa text. arg. e med., Areias Quartzosas Hidromorficas alicas e Gley Pouco Humico alico at. baixa text. indisc. sav. rel. pl.
sol	105	-999	-999	HLa6	GUAPORE LATERITA HIDROMORFICA ALICA at. baixa text. med. cont. sav./ fl., Areias Quartzosas Hidromorficas alicas sav. rel. pl. e Podzolico Vermelho-Amarelo distrofico at. baixa text. med. cont. sav./fl. rel. s. ond.
sol	106	36	19	Ctd1	GUAPORE CAMBISSOLO TROPICAL DISTROFICO at. alta text. arg., Solos Litolicos distroficos at. alta text. med. rel. s. ond. e Areias Quartzosas distroficas sav. rel. pl.
sol	107	21	47	Ctd2	GUAPORE CAMBISSOLO TROPICAL DISTROFICO at. alta text. med. sav. rel. s. ond., Solos Litolicos eutroficos at. alta text. med. cont. sav./fl. e Afloramentos Rochosos rel. ond.
sol	108	-999	-999	HGPd	GUAPORE GLEY POUCO HUMICO DISTROFICO at. baixa text. indisc. e Solos Aluviais distroficos at. baixa text. indisc. fl. rel. pl.
sol	109	-999	-999	HGPa1	GUAPORE GLEY POUCO HUMICO ALICO at. baixa text. arg. e Solos Aluviais distroficos at. baixa text. indisc. fl. rel. pl.
sol	110	-999	-999	HGPa2	GUAPORE GLEY POUCO HUMICO ALICO at. baixa text. indisc. e Areias Quartzosas Hidromorficas alicas fl. rel. pl.
sol	111	-999	-999	HGPa3	GUAPORE GLEY POUCO HUMICO ALICO at. baixa text. indisc. fl. e Planossolo alico at. baixa text. arg. sav. rel. pl.
sol	112	21	65	HGPa4	GUAPORE GLEY POUCO HUMICO ALICO at. baixa text. indisc., Solos Aluviais distroficos at. baixa text. indisc. fl. e Areias Quartzosas Hidromorficas distroficas form. pion. rel. pl.
sol	113	-999	-999	AQd1	GUAPORE AREIAS QUARTZOSAS DISTROFICAS fl. rel. pl.
sol	114	9	81	AQd2	GUAPORE AREIAS QUARTZOSAS DISTROFICAS fl. rel. pl. e s. ond.
sol	115	9	74	AQd3	GUAPORE AREIAS QUARTZOSAS DISTROFICAS fl. rel. pl. e Cambissolo Tropical distrofico at. baixa text. med. cont. sav./ fl. rel. ond.
sol	116	-999	-999	AQd4	GUAPORE AREIAS QUARTZOSAS DISTROFICAS rel. pl. e Latossolo Vermelho-Escuro distrofico text. med. fl. rel. s. ond. e ond.
sol	117	-999	-999	AQd5	GUAPORE AREIAS QUARTZOSAS DISTROFICAS e Solos Litolicos distroficos at. baixa text. med. sav. rel. s. ond.
sol	118	-999	-999	AQd6	GUAPORE AREIAS QUARTZOSAS DISTROFICAS sav. rel. pl., Latossolo Vermelho-Amarelo distrofico text. med. fl. e Latossolo Vermelho-Amarelo distrofico concrecionario text. med. cont. sav./fl. rel. s. ond.
sol	119	-999	-999	AQd7	GUAPORE AREIAS QUARTZOSAS DISTROFICAS, Solos Litolicos distroficos concrecionarios at. baixa text. med. sav. e Latossolo Vermelho-Amarelo distrofico concrecionario text. med. fl. rel. s. ond.
sol	120	-999	-999	AQd8	GUAPORE AREIAS QUARTZOSAS DISTROFICAS rel. s. ond., Solos Litolicos distroficos concrecionarios at. baixa text. media sav. rel. ond. e Afloramentos Rochosos rel. f. ond.
sol	121	-999	-999	AQa1	GUAPORE AREIAS QUARTZOSAS ALICAS sav. rel. pl.
sol	122	6	90	AQa2	GUAPORE AREIAS QUARTZOSAS ALICAS cont. sav./fl. rel. pl. e s. ond.
sol	123	0	96	AQa3	GUAPORE AREIAS QUARTZOSAS ALICAS fl. e Areias

					Quartzosas Hidromorficas alicas form. pion. rel. pl.
sol	124	19	20	Ad	GUAPORE SOLOS ALUVIAIS DISTROFICOS at. baixa text. indisc., Solos Hidromorficos Gleyzados eutroficicos at. baixa text. indisc. e Solos Hidromorficos Gleyzados distroficicos at. baixa text. indisc. fl. rel. pl.
sol	125	4	78	Re	GUAPORE SOLOS LITOLICOS EUTROFICOS at. baixa text. indisc. rel. f. ond. e mont., Podzolico Vermelho-Amarelo Eutrofico raso at. baixa text. arg. fl. rel. f. ond. e Afloramentos Rochosos rel. f. ond. e mont.
sol	126	-999	-999	Rd1	GUAPORE SOLOS LITOLICOS DISTROFICOS at. baixa text. aren. cont. fl./sav. e Afloramentos Rochosos rel. s. ond. e ond.
sol	127	-999	-999	Rd2	GUAPORE SOLOS LITOLICOS DISTROFICOS concrecionarios at. baixa text. media rel. ond. e f. ond. e Areias Quartzosas distroficicas fl. rel. s. ond.
sol	128	-999	-999	Rd3	GUAPORE SOLOS LITOLICOS DISTROFICOS concrecionarios at. baixa text. med. fl. rel. f. ond., Cambissolo Tropical alico at. baixa text. med. sav. rel. ond. e Areias Quartzosas distroficicas fl. rel. s. ond.
sol	129	-999	-999	Rd4	GUAPORE SOLOS LITOLICOS DISTROFICOS at. baixa text. media rel. s. ond., Areias Quartzosas alicas sav. rel. pl. e Afloramentos Rochosos rel. s. ond.
sol	130	28	45	Rd5	GUAPORE SOLOS LITOLICOS DISTROFICOS at. baixa text. indisc., Podzolico Vermelho-Amarelo Alico raso at. baixa text. arg. fl. e Afloramentos Rochosos rel. f. ond. e mont.
sol	131	14	57	Ra	GUAPORE SOLOS LITOLICOS ALICOS at. baixa text. indisc., Podzolico Vermelho-Amarelo Eutrofico raso at. baixa text. media fl. e Afloramentos Rochosos rel. f. ond. e mont.
sol	132	-999	-999	AR	GUAPORE AFLORAMENTOS ROCHOSOS rel. f. ond. e mont., Solos Litolicos alicos at. baixa text. med. e Cambissolo Tropical alico at. baixa text. med. sav. rel. ond.

VEGETATION CATEGORIES

COVER	CAT	HVEG	ABREV	DESCRIPTION
veg	1	13	Sad	PORTO-VELHO REGIAOES FITOECOLOGICAS; SAVANA, Arborea densa Relevo Residual do Sul da Amazonia
veg	2	13	Sad	PORTO-VELHO REGIAOES FITOECOLOGICAS; SAVANA, Arborea densa Superficie Pediplanada
veg	3	12	Sd	GUAPORE REGIAOES FITOECOLOGICAS; SAVANA, Arborea densa
veg	4	3	Saa	PORTO-VELHO REGIAOES FITOECOLOGICAS; SAVANA, Arborea aberta Relevo Residual do Sul da Amazonia
veg	5	3	Saa	PORTO-VELHO REGIAOES FITOECOLOGICAS; SAVANA, Arborea aberta Superficie Pediplanada
veg	6	3	Sas	GUAPORE REGIAOES FITOECOLOGICAS; SAVANA, Arborea aberta sem floresta de galeria
veg	7	3.5	Saf	GUAPORE REGIAOES FITOECOLOGICAS; SAVANA, Arborea aberta com floresta de galeria
veg	8	1.5	Sp	PORTO-VELHO REGIAOES FITOECOLOGICAS; SAVANA, Parque Relevo Residual do Sul da Amazonia
veg	9	1.5	Sp	PORTO-VELHO REGIAOES FITOECOLOGICAS; SAVANA, Parque

Superfície Pediplanada

veg	10	1.5 Sps	GUAPORE REGIAOES FITOECOLOGICAS; SAVANA, Parque sem floresta de galeria
veg	11	2 Spf	GUAPORE REGIAOES FITOECOLOGICAS; SAVANA, Parque com floresta de galeria
veg	12	.5 Sg	PORTO-VELHO REGIAOES FITOECOLOGICAS; SAVANA, Gramineo-lenhosa Relevo Residual do Sul da Amazonia
veg	13	.5 Sg	PORTO-VELHO REGIAOES FITOECOLOGICAS; SAVANA, Gramineo-lenhosa Superfície Pediplanada
veg	14	.3 Sgs	GUAPORE REGIAOES FITOECOLOGICAS; SAVANA, Gramineo-lenhosa sem floresta de galeria
veg	15	.5 Sgf	GUAPORE REGIAOES FITOECOLOGICAS; SAVANA, Gramineo-lenhosa com floresta de galeria
veg	20	20 Pap	PORTO-VELHO REGIAOES FITOECOLOGICAS; FORMACOES PIONEIRAS, Arborea, areas periodicamente inundadas Areas de Acumulacao inundaveis
veg	21	20 Pfb	GUAPORE REGIAOES FITOECOLOGICAS; FORMACOES PIONEIRAS, Influencia Fluvial buritizal
veg	22	30 Pau	PORTO-VELHO REGIAOES FITOECOLOGICAS; FORMACOES PIONEIRAS, Arbustiva, depressoes periodicamente inundadas Areas de Acumulacao inundaveis
veg	23	30 Pau	PORTO-VELHO REGIAOES FITOECOLOGICAS; FORMACOES PIONEIRAS, Arbustiva, depressoes periodicamente inundadas Depressoes nos interfluvios Tabulares do Terciario
veg	24	30 Pfs	GUAPORE REGIAOES FITOECOLOGICAS; FORMACOES PIONEIRAS, Influencia Fluvial arbustiva, sem palmeiras
veg	25	1.6 Pag	PORTO-VELHO REGIAOES FITOECOLOGICAS; FORMACOES PIONEIRAS, Graminosa, areas periodicamente inundadas Areas de Acumulacao inundaveis
veg	26	1.6 Pag	PORTO-VELHO REGIAOES FITOECOLOGICAS; FORMACOES PIONEIRAS, Graminosa, areas periodicamente inundadas Depressoes nos interfluvios Tabulares do Terciario
veg	27	1.6 Pfh	GUAPORE REGIAOES FITOECOLOGICAS; FORMACOES PIONEIRAS, Influencia Fluvial graminoide
veg	30	25 Fdp	PORTO-VELHO REGIAOES FITOECOLOGICAS; FLORESTA TROPICAL Densa, Aluvial, planicie periodicamente inundada Sub-regiao Aluvial da Amazonia
veg	31	25 Fdc	PORTO-VELHO REGIAOES FITOECOLOGICAS; FLORESTA TROPICAL Densa, Aluvial, terracos Sub-regiao Aluvial da Amazonia
veg	32	35 Fdb	PORTO-VELHO REGIAOES FITOECOLOGICAS; FLORESTA TROPICAL Densa, Terras baixas, plato Sub-regiao dos Baixos Platos da Amazonia
veg	33	35 Fda	PORTO-VELHO REGIAOES FITOECOLOGICAS; FLORESTA TROPICAL Densa, Terras baixas, relevo dissecado Sub-regiao dos Baixos Platos da Amazonia
veg	34	35 Fdo	PORTO-VELHO REGIAOES FITOECOLOGICAS; FLORESTA TROPICAL Densa, Terras baixas, relevo ondulado Sub-regiao dos Baixos Platos da Amazonia
veg	35	30 Fdn	PORTO-VELHO REGIAOES FITOECOLOGICAS; FLORESTA TROPICAL Densa, Submontana, relevo dissecado Altos Xingu/ Tapajos/ Madeira
veg	36	30 Fds	PORTO-VELHO REGIAOES FITOECOLOGICAS; FLORESTA TROPICAL Densa, Submontana, relevo ondulado Altos Xingu/ Tapajos/ Madeira
veg	37	30 Fdt	PORTO-VELHO REGIAOES FITOECOLOGICAS; FLORESTA

			TROPICAL Densa,Submontana,baixas cadeias de montanhasSul da Amazonia
veg	38	30 Fdr	PORTO-VELHO REGIAOES FITOECOLOGICAS;FLORESTA TROPICAL Densa,Submontana platoCobertura de Plataforma Pre-Cambriana
veg	39	30 Fdu	PORTO-VELHO REGIAOES FITOECOLOGICAS;FLORESTA TROPICAL Densa,Submontana relevo dissecadoCobertura de Plataforma Pre-Cambriana
veg	40	30 Fdi	PORTO-VELHO REGIAOES FITOECOLOGICAS;FLORESTA TROPICAL Densa,Submontana relevo onduladoCobertura de Plataforma Pre-Cambriana
veg	41	25 Dae	GUAPORE REGIAOES FITOECOLOGICAS;FLORESTA TROPICAL Ombrofila Densa ,Aluvial,dossel emergente
veg	42	30 Dse	GUAPORE REGIAOES FITOECOLOGICAS;FLORESTA TROPICAL Ombrofila Densa ,Submontana,dossel emergente
veg	43	22 Fap	PORTO-VELHO REGIAOES FITOECOLOGICAS;FLORESTA TROPICAL Aberta,Aluvial,planicie periodicamente inundadaSub-regiao Aluvial da Amazonia
veg	44	22 Fac	PORTO-VELHO REGIAOES FITOECOLOGICAS;FLORESTA TROPICAL Aberta,Aluvial,terracosSub-regiao Aluvial da Amazonia
veg	45	22 Fal	PORTO-VELHO REGIAOES FITOECOLOGICAS;FLORESTA TROPICAL Aberta,Aluvial,superficie aplainadaSuperficie Aplainada de Acumulacao
veg	46	30 Fab	PORTO-VELHO REGIAOES FITOECOLOGICAS;FLORESTA TROPICAL Aberta,Terras baixas,platoSub-regiao dos Baixos Platos da Amazonia
veg	47	30 Faa	PORTO-VELHO REGIAOES FITOECOLOGICAS;FLORESTA TROPICAL Aberta,Terras baixas,relevo dissecadoSub-regiao dos Baixos Platos da Amazonia
veg	48	30 Fao	PORTO-VELHO REGIAOES FITOECOLOGICAS;FLORESTA TROPICAL Aberta,Terras baixas,relevo onduladoSub-regiao dos Baixos Platos da Amazonia
veg	49	25 Fan	PORTO-VELHO REGIAOES FITOECOLOGICAS;FLORESTA TROPICAL Aberta,Submontana,relevo dissecadoAltos Xingu/Tapajos/Madeira
veg	50	25 Fas	PORTO-VELHO REGIAOES FITOECOLOGICAS;FLORESTA TROPICAL Aberta,Submontana,relevo onduladoAltos Xingu/Tapajos/Madeira
veg	51	25 Far	PORTO-VELHO REGIAOES FITOECOLOGICAS;FLORESTA TROPICAL Aberta,Submontana platoCobertura de Plataforma Pre-Cambriana
veg	52	25 Fau	PORTO-VELHO REGIAOES FITOECOLOGICAS;FLORESTA TROPICAL Aberta,Submontana relevo dissecadoCobertura de Plataforma Pre-Cambriana
veg	53	25 Fai	PORTO-VELHO REGIAOES FITOECOLOGICAS;FLORESTA TROPICAL Aberta,Submontana relevo onduladoCobertura de Plataforma Pre-Cambriana
veg	54	32 Abc	GUAPORE REGIAOES FITOECOLOGICAS;FLORESTA TROPICAL Ombrofila Aberta ,Terras Baixas com cipos
veg	55	25 Abp	GUAPORE REGIAOES FITOECOLOGICAS;FLORESTA TROPICAL Ombrofila Aberta ,Terras Baixas com palmeiras
veg	56	22 Asc	GUAPORE REGIAOES FITOECOLOGICAS;FLORESTA TROPICAL Ombrofila Aberta ,Submontana com cipos
veg	57	22 Asp	GUAPORE REGIAOES FITOECOLOGICAS;FLORESTA TROPICAL Ombrofila Aberta ,Submontana com palmeiras
veg	58	18 Fae	GUAPORE REGIAOES FITOECOLOGICAS;FLORESTA TROPICAL estacional Semidecidual ,Aluvial dossel emergente
veg	59	23 Fbe	GUAPORE REGIAOES FITOECOLOGICAS;FLORESTA TROPICAL estacional Semidecidual ,Terras Baixas dossel

## emergente

veg	60	25 Fae	GUAPORE REGIAOES FITOECOLOGICAS;FLORESTA TROPICAL estacional Semidecidual ,Submontana dossel emergente
veg	61	20 Sad	PORTO-VELHO AREAS DE TENSAO ECOLOGICA Contato Savana/Floresta,Savana Arbores densa
veg	62	18 Sd2	GUAPORE AREAS DE TENSAO ECOLOGICA Contato Savana/Floresta Estacional,Savana, Arborea densa
veg	63	15 Saa	PORTO-VELHO AREAS DE TENSAO ECOLOGICA Contato Savana/Floresta,Savana Arbores aberta
veg	64	13 Sas2	GUAPORE AREAS DE TENSAO ECOLOGICA Contato Savana/Floresta Estacional,Savana, Arborea Aberta sem floresta de galeria
veg	65	15 Saf2	GUAPORE AREAS DE TENSAO ECOLOGICA Contato Savana/Floresta Estacional,Savana, Arborea Aberta com floresta de galeria
veg	66	8 Sp	PORTO-VELHO AREAS DE TENSAO ECOLOGICA Contato Savana/Floresta,Savana Parque
veg	67	8 STE3	GUAPORE AREAS DE TENSAO ECOLOGICA Contato Savana/Savana Estepica,Ecotomo
veg	68	23 FSm	PORTO-VELHO AREAS DE TENSAO ECOLOGICA Contato Savana/Floresta,Ecotomo
veg	69	23 SNe2	GUAPORE AREAS DE TENSAO ECOLOGICA Contato Savana/Floresta Estacional,Ecotomo
veg	70	23 Fbe2	GUAPORE AREAS DE TENSAO ECOLOGICA Contato Savana/Floresta Estacional,Floresta SemidecidualTerras Baixas dossel emergente
veg	71	23 Fse2	GUAPORE AREAS DE TENSAO ECOLOGICA Contato Savana/Floresta Estacional,Floresta SemidecidualSubmontana dossel emergente
veg	72	23 SOe1	GUAPORE AREAS DE TENSAO ECOLOGICA Contato Savana/Floresta Ombrofila, Ecotomo
veg	73	23 Abc1	GUAPORE AREAS DE TENSAO ECOLOGICA Contato Savana/Floresta Ombrofila, Floresta abertaTerras Baixas com cipos
veg	74	20 Asc1	GUAPORE AREAS DE TENSAO ECOLOGICA Contato Savana/Floresta Ombrofila, Floresta abertaSubmontana com cipos
veg	75	20 Fac	PORTO-VELHO AREAS DE TENSAO ECOLOGICA Contato Savana/Floresta,Floresta Tropical Aberta,Aluvial,terracosSub-regiao Aluvial da Amazonia
veg	76	25 Fab	PORTO-VELHO AREAS DE TENSAO ECOLOGICA Contato Savana/Floresta,Floresta Tropical Aberta,Terras baixas,platoSub-regiao dos Baixos Platos da Amazonia
veg	77	25 Fao	PORTO-VELHO AREAS DE TENSAO ECOLOGICA Contato Savana/Floresta,Floresta Tropical Aberta,Terras baixas,relevo onduladoSub-regiao dos Baixos Platos da Amazonia
veg	78	22 Fan	PORTO-VELHO AREAS DE TENSAO ECOLOGICA Contato Savana/Floresta,Floresta Tropical Aberta,Submontana,relevo dissecadoAltos Xingu/Tapajos/Madeira
veg	79	22 Fas	PORTO-VELHO AREAS DE TENSAO ECOLOGICA Contato Savana/Floresta,Floresta Tropical Aberta,Submontana,relevo onduladoAltos Xingu/Tapajos/Madeira
veg	80	22 Far	PORTO-VELHO AREAS DE TENSAO ECOLOGICA Contato Savana/Floresta,Floresta Tropical Aberta,Submontana platoCobertura de Plataforma

Pre-Cambriana			
veg	81	22 Fau	PORTO-VELHO AREAS DE TENSÃO ECOLÓGICA Contato Savana/Floresta, Floresta Tropical Aberta, Submontana relevo dissecado Cobertura de Plataforma Pre-Cambriana
veg	82	22 Fai	PORTO-VELHO AREAS DE TENSÃO ECOLÓGICA Contato Savana/Floresta, Floresta Tropical Aberta, Submontana relevo ondulado Cobertura de Plataforma Pre-Cambriana
veg	83	25 Fdr	PORTO-VELHO AREAS DE TENSÃO ECOLÓGICA Contato Savana/Floresta, Floresta densa, Submontana plato
veg	84	25 Fdu	PORTO-VELHO AREAS DE TENSÃO ECOLÓGICA Contato Savana/Floresta, Floresta densa, Submontana relevo dissecado
veg	85	25 Fdi	PORTO-VELHO AREAS DE TENSÃO ECOLÓGICA Contato Savana/Floresta, Floresta densa, Submontana relevo ondulado
veg	86	20 Cbe4	GUAPORE AREAS DE TENSÃO ECOLÓGICA Contato Savana Estepica/Floresta Estacional, Floresta Decidual Terras Baixas dossel emergente
veg	87	24 Fbe5	GUAPORE AREAS DE TENSÃO ECOLÓGICA Contato Floresta Ombrofila/Floresta Estacional, Floresta Semidecidual Terras Baixas dossel emergente
veg	88	27 Fse5	GUAPORE AREAS DE TENSÃO ECOLÓGICA Contato Floresta Ombrofila/Floresta Estacional, Floresta Semidecidual Submontana dossel emergente
veg	89	25 ONe5	GUAPORE AREAS DE TENSÃO ECOLÓGICA Contato Floresta Ombrofila/Floresta Estacional, Ecotomo
veg	90	20 Pap	PORTO-VELHO AREAS DE TENSÃO ECOLÓGICA Contato Formacoes Edaficas/Floresta, Arborea areas periodicamente inundadas
veg	91	25 Fdp	PORTO-VELHO AREAS DE TENSÃO ECOLÓGICA Contato Formacoes Edaficas/Floresta, Floresta Tropical Densa Aluvial planicie, Sub-regiao Aluvial da Amazonia
veg	92	25 Fdc	PORTO-VELHO AREAS DE TENSÃO ECOLÓGICA Contato Formacoes Edaficas/Floresta, Floresta Tropical Densa Aluvial terracos, Sub-regiao Aluvial da Amazonia
veg	93	22 Fap	PORTO-VELHO AREAS DE TENSÃO ECOLÓGICA Contato Formacoes Edaficas/Floresta, Floresta Tropical Aberta Aluvial planicie, Sub-regiao Aluvial da Amazonia
veg	94	22 Fac	PORTO-VELHO AREAS DE TENSÃO ECOLÓGICA Contato Formacoes Edaficas/Floresta, Floresta Tropical Aberta Aluvial terracos
veg	95	22 Fag	PORTO-VELHO AREAS DE TENSÃO ECOLÓGICA Contato Formacoes Edaficas/Floresta, Floresta Tropical Aberta Aluvial planicie
veg	96	30 Fao	PORTO-VELHO AREAS DE TENSÃO ECOLÓGICA Contato Formacoes Edaficas/Floresta, Floresta Tropical Aberta Terras baixas, relevo ondulado
veg	100	.5 Ap	Agropecuaria

**Attachment 4 :**  
**Background note on European involvement in LBA**





## The "LBA-minisummit"

23 June 1997

Hotel 't Paviljoen  
Grebbeweg 103 - 105, Rhenen, the Netherlands  
tel. 0317 - 619003, fax 0317 - 617213

### Background note on European involvement in LBA

#### Background

Despite widespread concern and increased international efforts at conservation, the world's tropical rainforests continue to disappear at an unprecedented rate. Conversion of tropical rain forest to pasture or agricultural land therefore presents one of the most profound ecological trends in the current era. In many parts of the world, large areas of rainforest are currently in a transition phase from their natural state into intensively exploited land of considerable economic importance. Of vital importance in developing sustainable management systems for tropical rainforests is the question how the human interference affects the forest's basic capacities to renew itself, and how to safeguard the basic ecological, hydrological and climatological processes, such as water, carbon and nutrient cycling and biological and agricultural productivity.

Altered cycles of water, energy, carbon and nutrients, resulting from the changes in vegetation cover following deforestation, are expected to have climatic and environmental

consequences at local, regional and global scales. Deforestation will affect the functioning and composition of the atmosphere at geographical scales many times larger than those occupied by the tropical rainforest themselves. It will lead to a drastic impoverishment of the world's biodiversity resources, to profound changes in the global carbon balance and it may have a substantial effect on the global climate. Tropical deforestation is truly a global issue and therefore of a great concern to many nations and continents, including Europe.

To understand the consequences of tropical deforestation and to mitigate its negative effects, enhanced knowledge is needed of the functioning of both the existing natural forest systems, as well as systems which have already been converted to various other forms of land use or secondary regrowth. In the early nineties the Brazilian scientific community, in response to the world-wide concern about the fate of the world's largest remaining tropical rainforest - in Amazonia - called for a new multi-disciplinary research effort. This international

effort will be initially built around a comprehensive field experiment, to be put in place in Amazonia: the Large Scale Biosphere - Atmosphere Experiment in Amazonia (LBA).

## **LBA**

LBA is an international initiative designed to create new knowledge needed to understand climatological, ecological, biogeochemical, and hydrological functioning of Amazonia, the impact of land use change on these functions, and the interactions between Amazonia and the Earth's system. In LBA emphasis is given to observations and analyses in six general areas: Physical Climate, Carbon Storage and Exchange, Biogeochemistry and Nutrient Cycling, Atmospheric Chemistry, Land Surface Hydrology and Land Use and Land Cover Change. In an integrated, multi-disciplinary way, LBA will generate data to define the present state of the system and its response to the observed anthropogenic and climatic perturbations, complemented by modelling to provide insight into possible changes in the future. LBA has been designed to address major issues raised at the United Nations Earth Summit in Rio de Janeiro in 1992, where the attending nations and organisations agreed that a world-wide progressive destruction of the environment and the climate changes are to be encountered by combined global efforts.

LBA foresees highly integrated research and development activities to be carried out by Brazilian, other Amazonian,

European and North American groups over period of 1997 - 2003. The total budget needed for LBA-implementation is estimated at 90 million US\$. Major national and international funding programmes and agencies in three continents, South- and North America and Europe have been presented with this challenge. In the US, a budget of about 40 million US\$ has been already allocated to LBA through several NASA-programmes. In Brazil funding commitments of several agencies are under progress. In Europe, a number of initiatives started to support European contribution to the project.

## **European contribution to LBA**

European expertise and contribution to LBA is considered an important precondition to meet the overall objectives of the project by Brazil and by other non-Brazilian agencies involved.

Between 1994 and 1996, EU-Directorate General-XII (Environment and Climate) has supported a project called "Use of Integrated Modelling for LBA - Experiment Design". The project had a budget of 1,2 MECU, shared between the EU - DG-XII and the participating institutions in the Netherlands, France, Germany and the UK. The objectives of the project were two-fold: to use existing data and models to design the LBA mesoscale field experiment and to contribute to the LBA-overall preparatory activities in order to define a specific research contribution of Europe to the main phase of the project.

Independently of the activities supported by EU - DG-XII, and in response to the European Council Regulation no. 3062/95, a total Community funding of 200 million ECU has been allocated to an initiative called "Operations to promote tropical forests" over the period of four years (1996-1999). The budgets for this initiative are jointly operated by the EU through its Directorates General I-B (External Relations: Southern Mediterranean, Middle and Near East, Latin America, South and South-East Asia and North-South Cooperation), DG-XI (Environment, Nuclear Safety and Civil Protection), and DG-VIII (Bilateral and Development Cooperation Relations with Africa, the Caribbean and the Pacific; Lomé Convention). Through this initiative, the European Union became a major contributor to the G-7 "Pilot Programme to Conserve the Brazilian Rain Forest" (PPG-7). In relation to LBA, two budget lines managed by DG-I and DG-VIII are especially relevant: B7-6021 (50 MECU/year) and B7-6200 (20 MECU/year). In addition, DG-XI manages a programme of 3 MECU which may also contribute to LBA.

Based on these initiatives, the following combined funding strategy for a European contribution to LBA is under consideration:

a) Within the 1996/1997 budget lines B7-6021, B7-6000 and B7-8100 LBA will be supported through two subsequent projects of respectively 0.9 and 1.5 MECU. These projects will focus on preparatory studies and on setting up of some of the

infrastructure needed for the field measurements. The projects will involve joint European-Brazilian work, and support will be given for organisation of European LBA-workshop and for related coordination activities.

b) For the main phase of LBA (1998-2002), a substantial part of the European contribution to LBA will be associated with EU-involvement in the second phase of the PPG-7. LBA will be proposed as a bilateral EU-Brazil project, which will establish a liaison with other EU-activities in PPG-7, but will maintain its own management and budgetary structure. Total funding needed to support joint Europe-Brazil LBA-projects is up to 20 MECU for the main LBA-phase 1998-2002.

c) Directorate General XII-D (Science, Research and Development) has recently approved a LBA-related research project focusing on the role of the Amazon in the global budgets of carbon and greenhouse gases (total project budget 1.8 MECU; EU contribution 1.3 MECU).

d) Directorate General XII has also recently approved a LBA-related project in a framework of the European Network on Research on Global Change (ENRICH). The project (EU - contribution of 0.3 MECU) focuses on European-Amazonian collaboration, and on strengthening the research capacity to address regional and global implications of Amazonian deforestation and its contribution to global change.

### **Charge of the European LBA Workshop**

The LBA -Europe workshop aims at a thematic definition of the European contribution to LBA in compliance with the overall LBA planning and with the European LBA - funding prospects. The workshop follows from negotiations about the European LBA component, held at the EU-delegation in Brasilia in July 1996 and later during the annual meeting of the Pilot Programme for Preservation of Tropical Rainforest (PPG-7) in September 1996 in Bonn, Germany.

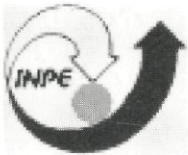
The workshop will address:

1. Key LBA issues to be addressed by each thematic European contribution;
2. Specification of the research, field, and development and dissemination activities, in support of Amazonian development policies, to be carried out in the European LBA contribution
3. Relation and tuning with other activities within the overall LBA-programme (NASA, Brazil, other Amazonian countries);
4. Relation with already funded EU-LBA activities and with other European LBA-activities (nationally supported projects);
5. Project partnership and cooperative networks (Europe-Brazil);

The workshop will result in the definition of a set of well balanced European - South American LBA projects.



sc-dlo



**Institute of  
Hydrology**



**UNIVERSIDADE DE SÃO PAULO  
INSTITUTO ASTRONÔMICO E GEOFÍSICO  
DEPARTAMENTO DE CIÊNCIAS ATMOSFÉRICAS**

